INVESTIGATIONS OF DNA-MEDIATED ELECTRON TRANSFER REACTIONS WITH METALLOINTERCALATORS

Thesis by

Michelle R. Arkin

In Partial Fulfillment of the Requirements

of the Degree of

Doctor of Philosophy

California Institute of Technology

Pasadena, California

1997

(Submitted January 23, 1997)

ACKNOWLEDGEMENTS

If I have become a tougher and more independent person while at Caltech, I owe this growth not only to the turmoils of graduate school, but also to the support and wisdom of friends and colleagues. First and foremost, I thank my graduate advisor Dr. Jackie Barton who, among other things, told me always to "be a classy person." Jackie has been a very supportive boss and continues to be an extremely creative scientist, and I wish her the very best success. Parenthetically, she is also a super proofreader, and I thank her for reading and commenting on this dissertation.

Even as I look forward to a new job and new environment, I know that I will miss the comraderie and helpfulness of many members of the Barton research group. In particular, I owe tremendous thanks to Dr. Eric Stemp. Not only is he an excellent scientist, but also a dear friend, like a wacky older brother. I am very proud of him in his new professorship, and hope his new house is filled with happiness. Before there was Eric, Dr. Cathy Murphy was my "big" sister who took me under her wing and taught me a great deal in my first two years at Caltech; Cathy is also largely responsible for the success of my love-life. I also thank the small group of Bartonites in the Beckman Institute - Dr. Kim Waldron, Dr. Shiela David, Dr. Cindy Dupureur, Dr. Sonya Franklin, and Shana Kelley - for their advice and friendship. As for the Noyes contingent of the laboratory, I thank everyone for teaching me at one time or another. In particular, I recall how I admired and looked-up-to Ayesha Sitlani and Niranjan Sardesi. I also thank Dr. Yonchu Jenkins for many personal and professional interactions; I am looking forward to many fun times together in San Franscisco. I also want to acknowledge the very talented group of students and postdocs with whom I worked most closely - Eric, Cathy, Yonchu, Dan Hall, Erik Holmlin, Shana, Dr. Sabine Coates Pulver, and Dr. Pete Dandliker. The strong collaborations within our "subgroup" have greatly accelerated our research, and I sincerely hope that the spirit of teamwork continues. Of course, I must thank Mo Renta, for going the extra mile.

Much of the work described in this thesis could not have been accomplished without the collaboration of the groups of Dr. Nick Turro at Columbia University and Dr. Paul Barbara at the University of Minnesota. I especially enjoyed working with Dr. Claudia Turro at Columbia University, and thank her for entertaining me when I visited their laboratory. I am also grateful for the expert assistance of Dr. Jay Winkler and the BILRC staff. For advice and help with lasers, I thank Dr. Angelo di Bilio, Don Low, and Dr. Max Bachrach.

Working with the students and postdoctoral fellows in Dr. Peter Dervan's group has been a great advantage to keeping by lab bench in the Beckman Institute. Dr. Yitzak Torr was very helpful and supportive during my first two years of school. I truly appreciated the interest he took in my education and in his sincere enjoyment of chemistry. More recently, I have had the pleasure to work with a number of helpful members of the BI; I especially want to thank Scott Carter, Dr. Brian Takasaki, Dr. Rob Hudson, and Dr. Thomas Lehmann for assistance with instrumentation, lab management, and synthetic advice.

One of the nicest aspects of working at Caltech is the helpful and friendly staff. Dian Buchness and Beth Kerns present cheerful smiles and good advice to perspectives and graduates in the Graduate office. Steve Gould, Elly Noe, and the VWR stockpersons have carried many a box and cleared up many an order problem -thanks! Additionally, I would like to thank Dana Roth of the Millikan Library; I expect never to meet a more calm and helpful librarian.

I have been very fortunate to have wonderful mentors throughout college and graduate school. Dr. Sharon Burgmayer was a terrific advisor when I was an undergraduate at Bryn Mawr, and I am grateful for her continued advice and friendship. Professor Gridley McKim-Smith has had a strong impact on my life as a teacher and a friend. Her incredible strength and wisdom will always touch and inspire me. At Caltech, I have enjoyed working with Dr. George Rossman, chemist-*cum*-mineralogist. During

two courses and one term of research, I came to know George as an energetic teacher and scientist. My thanks to them and my other teachers for their patience and support.

On a more personal note, I extend my sincere thanks and warmest wishes to friends and confidants: for research advice and good cheer, my gratitude to Dr. Mike Hill and Dr. Vince Catallano; for four years of weekly breakfasts, I thank Roian Egnor; for as many coffees and walks, my thanks to Carlos Brody; for helping me through props and thesis writing, my gratitude to Dr. Sonya Franklin, Sabine, and Shana. Wayne and I have been lucky to live with a terrific group of people, and for their friendship I thank Terry Stone, Pam Strugar, Pat Campbell, Chris Staves, and Larry and Annie Enscoe.

Lastly and lastingly, I thank the Arkin family. I could not envision a warmer and more loving group than my mother Merry, my father Roy, and my brother Jeremy. And to the newest member of the clan - welcome, Marion! To Dr. Wayne Larson - what can I say? My dear, I thank you for the smell of barns, the scent of roses, and an endless supply of love and understanding.

ABSTRACT

The array of π-stacked base pairs in DNA represents a novel medium for electron transfer reactions, and metallointercalators have served as useful tools to study this chemistry. Ultrafast kinetic measurements indicate that photoinduced electron transfer reactions between $M(phen)_2(X_2dppz)^{2+}$ (M = Ru, Os; dppz = dipyrido[3,2-a:2,3-c]phenazine; X = H, CH_3) [M(II)] and $Rh(phi)_2bpy^{3+}$ (phi = phenanthrenequinone diimine) [Rh(III)] can occur with rates > 3 x 10^{10} s^{-1}. Recombination reactions between M(III) and Rh(II) are also very fast (~10^{10} s^{-1}), and rates are found to be independent of the loading of Δ-$Rh(phi)_2bpy^{3+}$ on DNA. However, reaction rates and efficiencies are highly sensitive to i) the structure and chirality of intercalators and ii) the sequence and conformation of the DNA double helix. Photoinduced reactions between Ru(II) and Rh(III) bound to the DNA helix and to SDS micelles, which lack the ordered π-stacked array, are also compared. In contrast to DNA, quenching in micelles occurs by diffusion. The details of intercalation and DNA sequence are thus found to be important characteristics of DNA-mediated ET reactions.

To study long-range reactions through DNA, metallointercalator-DNA conjugates have been prepared. Rh(III) and novel trisheteroleptic complexes of Ru(II) are tethered to the 5'-termini of oligonucleotides by solid- and solution-phase methods, and these complexes have provided spectroscopic and photochemical tools to characterize chimeric structures. In addition to experiments in which DNA serves as a molecular bridge connecting donor and acceptor, the double helix may also serve as a reactant in electron transfer chemistry. Ru(III) oxidants have been generated *in situ* by a flash-quench methodology and have been found, by transient absorption spectroscopy, to oxidize G residues in DNA. Furthermore, using a tethered Ru(III)-DNA conjugate, oxidation products are observed 37 Å from the metallointercalator. These investigations of DNA-mediated electron transfer reactions contribute to our understanding of oxidative damage in DNA and may lead to a novel class of DNA-based biosensors.

TABLE OF CONTENTS

LIST OF FIGURES

LIST OF SCHEMES

LIST OF TABLES

Chapter 1

DNA as a Medium for Electron Transfer Reactions

1.1 Introduction

Electron transfer (ET) is among the most important chemical reactions in biology, and is central to the processes of respiration and photosynthesis.[1] In addition, chemical oxidants are known to cause a variety of reactions which can lead to DNA mutagenesis and cancer.[2,3] How biomolecules such as proteins and nucleic acids mediate ET chemistry and respond to oxidative stress is thus critical to our understanding of cell function and homeostasis.

For several years, our laboratory has been interested in the properties of DNA-mediated ET.[4,5,6] Double helical DNA is a water-soluble polymer which contains an electronically well-coupled stack of aromatic heterocyclic base pairs; does this π-stacked array serve as a medium for electron transfer? If so, what are the chemical consequences to the DNA itself? This chapter will introduce some the relevant ET theories and experiments and will describe early data from our laboratory using photoexcited donors and acceptors bound to DNA as probes to study electron transfer. The following text will then describe our recent efforts to address what fundamental role DNA structure plays in modulating ET chemistry.

The study of DNA-mediated ET will contribute to our understanding of radiation biology, ET theory, and molecular electronics. As the carrier of genetic information, DNA must be protected from the damage caused by oxidation.[2,3] However, in addition to its biological function, this polymer also represents a prototypical π-stacked column and therefore a novel medium through which to examine electron transfer reactions. Several theories have proposed that the chemical nature of the medium exerts a strong effect on rates of ET,[7] but few studies have directly addressed ET reactions through a π-stack. In the field of materials research, the synthesis of one-dimensional conductors, or molecular wires,[8] may lead to development of molecular devices, and polymeric π-stacks could have advantages over other conducting polymers.[9] By combining the selectivity and sensitivity of biological molecules with emerging nanoscale technologies, it may

even be possible to design a new class of DNA-based electronic biosensors.[10] If structural perturbations in the DNA medium modulate the rates and efficiencies of ET, such biosensors would be sensitive to nucleic acid sequence, base mismatches, and DNA-binding proteins. Thus, by exploiting the well-characterized biochemistry of DNA, and the throroughly researched field of electron transfer, insights into fundamental reactions will be gained and potential technologies explored.

1.2 Long-range electron transfer reactions

1.2.1 Pathway theory of ET

Marcus has provided a theoretical framework for considering ET reactions:[7,11]

$$k_{et} = (4\pi/h^2\lambda k_B T)^{1/2}[H_{ab}]^2 \exp-[(\Delta G^\circ + \lambda)^2/4\lambda k_B T],$$

where λ is the energy required to reorganize the donor, acceptor, and the solvent, $[H_{ab}]$ is the matrix coupling element, and ΔG° is the thermodynamic driving force. Electronic coupling, determined by $[H_{ab}]^2$, is related to the distance between the reactants and the overlap of the donor-acceptor wavefunctions such that

$$k_{et} \propto e^{-\beta R},$$

where ß is the electronic coupling factor and R the donor-acceptor distance. For reactants separated by a molecular spacer of length R, superexchange theory explains how electronic communication between donor and acceptor may be facilitated by electronic overlap with wavefunctions in the intervening spacer.[12] Several elegant experimental studies have validated the predictions of Marcus theory and superexchange by characterizing the variations in ET rates as a function of driving force, reorganization energy, temperature, and distance.[7] For example, Closs, Miller, and coworkers have demostrated that k_{et} decays exponentially as the length of a rigid, σ-bonded spacer increases;[13,14] furthermore, using donors and acceptors separated by a steroid bridge, these researchers showed that ET rates follow the predicted parabolic dependence on ΔG°

(including the famed "inverted region" in which k_{et} decreases with increasing ΔG° for $\Delta G^\circ > \lambda$). [13]

The coupling factor (ß), and thus k_{et}, depends sensitively on the electronic structure of the bridge between electron donor and acceptor, and a number of theorists have refined the notion of superexchange to describe medium-dependent effects.[12,15,16] One such "pathway" model has been proposed by Beratan, Onuchic, and coworkers to describe intraprotein ET reactions.[15] This model replaces the through-space distance R with a "tunneling length" σ which accounts for the empirical observation that electron-transfer rates are slower through H-bonded paths and through-space jumps than through σ-bonded media. Siddarth and Marcus have further devised a method for calculating the optimum ET pathway through a protein using an artificial intelligence approach.[12b] Both studies conclude that the nature of the protein medium has an important effect on rates of ET reactions.

Because biologically important ET reactions can occur over tens of ångstroms within a protein matrix, many laboratories have investigated the effect of distance and protein structure on rates of ET. One notable example is the work of Gray, Winkler, Richards, and colleagues who have developed a "flash-quench" strategy (Figure 1.1) to monitor ET between an electron donor within the protein (eg Fe^{2+}heme) and an electron acceptor $Ru(bpy)_2(imidazole)(histidine)^{3+}$ covalently bound to the protein surface.[17,18] By engineering histidine residues on the surface of cyctochrome c, these authors have measured k_{et} for several heme-protein-Ru(III) pathways. While results did not track with the direct, through-space distance R, data were well-correlated with the tunnelling distance σ. It is interesting that a single aromatic residue (tryptophan or tyrosine) did not seem to enhance ET rates in these experiments;[18] however, it is not known if an extended aromatic pathway in a protein, such as the 5 tryptophan and phenylalanine residues in the enzyme DNA photolyase,[19] functions as a pathway for long-range ET.

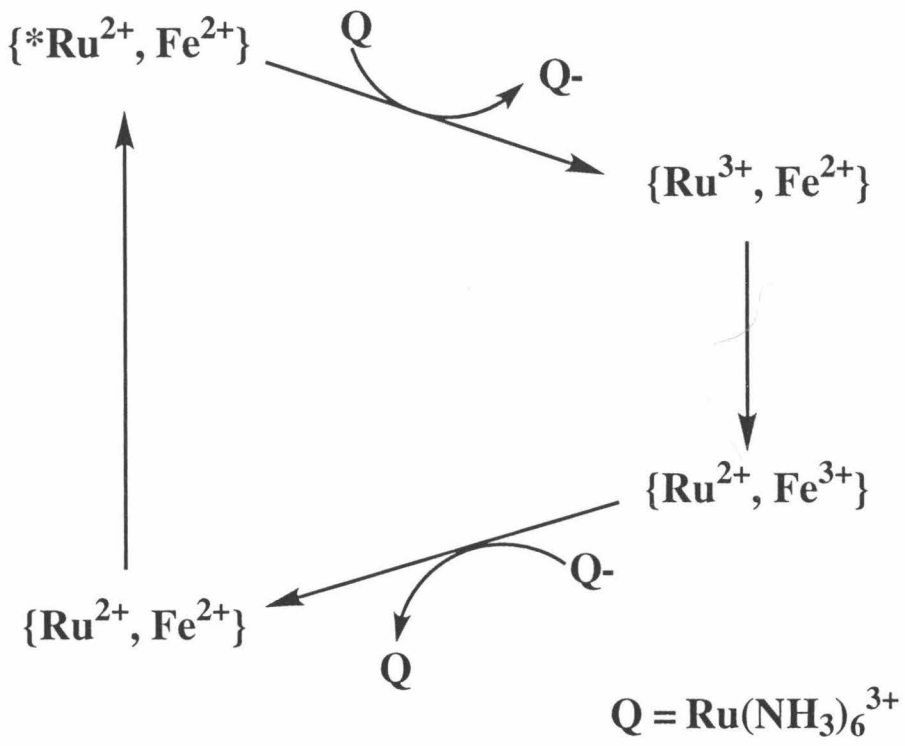

Figure 1.1

Flash-quench cycle for measuring rates of ET in cyctochrome c. In this scheme, *$Ru(bpy)_2(imidazole)(his)^{2+}$ [*Ru^{2+}] is quenched by $Ru(NH_3)_6^{3+}$ to form Ru^{3+}. The ferrous heme center [Fe^{2+}] of cytochrome c then transfers an electron to reduce Ru^{3+}. The ground state reaction between Fe^{2+} and Ru^{3+} is typically monitored by transient absorption spectroscopy which monitors color changes between the reduced and oxidized heme. Adapted from reference 18.

Finally, some exceptions to the relationship $k_{et} \propto e^{-R}$ have been reported. Shallow distance-dependences have been attributed to conformational gating in proteins[20] and to strong electronic coupling in conjugated π-networks.[21] Rates of ET between metal complexes separated by a polyproline spacer have been described for linkers up to nine proline residues long (~41 Å).[22] Isied, Wishart, and coworkers found that, for long spacers (4-9 proline units), k_{et} showed a small dependence on distance; for each additional unit (3.1 Å), only a ~3-fold decrease in rate was observed. The authors attribute this shallow distance-dependence to several factors, including efficient through-bond coupling with long oligomers. Thus, several studies have indicated that the reaction medium has a strong impact on the efficacy of electron transfer.

1.2.2 ET in π-stacked systems

Among the many ideas put forth concerning how the medium may serve to modulate electron transfer has been the notion that stacked aromatic heterocyclic moieties serve as "π-ways" through which electron transfer reactions might be promoted efficiently. A number of reports have described ET reactions through π-stacked arrays of aromatic heterocycles such as porphyrins and phthalocyanins (Figure 1.2).[9,23-28] These solid-state π-stacks are insulators until charge carriers are generated by pulse radiolysis, electrochemistry, or chemical oxidation (doping). According to theory, a sufficient amount of "fractional charge" must be generated to produce an energetically flat, extended electron pathway; interestingly, conductivity also shows strong sensitivity to lattice vibrations (phonons) and therefore to the extended structure of the crystal.[9] Marks and coworkers developed a series of π-stacks composed of phthalocyanins stabilized by covalent M-O-M bonds, where M = Ni, Si, Ge (Figure 1.2).[9,28] Co-crystalization of the components with iodide produced one-dimensional arrays of these π-columns with formal fractional charges of +0.33. Addition of different metals provided a series of stacks with varying monomer spacings; conductivity was found to be strongly dependent on the inter-

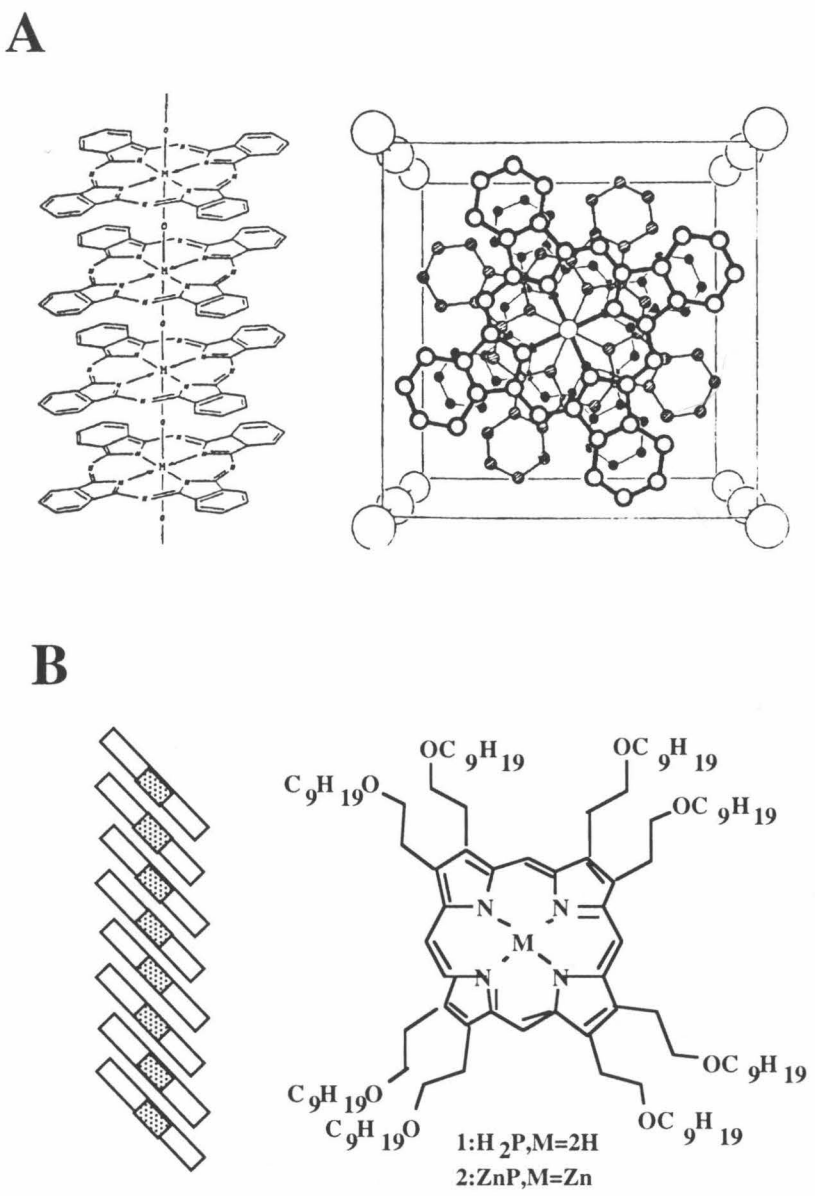

Figure 1.2

Molecular structures of π-stacked phthalocyanins (A) and porphyrins (B). The stacked structure of phthalocyanins in A is maintained by covalent metal-oxide bonds (M = Ni^{4+}, Si^{4+}, Ge^{4+}). Figure adapted from reference 9. Columnar porphyrin structures, on the other hand, are ordered only by intramolecular stacking interactions; columns are electronically and structurally insulated from one another by long aliphatic chains.[23] Both π-stacked arrays are highly conductive when doped.[9,23]

phthalocyanin distance, dropping from 700 $\Omega^{-1}cm^{-1}$ (3.244 Å separations) to ~100 $\Omega^{-1}cm^{-1}$ (3.3 Å) and ~10 $\Omega^{-1}cm^{-1}$ (3.5 Å). Thus, noncovalent stacking between π-systems was critical for mediating charge transfer.

Electron mobility in stacked porphyrins and phthalocyanins has also been investigated for columar stacks insulated from one another by long, aliphatic side chains.[23,24] Charge separation in these noncovalent arrays was attained by pulsed radiolysis, and conductivity was measured by time-resolved microwave conductivity (TRMC). As with the covalently ordered π-stacks, high charge mobilities (μ) were measured for these systems, with $\mu \sim 10^{-6}$ m^2/Vs. Mobilities of this size indicate a hopping mechanism for charge transfer (small polaron motion) in which a relatively localized charge jumps between adjacent π-systems. Two experiments directly addressed the importance of the π-stack in mediating charge transfer.[23] First, the temperature-dependence of conductivity was closely correlated with the degree of discotic order, with charge mobility dropping sharply at the transition temperatures between the solid, liquid crystalline, and isotropic liquid phases. Second, conductivity was found to increase exponentially with column length, indicating that charges were transfered along the columnar axis. In fact, these systems mediate electron transfer quite rapidly; from the calculated value of μ, the authors determined a mean jump time between stacked heterocycles of < 0.14 ps for phthalocyanins and < 0.6 picoseconds (ps) for porphyrins.

ET through π-systems has also been studied in polymers containing aromatic side chains.[25,26] For example, Tanaka, *et al.* prepared a copolymer containing biphenyl pendant groups mixed with a small number (< 2%) of pyrenyl groups. Excess electrons were added to the polymer by pulse radiolysis and electron transfer was monitored by transient absorption spectroscopy, which monitors the differences in color between the reactants and intermediate species. Data indicated that electrons were able to step across biphenyl rings until being trapped by the lower energy pyrenyl groups; ET rate constants between two aromatic groups were estimated to be ~3 x 10^9 s^{-1}. For these flexible

polymers, distances between pendant groups varied from 3 - 8 Å, depending on conformation; given the strong dependence of ET rates on the distance between adjacent π-systems, it is possible that the ET rates are limited by "bad" conformations which isolate radicals (•). In general, results with stacked heterocycles and aromatic assemblies underscore the importance of a closely-spaced, well-organized π-stacked array for mediating charge transfer.

1.2.3 DNA as a π-stacked polymer

The structure of DNA incorporates many of the features of an ideal π-stacked polymer. The double helix contains a relatively rigid, electronically coupled column of stacked base pairs within a water-soluble polyanion, the sugar-phosphate backbone.[29,30] Electronic coupling within the column is reflected in the extensive hypochromicity of the stacked double helix compared to the random coil, and it is this stacking interaction that accounts substantially for the stabilization of the helical form.[29] Using solid-state synthesis and cloning strategies, the chemical components of the DNA π-stack can be varied with precision, and thus the effects of polymer composition can be studied. This polymer is among the most extensively characterized molecule in chemistry, and thus x-ray crystallography,[31] NMR spectroscopy,[32] biochemical methods[33] and a host of other physical techniques have been developed to provide structural and dynamic information about the DNA ET bridge.

The molecular structure of a canonical B-form DNA double helix is illustrated in Figure 1.3A. Each base step is accompanied by a 36° twist and 3.4 Å rise; adjacent base pairs are approximately parallel to each other and tilted at a 12° angle relative to the dyad axis.[30] The two types of base pair are shown in Figure 1.3B. The DNA bases are attached at the N1 position by an N-glycosidic bond to the C1 position of the ribose sugar, and complementary bases are joined by hydrogen bonds. The asymmetry of the base pair structure creates two distinct grooves in B-form DNA; the major groove is 11.7

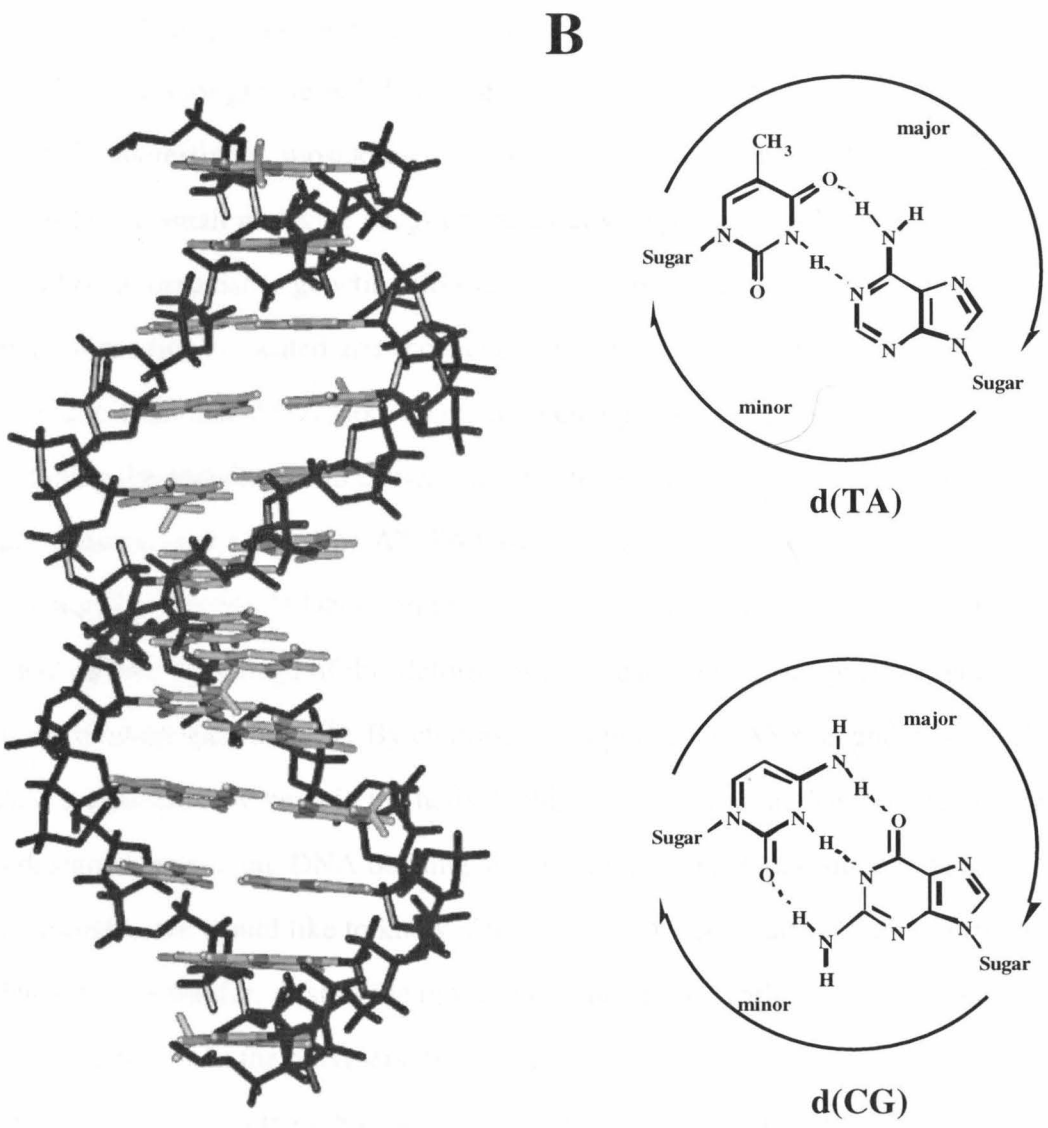

Figure 1.3

Structure of B-form DNA. A) Molecular model of double-helical DNA derived from canonical B-form parameters (InsightII; BIOSYM/Molecular Simulations). The ribose-phosphate backbones are shown in black; the stacked base pairs are shown in grey. B) Molecular structure of the bases of DNA showing hydrogen bonding between complementary bases and the attachment of the sugar-phosphate backbone. Arrows indicate the surfaces of the major and minor grooves. Bases are as follows: A = adenine, T = thymine, G = guanine, C = cytosine.

Å wide and 8.8 Å deep, and contains many of the functional groups presented by the bases, while the minor groove is 5.7 Å wide and 7.5 Å deep, and primarily hydrophobic in character. Interestingly, most known DNA-recognition proteins bind in the major groove, and most small molecule drugs preferentially target the smaller minor groove.

All of an organism's genetic information is stored in this simple, four-base code; how this information is located and accessed within the cell is an interesting and important question. For this reason, there has been a great deal of interest in understanding the sequence- and context-dependent structure of the DNA polymer. For example, sequences of alternating AT-TA basepairs have been found to be conformationally flexible;[34] DNA-binding proteins[35] and small molecules[36] have been "designed" to take advantage of this deformability to catalyze transcription initiation[35] or to increase binding specificity.[36] By contrast, homopolymeric AT sequences are rigid and cause a characteristic bend in the helix;[37] this unusual structure has been exploited in assays designed to measure DNA bending and unwinding. From the standpoint of electron transfer, we would like to know if the four DNA bases vary in their ability to modulate electron tranfer. Just as the molecular structure of synthetic π-stacks impacted the charge mobilities in the polymers described above,[9,23-27] differences in the molecular and extended structure in the DNA polymer could have a large impact on the rates of charge migration through the double helix.

1.3. Oxidative damage of DNA

1.3.1 Radiation biology

The effects of ionizing radiation on DNA has been the focus of much research. Radiation, in the form of UV light, x-rays, and γ-rays, has been shown to react with H_2O to generate hydroxyl radicals (OH•) and hydrated electrons (e^-) and also to directly ionize the DNA molecule.[3] OH• is highly reactive, and causes oxidative damage to DNA in the form of single-strand breaks and base modifications. Additives are sometimes used to

generate less reactive radicals such as $SO_4^{\bullet -}$ and $COO^{\bullet -}$ which only attack DNA and other easily reducible species. Electron spin resonance (ESR) and transient absorption spectroscopy studies indicate that positively charged holes generated by pulse radiolysis migrate to G residues to create $G(-H^+)^\bullet$ while reductive species ultimately form $C^{\bullet -}$ or $T^{\bullet -}$. Irradiation by UV light leads to direct biphotonic (248 nm) and monophotonic (193 nm) excitation of the DNA bases. At 248 nm the primary damage product is the thymine dimer which results from a 2+2 cycloaddition of adjacent T residues. At 193 nm, by contrast, most permanent damage products are modified guanines, such as 8-oxo-G. In single-stranded DNA, migration of radiation damage to $G^\bullet$ has been found to be sequence-dependent and to be blocked by intervening C residues.[38]

Several experiments have sought to measure the distance of charge migration through DNA following treatment with ionizing radiation. Table 1.1 indicates that results have varied widely, and mean migration distances of 1 - 200 base pairs (bp) have been reported. Since experimental and detection methods differ dramatically, it is difficult to rationalize these discrepancies. However, studies in which intercalators have been used as electron/hole traps are particularly interesting. Pulse radiolysis studies of i) "dry" DNA at room temperature and ii) frozen DNA glass at 77 K have both shown that dilute concentrations of intercalators suppress the formation of base radicals.[41,44] These data were taken as evidence that charge could migrate through DNA until reaching a charge trap; based on the ratio of DNA/drug, mean migration distances were estimated to be ~100 bp. In related work, Houée-Levin *et al.* monitored the disproportionation of the intercalated daunorubicin semiquinone in both the presence and absence of DNA.[48] These authors proposed that electron-transfer between semiquinones occurred through the DNA and estimated that $\mu \sim 4 \times 10^{-11}$ m^2/Vs. While this charge mobility is similar to that found for doped organic polymers, it is much lower than has been observed in stacked porphyrins (Section 1.2.2).[23] The lower, but nonzero, conductivity of DNA

Table 1.1. Distances for radiation-induced charge migration in DNA.[a]

Distance (bp)	Conditions	Comments[b]
100[c]	"Dry" DNA, ~77 K	PR, luminescence, bromouracil trap in DNA
25 mean[d]	Doped "dry" DNA, ~77 K	PR, luminescence from DNA/misonidazole trap
90 average[e]	Doped "dry" DNA ~300 K	PR, diffuse reflectance, misonidazole trap
30 max[f]	DNA ± H_2O, ~77 K	PR, conductivity, estimated upper limit
100 max[g]	DNA ± H_2O, ~77 K	PR, long-range migration seen in pthalocyanine model
110[h]	DNA/trap + H_2O, ~77 K	ESR, intercalated trap in DNA
"No evidence"[i]	Oriented DNA films, ~30% H_2O, 77 K	ESR, γ and proton irradiation
3[j]	DNA/trap + H_2O, 293 K	PR, solvated electrons, intercalated trap in DNA
5 max[k]	DNA/trap + H_2O, 293 K	PR, solvated electrons, intercalated trap in DNA
~100[l]	DNA+ H_2O, room temperature	PR, disproportionation of intercalated semiquinone of daunorubicin

[a] O'Neill *et al.*, reference 3. [b] PR = pulse radiolysis. [c] Fielden *et al.*, reference 39. [d] Al-Kazwini *et al.*, reference 40. [e] O'Neill *et al.*, reference 41. [f] van Lith *et al.*, reference 42. [g] Warman *et al.*, reference 43. [h] Cullis *et al.*, reference 44. [i] Miller *et al.*, reference 45. [j] Anderson *et al.*, reference 46. [k] Whillans *et al.*, reference 47. [l] Houée-Levin *et al.*, reference 48.

compared to these columnar crystals qualitatively agrees with the results of Warman *et al.* who have monitored the conductivities of both systems by TRMC (Table 1.1).[43]

Although the effects of ionizing radiation on DNA have important biological consequences, pulse radiolysis might not be an ideal method to measure the kinetics of DNA-mediated ET. Because radiolysis creates a number of high energy radicals, it is challenging to monitor only the reactions involving charge transfer *through* the DNA. Additionally, since ultraviolet light excites nearly all molecular components in DNA, it is difficult to determine from where mobile charges originated. Thus, the distance and rate of ET reactions must be derived statistically. To address these issues, it would be more convenient to initiate charge separation by a selective reaction, such as visible photoexcitation of a chromophore bound to DNA.

1.3.2 Theory of charge-transfer in DNA

Theoretical studies have proposed the importance of charge transfer in nucleic acids for some time.[16,49-53] Many such studies have been inspired by early experiments correlating the oxidation potential of aromatic compounds with their carcinogenicity.[54] Conductivity measurements of DNA pellets has also suggested that such solids behave as semiconductors,[55] although it is now generally agreed that DC charge conduction is mediated by mobile ions in the hydration shell of "dry" DNA.[55c]

Dee and Bauer proposed the first detailed theoretical approach to characterizing charge transfer through mixed sequences of DNA.[49] These authors used a model in which localized charges hop between adjacent bases, arguing that this approach is more reasonable than a model requiring a DNA band structure, since the absorption spectrum of DNA does not indicate extensive electronic delocalization. Instead, the energies of the molecular orbitals of the individual bases were calculated and the energies between them determined; the time-evolution of charge transfer between bases in the DNA helix was then calculated using a stochastic (probabilistic) equation. From this model, the mean

jump time was found to be ~10 fs, ten times faster than that estimated for phthalocyanin crystals (Section 1.2.2). The helical structure of DNA caused the rates of forward and reverse hopping to be different and sequence-dependent; thus, even though each hopping event was independent, after ~200 fs the probability of the electron's position was found to be spread over 20 basesteps, indicating long-range migration on the picosecond timescale.

Other quantum-mechanical calculations have considered the possibility of a "quasi π-type" band structure in helical DNA. Clementi, Ladik, and coworkers have performed *ab initio* self-consistent field (SCF) calculations on the nucleotide units and small fragments of B-form DNA.[50,51] The authors conclude that the DNA band gap is ≤ 10 eV, with a conduction band width of 0.2 - 0.8 eV, depending on sequence. The authors noted that significant charge transfer occurs *within* the nucleotide unit, such that a charge of ≥ -0.24 is placed on each base in a cooperative manner along the base stack. This formal partial charge is comparable to that described by Marks for doped phthalocyanin crystals (Section 1.2.2); however, no intrinsic semiconduction has been suggested by calculations with DNA.[51] It was noted, moreover, that charge migration might be observed if free charge carriers were formed in DNA.

Recently, Beratan and coworkers have applied similar SCF calculations to larger DNA structures containing electron donors and acceptors bound to the double helix.[16] The primary advance in these calculations was the use of large atomic basis sets requiring intensive mathematical computation. Calculations indicated that electron tunneling occurs through the DNA π-stack, instead of through the sugar-phosphate backbone, and decays sharply with distance (ß = 1.2 - 1.6 $Å^{-1}$). While these calculations do qualitatively agree with some measurements,[56-58] they do not predict a large number of experimental results.[39,44,48,59-62] Further theoretical and experimental work is needed before the electronic structure of DNA and the factors controlling charge migration through DNA will be well-understood.

1.4 Donor-acceptor pairs noncovalently associated with DNA

Given the importance of charge transfer in DNA, it is not surprising that chemists have sought to characterize this phenomenon.[4-6,63] A number of researchers have monitored ET reactions between donors and acceptors bound to DNA and have compared results to other "supramolecular" systems in which reactants are noncovalently associated with larger arrays such as micelles (Chapter 3)[64] or charged polymers.[65] In contrast to the radiation techniques described above, the use of small, photoactivated donors and acceptors offers well-described chemistry and a defined initiation point for ET. Furthermore, a great deal of research has been directed towards the design of small molecules which bind to DNA.[66-68] For such systems, three modes of binding have been identified, including i) electrostatic interactions with the sugar-phosphate backbone, ii) groove-binding between organic moieties and the hydrophobic floor of the grooves, and iii) intercalation of a flat, polarizable aromatic surface between two base pairs in the DNA π-stack. Due to the many possible binding orientations, it is important to define how donors and acceptors interact with DNA, and to ascertain if the mode of binding modulates ET chemistry.

1.4.1 Organic compounds and porphyrins

Some of the earliest studies utilizing DNA-bound reactants employed the well-known nucleic acid stain ethidium (Figure 1.4).[56,69-72] The luminescence lifetime of this dye is enhanced ~10-fold upon intercalation into DNA (from ~2 ns to 23 ns) due to protection of exocyclic amines from proton-transfer quenching by H_2O. Baguley and coworkers found that the emission of ethidium bound to poly(dA-dT) was highly quenched upon addition of intercalating derivatives of 9-anilinoacridine.[69] Only one equivalent (equiv) of the best quencher, 9-aminoacridine, was needed to quench 45% of ethidium luminescence. Interestingly, different efficiencies of quenching were observed in different DNA sequences; poly(dA-dT) supported the greatest yield of quenching,

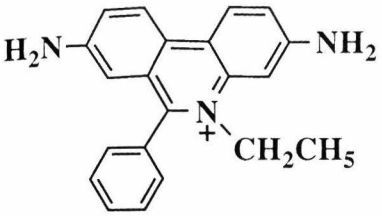

Ethidium

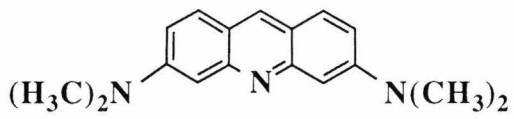

Acridine orange

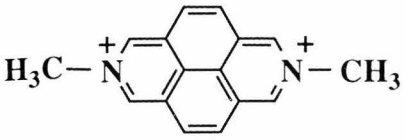

DAP^{2+}

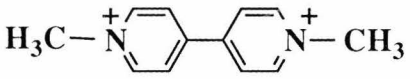

Methyl viologen

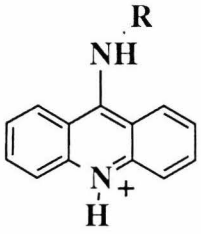

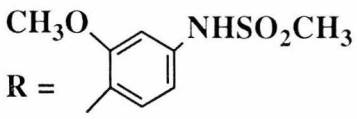

Amsacrine

R = H
9-aminoacridine

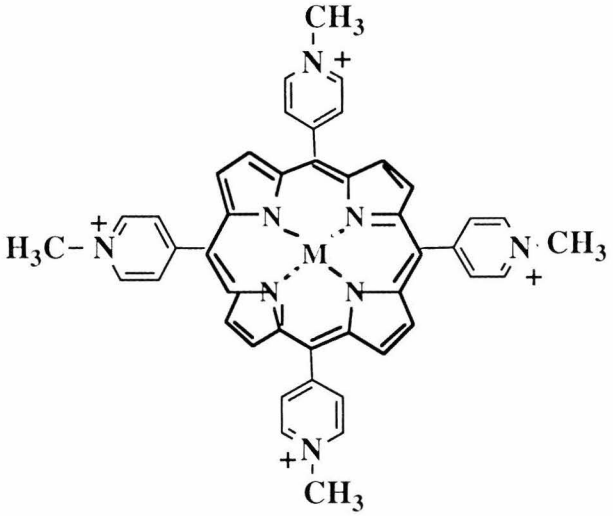

Porphyrin: MT4

Figure 1.4
Structures of organic and porphyrin donors and acceptors.

followed by mixed sequences and finally by poly(dG-dC). Time-resolved luminescence measurements indicated biphasic emission, with one quenched lifetime which could not be resolved, and was thus given a limit of $< 10^8$ s^{-1}, and a longer lifetime corresponding to unquenched ethidium. These data are consistent with a "static mechanism" of quenching in which reaction occurs between DNA-bound molecules without molecular diffusion. The mechanism of quenching was assigned as ET from acridine to photoexcited ethidium based on the lack of spectral overlap required for energy transfer and a qualitative correlation between the amount of quenching and the oxidation potential of several derivatives of 9-anilinoacridine. Interestingly, the electron-donating properties of quenchers also correlated with their *in vitro* antitumor activity. The authors conclude that "the effects of electron donation into the DNA" π-stack should be considered in the mechanism of antitumor drugs.

The quenching of DNA-bound ethidium by electron transfer has also been studied using the groove-bound methyl viologen (MV^{2+}) as a quencher. Fromhertz and Reiger were interested in using the DNA helix as a scaffold for attaining efficient charge separation, the first step in designing molecular electronics.[70] For ethidium quenched by MV^{2+}, they found an enhancement in ET rates of 5×10^5 over the solution phase reaction. Bimolecular rate constants k_q were obtained by the Stern-Volmer equation

$$I_o/I = 1 + K_{sv}[Q]; \; K_{sv} = k_q\tau_o,$$

where I_o and I are the emission intensities of the donor in the absence and presence of the quencher Q, respectively, and τ_o is the luminescence lifetime of the donor in the absence of Q. Linear plots of Io/I vs [Q] are expected for a reaction which occurs by a diffusional mechanism. The authors concluded that the increased rate of ET was due primarily to restricted diffusion along the one-dimensional DNA lattice. Further characterization of this ET reaction by transient absorption spectroscopy indicated that most of the reduced MV^+ recombined rapidly with ethidium, while ~2% escaped from the DNA surface into bulk solution.[71] Thus, when one reactant was diffusible, reactions were facilitated by the

diffusion along the surface of the DNA polymer; only when both donor and acceptor were intercalated into DNA was static quenching observed.

More recently, Brun and Harriman completed a photophysical study of ET reactions between photoexcited donors ethidium or acridine orange (Figure 1.4) and the intercalating acceptor N,N'-dimethyl-2,7-diazapyrenium (DAP^{2+}).[56] Picosecond time-correlated single photon counting (TCSPC) measurements showed that both ethidium and acridine orange bound to a mixed sequence of DNA decayed nonexponentially upon addition of small concentrations of DAP^{2+}. Decay traces were fit to a triexponential function, and the different emission decay constants were attributed to photoexcited (*) donor in three distinct environments. As the concentration of quencher was increased, the fraction of the two fast decays (0.7 and 8 ns for ethidium) increased while the decay corresponding to unquenched donor decreased. Assuming a *nonrandom distribution*, these authors assigned these decays to the rates of ET reactions between donors and acceptors separated by 3,4, and ≥ 5 bp. The three rates obtained for each donor were then fit to the Marcus equation $k_{et} = Ae^{-\beta R}$, from which a ß of ~0.9 $Å^{-1}$ was obtained; interestingly, this value is similar to the lowest values obtained in protein systems (Section 1.2). However, the model for ET in DNA did not provide evidence for a nonrandom distribution of intercalators on the DNA. It is also noteworthy that ET occurs efficiently even at the very low driving forces of these reactions (25 mV for ethidium, 65 mV for acridine orange).

In a second study, the same authors measured the rates of Dexter (exchange) energy transfer between intercalated acridine orange and intercalated or groove-bound palladium(II) porphyrins [tetrakis(x-*N*-methyl-pyridinium)porphyrins, where x = 2-4] (Figure 1.4).[57] Dexter energy transfer involves the exchange of two electrons between energy-matched donors and acceptors and is therefore similar to ET in its distance-dependence. The slow rates of energy transfer and high loadings of donors and acceptors employed led the authors to conclude that DNA was a poor medium for electron

exchange, and they presented a ß ~ 1.4 $Å^{-1}$. While not noted by the authors, the discrepancy between estimated ß values could be related to differences in intercalation between DAP^{2+} and Pd(II) porphyrins. For example, whereas the small, planar donors and DAP^{2+} are not likely to cause large disruptions to the DNA basestack, CuT4 [T4 = tetrakis(4-*N*-methyl-4-pyridinium)porphyrin][72] has been shown by x-ray crystallography to cause distortions in the DNA structure, including the removal of a cytosine base from the π-stack. Importantly, the porphyrin is shown not to "form van der Waals stacking contacts with adjacent bases."[73] The poor reactivity of "hemi-intercalated" porphyrins thus supports the notion that donor and acceptor must be well-stacked in order to communicate via the DNA base stack.

DNA-binding porphyrins have also been used to study Förster energy transfer through the double helix. Pasternack *et al.* have monitored the quenching of intercalated ethidium by intercalated and groove-bound H_2T4, ZnT4, and NiT4.[72] Förster energy transfer arises from dipole-dipole interactions and requires an energy match between the excited-state of the donor (emission spectrum) and the ground-state of the acceptor (absorption spectrum).[74] Theoretically, the efficiency of Förster energy transfer decays as R^6 and is therefore expected to increase strongly with [Q], since the average distance between donor and quencher should decrease. In the presence of DNA, however, the quenching efficiency (I_o/I) was found to increase only exponentially with [Q].[72] This anomalous behavior is consistent with a "sphere-of-action" model, first derived by Perrin, in which quenching occurs with perfect efficiency within a given donor-acceptor distance R_o and not at all beyond this critical separation.[75] The calculated R_o of ~20-30 Å implies that electronic coupling by the DNA π-stack effectively extends dipolar interations between the donor and acceptor.[72]

1.4.2 Octahedral transition-metal complexes

Concurrent with research utilizing ethidium as an intercalating donor, Barton, Turro, and coworkers were characterizing the binding and reactivity of $M(phen)_3^{n+}$ (phen = 1,10-phenanthroline; M = Ru^{2+}, Rh^{3+}, Co^{3+}, Cr^{3+}, Ni^{3+}) complexes bound to DNA.[65,76-82] Through a variety of spectroscopic techniques, it was determined that complexes such as $Ru(phen)_3^{2+}$ associates noncovalently with DNA by both groove-binding and intercalation, with an overall association constant $K_b \sim 10^3\ M^{-1}$.[76] Moreover, an enantioselectivity in these binding modes was observed. In the presence of DNA, emission from Δ-*$Ru(phen)_3^{2+}$ was found to decay with two lifetimes, 0.6 and 1.7 μs.[78] The longer lifetime, which also maintained polarization of luminescence, was attributed to an intercalative mode of binding, and ^1H NMR studies provided evidence for insertion of the 5,6 positions of one phen ligand between the DNA base pairs.[79] Support for surface binding, particularly for the Λ-enantiomer, was provided by ^1H NMR studies in which paramagnetic Ni(III)- and Cr(III)- phenanthroline complexes selectively perturbed protons in the minor groove of DNA. ESR studies with $Ru(phen)_2(TEMPO\text{-}phen)^{2+}$ [TEMPO = 2,2,6,6,-tetramethylpiperidine-N-oxyl] also indicated three distinct components which were attributed to free, groove-bound, and intercalated species.[80]

Figure 1.5 illustrates a model for binding of $M(phen)_3^{n+}$ complexes based on these data. Enantioselective binding of the isomers of $M(phen)_3^{n+}$ was ascribed to the "symmetry matching" of $M(phen)_3^{n+}$ isomers with the right-handed twist of B-DNA.[77] When Δ-$M(phen)_3^{n+}$ is intercalated, the two ancillary phen ligands follow the shape of the major groove, avoiding steric clashes with the sugar-phosphate backbone. For the left-handed Λ-isomer, such clashes make intercalation unfavorable; this enantiomer instead takes advantage of hydrophobic surface area and nestles in the floor of the minor groove.

Barton, Turro, and coworkers exploited the shape-selective binding of metal complexes to DNA to address the importance of molecular diffusion and long-range ET

Figure 1.5

Binding to DNA by enantiomers of tris(phenanthroline) metal complexes. The computer graphic representation depicts the model for noncovalent binding to right-handed double helical DNA by the Δ-(right) and Λ- (left) isomers. Δ-$[M(phen)_3]^{n+}$ is shown bound to the lower half of the helix through intercalation in the major groove. In this binding mode, preferred for the Δ-isomer, one ligand is partially stacked between the DNA base pairs. Λ-$[M(phen)_3]^{n+}$ is shown bound to the upper half of the DNA helix against the minor groove. This binding mode, preferred for the Δ-isomer, is stabilized through hydrophobic interactions.[76] Model built with InsightII (BIOSYM/ Molecular Simulations).

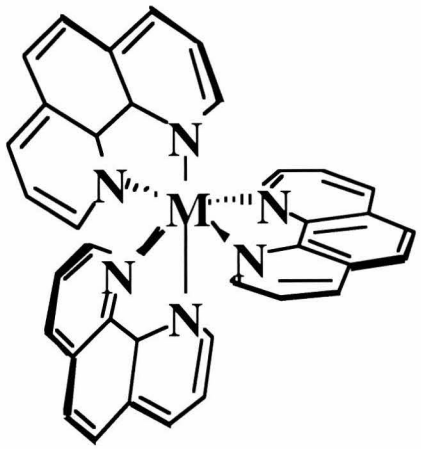

Λ-M(phen)$_3^{n+}$

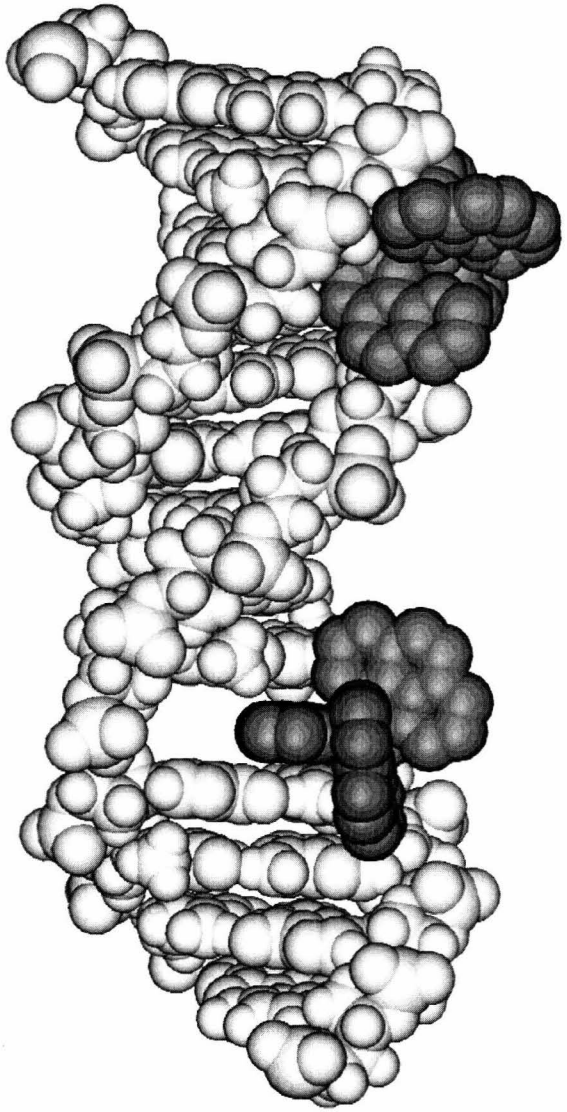

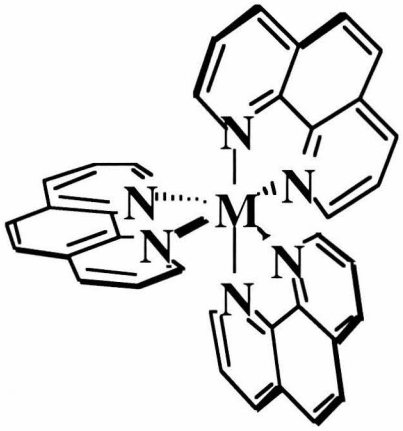

Δ-M(phen)$_3^{n+}$

through DNA.[65,81,82] In their initial study, emission quenching of $*Ru(L)_3^{2+}$ by $Co(L)_3^{3+}$ [L = bpy (2,2'-bipyridine), phen, 4,7-diphenylbpy] was found to be ~100-fold faster in the presence of DNA than in aqueous solution; moreover, Stern-Volmer plots were downward-curving, reaching saturation at high [Q].[81] Rate enhancements were attributed primarily to increases in local concentration and facilitated diffusion. A second study further explored the contributions of diffusion and long-range ET quenching using $*Ru(phen)_3^{2+}$ as donor and $M(phen)_3^{3+}$ (M = Co, Cr, Rh) as acceptors.[82] Some of the data are summarized in Table 1.2. At the low Ru(II)/(DNA bp) ratios (1/75 to 1/150) used in these experiments, quenching was more efficient for surface bound complexes than for intercalators. Furthermore, two experiments indicated a mechanism other than diffusion to account for accelerated ET rates. First, experiments were carried out in high viscosity solutions ($\leq$ 92% glycerol) through which diffusion was limited; nevertheless, reaction rates were still enhanced over quenching in the absence of DNA. Second, three quenchers with varying reduction potentials were studied. The solution-phase ET rates increased with reaction driving force, as expected from Marcus theory; in the presence of DNA and glycerol, however, rates of quenching were fastest for $Cr(phen)_3^{3+}$, the acceptor with intermediate driving force. The authors concluded that the observed rate enhancements were due to a combination of i) increases in local concentration of complexes bound to DNA, ii) facilitated diffusion along the DNA helix, and iii) long-range electron transfer through the DNA medium. The rapid equilibration between binding modes and the weak binding of $M(phen)_3^{n+}$ complexes to DNA, however, made it difficult to evaluate the relative importace of each factor.

1.5 Metallointercalators as donors and acceptors

The experiments described above (summarized in Table 1.3) strongly suggest that the binding of both donor and acceptor plays an important role in the ability of DNA to mediate electron transfer. In order to selectively probe the role of the DNA π-stack, more

Table 1.2. Parameters for ET reactions between *$Ru(phen)_3^{2+}$ and $M(phen)_3^{n+}$ bound to DNA.[a]

Acceptor	ΔG^o (V)	Rate constants (x 10^{10} M^{-1} s^{-1})[b] k_q^c	k_q^s	k_q^i
$Co(phen)_3^{3+}$	1.29	0.14[c]	2.4[d]	0.2[d]
$Cr(phen)_3^{3+}$	0.64	0.05[c]	5.0[d]	0.64[d]
$Rh(phen)_3^{3+}$	0.22	0.02[c]	0.14[d]	0.086[d]

[a] adapted from Purugganan *et al.*, reference 82. Conditions were 4 μM $Ru(phen)_3^{2+}$, 300 μM bp DNA, in a buffer of 5 mM tris, 50 mM NaCl, pH 7.2. [b] superscripts denote the following: c = free donor in solution, s = donor surface-bound to DNA, i = donor intercalated into DNA. [c] 293 K. [d] 253 K.

Table 1.3. Luminescence quenching of photoexcited donors in the presence of DNA.[a]

Donor	Acceptor	DNA[b]	bp/donor	I_o/I at 5 equiv Q	Intercalative binding
Ethidium	Amsacrine	Mixed sequence	10	2.5	Both donor and acceptor
Ethidium	Methyl viologen	Mixed sequence	50	1.5[c]	Donor only
Ethidium	DAP^{2+}[d]	Mixed sequence	10	3.0[c]	Both donor and acceptor
Pd^{2+} Porphyrins	Methyl viologen	Mixed sequence	20	1.03	Donor only
$Ru(phen)_3^{2+}$	$Co(bpy)_3^{2+}$	Mixed sequence	23	1.35	Donor only
$Ru(phen)_3^{2+}$	$Co(bpy)_3^{2+}$	sonicated	23	1.1	Donor only
$Ru(phen)_2dppz^{2+}$	$Ru(NH_3)_6^{3+}$	Mixed sequence	50	1.5	Donor only
$Ru(phen)_2dppz^{2+}$	$Rh(phi)_2phen^{3+}$	Mixed sequence	50	3.5	Both donor and acceptor

[a] adapted from Stemp and Barton, reference 5. All data referenced in text. For all systems, quenching was measured at ambient temperature, in aqueous buffers with pH ~ 7. [b] "mixed sequence" denotes highly polymerized calf thymus DNA; "sonicated" denoted shorter (~2000 bp) strands of calf thymus DNA. [c] Values reported for 2 equiv of quencher. [d] DAP^{2+} = *N, N'*-dimethyl-2,7-diazapyrenium.

recent studies in our laboratory have utilized avid metallointercalators with binding constants for intercalation of $\geq 10^7$ M^{-1}.[4-6] The strong preference of these molecules to intercalate rather than groove-bind clarifies the relationship of the donor and acceptor to the DNA medium. Additionally, the binding of these molecules to B-form DNA has been characterized by a number of techniques, and thus binding can be correlated with reactivity.

Figure 1.6 illustrates the donor $Ru(phen)_2dppz^{2+}$ (dppz = dipyrido[3,2-a:2,'3'-c]phenazine) [Ru(II)], the acceptor $Rh(phi)_2phen^{3+}$ (phi = 9,10-phenanthrenequinone diimine) [Rh(III)] and their interactions with DNA. Not only do these complexes bind tightly to DNA by intercalation, but their electronic structures are particularly well-suited to engage in ET reactions through the DNA π-stack.[59] The absorption spectrum of Ru(II) is characterized by metal-to-ligand charge transfer (MLCT), [83-87] and studies of $Ru(bpy)_2dppz^{2+}$ in the absence of DNA have shown that the photoexcited electron is centered on the phenazine ring of the intercalated dppz ligand.[87] The electron acceptor $Rh(phi)_2phen^{3+}$ is known to bind tightly to nucleic acids via intercalation of the phi ligand;[88-90] furthermore, the lowest energy absorption bands of this complex results from transitions centered on the phi ligand.[90,91] We were intrigued by the possibility that intercalation of the ruthenium and rhodium complexes could afford easy access to the π-way, where the stacked bases might readily accept and direct an electron from the donor to the intercalated acceptor.[59]

1.5.1 Dipyridophenazine complexes of Ru(II) and Os(II)

Evidence for intercalation of the dppz ligand of complexes such as $Ru(phen)_2dppz^{2+}$ is provided by DNA unwinding studies,[86] UV-absorption and emission titrations,[86,93-96] resonance raman spectroscopy,[87] and ^1H NMR.[97] The absorption spectrum of $Ru(phen)_2dppz^{2+}$, given in Figure 1.7A, indicates MLCT centered at 440 nm, phen π-π* transitions at 272 nm, and π-π* transitions within the dppz ligand at 384

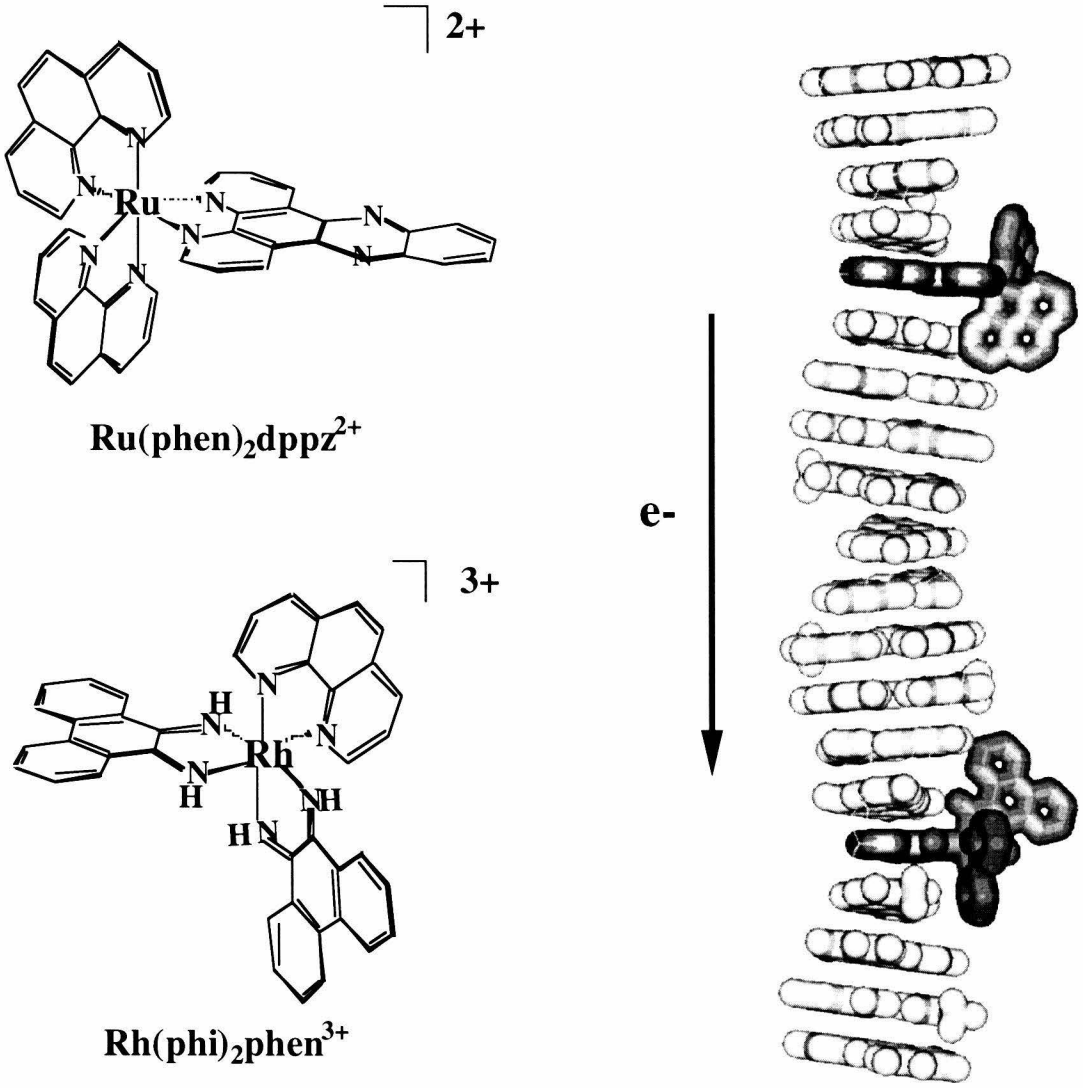

Figure 1.6

Structures of metallointercalators $Ru(phen)_2dppz^{2+}$ and $Rh(phi)_2phen^{3+}$ and a schematic illustration of a possible electronic pathway from the photoexcited $Ru(phen)_2dppz^{2+}$ donor through the stacked bases of DNA to the $Rh(phi)_2phen^{3+}$ acceptor.

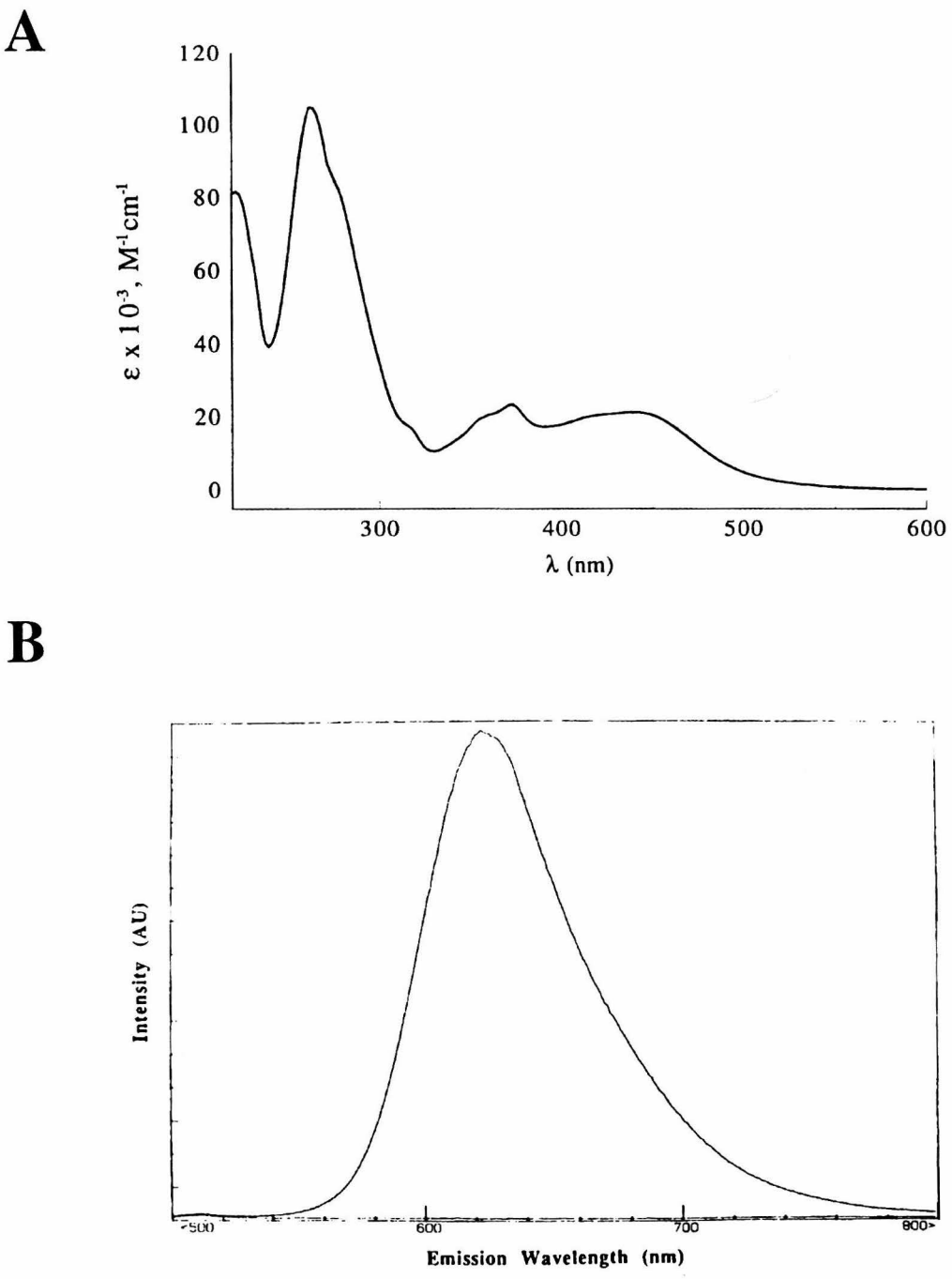

Figure 1.7

Photophysical properties of $Ru(phen)_2dppz^{2+}$. A) UV-visible absorption spectrum of Ru(II) in aqueous solution in the absence of DNA. B) Emission spectra of Ru(II) in the absence (baseline spectrum) and presence (top spectrum) of B-form DNA.

nm. Theory and experiment both indicate that charge transfer is localized on the dppz π-system.[83-87,98] In aqueous solution, the emission resulting from the MLCT excited state is deactivated through an interaction between the phenazine nitrogens and solvent water molecules[83,86] and no steady-state emission is observed. When the complex intercalates into double stranded DNA, however, the stacked bases protect the phenazine nitrogens from water, and intense photoluminescence is apparent (Figure 1.7B); emission enhancements upon intercalation are estimated to be > 10^4 for $Ru(phen)_2dppz^{2+}$. While not known in detail, the mechanism of water quenching had been ascribed to either energy- or proton transfer. Recently, ultrafast laser spectroscopy has been used to determine the lifetimes, spectral properties, and decay mechanisms of the Ru^{III}-$dppz^{\bullet-}$ charge-transfer state (Chapter 2).[61]

Table 1.4 presents the steady-state and time-resolved emission characteristics of $Ru(phen)_2dppz^{2+}$ upon binding to various DNAs.[86] The time-resolved luminescence of DNA-bound Ru(II) is characterized by a biexponential decay, consistent with the presence of at least two binding modes for the complex. That both modes involve intercalation of the dppz ligand is supported by $[Fe(CN)_6]^{4-}$ quenching,[86] proton-transfer quenching,[99] and ^1H NMR experiments.[97] ^1H NMR measurements also indicate that both modes involve intercalation from the major groove and that the average dissociation rate for Ru(II) from DNA is ≤ 70 s^{-1}. Based on quenching and ^1H NMR experiments as well as photophysical studies of derivatives of Ru(II), two families of intercalative binding modes have been proposed (Figure 1.8): i) a perpendicular mode in which the dppz ligand intercalates from the major groove such that the long axis of the metal complex lies along the dyad axis and ii) a side-on mode where the long axis of the dppz lies more closely to the long axis of the base pairs.[94] It is noteworthy that the differences in lifetimes do not imply that the binding of the perpendicular mode is stronger than that of the side-on mode; in fact, the higher percentage of short lifetime in most DNA environments (Table 1.4) suggests that the binding of the latter orientation is

Table 1.4. Luminescent Parameters for Photoexcited $Ru(phen)_2dppz^{2+}$ Bound to Nucleic Acids.[a]

Nucleic Acid	τ (ns)[b,c]	%[d]	λ_{max} (nm)	Φ[e]
Calf thymus DNA[f]	770 120	40 60	617	0.039
Z-form poly[d(GC)][f]	270 70	60 40	608	0.025
poly [r(AU)][f]	490 80	20 80	620	0.004
poly (dT)•poly (dA)•poly (dT)[f]	530 170	60 40	621	0.061
Δ-$Ru(phen)_2dppz^{2+}$, calf thymus DNA[g]	850 160	20 80	617	~0.08
Λ-$Ru(phen)_2dppz^{2+}$, calf thymus DNA[g]	150 40	15 85	617	~0.01

[a] All steady-state and time-resolved measurements conducted at 20°C using instrumentation described in reference 28. $Ru(phen)_2dppz^{2+}$ is racemic mixture unless otherwise noted. [b] Error estimated to be ± 10% for both steady-state and time-resolved measurements. [c] Samples used in steady-state and time-resolved measurements contained 10 μM ruthenium complex/100 μM nucleotides. [d] Lifetime ratios calculated from the magnitudes of the pre-exponential factors produced by the program used in the deconvolution of the time-resolved data. [e] Quantum yields, Φ, were determined relative to $[Ru(bpy)_3]^{2+}$ (Φ = 0.042) (48). [f] Adapted from Jenkins *et al.*, reference 86. [g] Ratio Ru(II)/DNA bp = 1/50. Adapted from Arkin *et al.*, reference 61.

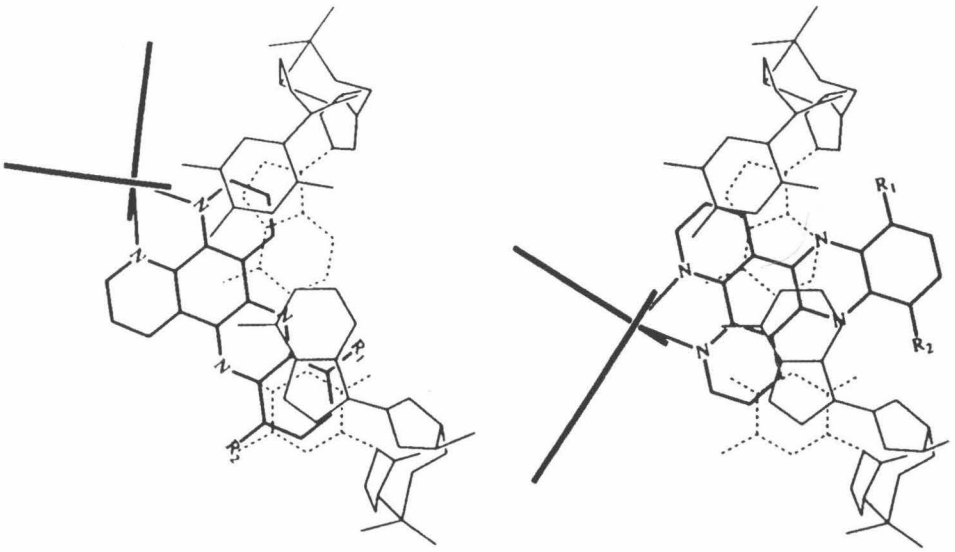

Figure 1.8

Illustration of the side-on (left) and perpendicular (right) models proposed for intercalation of $Ru(phen)_2dppz^{2+}$ in DNA. View is shown along the helical axis, with the major groove to the left, and depicts the possible overlap of dppz (bold lines) with the base pairs above (solid lines) and below (dashes) the intercalated ligand. In the side-on orientation, one phenazine nitrogen atom is positioned towards solvent. In the perpendicular intercalation mode, both sides of the ligand are protected from water. Adapted from reference 94.

thermodynamically favored. Table 1.4 also indicates that both enantiomers of $Ru(phen)_2dppz^{2+}$ intercalate with two binding orientations.[61,96] Emission lifetimes are significantly longer for the Δ-isomer and the steady-state emission intensity is ~8-fold higher than for the Λ enantiomer; the greater protection of Δ-Ru(II) from water quenching is consistent with the symmetry matching of the right-handed isomer and the helical structure of B-form DNA. Because of the much higher emission intensity of Δ- compared to Λ-Ru(II), the emission lifetimes of *rac*-$Ru(phen)_2dppz^{2+}$ approximate that of the Δ-isomer.

As also described in Table 1.4, the luminescent parameters for the metal complex bound to different conformations of DNA can be correlated with the accessibility of the phenazine ligand to water.[83] This correlation is most clearly illustrated in the examples of A-form poly[r(AU)] and the triple helix poly(dT)•poly(dA)•poly(dT). In A-form nucleic acids, the base pairs are pushed back toward the periphery of the major groove, creating a major groove which is both very deep and very narrow.[30] The shape of this cavity likely hinders the intercalation of the dppz ligand; this relatively poor protection results in short excited-state lifetimes and correspondingly low luminescent intensities. Intercalation into the triplex, on the other hand, results in an interaction where the base triples adjacent to the intercalating ligand completely surround the phenazine nitrogens, resulting in greater protection from water and therefore longer luminescent lifetimes and higher luminescent intensities.[83] After $Ru(bpy)_2dppz^{2+}$ was shown to serve as a sensitive indicator of solvent accessibility in DNA, this luminescent probe was similarly used to describe solvent channels in Nafion films[100] and to characterize the binding of polypyridyl complexes to anionic micelles.[64,101]

Osmium(II) complexes of dppz preserve some of the properties of Ru(II) complexes, but with important variations.[102] Since the Os(II) and Ru(II) complexes are isostructural, both complexes are expected to bind identically to DNA; indeed, absorption and emission titrations indicate that $Os(phen)_2dppz^{2+}$ does intercalate into B-form DNA.

Importantly, the photophysical attributes of Os(II) are characteristically different from those of Ru(II). The visible spectrum of Os(II) shows significant absorption of light from 550-650 nm, indicating direct population of a ^{3}MLCT excited-state, as expected from the greater spin-orbit coupling of third row transition metals.[103] Compared to Ru(II), the emission maximum (λ_{max}) from Os(II) complexes is red-shifted (λ_{max} ~760 nm) and the emission lifetimes are much shorter (2 - 12 ns).[102] Recent work has been focused on the characterization of Os(II) as a photoexcited electron donor in DNA,[104] and comparisons between Os(II) and Ru(II) are discussed in Chapter 2.[61] In particular, we are interested to learn whether ET reactions are governed by intercalation, photophysics, or a combination of both.

The sensitive emission properties of $Ru(phen)_2dppz^{2+}$ and its derivatives make these complexes ideal electron donors in the study of DNA mediated electron transfer. Since luminescence is due to intercalated species, photophysical studies probe only those complexes bound to DNA. The steady-state and time-resolved luminescence properties of Ru(II) complexes also serve to characterize novel metal/DNA assemblies. Additionally, many derivatives of $M(phen)_2dppz^{2+}$ can be readily prepared,[105] providing a large pool of structurally related photoexcited donors.

1.5.2 Phenanthrenequinone diimine complexes of Rh(III)

Phi complexes of rhodium(III) bind avidly to DNA through intercalation,[67] as shown by UV-absorption spectroscopy,[88,89] helical unwinding studies, and ^{1}H NMR spectroscopy.[90] UV-absorption spectra of a series of complexes indicate strong hypochromism of electronic transitions between 330-400 nm (Figure 1.9); spectroscopic and electrochemical studies with a number of phi complexes of Rh(III) and Ir(III) indicate that these low energy absorbance bands arise from π-π^* and intraligand CT in the phi moiety.[92] Furthermore, ^{1}H NMR measurements of Δ-$Rh(phen)_2phi^{3+}$, $Rh(en)_2phi^{3+}$ (en = ethylenediamine) and $Rh(Me_2trien)phi^{3+}$ (Me_2trien = 2,9-diamino-

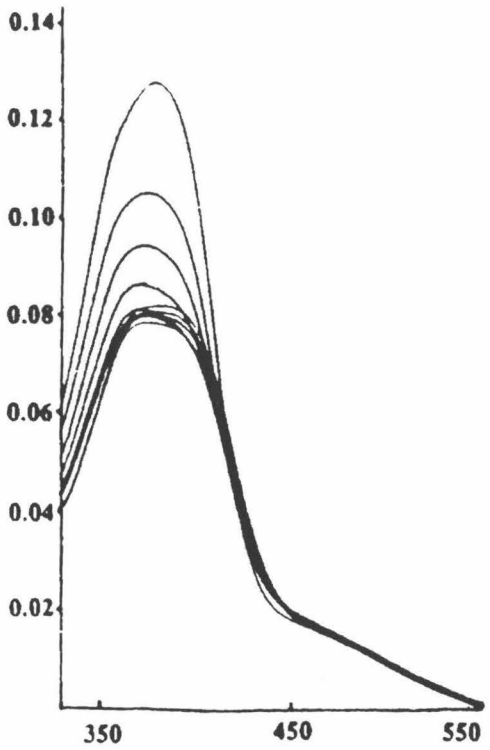

Figure 1.9

UV-visible absorption spectrum of $Rh(phi)_2bpy^{3+}$ upon addition of B-form DNA. The hypochromicity (31%) and red-shift (11 nm) evident in the phi-centered absorbance bands between 350 nm and 550 nm are indicative of intercalative binding of the complex via the phi ligand. Conditions are 11.4 μM Rh(III), 0 - 127 μM nucleotides DNA, in an aqueous buffer of 5 mM tris, 50 mM NaCl, pH 7.5. Adapted from reference 88.

4,7-diazadecane) bound to oligonucleotide duplexes show large upfield shifts in phi protons (.5-1.2 ppm) indicative of deep intercalation of this ligand.[90,106,107] In each study, two-dimensional NOESY experiments indicate a selective loss of the intramolecular NOE between the central base and the adjacent sugar, providing compelling evidence for intercalation of the rhodium(III) complex at that base step. As in ^{1}H NMR measurements of Ru(phen)$_2$dppz^{2+},[97] NOESY experiments with phi complexes of Rh(III) also indicate intermolecular NOE's between the metallointercalator and protons in the DNA major groove.[90,106,107]

Rhodium complexes have proven to be particularly useful probes of DNA structure and recognition because these complexes promote strand breaks in DNA and RNA upon photoactivation.[67,88] The DNA-derived products of this photocleavage reaction are consistent with abstraction of the C3' hydrogen atom from the nucleotide in the 5' position of the intercalation site. Because cleavage occurs directly at the base step of intercalation, these complexes have served as novel probes of higher-order structures in nucleic acids and as high-resolution DNA photofootprinting reagents.[67,108,109,110]

The nucleic-acid recognition properties of phi complexes of rhodium may be optimized by altering the ancillary ligands (Figure 1.10).[36,110-113] The recognition of these octahedral intercalators is governed by the ensemble of noncovalent interactions between the metal complex and the nucleic acid binding site. Such interactions arise from i) the complementarity of the three-dimensional shapes of the metal complex and its site and ii) the positioning of ligand functionalities for hydrogen bonding and van der Waals contacts to functional groups in the DNA major groove. An elegant example of recognition by functional group complementarity is provided by Rh(Me$_2$trien)phi^{3+}.[111] This complex recognizes the sequence 5'-TCGA-3' through hydrogen bonding between axial amines on the complex and carbonyl groups on the GC basepairs and through van der Waals contacts between methyl groups on the trien ligand and on the thymine bases. Δ-Rh(phen)$_2$phi^{3+} provides an example of shape-selective binding.[112] This hydrophobic

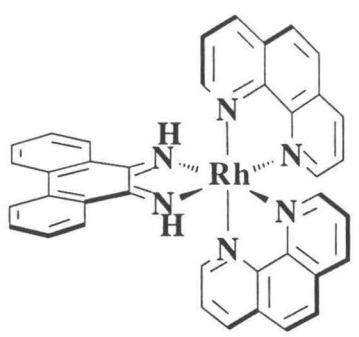

$[Rh(phen)_2(phi)]^{3+}$

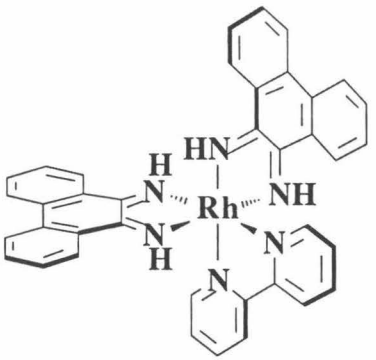

$[Rh(phi)_2(bpy)]^{3+}$

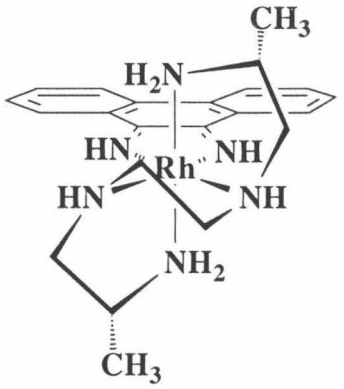

Δ,α-(R,R)-$[Rh(Me_2trien)(phi)]^{3+}$

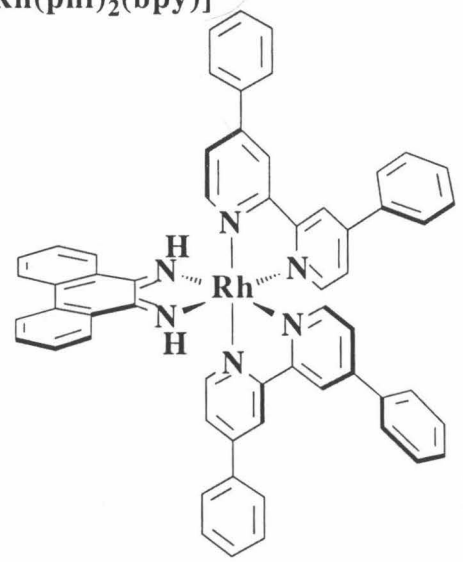

$[Rh(4,4'\text{-diphenylbpy})_2(phi)]^{3+}$

Figure 1.10

Phi complexes of rhodium(III). Clockwise, from upper left: $[Rh(phen)_2phi]^{3+}$ recognizes 5'-pyr-pyr-pur-pur-3' sequences, characterized by an open major groove.[112] $[Rh(phi)_2(bpy)]^{3+}$ binds and cleaves B-form DNA without sequence selectivity, making it a high resolution photofootprinting reagent.[110] Δ-$[Rh(4,4'\text{-dimethylbpy})_2(phi)]^{3+}$ recognizes the palindromic sequence 5'-CTCTAGAG-3' and displays striking enantioselectivity.[113] Δ,α, -(R,R) $[Rh(Me_2trien)(phi)]^{3+}$ recognizes 5'-TGCA-3' sequences through a combination of van der Waals interactions involving the methyl groups on the ligand and hydrogen bond donation by the axial amines.[106,111]

complex binds preferentially at base steps with an open major groove, since only at such sites are steric clashes of the phen protons with the bases relieved. This specificity can be contrasted with the sequence-neutral binding of $Rh(phi)_2bpy^{3+}$; in this complex the ancillary phi is pulled away from the helix and steric clashes with protons in the major groove are avoided.[110] Finally, Δ-Rh(4,4'-diphenylbpy)$_2$phi^{3+} provides a dramatic example of shape-selection; this bulky complex recognizes the 8 base-pair sequence 5'-CTCTAGAG-3' with a specificity and binding strength that rivals DNA-binding proteins.[113] Moreover, the concentration dependence of photocleavage indicates that Δ-Rh(4,4'-diphenylbpy)$_2$phi^{3+} binds to its DNA site as a dimer (K_{dimer} ~ 2 kcal/mol), and modeling suggests that this extra affinity is provided by van der Waals contact between the phenyl and bipyridine rings on the nonintercalated ligands.

$Rh(phi)_2phen^{3+}$ is a particularly suitable luminescence quencher for investigations of ET reactions on DNA. Its electronic properties are favorable for electron transfer, and this rhodium complex is primarily sequence neutral, so that nearly random binding of the donor and acceptor is expected. Moreover, the photocleavage reaction can be exploited to identify the binding sites of the acceptor on the DNA double helix.

1.6 *Ru(phen)$_2$dppz^{2+} as electron donor in DNA

1.6.1 Comparison of quenching by $Ru(NH_3)_6^{3+}$ and $Rh(phi)_2phen^{3+}$

Figure 1.11 shows the electron transfer cycle for photoinduced ET between Ru(II) and a quencher Q. Following excitation with visible light, *Ru(II) is quenched by ET to Q. The charge-shifted intermediates Ru(III) and Rh(II) then recombine to regenerate the starting materials. Typically, photoinduced ET is monitored by luminescence quenching; the recombination reaction, on the other hand, is monitored by transient absorption spectroscopy, since this reaction involves only ground-state species.

Initial studies with *Ru(phen)$_2$dppz^{2+} focused on luminescence quenching in the presence of mixed sequences of DNA.[59] The importance of intercalation was

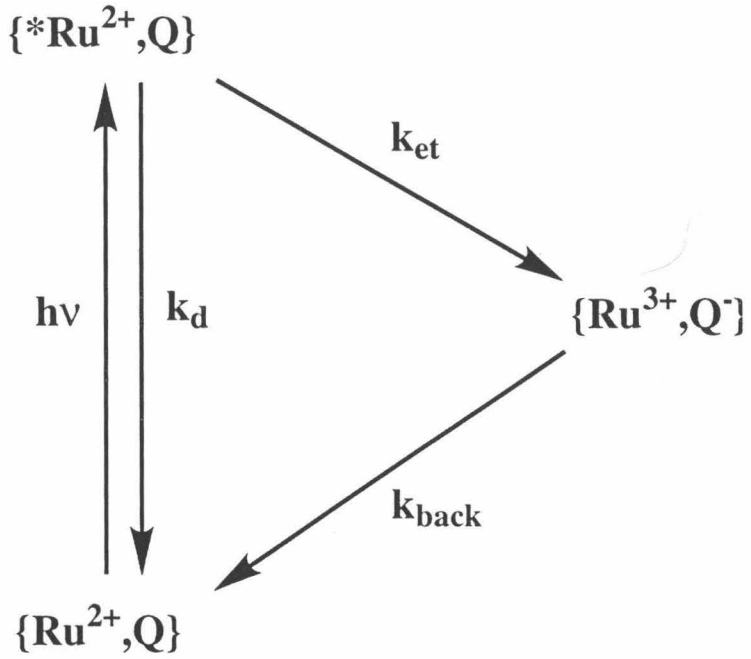

Figure 1.11

Photoinduced electron transfer cycle. Photoexcited $Ru(phen)_2dppz^{2+}$ ($*Ru^{2+}$) transfers an electron to a quencher Q, such as $Ru(NH_3)_6^{3+}$ or $Rh(phi)_2phen^{3+}$, to form the intermediates Ru^{3+} and Q^-. Ru^{3+} and Q^- then recombine to generate the starting materials; this ground-state reaction is followed by transient absorption spectroscopy.

investigated by comparing quenching of *Ru(II) by groove-bound and intercalated acceptors. Hexa(amine)ruthenium(III) [$Ru(NH_3)_6^{3+}$] served as the nonintercalated acceptor since it is a known oxidative quencher of ruthenium(II) polypyridyl complexes[17,114] and has been shown to bind DNA by electrostatic and hydrogen bonding interactions.[115] Additionally, the reduction potential of $Ru(NH_3)_6^{3+}$ was shown to be very similar to that of the intercalating acceptor $Rh(phi)_2phen^{3+}$ (+0.1 *versus* -0.03 V vs. NHE, respectively), and thus ΔG° for both ET reactions were comparable.[59] Time-resolved emission measurements (Figure 1.12A) indicated Stern-Volmer quenching of $*Ru(phen)_2dppz^{2+}$ by $Ru(NH_3)_6^{3+}$ in the presence of B-form DNA; plots of intensity (I_o/I) and lifetime (τ_o/τ) quenching were linear with [Q] and similar quenching rate constants ($k_q \approx 10^{10}\ M^{-1}s^{-1}$) were calculated. These kinetics reflected dynamic quenching in which the donor and acceptor molecules were brought together by the molecular diffusion of $Ru(NH_3)_6^{3+}$. Interestingly, the short emission lifetime was quenched more efficiently than the long lifetime; this difference in k_q is consistent with proton-transfer quenching and solvent-isotope studies which indicated that the intercalated species with the shorter emission lifetime was more accessible to solvent.

The quenching of $*Ru(phen)_2dppz^{2+}$ by $Rh(phi)_2phen^{3+}$ contrasted strongly to quenching caused by the diffusible $Ru(NH_3)_6^{3+}$.[59] When the intercalating $Rh(phi)_2phen^{3+}$ was titrated into a sample containing a mixed sequence of DNA and $Ru(phen)_2dppz^{2+}$, the luminescence intensity of *Ru(II) was highly quenched, whereas the emission lifetimes were only slightly affected. Time-resolved emission measurements further indicated that the quenching rate was faster than the instrument response, and thus occurred within 10 ns. As Figure 1.12B shows, Stern-Volmer plots of intensity quenching were sharply upward-curving, while the corresponding changes in lifetime were roughly linear and small. Repeating the emission quenching experiment with a 28 bp sequence of DNA gave similar results, except that the intensity quenching was even more dramatic. The more efficient reaction with the shorter DNA strand further

Figure 1.12

Stern-Volmer plots of $Ru(phen)_2dppz^{2+}$ luminescence quenching by $Ru(NH_3)_6^{3+}$ (A) and $Rh(phi)_2phen^{3+}$ (B). A) Quenching of luminescence intensity (●), short emission lifetime (▲), and long emission lifetime (◆) in the presence of $Ru(NH_3)_6^{3+}$. B) Quenching of luminescence intensity (●), short emission lifetime (▲), and long emission lifetime (▼) in the presence of $Ru(NH_3)_6^{3+}$. Reaction conditions are 10 μM $Ru(phen)_2dppz^{2+}$, 500 μM DNA bp in an aqueous buffer of 5 mM tris, 50 mM NaCl, pH 7.2 at ambient temperature. Adapted from reference 59.

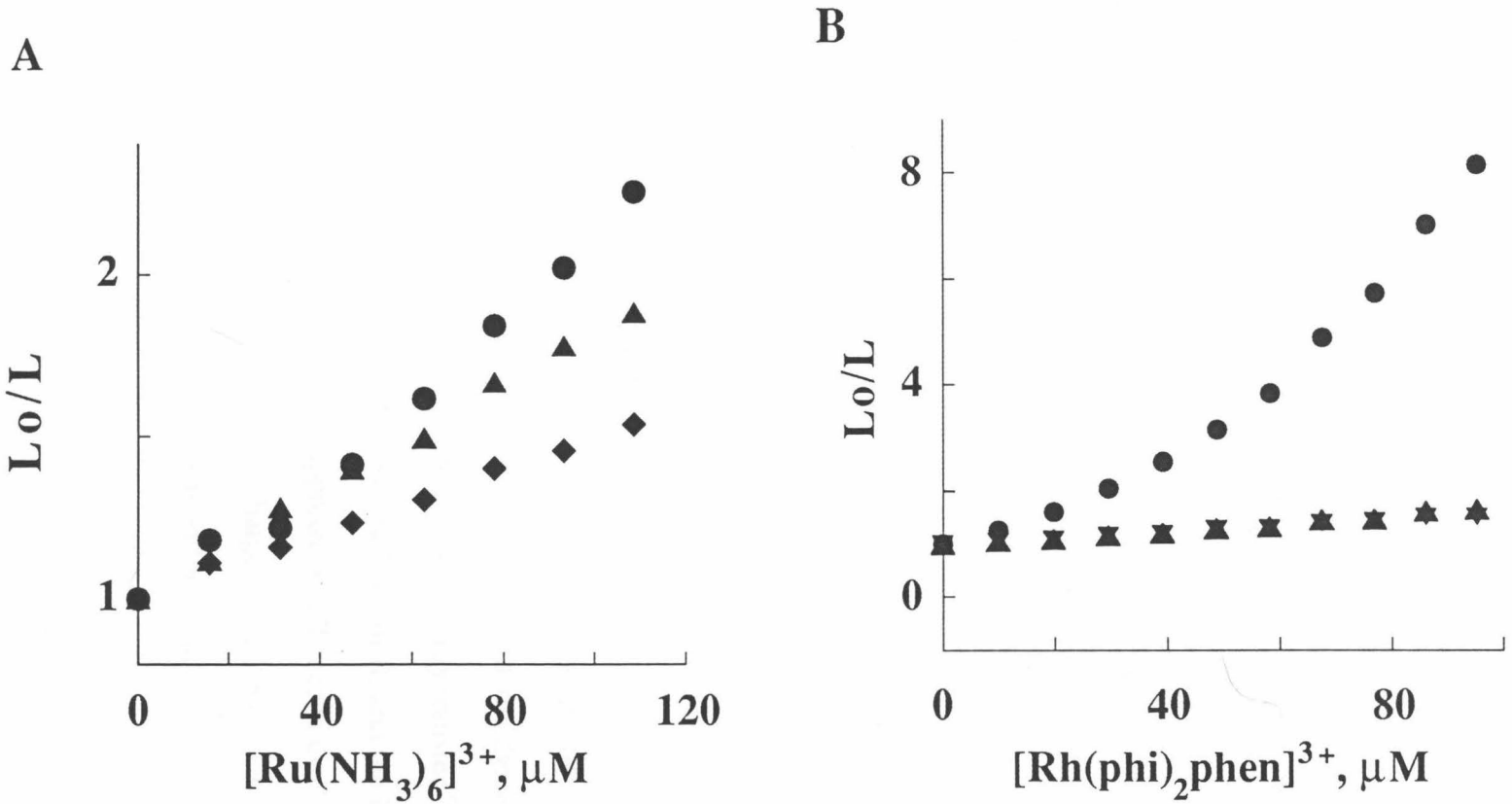
A
Lo/L
2
1
0
40
80
120
[Ru(NH3)6]3+, μM
B
Lo/L
8
4
0
0
40
80
[Rh(phi)2phen]3+, μM

indicated that quenching was not due to facilitated diffusion of complexes, since the opposite result was obtained for $M(L)_3^{n+}$ complexes weakly bound to DNA (Section 1.4.2). The large loss of intensity and small decrease in the lifetimes of $*Ru(phen)_2dppz^{2+}$ in the presence of $Rh(phi)_2phen^{3+}$ is consistent with a "static" mechanism of quenching which occurs faster than molecular diffusion.

The contrast between the reactivity of the intercalated acceptor and the diffusible $Ru(NH_3)_6^{3+}$ mirrors the results of experiments described in Section 1.4; in each case, fast and/or efficient electron transfer was only observed when both donor and acceptor were intercalated into DNA. It seems, therefore, that *intercalation provides access to the DNA π-stack.* This simple hypothesis has directed much of the work discussed in this dissertation, and these initial experiments have prompted a number of further studies. For example, we wanted to demonstrate that the mechanism of quenching was, in fact, electron transfer (Section 1.6.2; Chapter 2),[61,116] and to explore the possibility that ET reactions between intercalators could occur over long distances (Section 1.7; Chapter 2, Chapter 4).[60,61]

1.6.2 Evidence for ET mechanism of quenching

In the initial reports of quenching of DNA-bound *Ru(II) by Rh(III), the quenching mechanism was assigned as ET because of the strong thermodynamic driving force (~0.6 V) and the lack of spectral overlap necessary for energy transfer.[59] Analogous photophysical studies of covalently-linked ruthenium(II) and rhodium(III) polypyridyl complexes without DNA have also supported an ET mechanism.[117] Direct evidence for ET, however, requires detection of the charge-shifted intermediates; transient absorption spectroscopy is one popular method for monitoring the formation and/or decay of such transient ET products.

The transient difference spectra for $*Ru(phen)_2dppz^{2+}$ - $Ru(phen)_2dppz^{2+}$ and $Ru(phen)_2dppz^{3+}$ - $Ru(phen)_2dppz^{2+}$, shown in Figure 1.13, are characteristic of

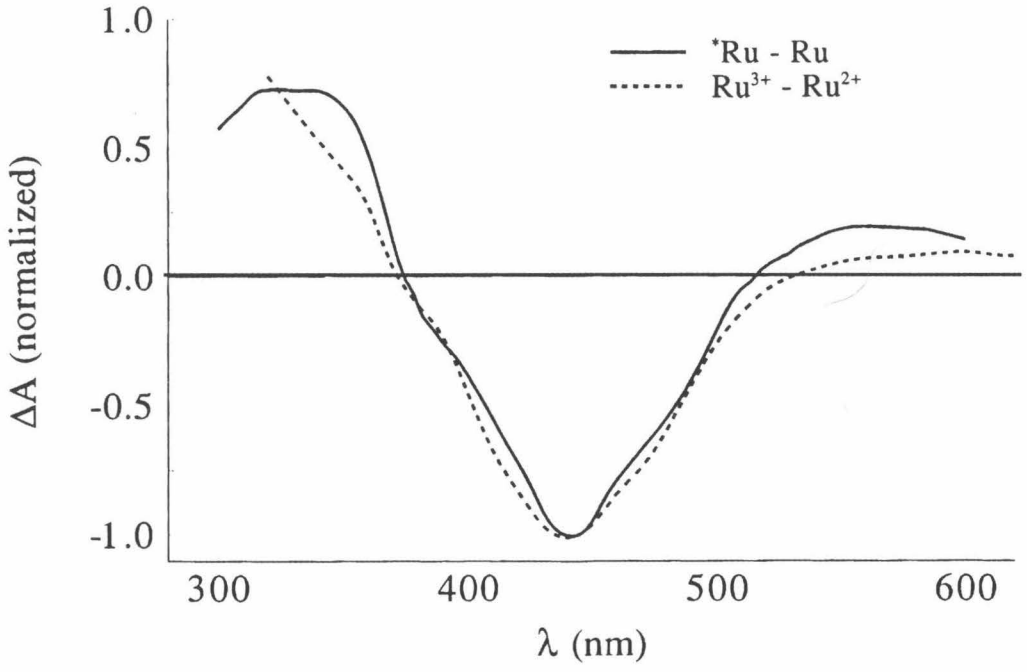

Figure 1.13

Transient absorption spectra of $Ru(phen)_2dppz$ species bound to DNA. The *Ru(II) - Ru(II) difference spectrum (solid line) was obtained by measuring the intensity of absorption (ΔA) immediately following photoexcitation (480 or 532 nm) of $Ru(phen)_2dppz^{2+}$ bound to a mixed sequence of DNA. The Ru(III) - Ru(II) difference spectrum (dashed line) was obtained by measuring ΔA at times much longer than the excited-state lifetime of *Ru(II) for intercalated $*Ru(phen)_2dppz^{2+}$ quenched by $Ru(NH_3)_6^{3+}$.[118]

polypyridyl complexes of ruthenium.[118,119] The Ru(III) - Ru(II) difference spectrum was obtained by oxidation of *Ru(II) by $Ru(NH_3)_6^{3+}$; the very small absorptivity and high cage-escape yield of this diffusible quencher has made it a very useful tool for measuring the properties of ruthenium polypyridyl complexes.[17] Both *Ru(II)-Ru(II) and Ru(III)-Ru(II) difference spectra show positive absorbance at 325 nm arising from LMCT and a negative signal at ~400 - 500 nm due to bleaching of the MLCT; additionally, the *Ru(II) - Ru(II) spectrum is small and positive after ~515 nm from the absorption of a ligand radical anion. The strong similarity between these two difference spectra does not permit detection of the formation of the Ru(III) ET product; however, the decay of this transient species can be monitored at time scales after the decay of *Ru(II).

The first direct evidence for ET between metallointercalators bound to a mixed sequence of DNA was obtained with the donor $Ru(DMP)_2dppz^{2+}$ (DMP = 4,7-dimethyl-1,10-phenanthroline) and the acceptor $Rh(phi)_2bpy^{3+}$.[116] Spectral characterization was facilitated by use of the pure Δ enantiomers of both the donor and acceptor (Chapter 2). Δ-$Ru(DMP)_2dppz^{2+}$ was found to intercalate into B-form DNA and maintained the "light switch" characteristic of the parent complex $Ru(phen)_2dppz^{2+}$. Furthermore, fast luminescence quenching was found upon addition of Δ-$Rh(phi)_2bpy^{3+}$ to Δ-$Ru(DMP)_2dppz^{2+}$ bound to DNA. Figure 1.14 shows transient absorption data obtained on the 50 μs time scale following the quenching reaction. At both 325 and 440 nm, a fast decay due to unquenched *Ru(II) was observed as well as a slow signal due to decay of Ru(III); the inset compares the spectrum of the transient formed in the presence of DNA by both $Rh(phi)_2bpy^{3+}$- and $Ru(NH_3)_6^{3+}$-induced quenching. Based on the amount of emission quenching and relative yields of $Ru(DMP)_2dppz^{3+}$ for these reactions, it was estimated that the long-lived transient formed by Rh(III) quenching accounted for < 30% of the yield of ET between the two metallointercalators. It was also assumed, based on transient and steady-state absorption spectra of $Ru(DMP)_2dppz^{3+}$, that the Rh(II) species

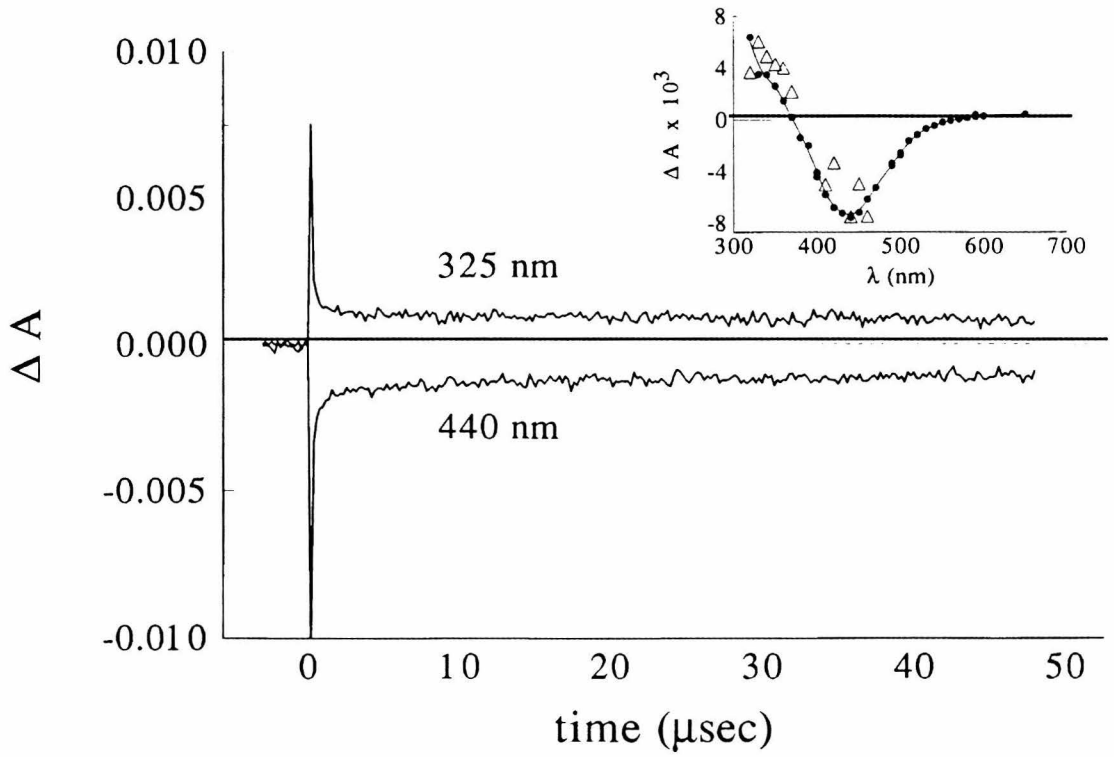

Figure 1.14

Kinetic profiles at 325 and 440 nm for transients formed upon 480 nm excitation of Δ-$Ru(DMP)_2dppz^{2+}$ (20 μM) in the presence of Δ-$Rh(phi)_2bpy^{3+}$ (118 μM) and DNA (1 mM bp) in a buffer of 5 mM tris, 50 mM NaCl (pH 8.5) at room temperature. The inset shows the Ru(III) - Ru(II) difference spectrum (●) obtained by measuring ΔA at ΔA at times much longer than the excited-state lifetime of *Ru(II) for intercalated *Δ-$Ru(DMP)_2dppz^{2+}$ (10 μM) quenched by $Ru(NH_3)_6^{3+}$ (300 μM). Also shown are the absorbance changes extrapolated to t = 0 for *Δ-$Ru(DMP)_2dppz^{2+}$ quenched by Δ-$Rh(phi)_2bpy^{3+}$ (Δ). Adapted from reference 116.

formed in the ET reaction did not contribute significantly to the transient absorption signal. The complex kinetics of the recombination reactions were attributed to i) variations in binding orientations for the donor and acceptor, ii) the large numbers of donor-acceptor separation distances, and iii) dissociation of intermediates on the millisecond time scale. It was further proposed that the rate of $Ru(DMP)_2dppz^{3+}$ decay could be limited by the low energy of donor and acceptor relative to the DNA bridge in the ground-state recombination reaction, compared to the high energy of *Ru(II) in the photoinduced forward reaction.

Subsequent transient absorption experiments provided a great deal of information concerning the kinetics of DNA-mediated ET between metallointercalators.[61,104] ET products have also been detected on long time scales following quenching of $Os(phen)_2dppz^{2+}$ by $Rh(phi)_2bpy^{3+}$,[104] but not in reactions where $Ru(phen)_2dppz^{2+}$ served as the electron donor.[59] While the precise reasons for these differences have not been determined, it is noteworthy that $Os(phen)_2dppz^{3+}$ and $Ru(DMP)_2dppz^{3+}$ have been shown to be more stable in aerated aqueous solutions.[104,118] Thus, it is possible that alternative pathways for reduction of $Ru(phen)_2dppz^{3+}$ exist. Moreover, Chapter 2 describes results from transient absorption spectroscopic measurements on the picosecond time scale in which a series of Ru(II) donors and DNA sequences were studied.[61]

1.7 ET reactions between metallointercalators bound covalently to DNA

To begin investigating the distance- and sequence-dependence of DNA-mediated ET, an assembly was prepared in which the donor and acceptor metallointercalators were tethered to the ends of a 15 bp DNA duplex (Figure 1.15).[60] A number of synthetic schemes have been developed to tether small molecules to DNA, including modification of the DNA bases, the sugars and phosphates within the backbone, and the 5' and 3' backbone termini.[120-122] For our ET studies,[60] metal complexes were tethered to the 5'

Figure 1.15

Structure of metallointercalators tethered to complementary 15 bp oligonucleotides. Peptide coupling methods were used to attach both $Ru(phen')_2dppz^{2+}$ (phen' = 5-amidoglutaric acid-1,10-phenanthroline) and $Rh(phi)_2(phen')^{3+}$ to a purified oligonucleotide containing a free amino group at the 5' terminus (Applied Biosystems). Hybridization of the strands by slow cooling provided the doubly metallated duplex shown.[60]

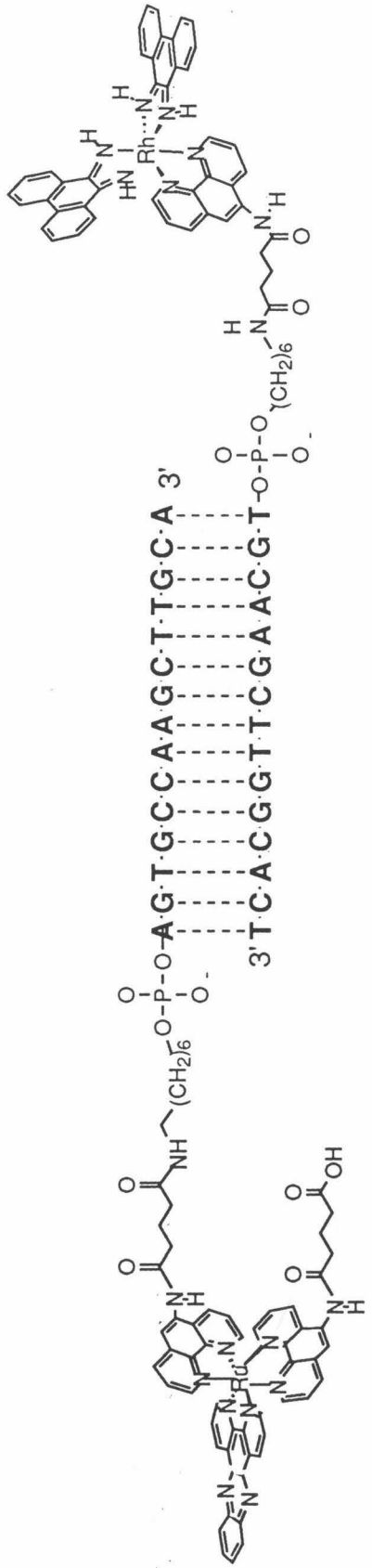

terminus of complementary oligonucleotides through a flexible linker; this design allowed the formation of a well-defined electron transfer assembly in which donor and acceptor were able to intercalate into the duplex at distinct positions with a discrete distance of separation. Covalent attachment of each metal complex to complementary oligonucleotides permitted two companion experiments, represented in Figure 1.16, which were used to characterize intercalation and intramolecular ET. The luminescence properties of the ruthenated oligonucleotide hybridized to its unmodified complement (Ru-DNA) provided a means to characterize the intercalated donor. Similarly, photocleavage reactions on the rhodium-modified oligonucleotide hybridized to its unmodified complement (Rh-DNA) was used to measure the position of the tethered intercalator in the DNA duplex.

1.7.1 Luminescence of $Ru(phen')_2dppz^{2+}$ tethered to DNA

When the ruthenium-modified oligomer was annealed to its unmetalated complement, intense luminescence due to Ru(II) intercalation was observed.[60,123] By contrast, the ruthenium-modified oligonucleotide displayed little luminescence as the single strand or in the presence of non-complementary single-stranded DNA. These results were consistent with previous studies in which luminescence was observed in aqueous solution only when the dppz ligand was intercalated into a B-DNA duplex (Section 1.5.1).[86] Table 1.5 indicates that the luminescent lifetimes and the relative luminescent intensities for the covalently bound duplex and its noncovalently intercalated Ru(II) analog were similar.[60] As with $Ru(phen)_2dppz^{2+}$, a biexponential decay in emission was observed for Ru-DNA; additionally, a small shift in the wavelength of emission compared to the noncovalent complex was found. The longer lifetimes and blue shift likely reflected the sensitivity in emission to the particular stacking of the two complexes in their intercalation sites (Table 1.4).[61,86,96]

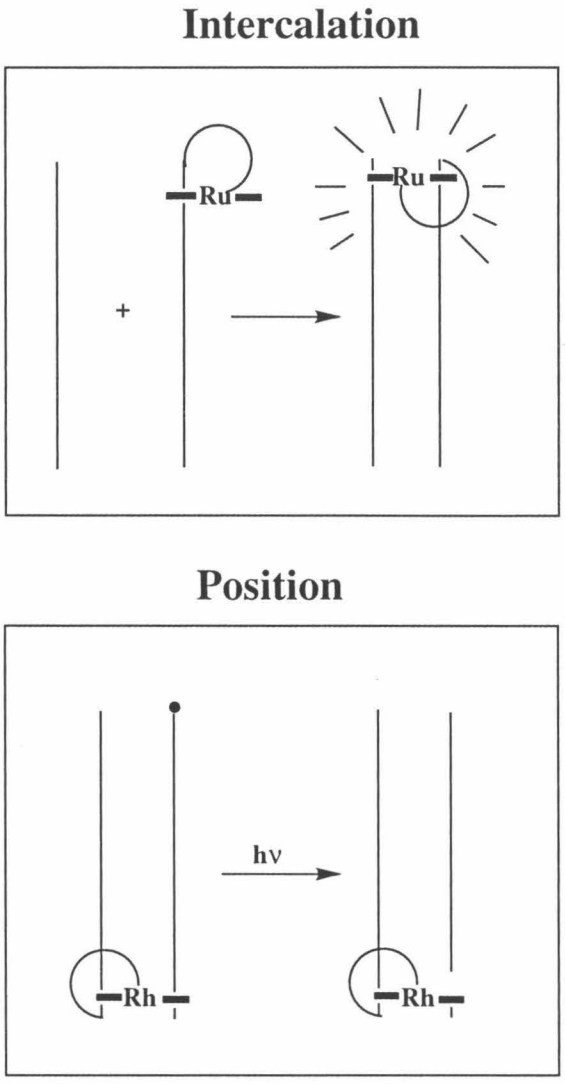

Figure 1.16

Schematic drawing of intramolecular, covalently bound intercalators on an oligonucleotide. The luminescent properties of the ruthenium-modified duplex provide information about the mode of intercalation; photocleavage of the oligonucleotide by covalently bound rhodium provides a determination of the position(s) of intercalation.

Table 1.5. Excited state lifetimes and integrated intensities for Ru(II)-DNA and its non-covalent analog.[a]

Sample	τ (ns)[b,c]	%[d]	λ_{max} (nm)	Φ[b,e,f]
Ru———	500	60	598	0.0071
	110	40		
Ru + ———	420	35	610	0.0063
	90	65		

[a]All steady-state and time-resolved measurements conducted at 20 °C. Adapted from reference 60. [b]Error estimated to be ± 10% for both steady-state and time-resolved measurements. [c]Samples used in time-resolved measurements contained either 5 μM of the covalently bound duplex or 5 μM $[Ru(phen)_2(dppz)]^{2+}$ and 5 μM of the analogous 15-mer duplex. [d]Lifetime ratios calculated from the magnitudes of the pre-exponential factors produced by the program used in the deconvolution of the time-resolved data. [e]Quantum yields, Φ, were determined relative to $[Ru(bpy)_3]^{2+}$ (Φ = 0.042). [f]Samples used in steady-state measurements contained either 4 μM of the covalently bound duplex or 4 μM $[Ru(phen)_2(dppz)]^{2+}$ and 4 μM of the analogous 15-mer duplex.

Three experiments were designed to address whether intercalation of tethered Ru(II) was inter- or intramolecular.[123] Emission from Ru-DNA was linear with concentration, suggesting that intercalation was intramolecular at concentrations ≤ 5 μM duplex. Also, addition of unmodified duplex to ruthenated duplex resulted in ≤ 5% change in the luminescence, indicating no change in binding as the number of DNA sites increased. Finally, steady-state luminescence measurements compared the binding of tethered Ru(II) in Ru-DNA duplexes containing mismatches in various positions in the sequence. Luminescence was found to be higher for mismatches near the ruthenated end of the oligomer, where the ruthenium complex could intercalate intramolecularly and stabilize the mismatched site.

Luminescence titrations further demonstrated that the ruthenated duplex behaved as a 15 mer bearing one intercalator.[60] As free $Ru(phen)_2dppz^{2+}$ was added to a solution of unmetallated 15 mer duplex, steady-state luminescence increased linearly until reaching saturation at ~3 equiv of Ru(II) per duplex, consistent with competitive binding of $Ru(phen)_2dppz^{2+}$ to the 15 mer duplex and an average binding site size of ~4 bp. When the analogous experiment was conducted with Ru-DNA, saturation of luminescence occurred after the addition of ~2 equiv Ru(II). Thus, covalently bound ruthenium(II) complex was not displaced by additional intercalators.

1.7.2 Binding of $Rh(phi)_2(phen')^{3+}$ tethered to DNA

Hybridization of the Rh(III)-modified oligonucleotide with its unmodified complement permitted the position of intercalation on the helix to be determined, since photoactivation of phi complexes of rhodium promotes strand cleavage at the site of intercalation (Section 1.5.2).[88] The complementary strand was radioactively labeled at its 5'-end, annealed to the rhodium-modified strand and irradiated at 313 nm.[60] Separation of the resultant products by gel electrophoresis indicated that covalently bound Rh(III) damaged the duplex with high specificity at sites 2 and 3 from the 3' terminus of the ^{32}P-

labeled strand (Figure 1.17A). DNA cleavage by untethered $Rh(phi)_2phen^{3+}$, by contrast, yielded reaction at all positions on the oligomer. Thus, tethered Rh(III) bound with similar probability one or two base-pairs in from the 5' end of the modified strand. The specificity of the Rh(III) cleavage also argued that intercalation of the covalently attached complex was largely intramolecular. Assuming that the tethered Ru(II) donor was also bound at the two closest base steps to the end, the separation between Ru(II) and Rh(III) in the doubly metallated oligonucleotide duplex was taken to be ≥ 41 Å (Figure 1.17B). Figure 1.18 schematically illustrates the tethered DNA assembly.

1.7.3 Quenching of *Ru(II) by Rh(III) in covalent DNA assembly

Figure 1.19 shows the steady-state emission spectra from the ruthenated oligonucleotide hybridized to unmetallated complement and also to Rh(III)-tethered complement.[60] The complete quenching of luminescence was observed in the donor-DNA-acceptor assembly. TCSPC measurements did not detect emission from the doubly metallated oligonucleotide and the quenching rate was thus found to be $< 10^9$ s^{-1}. Several control experiments supported the hypothesis that quenching occurred intramolecularly between intercalated metal complexes (Table 1.6). For example, the addition of the doubly modified duplex to the ruthenium-modified duplex did not quench the luminescence from the ruthenium-modified duplex, demonstrating the absence of adventitious quenchers in the rhodium(III) sample. Addition of an equimolar amount of rhodium-modified duplex to ruthenium-modified duplex also did not promote significant quenching of the ruthenium duplex, consistent with the quenching being substantially intramolecular at these concentrations. Finally, the addition of a stoichiometric amount of $Rh(phi)_2phen^{3+}$ to the ruthenium-modified duplex caused substantial but not complete quenching of the ruthenium emission. This result was consistent with the independent binding of tethered Ru(II) and $Ru(phen)_2dppz^{2+}$ noted in Section 1.7.1. Since Ru-DNA was found to hold two additional intercalators, some duplexes contained two Rh(III)

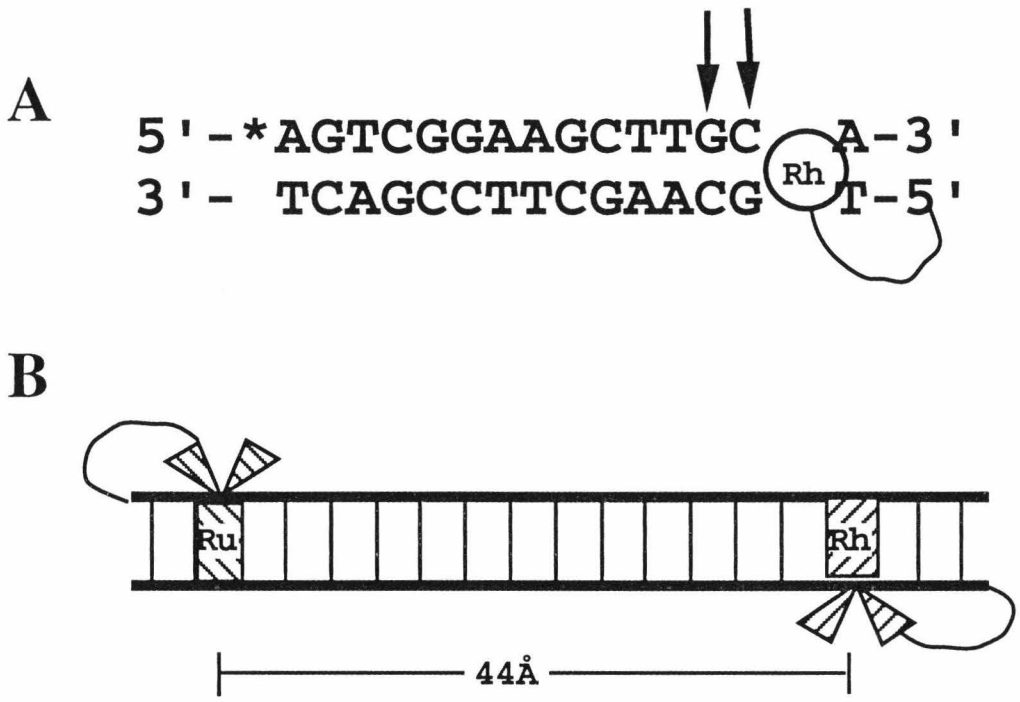

Figure 1.17

Schematic illustrations of covalently modified DNAs. A) Sequence of a 15mer oligonucleotide bearing covalently bound rhodium(III) complex, hybridized to its ^{32}P labeled complement. Arrows point to the sites of photocleavage by the metal complex, establishing that it is intercalated either adjacent to the first (as shown) or second base steps from the covalent linkage. B) Schematic of the doubly-modified duplex, showing a separation distance of the donor and acceptor. Assuming that both the rhodium and the ruthenium complex can intercalate one or two base pairs from their linkage with equal probability, 25% of the donor/acceptor pairs are separated by 41 Å, 50% by 44 Å, and 25% by 48 Å. Adapted from reference 60.

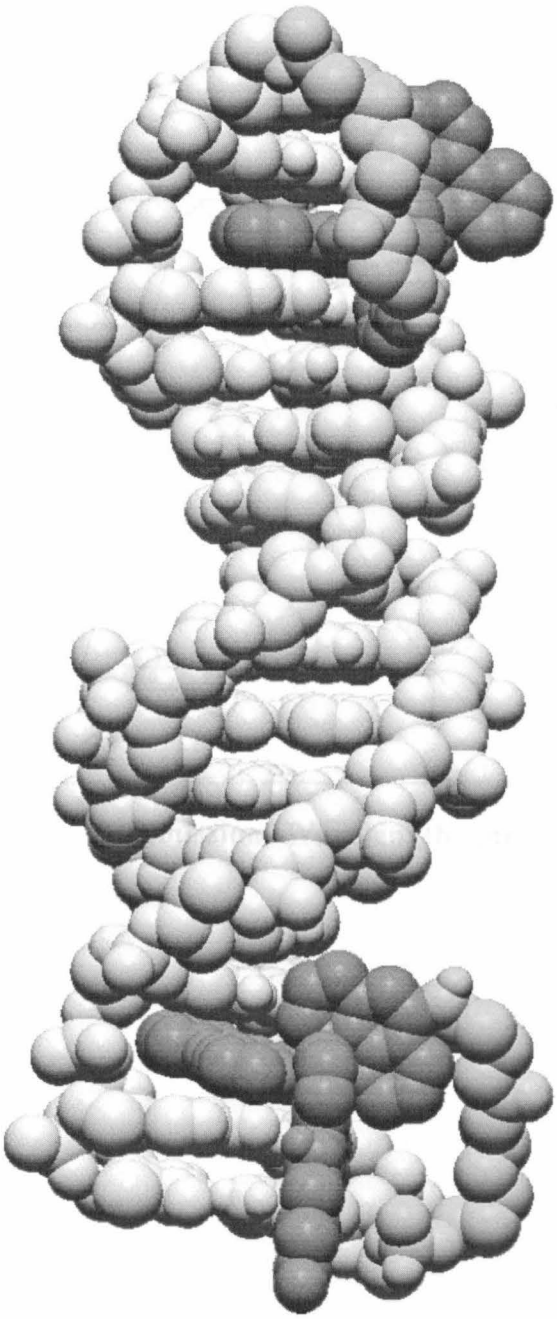

Figure 1.18

Computer graphics illustration of the doubly-modified oligonucleotide bearing the complexes $Ru(phen')_2dppz^{2+}$ and $Rh(phi)_2(phen')^{3+}$. In the graphics representation the tethered intercalators are bound two base pairs from either end of the 15-mer duplex for a separation distance between intercalated ligands of 41 Å. Adapted from reference 60.

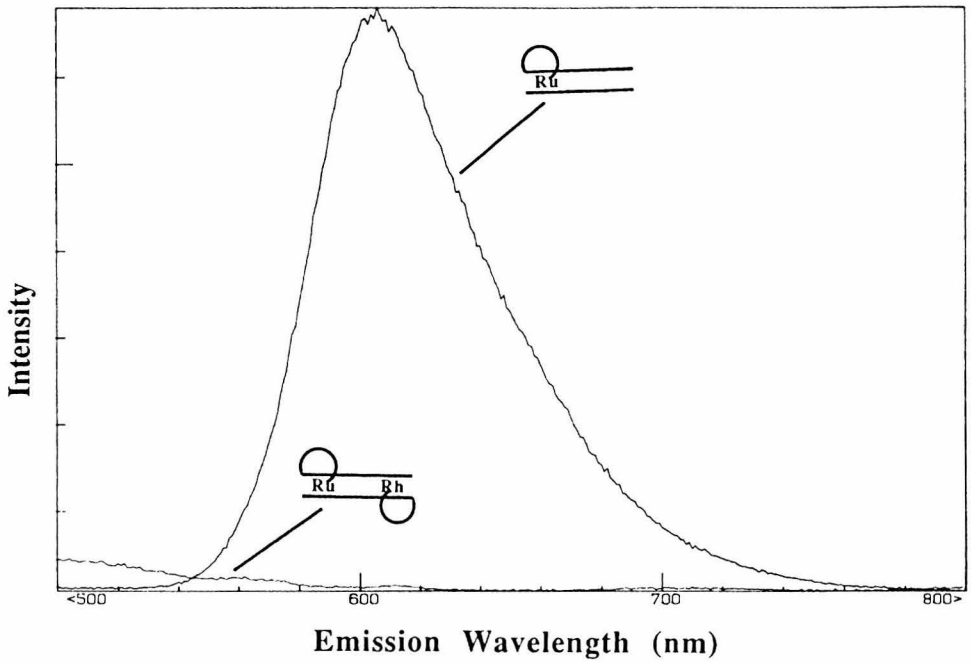

Figure 1.19

Emission spectrum of 5 μM Ru(dppz)(phen')$_2$-$(CH_2)_6$-5'-TGCAAGC-TTGGCACT-3' annealed to its unmodified complement (top) or Rh(III)-modified complement. The intense emission observed with Ru-DNA was quenched in the Ru-DNA-Rh sample. Adapted from reference 60.

Table 1.6. Luminescent Intensities of Covalent Metal-DNA Intercalation Complexes.[a]

Sample[b]	Relative Luminescence Intensity[c]
Ru═══	1.00
Ru═══Rh	0.00
1/2 Ru═══ + 1/2 Ru═══Rh	0.57
1/2 Ru═══ + 1/2 ═══Rh	0.43
Ru═══ + Ru(II)	2.78
Ru═══ + Rh(III)	0.08

[a] Adapted from reference 3. [b] Ru═══ refers to 5'-[Ru(phen')$_2$(dppz)]-AGTGCCAAGCTTGCA-3' annealed to its complement; Ru═══Rh refers to 5'-[Ru(phen')$_2$(dppz)]-AGTGCCAAGCTTGCA-3' annealed to 5'-[Rh(phi)$_2$(phen')]-TGCAAGCTTGGCACT-3'; Ru(II) and Rh(III) refer to $[Ru(phen')_2(dppz)]^{2+}$ and $[Rh(phi)_2(phen')]^{3+}$, respectively. Conditions are 5 μM DNA duplex, 5 mM tris, 50 mM NaCl, pH 7.2. [c] All spectra were taken on an SLM Aminco 8000 spectrofluorimeter. Intensities were integrated from 500 nm to 800 nm and are normalized to the luminescence intensity of Ru═══ . The uncertainty of integrated intensities is ± 10%.

complexes, leaving 8% of the ruthenium-modified duplexes unoccupied and therefore unquenched. Thus, complete quenching was observed only when the acceptor is covalently bound to the same duplex as the donor.

Figure 1.20 contrasts this tethered assembly to one bearing the weak intercalators $Ru(phen)_2(phen')^{2+}$ and $Rh(phen)_2(phen')^{3+}$ (phen' = 5-amidoglutaric acid-1,10-phenanthroline).[60] The luminescence characteristics of $Ru(phen)_2(phen')$-DNA clearly indicated that, in contrast to $Ru(phen')_2(dppz)$-DNA, this tethered complex did not intercalate; neither emission enhancement nor increase in emission lifetime was found, and emission was rapidly quenched by the anionic quencher $Fe(CN)_6^{4-}$.[86] Importantly, when the $Ru(phen)_2(phen')$-modified oligonucleotide was hybridized to $Rh(phen)_2(phen')$-modified complement, no luminescence quenching was observed.[60] While the driving force for this reaction is ~500 mV smaller than for ET reactions between $Ru(phen)_2dppz^{2+}$ and $Rh(phi)_2phen^{3+}$, ET has been demonstrated for the $M(phen)_3^{n+}$ couple in the presence of DNA (Section 1.4.2). Taking these results with those for the avid intercalators, it was thus concluded that intercalation was required for rapid electron transfer to occur.

The results for covalently-bound analogs of $Ru(phen')_2dppz^{2+}$ and $Rh(phi)_2(phen')^{3+}$ intercalated into a 15 mer oligonucleotide therefore demonstrated that photoinduced electron transfer between intercalators could occur rapidly over > 40 Å through a DNA helix over a pathway consisting of π-stacked base pairs. These experiments also provided an experimental framework to address a number of fundamental questions concerning DNA-mediated ET. What are the rates of these long-range reactions and how far can ET reactions occur? How does the DNA sequence in the binding site and in the intervening bridge modulate ET quenching? Before these issues could be tackled, however, the technology for preparing and analyzing metal-DNA assemblies required development. Towards this end, Chapter 4 describes our recent

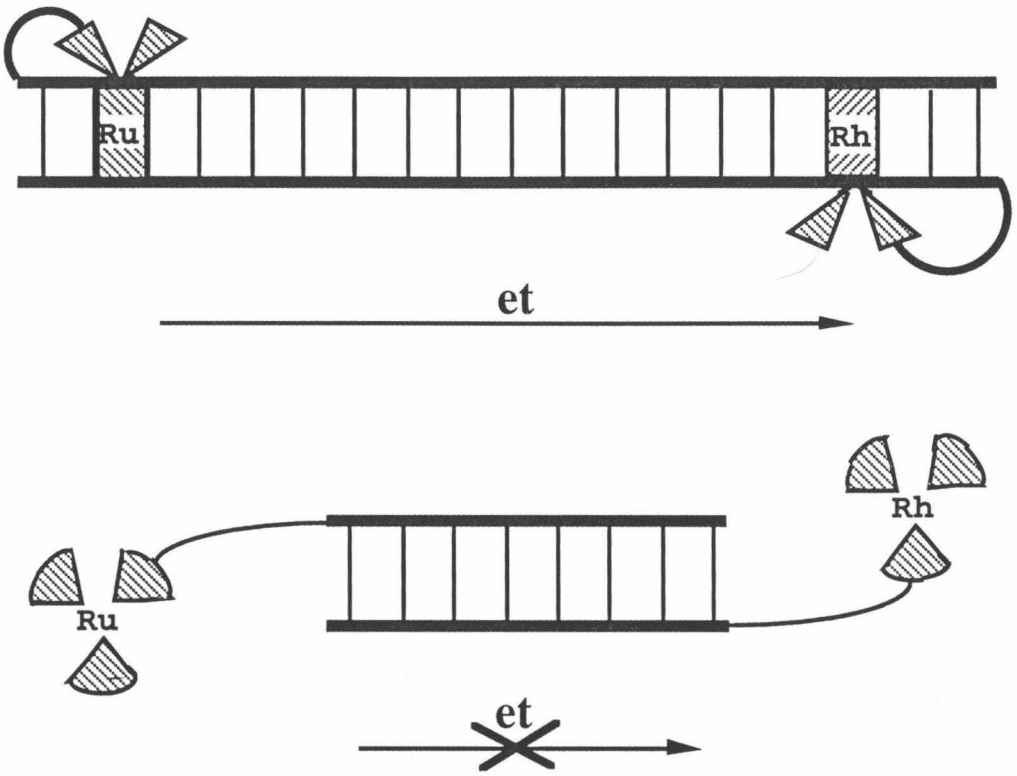

Figure 1.20

Schematic illustrations comparing electron transfer reactions in tethered systems. Fast ET quenching was observed when donor and acceptor were intercalated (top). In contrast, no quenching was seen for nonintercalated donors and acceptors (bottom).

advances in the synthesis and characterization of metallointercalators, linkers, and DNA-mediated ET assemblies.

1.7.4 DNA-mediated ET between tethered, unintercalated metal complexes

One other report has described the design and synthesis of an oligonucleotide duplex modified with a tethered donor and acceptor (Figure 1.21).[58] Meade and Kayyem sought to prepare a system in which the reactants bound covalently to DNA without perturbing the DNA structure, and thus attached two ruthenium coordination compounds to 2'-amino ribose rings placed at the 5'-termini of complementary 8 bp oligonucleotides. The complexes $Ru(bpy)_2(im)(X)^{2+}$ and $Ru(NH_3)_4(py)(X)^{3+}$ (im = imidazole, py = pyridine, X = aminoribose DNA) were closely related to reactants used in flash-quench studies with ruthenium-modified proteins and in pulse radiolysis experiments with polyproline oligomers (Section 1.2.1).[17,22]

The kinetics of the following ground-state ET reaction were monitored by transient absorption spectroscopy using both photoinduced ET and flash-quench techniques:[58]

$$Ru(bpy)_2(im)(X)^{3+} + Ru(NH_3)_4(py)(X)^{2+} \longrightarrow Ru(bpy)_2(im)(X)^{2+} + Ru(NH_3)_4(py)(X)^{3+}$$

The kinetics contained a slow decay ($1.6 \times 10^6\ s^{-1}$) which was assigned as the rate of ET through the 8 bp duplex. Because the oligonucleotide was rather short, experiments were done in 1 M salt to increase duplex stability; it would be interesting to see if this high salt concentration affected the ET rates (Section 1.3.2). While the authors noted that several sequences must be studied to deduce ß values for the DNA π-stack, they also noted that the rate obtained for the 8 bp system, with through-space separation of 21Å (~35Å through-bond distance), was similar to that measured for ET in cytochrome c (20Å through-space; ~30 Å through-bond) (Section 1.2.1).[17] This tethered system is complementary to the well-intercalated donors and acceptors discussed above. For Ru(II)

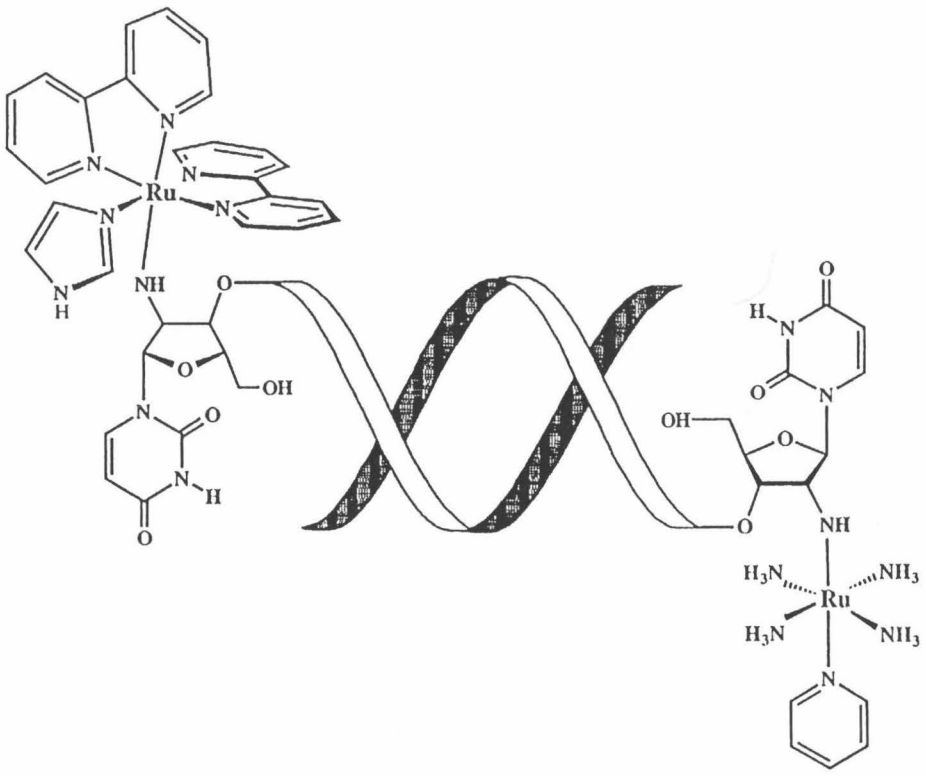

Figure 1.21

Schematic drawing of ruthenium donors and acceptors covalently bound to DNA. $Ru(bpy)_2(im)^{2+}$ and $Ru(NH_3)_4(py)^{3+}$ were complexed to complementary 8 bp oligonucleotides modified to contain a 2'-amino group on the 5' terminal ribose rings. The rate of ground-state electron transfer for this system was $1.6 \times 10^6\ s^{-1}$. Adapted from reference 58.

and Rh(III) intercalators, the electronic environment might be better described as hydrophobic and aromatic, and ET reactants are coupled to the DNA through noncovalent π-stacking interactions;[60] in contrast, the complexes used here are highly solvated Ru(II/III) complexes with large reoganization energies and are connected to the DNA only through covalent σ-bonded pathways.[58]

1.8 Oxidation reactions between DNA and intercalators

In addition to experiments described above, in which DNA serves as a molecular bridge connecting donor and acceptor, other studies have used intercalators as acceptors to remove an electron from the DNA itself. Small molecules have been developed which cause oxidative damage to G bases[124-128] and also effect repair of thymine dimers in DNA.[129,130] Since these two lesions are the most common forms of damage caused by ionizing radiation (Section 1.3.1),[3] such ET reactions complement radiation biology studies. Moreover, since these experiments utilize an intercalator to access the DNA bases, experiments are related to DNA-mediated ET reactions in which DNA serves as the bridge.[6] Perhaps most interesting from a chemistry perspective, ET reactions using the DNA bases as electron donors and acceptors lead to permanent chemical transformations. These experiments thus include additional reaction mechanisms as well as DNA-mediated charge separation.

An early study of DNA damage used a photochemical cosensitization strategy to cause strand breakage at guanine residues.[124] Through gel electrophoresis measurements, Dunn *et al.* found that the yield of strand breakage caused by intercalated ethidium was 10-fold higher in the presence of methyl viologen. The reaction mechanism for cleavage was closely related to the flash-quench strategy used to study protein-mediated ET;[17] photoexcited ethidium was quenched by ET to methyl viologen, leaving a stongly oxidizing ethidium$^{\bullet+}$.[124] A guanine base then donated an electron to ethidium and to form a G$^{\bullet}$ which could rearrange to cause direct strand scission with a

quantum yield (Φ) of 6 x 10^7 or react with an oxygen donor (H_2O, O_2) to form a modified base ($\Phi \sim 10^{-6}$). Thus, formation of an oxidant bound to DNA led to oxidative damage similar to that seen following treatment with ionizing radiation.

Other reports of G oxidation have initiated damage with a photoexcited electron acceptor. Intercalators (Figure 1.22) such as riboflavin, napthalamide, anthraquinone [2AQA(HEt_2)], and $Rh(phi)_2bpy^{3+}$ have been shown to cause base damage selectively at the 5'-G of 5'-GG-3' sequences.[125-128] In each case, damage was identified as 8-oxo-G and the site of damage determined by piperidine-mediated strand scission at the oxidized base. In the case of 2AQA(HEt_2), transient absorption spectroscopy indicated that reduced anthraquinone was generated within 20 ps of excitation.[126] The 5'-G selectivity was ascribed to charge migration through DNA, which slowed the recombination rate and allowed the radical to hop to a site of low energy before being trapped by water or molecular oxygen. In the presence of O_2, which reacted with 2AQA(HEt_2)$^{\bullet-}$ to form 2AQA(HEt_2) and superoxide, the quantum yield of G damage was ~ 1%, indicating an efficient reaction. It is noteworthy that the formation and decay of G$^{\bullet}$ could not be detected, presumably due to the intense color of the organic acceptor.

Recent theoretical work by Saito and coworkers has provided a rationale for the 5'-GG-3' selectivity.[127] *Ab initio* calculations indicated that 5'-GG'-3' and 5'-GGG-3' have the lowest ionization potentials of all DNA sequences; furthermore, computations showed that the molecular orbitals on adjacent guanine π-systems interact. Electron density maps of the highest occupied molecular orbital (HOMO) of a 5'-GG'-3' dinucleotide is strongly dependent on the relative orientations of the stacked bases; in B-form DNA, ~95% of the electron density was found to be centered on the 5'-G. Not only did these calculations accurately model experimental results, but they also suggested that electronic overlap between stacked bases is important in determining the reactivity of the DNA polymer.

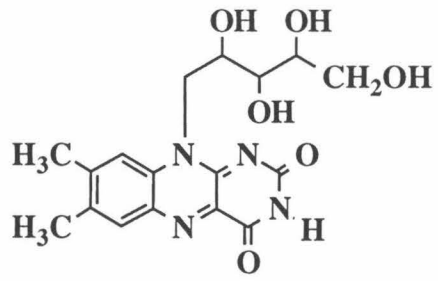

Riboflavin

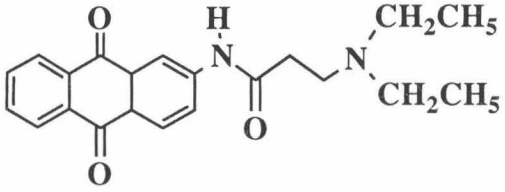

2AQA2(HEt_2)

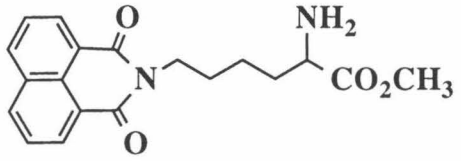

Napthalimide

Figure 1.22
Structures of organic photooxidants of DNA.

Hall *et al.* obtained the first definitive evidence that photoinduced G oxidation could occur over long distances through DNA.[128] These authors synthesized a tethered oligonucleotide duplex (Figure 1.23) analogous to the ET assembly described in Section 1.7. The photooxidant $Rh(phi)_2(bpy')^{3+}$ (bpy' = 4-butyric acid-4'-methyl-2,2'-bipyridine) (E_{ox} ~ 2 V) was found to promote the formation of piperidine-labile damage to 5'-G of 5'-GG-3' sequences over 37Å. The intercalation site of Rh(III) was determined by photocleavage at 313 nm, and this direct strand scission reaction contrasted to 5'-GG-3' damage caused by irradiation into the phi π-π^* transition at 365 nm ($\Phi \sim 10^{-8}$). Importantly, damage was caused with similar efficiency at 5'-GG-3' sequences placed 17Å and 34Å from *Rh(III) and with increased yield at a 5'-GGG-3' site placed 37Å from the photooxidant. The yield of damage was lowered by disruption of the base stack by a bulge in the DNA duplex.[128b] Thus, G oxidation reactions were reported to be sensitive to the oxidiation potential of G residues and to the coupling of the DNA π-stack, but not senstive to the distance between the G donor and *Rh(III) acceptor.

Not only can small molecules damage DNA, they can also photosensitize repair of thymine dimer lesions (Section 1.3.1). Using model compounds, researchers have shown that splitting of cyclobutane dimers can occur through either an oxidative or a reductive mechanism.[131] The enzyme photolyase has been shown to cause cycloreversion of pyrimidine dimers by adding an electron to the cyclobutane ring; the ring then splits and the electron is donated back to the enzyme.[19] The first reports of cycloreversion by a small molecule bound to DNA also invoked a reductive mechanism.[129] Hélène and coworkers found that indoles such as tryptophan could bind DNA and photosensitize dimer splitting, presumably through formation of a charge-transfer complex between the indole and dimer. Dandliker *et al.* demonstrated that dimers could be repaired over long-range by an oxidative mechanism.[130] These researchers prepared an assembly containing $Rh(phi)_2(bpy')^{3+}$ as a photooxidant separated by 16-26 Å from the dimer. Importantly, complete repair of the dimer was found after 30 min irradiation at 400 nm when a

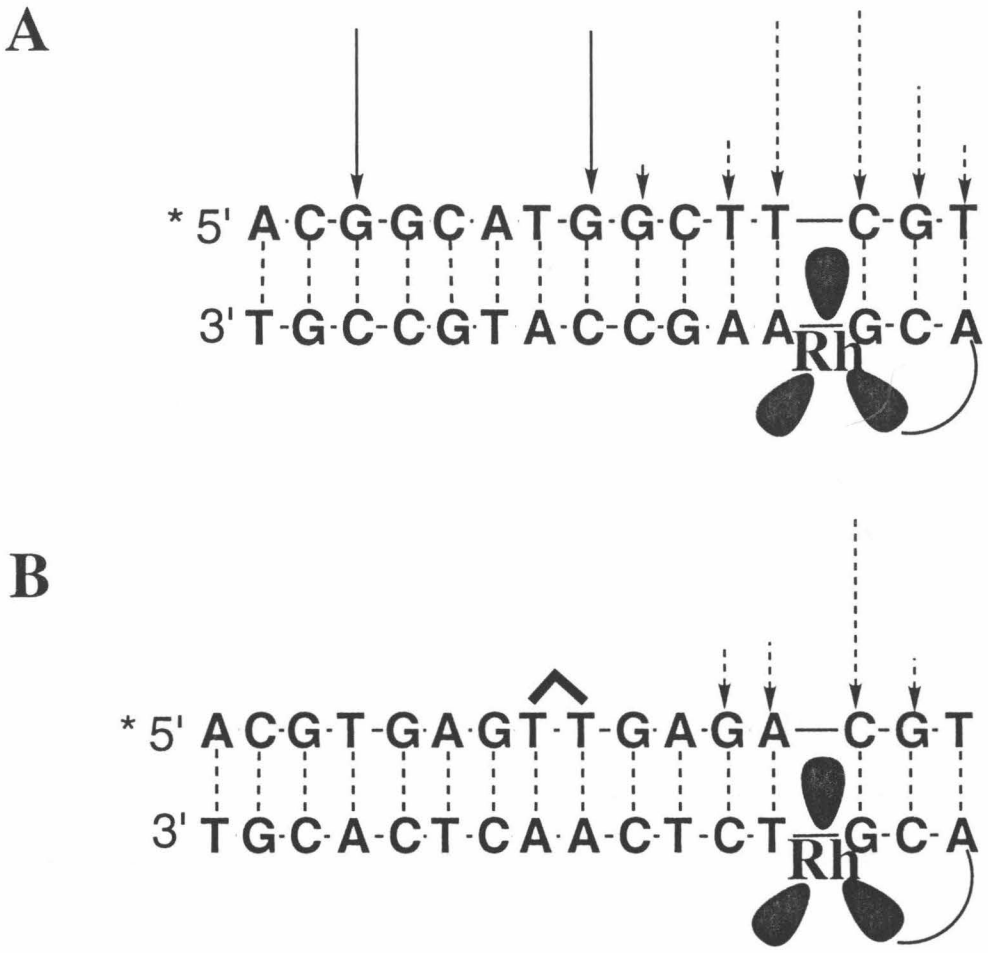

Figure 1.23

Rh-DNA assemblies used in studies of photooxidation reactions. A) $Rh(phi)_2(bpy')^{3+}$ tethered to a 15 bp oligonucleotide duplex containing two 5'-GG-3' sequences. The position of Rh(III) intercalation was determined by the sites of direct photocleavage caused by irradiation at 313 nm (dashed arrows). Long-range G oxidation was indicated by positions of piperidine-labile damage caused by irradiation at 365 nm (solid arrows).[128] B) $Rh(phi)_2(bpy')^{3+}$ tethered to a 16 bp oligonucleotide duplex containing a single thymine dimer (^). The position of Rh(III) intercalation was determined by the sites of direct photocleavage caused by irradiation at 313 nm (dashed arrows). Long-range repair of the thymine dimer was identified by gel electrophoresis and liquid chromatography measurements following irradiation at 400 nm.[130]

stoichiometric amount of $Rh(phi)_2(4,4'\text{-dimethylbpy})^{3+}$ complex was noncovalently bound to the oligonucleotide duplex. Furthermore, the reaction was catalytic, as full repair could be obtained when 0.03 equiv Rh(III) were present. As with oxidation of 5'-GG-3' sequences by *Rh(III), thymine dimer repair did not become less efficient with distance but was affected by disruption of the DNA π-stack.

The fact that metallointercalators can cause long-range damage of guanines and repair of thymine dimers demonstrates that DNA can mediate chemistry at a distance. In Chapter 5, we discuss another approach to monitoring long-range G oxidation through DNA. We have used a flash-quench strategy to monitor both the initial electron transfer reactions between a Ru(III) intercalator and DNA and the subsequent damage caused to guanine bases.[132] Such experiments are complementary to studies using the DNA as a bridge for photoinduced ET,[58,60] since they probe different DNA-mediated reactions. For instance, the mechanism of DNA oxidation has often been described by a hopping mechanism in which localized positive charges migrate through the helix.[126] By contrast, bridge-mediated ET monitors the transport of negative charges, and is often described by a tunneling mechanism in which DNA bridge states are high in energy relative to the mobile electron.[16,133] One long-term goal of our investigations into DNA mediated charge transfer reactions is to determine whether one mechanism can account for the various phenomena described throughout this introduction.

1.9 Perspectives

Several interesting issues have been raised by the results of ET theory and experiment. While conclusions vary from study to study, much work indicates that ET through DNA can occur rapidly and over long distances. Perhaps conclusions differ because factors critical to DNA-mediated ET have not been considered. We have sought to address some of these factors by measuring the properties of ET reactions between metallointercalators bound to DNA. Chapters 2 and 3 focus on intercalators

noncovalently associated with the double helix; using these systems, we have explored the kinetics of DNA-mediated ET and the importance of metal-DNA interactions and DNA sequence (Chapter 2). Additionally, we have compared ET reactions between donors and acceptors bound to DNA and to anionic micelles (Chapter 3). By tethering related metallointercalators to defined DNA sequences, we will be able to determine the distance-dependence of ET through DNA; in Chapter 4, we discuss recent advances in the synthesis, characterization, and quenching properties of tethered Ru-DNA-Rh assemblies. Finally, we have used these covalent assemblies to develop a flash-quench method to generate oxidizing intercalators at defined locations on DNA (Chapter 5).

Several conclusions can be drawn from the many studies of DNA-mediated electron transfer. One interesting feature seen in radiation biology, ET theory, and photophysical experiments is the strong dependence on the DNA sequence and structure in modulating ET reactions. In each study comparing DNA sequences, polymers containing AT sequences were superior mediators of ET to those containing GC.[16,61,69] Additionally, charge migration has been found to be more facile in well-stacked, double stranded DNA than in the flexible, single-stranded polymer.[3,38,128] The long-range migration of charge through DNA has also been demonstrated in several experimental studies,[3,58,61,62,128,130,132] and both hopping models and semiconductor models have been used to characterize experimental results.[48,50] Finally, close stacking of the π-systems is found to be critical for observing long-range reactions.[9,23,24] The base pairs themselves must be well-structured, as evidenced by thermodynamic and structural studies.[38,62,128,130] Furthermore, the electron donor and acceptor must also be well-coupled into the DNA π-stack, as demonstrated by binding studies[60] and by comparison of reactions in DNA and in micelles.[64] Clearly, ET reactions mediated by the π-stack differ from other systems in several important respects.

1.10 References

1. Moser, C. C.; Keske, J. M.; Warncke, K.; Farid, R. S.; Dutton, P. L. *Nature* **1992**, *355*, 796.
2. a) Pfeiffer, P.; Gottlich, B.; Reichenberger, S.; Feldmann, E.; Daza, P.; Ward, J. F.; Milligan, J. R.; Mullenders, L. H. F.; Natarajan, A. T. *Mut. Res. Rev. Genet. Tox.* **1996**, *366*, 69. b) Ward, J. F. *Radiation Res.* **1995**, *142*, 362. c) Hatahet, Z.; Purmal, A. A.; Wallace, S. S. *Ann. New York. Acad. Sci.* **1994**, *726*, 346. d) Von Sonntag, C.; Schuchmann, H. P. *Meth. Enzym.* **1990**, *186*, 511.
3. O'Neill, P.; Fielden, E. M. *Adv. Rad. Biol.* **1993**, *17*, 53, and references therein.
4. Arkin, M. R.; Jenkins, Y.; Turro, N. J.; Barton, J. K. *Adv. Chem. Ser.* **1995**, *246*,449.
5. Stemp, E. D. A.; Barton, J. K. *Metal Ions Biol. Syst.* **1996**, *33*, 325.
6. Holmlin, R. E. H.; Dandliker, P. D.; Barton, J. K. *Angew. Chem. Int. Ed. Engl.* in press **1997**.
7. a) Kalyanasundaram, K.; Nazeeruddin, Md. K. *Inorg. Chim. Acta.* **1994**, *226*, 312. b) Bowler B. E.; Raphael, A. L.; Gray, H. B. *Prog Inorg. Chem.* **1990**, *38*, 259, and references therein. c) Joran, A. D.; Leland, B. A.; Felker, P. M.; Zewail, A. H.; Hopfield, J. J.; Dervan, P. B. *Nature* **1987**, *327*, 508.
8. *Molecular Electronics*, (Ashwell, G. J., Ed.) Taunton: Research Studies Press, **1992**.
9. Marks, T. J. *Science* **1985**, *227*, 881.
10. a) Du, Z.; Hood, L.; Wilson, R. K. *Meth. Enzym.* **1993**, *218*, 104. b) D. Stahl, *Meth. Enzym.* **1993** *224*, 373. c) Pease, A. C.; Solas, D.; Sullivan, E. J.; Cronin, M. T.; Holmes, C. P.; Fodor, S. P. A. *Proc. Natl. Acad. Sci. USA* **1994**, *91*, 5022.
11. a) Marcus, R. A.; Sutin, N. *Biochim. Biophys. Acta* **1985**, *811*, 265. b) Siddarth, P.; Marcus, R. A. *J. Phys. Chem.* **1993**, *97*, 2400.
12. a) McConnell, H. M. *J. Chem. Phys.* **1961**, *35*, 508. b) Ratner, M. A. *J. Phys. Chem.* **1990**, *94*, 4876. c) Naleway, C. A.; Curtiss, L. A.; Miller, J. R. *J. Phys. Chem.* **1991**,

95, 8434. d) Mujica, V.; Kemp, M.; Ratner, M. A. *J. Chem. Phys.* **1994**, *101*, 6856. e) Mujica, V.; Kemp, M.; Ratner, M. A. *J. Chem. Phys.* **1994**, *101*, 6849.

13. Closs, G. L.; Calcaterra, L. T.; Green, N. J.; Penfield, K. W.; Miller, J. R. *J. Phys. Chem.* **1986**, *90*, 3673.
14. Closs, G. L.; Johnson, M. D.; Miller, J. R.; Piotrowiak, P. *J. Am. Chem. Soc.* **1989**, *111*, 3751.
15. Beratan, D. N.; Onuchic, J. N. *Adv. Chem. Ser.* **1991**, *228*, 71.
16. a) Risser, S. M.; Beratan, D. N.; Mead, T. J. *J. Am. Chem. Soc.* **1993**, *115*, 2508. b) Priyadarshy, S.; Risser, S. M.; Beratan, D. N. *J. Phys. Chem.* **1996**, *100*, 17678.
17. a) Chang, I. J.; Gray, H. B.; Winkler, J. R. *J. Am. Chem. Soc.* **1991**, *113*, 7056. b) Wuttke, D. S.; Bjerrum, M. J.; Winkler, J. R.; Gray, H. B. *Science* **1992**, *256*, 1007. c) Langen, R.; Chang, I. J.; Germanas, J. P.; Richards, J. H.; Winkler, J. R.; Gray, H. B. *Science* **1995**, *268*, 1733.
18. Casimiro, D. R.; Richards, J. H.; Winkler, J. R.; Gray, H. B. *J. Phys. Chem.* **1993**, *97*, 13073.
19. a) Park, H. W.; Kim, S.-T.; Sancar, A.; Deisenhofer, J. *Science* **1995**, *268*, 1866. b) Kim, S.-T.; Sancar, A. *Photochem. Photobiol.* **1993**, *57*, 895.
20. a) Hoffman, B. M.; Ratner, M. A. *J. Am. Chem. Soc.* **1987**, *109*, 6237. b) Brunschwig, B. S.; Sutin, N. *J. Am. Chem. Soc.* **1989**, *111*, 7454.
21. a) Beley, M.; Chodorowski-Kimmes, S.; Collin, J.-P. *et al. Angew. Chem. Int. Ed. Engl.* **1994**, *33*, 1775. b) Larsson, S. *Chem. Phys. Lett.* **1982**, *90*, 136.
22. Isied, S. S.; Ogawa, M. Y.; Wishart, J. F. *Chem. Rev.* **1992**, *92*, 381.
23. Schouten, P. G.; Warman, J. M.; deHaas, M. P.; Fox, M. A.; Pan, H.-L. *Nature* **1991**, *353*, 736.
24. Schouten, P. G., Warman, J. M.; de Haas, M. P. *et al. J. Am. Chem. Soc.*, **1994**, *116*, 6880.
25. Fox, M. A. *Accts. Chem. Res.* **1992**, *25*, 569.

26. Tanaka, M.; Yoshida, H.; Ogasawara, M. *J. Phys. Chem.* **1991**, *95*, 955.

27. Markovitsi, D.; Bengs, H.; Ringsdorf, H. *J. Chem. Soc. Faraday Trans.*, **1992**, *88*, 1275.

28. J. G. Gaudiello, G. E. Kellogg, S. M. Tetrick and T. J. Marks *J. Am. Chem. Soc.* **1989**, *111*, 5259.

29. Saenger, W.; Cantor, C. R., eds. *Principles of Nucleic Acid Structure*, NY: Springer-Verlag, **1984**.

30. Blackburn, G. M.; Gait, M. J. eds. *Nucleic Acids in Chemistry and Biology*, New York: Oxford University Press, **1990**.

31. Wing, R.; Drew, H.; Takano, T.; Broka, C.; Tanaka, S.; Itakura, D.; Dickerson, R. E. *Nature* **1980**, *287*, 755.

32. Wuthrich, K. *NMR of Proteins and Nucleic Acids*, New York: Wiley, **1986**.

33. Sambrook, J.; Fritsch, E. F.; Maniatis, T. *Molecular Cloning: A Laboratory Manual*, 2nd ed., New York: Cold Spring Harbor Laboratory, **1989.**

34. a) Vorlickova, M.; Kypr, J. *J. Biomolec. Struct. Dyn.* **1985**, *3*, 67. b) Hunter, C. A. *J. Mol. Biol.* **1993**, *230*, 1025. c) Yanagi, K.; Privé, G. G.; Dickerson, R. E. *J. Mol. Biol* **1991**, *217*, 201.

35. Kim, Y. C.; Geiger, J. H.; Han, S.; Sigler, P. B. *Nature*, **1993**, *365*, 512.

36. Terbrueggen, R. J.; Barton, J. K. *Biochemistry*, **1995**, *34*, 8227.

37. Haran, T. E.; Kahn, J. D.; Crothers, D. M. *J. Mol. Biol.* **1994**, *244*, 135.

38. Melvin, T.; Botchway, S.; Parker, A. W.; O'Neill, P. *J. Chem. Soc. Chem. Comm.* **1995**, 653.

39. Fielden, E. M.; Lillicrap, S. C.; Robins, A. B. *Radiat. Res.* **1971**, *48*, 421.

40. Al-Kazwini, A. T.; O'Neill, P.; Adams, G. E.; Fielden, E. M. *Radiat. Res.* **1990**, *121*, 149.

41. O'Neill, P.; Al-Kazwini, A. T.; Land, E. J.; Fielden, E. M. *NATO ASI Ser. Ser. H* **1991**, *54*, 125.

42. Van Lith, D.; de Haas, M. P.; Warman, J. M.; Hummel, A. *Biopolymers* **1983**, *22*, 807.

43. Warman, J. M.; de Haas, M. P.; Schouten, P. G. in *Radiation Research: A 20th-Century Perspective Volume II: Congress Proceedings* (Dewey, W. C.; Edington, M.; Fry, R. J. M.; Hall, E. J.; Witmore, G. F., Eds.), Academic Press, **1992**, 93.

44. Cullis, P. M.; McClymont, J. D.; Symons, M. C. R. *J. Chem. Soc. Faraday Trans.* **1990**, *86*, 591.

45. Miller, J. H.; Frasco, D. L.; Swenberg, C. E.; Rupprecht, A., in *Radiation Research: A Twentieth Century Perspective Vol .II* (Chapman, J. D.; Dewey, W. C.; Witmore, G. F., Eds.), San Diego: Academic Press, **1992**, 433.

46. Anderson, R. F.; Patel, K. B.; Wilson, W. R. *J. Chem. Soc. Faraday, Trans.1*, **1991**, *87*, 3739.

47. Whillans, D. W. *Biochimica et Biophysica Acta* **1975**, *414*, 193.

48. Houee-Levin, C.; Gardes-Albert, M.; Rouscilles, A.; Ferradini, C.; Hickel, B. *Biochemistry* **1991**, *30*, 8216.

49. Dee, D.; Baur, M. E. *J. Chem. Phys.* **1974**, *60*, 541.

50. Otto, P.; Clementi, E.; Ladik; J. *J. Chem. Phys.* **1983**, *78*, 4547.

51. Clementi, E.; Corongiu, G. *Int. J. Quant. Chem. Quant. Biol. Symp.* **1982**, *9*, 213.

52. Miller, J. H.; Swenberg, C. E. *Can. J. Phys.* **1990**, *68*, 962.

53. Baverstock, K. F.; Cundall, B. *Radiat. Phys. Chem.* **1988**, *32*, 553.

54. Szent-Gyorgyi, A.; Isenberg, I.; Baird, Jr., S. L. *Proc. Natl. Acad. Sci. USA* **1960**, *46*, 1444.

55. a) Snart, R. S. *Biopolymers* **1968**, *6*, 293. b) O'Konski, C. T.; Moser, P.; Shirai, M. *Biopol .Symp.* **1964**, *1*, 479. c) van Lith, D.; Warman, J. M.; de Haas, M. P., Hummel, A. *J. Chem. Soc. Faraday Trans. 1* **1986**, *82*, 2933.

56. Brun, A. M.; Harriman, A. *J. Am. Chem. Soc.* **1992**, *114*, 3656.

57. Brun, A. M.; Harriman, A. *J. Am. Chem. Soc.* **1994**, *116*, 10383.

58. Meade, T. J.; Kayyem, J. F. *Angew. Chem. Int. Ed. Engl.* **1995**, *34*, 352.

59. Murphy, C. J.; Arkin, M. R.; Ghatlia, N. D.; Bossmann, S.; Turro, N. J.; Barton, J. K. *Proc. Nat. Acad. Sci., US A*, **1994**, *91*, 5315.

60. Murphy, C. J.; Arkin, M. R.; Jenkins, Y.; Ghatlia, N. D.; Bossman, S.; Turro, N. J.; Barton, J. K. *Science* **262**, 1025 (1993).

61. Arkin, M. R.; Stemp, E. D. A.; Holmlin, R. E.; Barton, J. K.; Hörmann, A.; Olson, E. J. C.; Barbara, P. F. *Science*, **1996**, *273*, 475.

62. Kelley, S. O.; Holmlin, R. E.; Stemp, E. D. A.; Barton, J. K. unpublished results.

63. Meade, T. J. *Metal Ions Biol. Syst.* **1996**, *32*, 453.

64. Arkin, M. R.; Stemp, E. D. A.; Turro, C.; Turro, N. J.; Barton, J. K. *J. Am. Chem. Soc.* **1996**, *118*, 2267.

65. a) Turro, N. J.; Barton, J. K.; Tomalia, D. A. *Accts. Chem. Res.* **1991**, *24*, 332. b) Orellana, G.; Kirsch de Mesmaeker, A.; Barton, J. K.; Turro, N. J. *Photochem. Photobiol.* **1991**, *54*, 499.

66. Pyle, A. M.; Barton, J. K. *Prog Inorg. Chem.* **1990**, *38*, 259.

67. a) Dupureur, C. M.; Barton, J. K. *Comprehensive Supramolecular Chemistry V. 5*, J.-M. Lehn, ed. Pergamon Press, **1995**, 295. b) Johann, T. W.; Barton, J. K. *Trans. Royal Soc. (London) A.* **1996**, *354*, 299.

68. Lober, G. *J. Luminescence* **1981**, *22*, 221.

69. a) Baguley, B. C.; Le Bret, M. *Biochemistry* **1984**, *23*, 937. b) Davis, L. M.; Harvey, J. D.; Baguley, B. C. *Chem.-Biol. Interactions* **1987**, *62*, 45.

70. Fromherz, P.; Rieger, B. *J Am Chem Soc.* **1986**, *108*, 5361.

71. Atherton, S. J.; Beaumont, P. C. *J. Phys. Chem.* **1987**, *91*, 3993.

72. Pasternack, R. F.; Caccam, M.; Keogh, B. *et al. J. Am. Chem. Soc.* **1991**, *113*, 6835.

73. Lipscomb, L. A.; Zhou, F. X.; Presnell, S. R.; Woo, R. J.; Peek, M. E.; Plaskon, R. R.; Williams, L. D. *Biochemistry* **1996**, *35*, 2818.

74. Förster, T. *Discussions Faraday Soc.* **1959**, *27*, 7.

75. Perrin, F. *Compt. Rend.* **1924**, *178,* 1978.

76. Murphy, C. J.; Barton, J. D. *Meth. Enzym.* **1993**, *226*, 576.

77. Barton, J. K. *Science* **1986**, *233*, 727.

78. a) Barton, J. K.; Goldberg, J. M.; Kumar, C. V.; Turro, N. J. *J. Am. Chem. Soc.* **1986**, *108*, 2081. b) Kumar, C. V.; Barton, J. K.; Turro, N. J. *J. Am. Chem. Soc.* **1985**, *107*, 5518.

79. a) Rehmann, J. P.; Barton, J. K. *Biochemistry* **1990**, *29*, 1710. b) Rehmann, J. P.; Barton, J. K. *Biochemistry* **1990**, *29*, 1701.

80. Ottaviani, M. F.; Ghatlia, N. D.; Bossmann, S. H.; Barton, J. K.; Dürr, H.; Turro, N. J. *J. Am. Chem. Soc.* **1992**, *114*, 8946.

81. Barton, J. K.; Kumar, C. V.; Turro, N. J. *J. Am. Chem. Soc.* **1986**, *108*, 6391.

82. Purugganan, M. D.; Kumar, C. V; Turro, N. J.; Barton, J. K. *Science* **1988**, *241*, 1645.

83. Friedman, A. E.; Chambron, J.-C.; Sauvage, J.-P.; Turro, N. J.; Barton, J. K. *J. Am. Chem. Soc.* **1990**, *112*, 4960.

84. Chambron, J.-C.; Sauvage, J.-P.; Amouyal, E.; Koffi, P. *New J. Chem.* **1985**, *9*, 527.

85. E. Amouyal, A. Homsi, J.-C. Chambron and J.-P. Sauvage, *J. Chem. Soc. Dalton Trans.* **1990**, 1841 (1990).

86. Jenkins, Y.; Friedman, A. E.; Turro, N. J.; Barton, J. K. *Biochemistry* **1992**, *31*, 10811.

87. a) Coates, C. G.; Jacquet, L.; McGarvey, J. J.; Bell, S. E. J.; Al-Obaidi, A. H. R.; Kelly, J. M. *Chem. Comm.* **1996**, 35. b) Turro, C.; Bossmann, S. H.; Leroi, G. E.; Barton, J. K.; Turro, N. J. *Inorg. Chem.* **1994**, *33*, 1244.

88. Sitlani, A.; Long, E. C.; Pyle, A. M.; Barton, J. K. *J. Am. Chem. Soc.* **1992,** *14*, 2303.

89. Pyle, A. M.; Long, E. C.; Barton, J. K. *J. Am. Chem. Soc.* **1989**, *111*, 4520.

90. David, S. S.; Barton, J. K. *J. Am. Chem. Soc.* **1993**, *115*, 2984.

91. Pyle, A. M.; Chiang, M. Y.; Barton, J. K. *Inorg. Chem.* **1990**, *29*, 4487.

92. Turro, C.; Evenzahav, A.; Bossmann, S. H.; Barton, J. K.; Turro, N. J. C. *Inorg. Chim. Acta* **1996**, *243*, 101.

93. Friedman, A. E.; Kumar, C. V.; Turro, N. J.; Barton, J. K. *Nucleic Acids Res.* **1991**, *19*, 2595.

94. Hartshorn, R. M.; Barton, J. K. *J Am. Chem. Soc*, **1992**, *114*, 5925.

95. Gupta, N.; Grover, N.; Neyhart, G. A.; Singh, P.; Thorp, H. H. *Inorg. Chem.* **1993**, *32*, 310.

96. Hiort, C.; Lincoln, P.; Norden, B. *J. Am. Chem. Soc.* **1993**, *115*, 3448.

97. a) Dupureur, C. M.; Barton, J. K. *J. Am. Chem. Soc.* **1994**, *116*, 10286. b) Dupureur, C. M.; Barton, J. K. submitted for publication.

98. Fees, J.; Kaim, W.; Moscherosch, M.; Matheis,W.; Klima, J.; Krejcik, M.; Zalis, S. *Inorg. Chem.* **1993**, *32*, 166.

99. Turro, C.; Bossmann, S. H.; Jenkins, Y.; Barton, J. K.; Turro, N. J. *J. Am. Chem. Soc.* **1995**, *117*, 9026.

100. Sabatani, E.; Nikol, H. D.; Gray, H. B.; Anson, F. C. *J. Am. Chem. Soc.* **1996**, *118*, 1158.

101. Chambron, J.-C.; Sauvage, J.-P. *Chem. Phys. Lett.* **1991**, *182*, 603.

102. Holmlin, R. E.; Barton, J. K. *Inorg. Chem.* **1995**, *34*, 7.

103. Demas, J. N.; Crosby, G. A. *J. Am. Chem. Soc.* **1971**, *93*, 2841.

104. Holmlin, R. E.; Stemp, E. D. A.; Barton, J. K. *J. Am. Chem. Soc.* **1996**, *118*, 5236.

105. Juris, A.; Balzani, V.; Barigelletti, F., *et al. Coord. Chem. Rev.* **1988**, *84*, 85.

106. Hudson, B.; Dupureur, C. M.; Barton, J. K. *J. Am. Chem. Soc.*, **1995**, *117*, 9379.

107. a) Collins, J. G.; Shields, T. P.; Barton, J. K. *J. Am. Chem. Soc.* **1994**, *116*, 9840. b) Shields, T. P.; Barton, J. K. *Biochemistry*, **1995**, *34*, 15049.

108. Chow, C. S.; Behlen, L. S.; Uhlenbeck, O. C.; Barton, J. K. *Biochemistry* **1992**, *31*, 972.

109. Lee, I.; Barton, J. K. *Biochemistry*, **1993**, *32*, 6121.

110. Uchida, K.; Pyle, A. M.; Morii, T.; Barton, J. K. *Nucleic Acids Res.* **1989**, *17*, 10259.

111. Krotz, A. H.; Hudson, B. P.; Barton, J. K. *J. Am. Chem. Soc.* **1993**, *115*, 12577.

112. Campisi, D.; Morii, T.; Barton, J. K. *Biochemistry*, **1994**, *33*, 4130.

113. Sitlani, A.; Dupureur, C. M.; Barton, J. K. *J. Am. Chem. Soc.* **1993**, *115*, 12589.

114. Navon, G.; Sutin, N. *Inorg. Chem.* **1974**, *13*, 2159.

115. Ho, P. S.; Frederick, C.; Saal, D.; Wang, A. H.-J.; Rich, A. *J. Biomol. Struct. Dynam.* **1987**, *4*, 521.

116. Stemp, E. D. A.; Arkin, M. R.; Barton, J. K. *J. Am. Chem. Soc.* **1995**, *117*, 2375.

117. a) Indelli, M. T.; Bignozzi, C. A.; Harriman, A.; Schoonover, J. R.; Scandola, F. *J. Am. Chem. Soc.* **1994**, *116*, 3768. b) Nozaki, K.; Ohno, T.; Haga, M. *J. Phys. Chem.* **1992**, *96*, 10880. c) Kalyanasundaram, K.; Gratzel, M.; Nazeeruddin, Md. K. *J. Phys. Chem.* **1992**, *96*, 5865. d) Furue, M.; Hirata, M.; Kinoshita, S.; Kushida, T.; Kamachi, M. *Chem. Lett.* **1990**, 206. e) Creutz, C.; Keller, A. D.; Sutin, N.; Zipp, A. P. *J. Am. Chem. Soc.* **1982**, *104*, 3618. f) Chan, S.-F.; Chou, M.; Creutz, C.; Matsubara, T.; Sutin, N. *J. Am. Chem. Soc.* **1981**, *103*, 369.

118. Stemp, E. D. A., unpublished results.

119. Kalyanasundaram, K; *Coord. Chem. Rev.* **1982**, *46*, 159.

120. General reviews: a) Goodchild, J. *Bioconjugate Chem.* **1990**, *1*, 165. b) Englisch, U.; Gauss, D. H. *Angew. Chem. Int. Ed. Engl.* **1991**, *30*, 613. c) Beaucage, S. L.; Iyer, R. P. *Tetrahedron* **1993**, *49*, 1925. d) Thuong, N. T.; Helene, C. *Angew. Chem. Int. Ed. Engl.* **1993**, *32*, 666.

121. Attachment to bases and sugars: a) Tesler, J.; Cruickshank, D. A.; Morrison, L. E.; Netzel, T. L.; Chan, C. *J. Am. Chem, Soc.* **1989**, *111*, 7221. Spaltenstein, A.; Robinson, B. H.; Hopkins, P. B. *J. Am. Chem. Soc.* **1989**, *111*, 2303. Wang, G.; Bergstrom, D. *Tet. Lett.* **1993**, *24*, 6721. Aurup, H.; Tuscgi, T.; Benseler, F.; Ludwig, J.; Eckstein, *Nuc. Acids. Res.* **1994**, *22*, 20.

122. Attachment to oligonucleotide terminus: Mergny, J. L.; Boutorine, S.; Garestier, T.; Belloc, F.; Rougee, M.; Bulychev, N. V.; Koshkin, A. A.; Bourson, J.; Levedev, A. V.; Valeur, B.; Thuorn, N. T.; Helene, C. *Nuc. Acids. Res.* **1994**, *22*, 920. Bannwarth, W.; Schmidt, D.; Stallard, R. L.; Hornung, C.; Knorr, R.; Müller, F. *Helv. Chim. Acta* **1988**, *71*, 2085. Bannwarth, W.; Schmidt, D. *Tet. Lett.* **1989**, *30*, 1513. Chen, C.-H. B.; Sigman, D. S. *Proc. Natl. Acad. Sci. USA* **1986**, *83*, 7147. Chu, B. C. F.; Orgel, L. E. *Proc. Natl. Acad. Sci. USA* **1985**, *82*, 963.

123. Jenkins Y.; Barton, J. K. *J. Am. Chem. Soc.* **1992**, *114*, 8737.

124. Dunn, D. A.; Lin, V. H.; Kochevar, I. E. *Biochemistry*, **1992**, *31*, 11620.

125. Ito, K.; Inoue, S.; Yamamoto, K.; Kawanishi, S. *J. Biol. Chem.* **1993**, *268*, 13221.

126. a) Ly, D.; Kan, Y.; Armitage, B.; Schuster, G. B. *J. Am. Chem. Soc.* **1996**, *118*, 8747. b) Breslin, D. and Schuster, G. B. *J. Am. Chem. Soc.* **1996**, *118*, 2311. c) Armitage, B.; Yu, C.; Devadoss, C.; Schuster, G. B. *J. Am. Chem. Soc.*, **1994**, *116*, 9847.

127. a) Saito, I.; Takayama, M.; Sugiyama, H.; Nakatani, K.; Tsuchida, A.; Yamamoto, M. *J. Am. Chem. Soc.* **1995**, *117*, 6406. b) Sugiyama, H. and Saito, I. *J. Am. Chem. Soc.* **1996**, *118*, 7063.

128. a) Hall, D. B; Holmlin, R. E.; Barton, J. K. *Nature*, **1996**, *382*, 731. b) Hall, D. B. and Barton, J. K., submitted for publication.

129. Charlier, M.; Hélène, C. *Photochem. Photobiol.* **1975**, *21*, 31.

130. Dandliker, P. J.; Holmlin, R. E.; Barton, J. K., *Science*, in press, **1996**.

131. Yang, D. Y.; Begley, T. P. *Tet. Lett.* **1993**, *34*, 1709.

132. a) Stemp, E. D. A., Arkin, M. R.; Barton, J. K. unpublished results. b) Arkin, M. R.; Stemp, E. D. A.; Barton, J. K. unpublished results.

133. For a theory incorporating thermal accessibility of DNA bridge, see: Felts, A. K.; Pollard, W. T.; Friesner, R. A. *J. Phys. Chem.* **1995**, *99*, 2929.

Chapter 2

Effects of Donor and DNA Sequence on DNA-mediated Electron Transfer Reactions between Metallointercalators*

* Adapted from Arkin, M. R.; Stemp, E. D. A.; Holmlin, R. E.; Barton, J. K.; Hörmann, A.; Olson, E. J. C.; Barbara, P. F. *Science*, **1996**, *273*, 475.

2.1 Introduction

Many researchers have considered whether the aromatic heterocyclic bases in duplex DNA offer a medium for fast, long-range electron transfer (ET).[1-12] Previous work in our laboratory, described in Chapter 1, indicates that intercalated electron donors and acceptors provide a direct probe of the DNA π-stack. Subnanosecond luminescence quenching of photoexcited Ru(II) donors by Rh(III) acceptors occurs when both complexes are intercalatively stacked into B-DNA, but fast quenching is not observed with a nonintercalating acceptor in a reaction with comparable driving force.[3,4] Transient absorption spectroscopy studies on the microsecond time scale indicate that quenching in these systems occurs by ET for both Ru(II) and Os(II) intercalators.[11,12] Furthermore, with metallointercalators covalently attached to a 15 base pair (bp) DNA duplex and separated by > 40 Å, a lower limit on the intramolecular quenching was set at ~ 3×10^9 s^{-1}.[4] The spectroscopic techniques used in these studies, however, had insufficient time resolution to measure rates for photoinduced forward reactions and did not provide complete kinetics for the recombination reaction between Ru(III) and Rh(II) intermediates. Towards the goal of resolving the kinetics of DNA-mediated ET reactions, we have employed ultrafast emission and absorption spectroscopies to examine reactions mediated by DNA with a series of noncovalently bound, intercalated metal complexes. These time-resolved measurements complement information gathered from steady-state emission quenching.

In addition to measuring reaction rates, we have begun to explore the effects of the intercalator structure and the DNA sequence in mediating ET chemistry. Photoexcited donors have the formula $M(L)_2dppz^{2+}$ (M = Ru, Os; L = derivative of 1,10-phenanthroline or 2,2'-bipyridine; dppz = derivative of dipyridophenazine), shown in Figure 2.1. As has been reported for the parent complex $Ru(phen)_2dppz^{2+}$, donors intercalate into DNA with a binding constant (K_b) of 10^7 M^{-1} and display large luminescence enhancements upon DNA intercalation.[13-17] Using ultrafast absorption and emission spectroscopies, we quantitate

Figure 2.1

A) Illustration of intercalating donors (M = Ru, Os) and acceptor Rh(III) and the electron-transfer cycle. Photoexcitation of M(II) forms the excited state *M(II), which can radiatively decay (k_d) or can be quenched by ET with Rh(III) (k_{et}) to form M(III)/Rh(II) and then recombine (k_{rec}). Photoinduced ET may yield either Rh(II)$(phi)_2$bpy or Rh(III)(phi)(phi^-)bpy, both symbolized as Rh(II). B) Schematic illustration of Ru(II) and Rh(III) bound to DNA at typical ratios used in these experiments; the donor-acceptor distance correspond to 17 and 85 Å for the placement of complexes as shown.

A

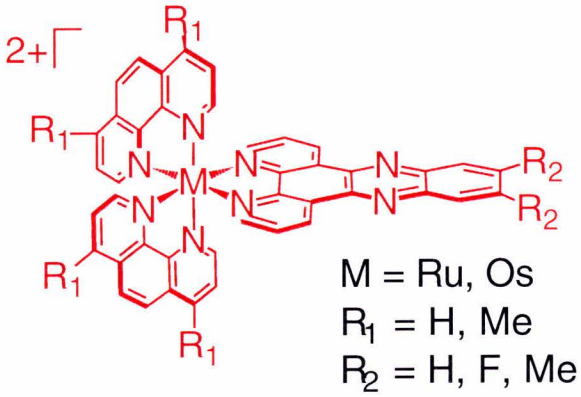

Ru(phen)$_2$dppz^{2+}derivatives

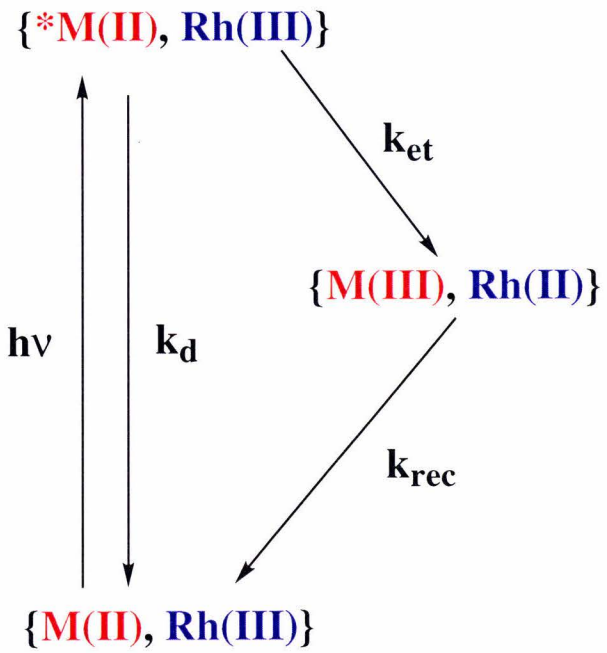

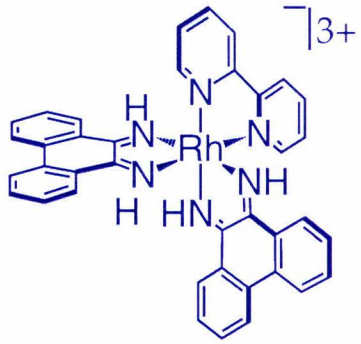

Rh(phi)$_2$bpy^{3+}

B

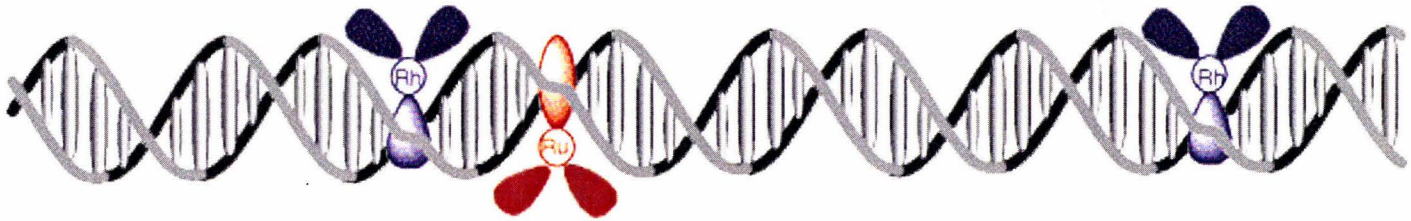

this "molecular light switch" effect by measuring the excited-state lifetimes of $M(L)_2dppz^{2+}$ complexes in the absence and presence of DNA. The electron acceptor is $Rh(phi)_2bpy^{3+}$ (phi = 9,10 phenanthrenequinone diimine) (Figure 2.1), analogous to the $Rh(phi)_2phen^{3+}$ complex used in previous studies (Chapter 1). Similar complexes have been shown to intercalate into DNA through a phi ligand, also with $K_b > 10^6 M^{-1}$.[18] Phi complexes of Rh(III) are known to cleave the DNA strand at the intercalation site when irradiated with ultraviolet (UV) light.[19,20] This photocleavage assay has attracted much attention as a structural probe of DNA,[21] and is used here to identify the binding sites of $Rh(phi)_2bpy^{3+}$. The electronic structures of both the donors and the acceptor are particularly well-suited for studying DNA-mediated electron transfer. For $M(L)_2dppz^{2+}$ derivatives, the lowest energy electronic transition is characterized by metal-to-ligand charge transfer (MLCT) directed onto the dppz ligand.[12,15,22,23] Excitation of the complexes bound to DNA promotes an electron onto this intercalating ligand, directing it into the stacked basepairs. The lowest energy transition of the acceptor $Rh(phi)_2bpy^{3+}$ is also centered on the intercalating phi ligand,[24] and thus $Rh(phi)_2bpy^{3+}$ is well-positioned to accept an electron through the DNA π-stack.

Figure 2.1 illustrates the photoinduced electron transfer cycle between $M(L)_2dppz^{2+}$ and $Rh(phi)_2bpy^{3+}$. In this chapter, we examine the photoinduced forward (k_{et}) and ground-state recombination (k_{rec}) ET reactions on the picosecond time scale by monitoring both the kinetics of the emission decay and the kinetics of the recovery in ground state absorption by Ru(II) and Os(II) donors. When possible, pure enantiomers of donors and acceptor are used because the binding of metallointercalators is sensitive to the chirality of the DNA double helix.[17,25] Steady-state and kinetic measurements indicate that photoinduced ET reactions are static on the picosecond time scale ($k_{et} > 3 \times 10^{10}\ s^{-1}$), and picosecond transient absorption spectroscopy demonstrates that recombination reactions are also very fast ($k_{rec} \sim 10^{10}\ s^{-1}$). Comparison of the kinetics of ground-state recovery of $M(L)_2dppz^{2+}$ in solution and in DNA indicates that quenching does not occur by reaction

with water or by displacement from the DNA. In fact, spectroscopic data provides evidence for an ET reaction mechanism mediated by the DNA over a distance of at least 10.2 Å. Analysis of different DNA sequences and preliminary studies with an A-form duplex suggest further that ET between metallointercalators depends on the DNA structure. Two important general observations are made: First, recombination rates are found to be independent of the loading of Δ-$Rh(phi)_2bpy^{3+}$ on DNA, and two models to describe these results are discussed. Second, ET reaction rates and efficiencies are found to be sensitive to the binding of complexes to DNA and to the stacking interations in the metal/DNA complex. Thus, the details of intercalation and DNA sequence are important characteristics of DNA-mediated ET reactions.

2.2 Experimental

Materials. The ligands (L) 1,10-phenanthroline (phen), 2,2'-bipyridine (bpy), and 4,4'-dimethyl-2,2'-bipyridine (DMP) were purchased from Aldrich. Dppz ligands, including dipyrido[3,2-a:3',2'-c]phenazine (dppz) and 7,8-dimethyl dipyridophenazine (Me_2dppz) were prepared according to literature procedures.[22] 7,8-difluoro-dipyridophenazine (F_2dppz) was the kind gift of Dr. C. M. Dupureur. $[Ru(L)_2dppz]Cl_2$, $[Os(phen)_2dppz]Cl_2$ and $[Rh(phi)_2bpy]Cl_3$ were prepared according to literature procedures[14,22] and further purified by high pressure liquid chromatography (HPLC). Enantiomers were resolved using standard protocols[16,18a,26] and analyzed by circular dichroism spectroscopy. Stock solutions were prepared in H_2O and quantitated by UV-visible absorption spectroscopy [ε_{440} = 21,000 $M^{-1}cm^{-1}$ for dppz complexes of Ru(II);[14] ε_{430} = 13,000 $M^{-1}cm^{-1}$ for $Os(phen)_2dppz^{2+}$; ε_{350} = 23,600 $M^{-1}cm^{-1}$ for $Rh(phi)_2bpy^{3+}$].[19] Mixed-sequence DNA (sonicated calf thymus), poly(dA-dT), and poly(dG-dC) (Pharmacia) were dialyzed against buffer and quantitated by UV absorption spectroscopy [ε_{260} = 6600 M^{-1} cm^{-1} for calf thymus and poly(dA-dT) DNAs; ε_{260} = 8400 $M^{-1}cm^{-1}$ for poly(dG-dC)]. Average lengths of DNA are 2000± 600 bp for sonicated calf

thymus DNA, 920 bp for poly(dG-dC), and 1050 bp for poly(dA-dT). Samples were prepared in an aerated buffer of 5 mM tris, 50 mM NaCl, pH 8.5 at ambient temperature.

The A-form oligonucleotide duplex was prepared by hybridization of the mixed RNA-DNA chimera 5'-d(AGAT)r(AGAAGGCCUGGU)d(TCCT)-3' and its all DNA complementary strand 5'-d(AGGAACCAGGCCTTCTATCT)-3'. Sequences were prepared by standard phosphoramidite chemistry[27] (Glen Research) on a model 394 DNA synthesizer (Applied Biosystems). Both strands were purified by anion exchange chromatography followed by reverse-phase chromatography. Conditions for ion exchange HPLC [Hewlett Packard HP1090, oligonucleotide column (Vydac)] were as follows: oven temperature = 40 ^{o}C; solvent A = 10 mM phosphate buffer, pH 7; solvent B = 10 mM phosphate, 0.9 M NaCl, pH 7; gradient = 40 - 100% B over 30 min. Conditions for reverse-phase HPLC [Hewlett Packard HP1050, C4 column (Vydac)] were as follows: solvent A = 100 mM NH_4OAc buffer, pH 6.5; solvent B = acetonitrile; gradient = 0 - 25% B over 40 min.

Laser instrumentation. Time-resolved measurements on the nanosecond time scale utilized the laser facilities in the Beckman Institute Laser Resource Center using an excimer-pumped dye laser containing Coumarin 480 (Exciton). Laser powers were 1.0 - 1.5 mJ at 10 Hz and the pulse width was ca. 20 ns. Details of this instrumentation are provided elsewhere.[12,28]

The time-correlated single photon counting (TCSPC) apparatus was constructed in the laboratory of Prof. P. F. Barbara and utilizes a cavity-dumped femtosecond mode-locked Ti:sapphire laser centered near 830 nm.[29] Samples are excited with frequency-doubled light at variable repetition rates (usually 40 kHz). Typical emission count rates are = 1 kHz detected with a Hamamatsu multichannel plate photomultiplier tube (R3809U-01). The data displayed represents the sum of several scans obtained in reverse timing. Full width at half height is ~ 50 ps.

The pump/probe transient absorption experiments, also done in collaboration with Prof. P. F. Barbara in his laboratory, employ a Ti:sapphire regenerative amplifier.[30] The system typically produces 140 fs pulses centered near 780 nm with a pulse energy of ~180 μJ at 2 kHz repetition rate. Amplified pulses are partitioned in a 30/70 beam splitter, initiating the pump and probe light sources. The larger fraction is focused into a spinning quartz disk for continuum generation. 420 nm probe light is selected by a variable-wavelength interference filter and split into signal and reference paths. The smaller fraction of the amplified pulse is mechanically chopped at 1 kHz and focused onto a 1-mm BBO crystal for second harmonic frequency generation. The resultant 390 nm pump light (~10 μJ/pulse) is focused and crossed with the probe light through a static 2 mm quartz sample cuvette. Time-resolved dynamics are obtained by scanning a variable delay in the probe light interaction with the sample relative to the pump light interaction. Signal and reference probe intensities were measured by large-area avalanche photodiodes (EG&G) and divided in an analog processor. The change in absorbance measured from probe intensity with the pump on relative to probe intensity with pump blocked was obtained from a boxcar operating in toggle mode. Typically, 2000 shots were averaged per time point and 2-8 scans were averaged per data set.

Methods. Determination of excited-state lifetimes of dppz complexes of Ru(II) and Os(II) in aqueous solution was accomplished by TCSPC and picosecond transient absorption spectroscopy. TCSPC data were obtained with λ_{exc} = 390 nm and λ_{obs} > 700 nm. Transient absorption data used λ_{exc} = 390 nm and λ_{obs} = 420 nm. Samples contained 40 μM complex in 5 mM tris, 50 mM NaCl, pH 8.5.

For donors bound to DNA, emission was monitored by both flash-photolysis and TCSPC. Luminescence decay data on the nanosecond time scale were taken with λ_{exc} = 480 nm and λ_{obs} = 616 nm [λ_{obs} = 738 nm for Os(II)]. Samples contained 10 μM metal complex, 500 μM base pairs (bp) calf thymus DNA in 5 mM tris, 50 mM NaCl, pH 8.5. All experiments were done at a ratio of 50 DNA bp to 1 electron donor, such that the

complexes are dilute on the helix. Steady-state luminescence intensities were determined by integrating the full emission decay curves. The amount of ultrafast quenching by Δ-$Rh(phi)_2bpy^{3+}$ was measured as the prompt loss in initial intensity of emission decay curves measured by flash-photolysis and TCSPC (λ_{exc} = 400 nm, λ_{obs} = 620 nm). TCSPC data were corrected for a response-limited emission decay of Δ-$Rh(phi)_2bpy^{3+}$.

For picosecond transient absorption spectroscopy, a separate, 200 μl sample was prepared for each point during a titration to avoid photobleaching. Transient absorption data were measured with λ_{exc} = 390 nm, λ_{obs} = 420 nm, using samples containing photoexcited donor (20 μM), DNA (1 mM bp), in the buffer described above. The absolute concentrations of reagents affected neither the reaction rates nor the yield of ET. Prior to data fitting, kinetic traces were corrected for a small contribution from *Rh(III) and normalized with respect to the change in absorbance (ΔA) at time zero. Transient absorption data were well described by both a single exponential function with an offset and by a biexponential function where the offset is represented by a slow decay constant. More complex expressions incorporating multiple exponential terms or distributions did not improve fit residuals.

Modelling kinetic data. Modelling involved the simulated loading of a one-dimensional lattice with two different intercalators to calculate the distribution of separations between donors and acceptors on DNA (using computer software developed by in the laboratory of Prof. P. Barbara).[31] For statistical descriptions of nearest-neighbor pairs (in the absence of clustering), 10^4 cycles of random loading were compiled.

Electrochemistry. Reduction potentials for $Rh(phi)_2bpy^{3+}$ and dppz complexes of Ru(II) and Os(II) were measured using instrumentation described previously[3] at a scan rate of 100 mV/s. Complexes were dissolved in dry DMF (Fluka) with 100 mM tetrabutylammonium hexafluorophosphate as supporting electrolyte. $M(L)_2dppz^{2+}$ complexes and $Rh(phi)_2bpy^{3+}$ gave reversible and quasi-reversible voltammagrams, respectively. Potentials were determined relative to Ag/AgCl and converted to NHE by

adding 0.2 V. ΔG^0 values for quenching and recombination reactions were then calculated by the equation $E(3+/*2+) = E_{00} - E(3+/2+)$, where $E(3+/*2+)$ is the excited-state reduction potential of the donor, E_{00} is the intersection of the donor absorption and emission spectra, and $E(3+/2+)$ is the ground-state reduction potential of the donor.

Photocleavage of DNA by Δ-Rh(phi)$_2$bpy^{3+}. The 180 bp fragment (Eco RI/PVU II) was isolated from pUC18 and 3'-^{32}P-end-labeled by standard protocols.[32] Labeled DNA was added to 20 μl samples containing Δ-Rh(phi)$_2$bpy^{3+} (10 μM), calf thymus DNA (500 μM bp) in a buffer of 5 mM tris, 50 mM NaCl, pH 8.5 in the presence or absence of Ru(II) complex. Samples were then irradiated at 313 nm with a 1000 W Hg/Xe lamp equipped with a monochrometer (~2 mW at 313 nm).[33] After irradiation, samples were dried and electrophoresed through a 20% denaturing polyacrylamide gel. The extent and sequence-dependence of photocleavage was quantitated by phosphorimagery (Imagequant).

2.3 Results

2.3.1 Binding of dppz complexes to DNA

The excited-state lifetimes have been determined for several complexes of the form M(L)$_2$dppz^{2+} in aqueous solution in both the absence and presence of B-DNA (Table 2.1). None of the derivatives given in Table 2.1 show significant steady-state luminescence in water, and this lack of emission serves as a sensitive assay for the purity of these complexes. Picosecond transient absorption spectroscopy indicates that the recovery of ground-state absorption occurs with lifetimes between 85 to 500 ps for Ru(II) and 10 to 30 ps for Os(II) without DNA. Ultrafast TCSPC confirms the kinetics observed by transient absorption spectroscopy, and it is noteworthy that the emission maxima occur at much lower energy in buffer than in DNA (<800 nm versus ~600 nm, respectively).[34]

Table 2.1 also reports the kinetics of luminescence decay for these complexes bound to DNA. DNA intercalation is shown to increase the lifetime of the excited state of

Table 2.1. Excited state lifetimes of photoexcited electron donors.

Donor[a]	aqueous solution[b] τ (ns)	% [d]	DNA[c] τ (ns)[e]	% [d]
Δ-Ru(phen)$_2$dppz^{2+}	0.25	97	160	80
			850	20
Λ-Ru(phen)$_2$dppz^{2+}			40	85
			150	15
rac-Ru(bpy)$_2$dppz^{2+}	0.21	95	100	90
			450	10
Δ-Ru(DMP)$_2$dppz^{2+}	0.11	96	30	80
			125	20
Δ-Ru(phen)$_2$(F$_2$-dppz)$^{2+}$			40	85
			280	15
rac-Ru(phen)$_2$(Me$_2$-dppz)$^{2+}$	0.085	8[f]	370	65
	0.49	50	1170	35
Δ-Os(phen)$_2$dppz^{2+}	0.0096	60[f]	1.5	75
	0.026	33	9.2	25
Δ-Ru(phen)$_2$dppz^{2+}, D$_2$O	0.56	96	400	75
			1240	25
Δ-Ru(phen)$_2$dppz^{2+}, poly(dA-dT)			120	75
			720	25
Δ-Ru(phen)$_2$dppz^{2+}, poly(dG-dC)			37	10
			280	90

[a] bpy = 2,2'-bipyridine, F_2-dppz = 7,8-difluoro dipyridophenazine, Me_2-dppz = 7,8-dimethyl dipyridophenazine, DMP = 4,7-dimethyl-1,10 phenanthroline. [b] Error in lifetimes is estimated to be $\leq$ 15%. [c] Error in lifetimes is estimated to be $\pm$ 10%. [d] The percentage indicates the magnitude of the preexponential factor in a biexponential fit; for aqueous solution data, there is a small residual offset. [e] The two excited state decays for bound species have been ascribed to two orientations of the intercalated dppz ligand within the base stack, which vary in their accessibility to solvent [see 11-14]. The excited state τs of Δ- and Λ-$Ru(phen)_2dppz^{2+}$ in the presence of DNA are sensitive to the metal/DNA ratio [see 12, 17]. [f] The observed biexponential decays probably reflect competing pathways for excited-state decay.

these complexes by three orders of magnitude. It has been reported that the emission lifetimes of $M(phen)_2dppz^{2+}$ complexes bound to DNA vary with the ratio of complex/DNA, and this sensitivity has been attributed to i) cooperative binding,[17] ii) self-quenching,[12] and iii) increasing rigidity in the DNA structure as a consequence of intercalation. We have found that the emission intensity of DNA-bound $Ru(phen)_2dppz^{2+}$ increases slightly when additional nonquenching, nonluminescent intercalators are added (data not shown). This observation supports the notion that Ru(II) emission is increased to due structural changes in DNA.

2.3.2 Emission quenching of Δ-$Ru(phen)_2dppz^{2+}$ by Δ-$Rh(phi)_2bpy^{3+}$

In Chapter 1, we described the static quenching of *rac*-$*Ru(phen)_2dppz^{2+}$ bound to DNA in the presence of the intercalating acceptor *rac*-$Rh(phi)_2phen^{3+}$.[3] When Δ-$Rh(phi)_2bpy^{3+}$ is added to Δ-$*Ru(phen)_2dppz^{2+}$ bound to DNA, a higher yield of static quenching is observed than with racemic complexes. Figure 2.2 presents two methods for plotting the time-resolved quenching data. The Stern-Volmer formalism[35] (Figure 2.1A) has been developed to characterize diffusion-controlled reactions, such as quenching of DNA-bound $*Ru(phen)_2dppz^{2+}$ by $Ru(NH_3)_6^{3+}$ (Chapter 1).[3] Plotting reaction efficiency as "fraction quenched" (Figure 2.2B) is particularly suitable for visualizing differences in quenching efficiency between two reactions and for comparing quenching titrations to transient absorption data and statistical analyses. Both types of plot provide the same information, however, and will be used interchangeably throughout this text.

Since nanosecond flash-photolysis measurements are unable to resolve the fast quenching of Δ-$*Ru(phen)_2dppz^{2+}$ by Δ-$Rh(phi)_2bpy^{3+}$, we attempted to monitor the quenching reaction on the picosecond time scale by TCSPC. However, Figure 2.3A shows that no change in the emission kinetics is observed when the quenching of Δ-*Ru(II) by Δ-Rh(III) is measured by TCSPC; instead, there is a large decrease in the luminescence intensity at zero time. This loss of intensity implies that emission quenching

Figure 2.2

Time-resolved emission quenching of Δ-$Ru(phen)_2dppz^{2+}$ by Δ-$Rh(phi)_2bpy^{3+}$ bound to a mixed sequence of DNA. A) Efficiency of quenching presented as a Stern-Volmer plot. Total intensity quenching (●) is much greater than quenching of the short emission lifetime (▲) or of the long emission lifetime (◆). B) Efficiency of quenching represented as the "fraction quenched." Plot includes intensity quenching (●), quenching of the short emission lifetime (▲), and quenching of the long emission lifetime (◆).

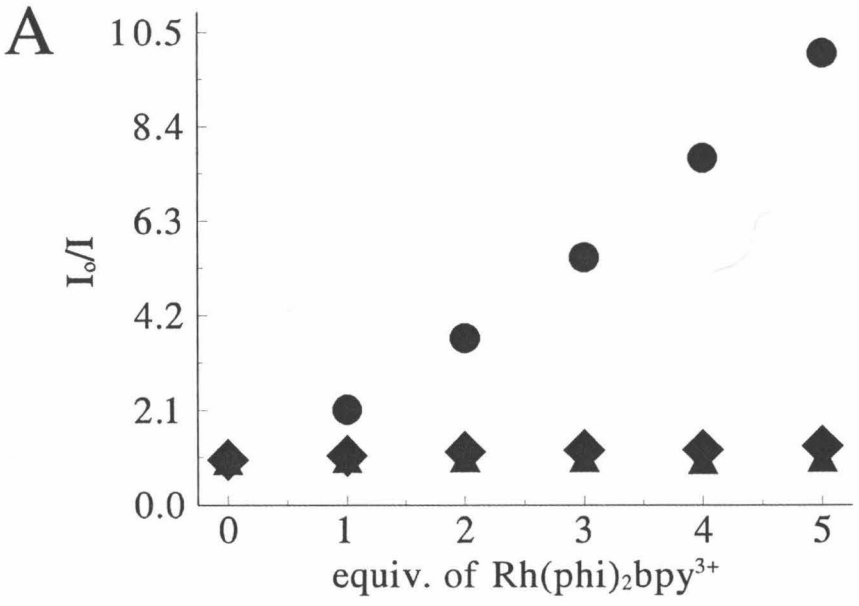
A
10.5
8.4
6.3
4.2
2.1
0.0
I_o/I
0
1
2
3
4
5
equiv. of $Rh(phi)_2bpy^{3+}$

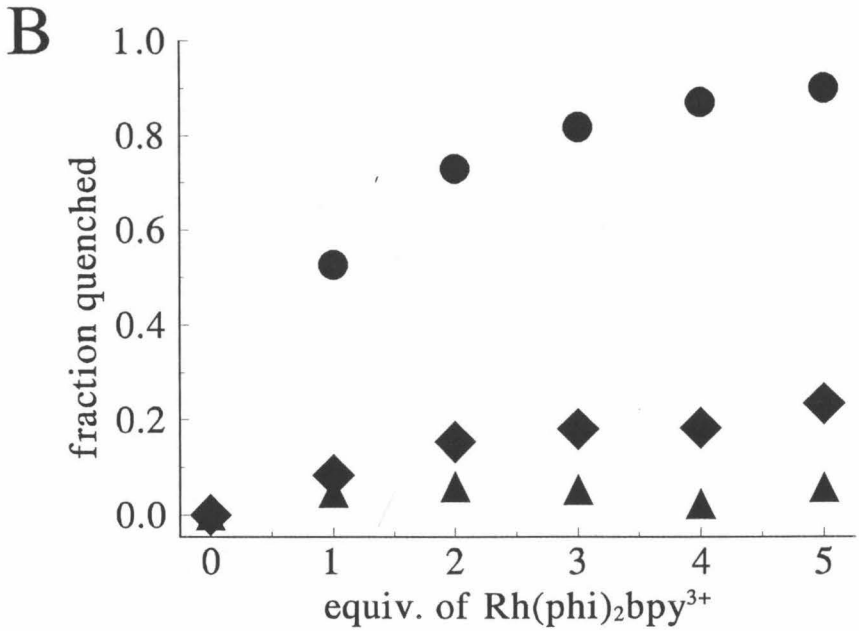
B
1.0
0.8
0.6
0.4
0.2
0.0
fraction quenched
0
1
2
3
4
5
equiv. of $Rh(phi)_2bpy^{3+}$

Figure 2.3

A) Time-resolved emission decays measured by time-correlated single photon counting (TCSPC), for Δ-*Ru (10 μM) bound to DNA (500 μM bp) in the presence of 0, 10, 20 μM Δ-Rh (bottom to top). IRF indicates the instrument response function. B) Fractional yields of the forward and recombination ET reactions. All measurements were done with 200 μl samples containing 10 μM Ru(II), 500 μM DNA bp, in an aerated buffer of 5 mM tris, 50 mM NaCl, pH 8.5. Steady-state (total) quenching determined by nanosecond laser flash photolysis (●); Quenching occurring with $k_{et} > 10^8\ s^{-1}$ (also measured by nanosecond laser flash photolysis) (◆); Quenching occurring with $k_{et} > 3 \times 10^{10}\ s^{-1}$ determined by picosecond TCSPC (×); Absorption recovery occurring with $k_{rec} = 9 \times 10^9 s^{-1}$ (▲). C) Time-resolved transient absorption data monitoring the ground-state recovery kinetics of Δ-$Ru(phen)_2dppz^{2+}$ bound to DNA as a function of Δ-$Rh(phi)_2bpy^{3+}$ concentration. From bottom to top: 0, 0.5, 1, 2, and 4 equiv Δ-Rh(III).

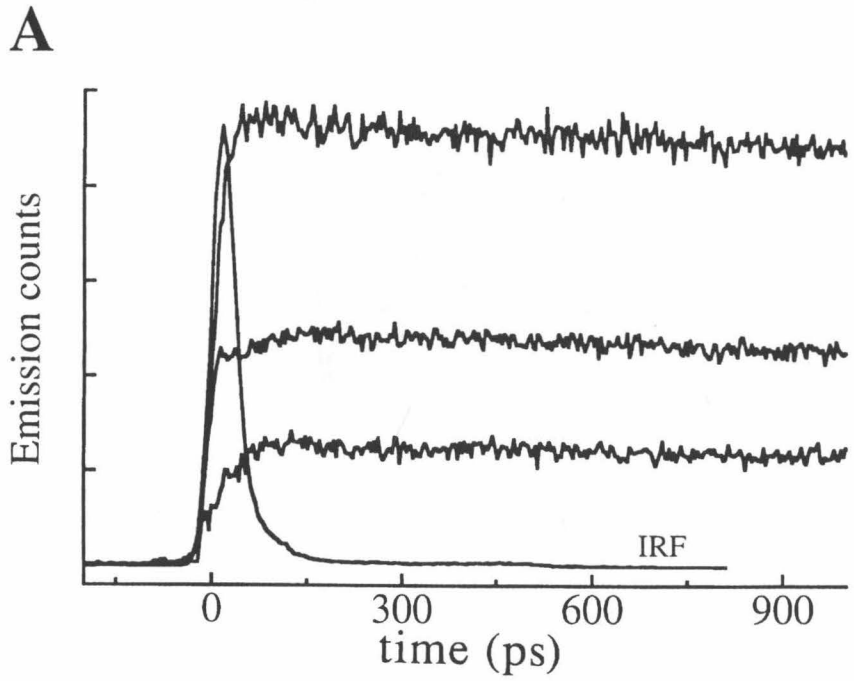

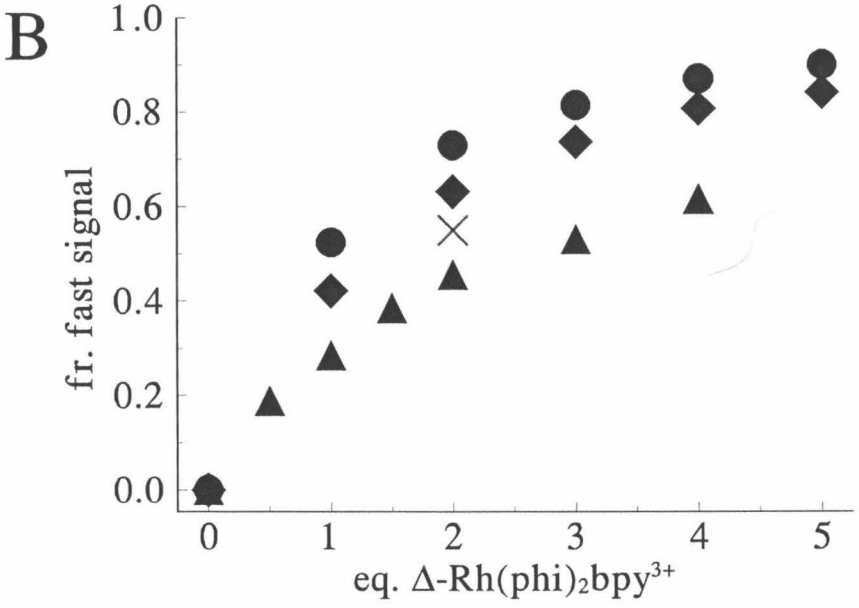
B
1.0
0.8
0.6
0.4
0.2
0.0
fr. fast signal
0
1
2
3
4
5
eq. Δ-Rh(phi)2bpy3+

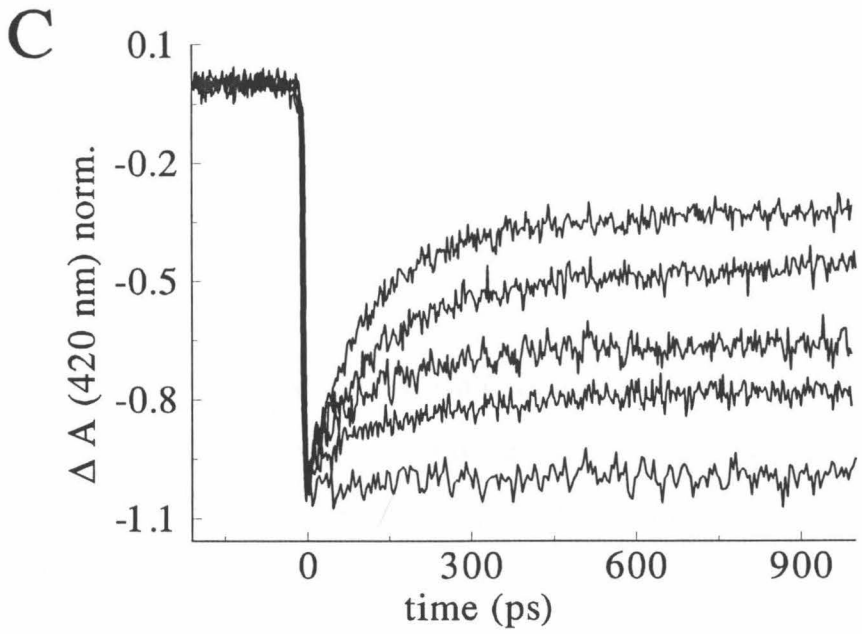
C
0.1
-0.2
-0.5
-0.8
-1.1
Δ A (420 nm) norm.
0
300
600
900
time (ps)

occurs faster than the time resolution of our instrumentation, so we assign a lower limit of ~3 x 10^{10} s^{-1} to k_{et} on the basis of the resolution of the TCSPC apparatus. Importantly, as the concentration of Δ-Rh(III) bound to DNA is increased, a corresponding decrease in the initial intensity is observed.

The fraction of excited states undergoing ET with $k_{et} > 3 \times 10^{10}$ s^{-1} is comparable to the total fraction of emission quenching observed by nanosecond laser flash photolysis (Figure 2.3B). Total, or steady-state quenching, is determined by integration of the full emission decay curves for nanosecond laser flash photolysis. The fraction of emission quenching that occurs faster than the 10-ns response of this instrument is revealed by the loss of initial intensity at zero time. These intensity losses are compared to the signal loss at zero time observed by picosecond TCSPC. It is noteworthy that TCSPC is primarily intended for kinetic measurements, and it is not an ideal technique for quantitating intensity losses. Nevertheless, the picosecond emission data reveals initial intensity losses comparable to those obtained by laser flash photolysis; moreover, no additional kinetic components were observed on the picosecond time scale. Thus, most of the quenching of Δ-Ru(II) by Δ-Rh(III) in DNA occurs with $k_{et} > 3 \times 10^{10}$ s^{-1} (Figure 2.3B). Because a small amount of reaction occurs on a timescale longer than 10 ns, there is a discontinuous distribution of photoinduced ET rates, composed of a substantial ultrafast component (with $k_{et} > 3 \times 10^{10}$ s^{-1}) and a smaller population with $k_{et} < 10^{8}$ s^{-1}.

2.3.3 Ground-state recovery of Δ-Ru(phen)$_2$dppz^{2+} bound to DNA

Picosecond transient absorption spectroscopy was used to follow the recovery of ground state absorption at 420 nm for DNA-bound Δ-Ru(phen)$_2$dppz^{2+} (Figure 2.3C). In the absence of quencher, the ground state absorption recovers on a time scale longer than 3 ns, consistent with the excited-state lifetimes of > 150 ns. (Table 2.1) As Δ-Rh(phi)$_2$bpy^{3+} is added to Δ-Ru(phen)$_2$dppz^{2+} bound to DNA, a fast component with k ~ 10^{10} s^{-1} is evident in the kinetics of ground-state recovery. The amplitude of this kinetic

component increases substantially with increasing Δ-Rh(III) concentration. A bleach in this absorption band of MLCT could indicate the presence of either excited-state donor or oxidized donor, or both.[11] TCSPC measurements, however, reveal that no quenching occurs with a rate constant of 10^{10} s^{-1} and that $k_{et} > 3 \times 10^{10}$ s^{-1} for the major component (Section 2.3.2). Therefore, the dynamics measured here by transient absorption spectroscopy correspond to decay of an ET intermediate, that is, Ru(III) + Rh(II) ---> Ru(II) + Rh(III).

Figure 2.3B correlates the yield of quenching with the yield of recovery of ground-state absorption ($\%_{rec}$). In order to quantitate the fraction of Ru(III) reacting to regenerate Ru(II) on this fast timescale, we have assumed that Δε at 420 nm is the same for both *Ru(II) and Ru(III).[36] If Δε is greater for *Ru(II) than for Ru(III), then Figure 2.3B gives the lower limit for $\%_{rec}$ which occurs on the picosecond time scale. This analysis also requires that Rh(II), formed in the initial ET reaction, does not contribute significantly to the size of the transient absorption signal for the ground-state recovery of M(II) (M = Ru, Os); this assertion has been validated by difference absorption spectra measured for Os(III) on the microsecond time scale.[12] The amplitude of fast recovery of ground-state absorption is therefore related to the fraction of M(III) reacting to regenerate M(II).

Since the fraction of fast absorption recovery is always less than the fraction of ultrafast emission quenching (Figure 2.2B), not all of the donor population quenched with high k_{et} also undergoes fast ($k_{rec} = 9 \times 10^9$ s^{-1}) back ET. For example, at 1 equivalent (equiv) Δ-Rh(III), the fraction of ultrafast quenching is 0.42, whereas the fraction of fast recombination is 0.28; therefore, at least 67% of the Ru(III)/Rh(II) intermediates react with $k_{rec} = 9 \times 10^9$ s^{-1}. No intermediate persists beyond the excited-state decay of unquenched Δ-*Ru(phen)$_2$dppz^{2+} ($t > 2$ μs); thus, the remaining ≤ 33% of intermediates react with 10^9 $s^{-1} > k_{rec} > 10^6$ s^{-1}. It is technically difficult to measure the recombination kinetics in this time window owing to interfering, spectrally similar signals from *M(II). For two other donors, however, transient intermediates have been observed on the microsecond

timescale,[11,12] and these long-lived ET products also might be generated in the ultrafast quenching process. Because recombination occurs on picosecond to microsecond time scales, the distribution of rates is wider for the recombination reaction than for the quenching reaction.

Regardless of whether the average loading of metal complexes is 1 in 33 bp or 1 in 10 bp, the fast dynamics exhibited by Δ-Ru(phen)$_2$dppz^{3+} are well described under all conditions by an exponential decay of 9.0 x 10^9 s^{-1} (Figure 2.4). The signal-to-noise ratio of the data does not allow one to distinguish between a single decay and a narrow distribution of rates centered at 10^{10} s^{-1}, but we see no evidence for kinetics other than this 10^{10} s^{-1} component for $t < 3$ ns. Because rates of ET typically decay exponentially with distance [$k \propto e^{-\beta R}$, were β = decay coupling parameter and R = distance],[37] a single rate suggests either that ET occurs over only one distance or that reaction occurs over a range of distances with a shallow distance-dependence (*vide infra*).

2.3.4 Solvent effects on recovery of ground-state absorption of Δ-Ru(II)

The rates of ground-state recovery were measured for Δ-Ru(phen)$_2$dppz^{2+} in buffered solutions of H_2O and D_2O. In the absence of DNA, the decay of the excited state is strongly solvent-dependent (k_H/k_D = 2.2) (Table 2.1). On the other hand, the recovery of ground-state absorption for Δ-Ru(III)+Δ-Rh(II) bound to DNA is not sensitive to the solvent isotope. These isotope effects, contrasted in Figure 2.5, indicate that the mechanism of excited-state decay does involve solvent whereas the recombination reaction in the presence of DNA does not.

2.3.5 Reactions of M(L)$_2$dppz^{2+} with Δ-Rh(phi)$_2$bpy^{3+} bound to DNA

We have characterized the reactivity of seven donor-acceptor pairs in mixed-sequence DNA by luminescence and transient absorption spectroscopy (Table 2.2). All donors are expected to bind tightly to DNA by intercalation, but complexes vary with

Figure 2.4

Recovery of ground-state absorption after photoexcitation for Δ-$Ru(phen)_2dppz^{2+}$ bound to DNA in the presence of 1 equiv (left) and 4 equiv (right) Δ-$Rh(phi)_2bpy^{3+}$. The plots show transient absorption data fit to the equation: $\Delta A(t) = \Delta A(t = 0)\ [\ f \exp(-k_1 t) + (1-f) \exp(-k_2 t)]$; fit residuals are displayed above the data. For the fits shown here, f = 0.28 and $k_2 = 4.0 \times 10^7\ s^{-1}$ for 1 equiv acceptor and f = 0.63 and $k_2 = 1.2 \times 10^8\ s^{-1}$ for 4 equiv acceptor; k_1 (= k_{rec}) was fixed at $8.7 \times 10^9\ s^{-1}$ in both cases. When not set, k_1 remains constant (± 15%) for each point in the titration.

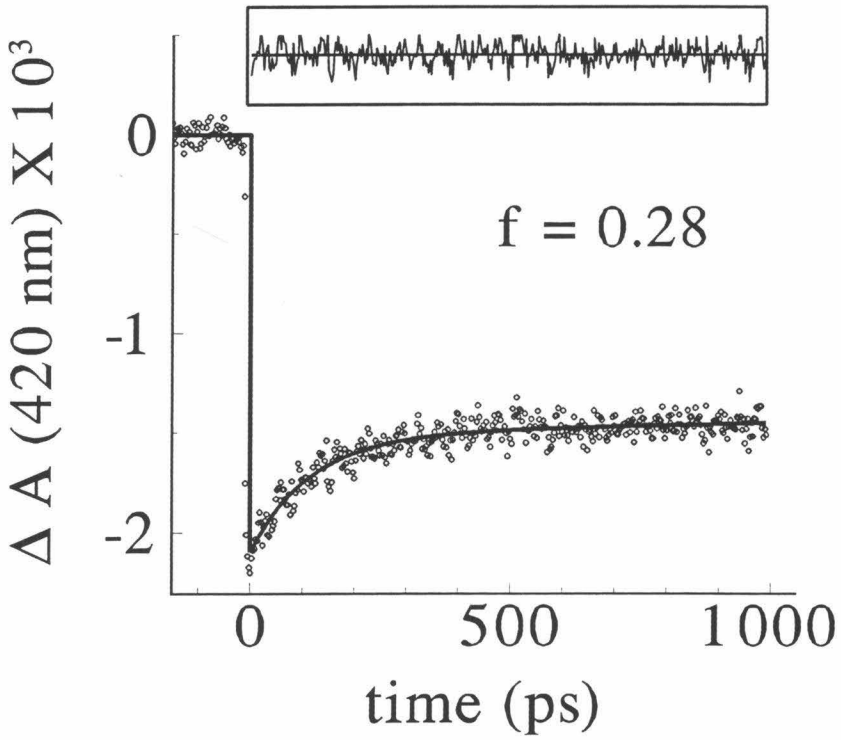
Δ A (420 nm) X 10^3
0
-1
-2
f = 0.28
0
500
1000
time (ps)

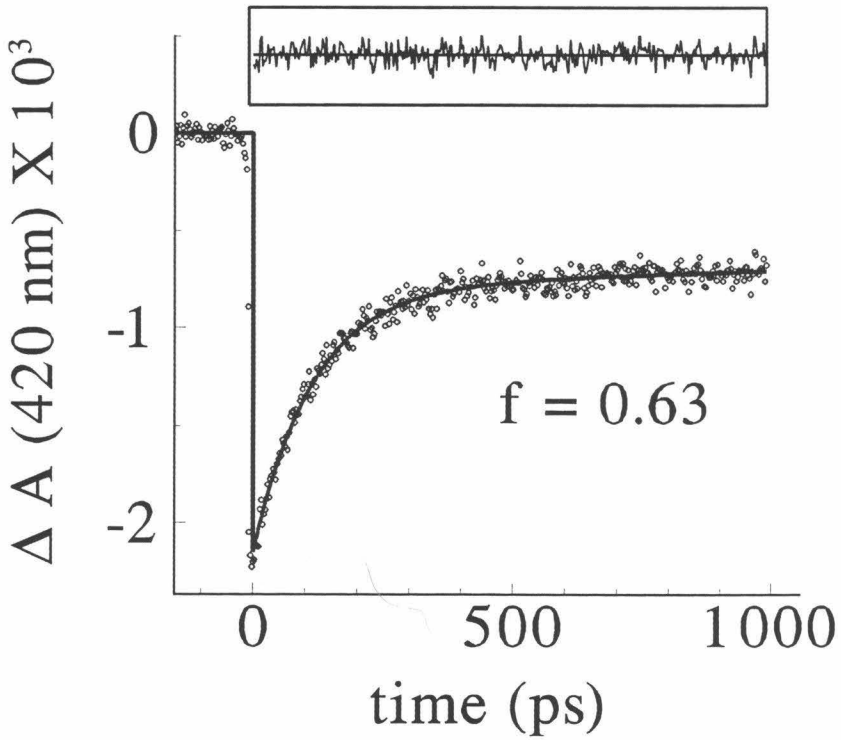
Δ A (420 nm) X 10^3
0
-1
-2
f = 0.63
0
500
1000
time (ps)

Figure 2.5

Time-resolved transient absorption data comparing the effect of D_2O on the recovery of ground-state absorption of *rac*-$Ru(phen)_2dppz^{2+}$ in an aqueous buffer of 5 mM tris, 50 mM NaCl, pH 8.5. A) 40 μM Ru(II) in aqueous solution. B) 20 μM Ru(II) bound to 1mM DNA bp and quenched by 60 μM Δ-$Rh(phi)_2bpy^{3+}$. Transient absorption trace in D_2O has been plotted with an offset of 0.1, so that both traces can be seen.

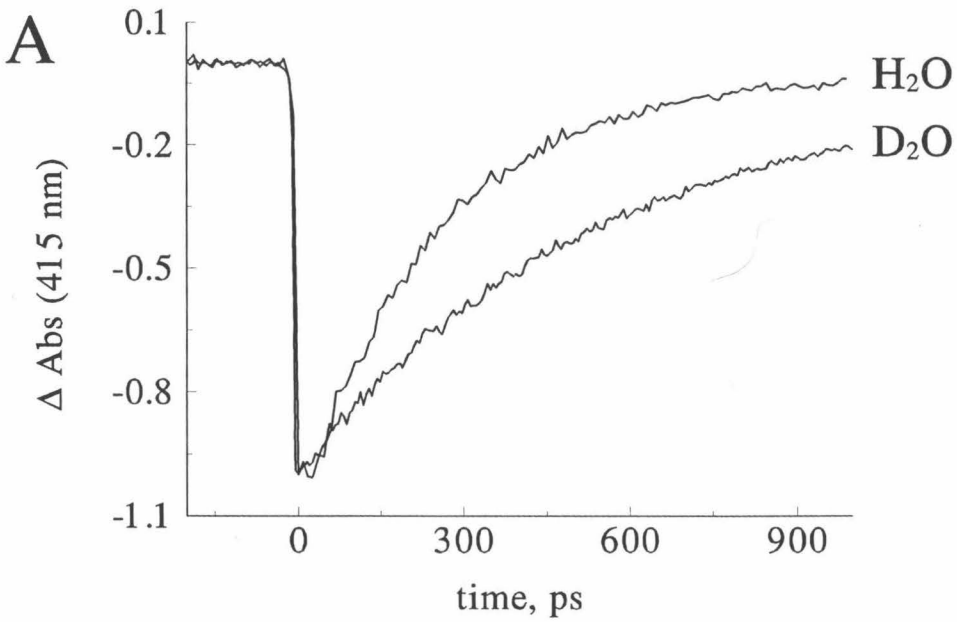
A
0.1
-0.2
-0.5
-0.8
-1.1
Δ Abs (415 nm)
0
300
600
900
time, ps
H2O
D2O

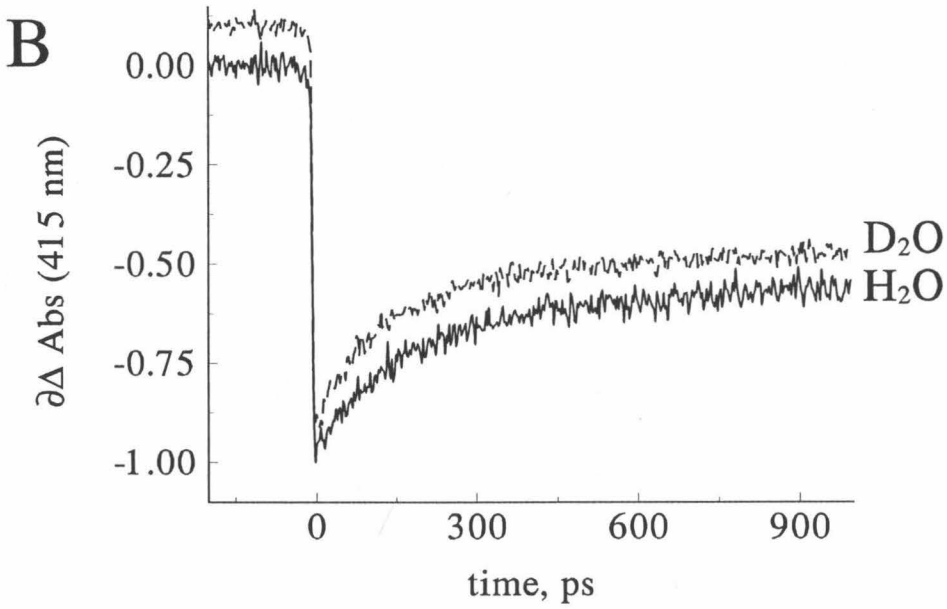
B
0.00
-0.25
-0.50
-0.75
-1.00
∂Δ Abs (415 nm)
0
300
600
900
time, ps
D2O
H2O

Table 2.2. Quenching and ground-state recombination (rec) of photoexcited electron donors bound to DNA.

Donor	k_{rec} (s^{-1})[a]	$\%_{quench}$[b]	$\%_{rec}$[c,a]	$-\Delta G^0$ quench (V)	$-\Delta G^0$ rec (V)
Δ - $Ru(phen)_2dppz^{2+}$	9.2 x 10^9	82	53	0.56	1.66
rac-$Ru(bpy)_2dppz^{2+}$	7.1 x 10^9	68	60[d]	0.52	1.69
Δ - $Ru(DMP)_2dppz^{2+}$	11 x 10^9	47	44	0.59	1.59
Δ - $Ru(phen)_2(F_2\text{-}dppz)^{2+}$	7.7 x 10^9	81	47	0.54	1.68
rac-$Ru(phen)_2(Me_2\text{-}dppz)^{2+}$	8.3 x 10^9	82	44	0.57	1.67
Δ - $Os(phen)_2dppz^{2+}$	11 x 10^9	80	64	0.73	1.21
Λ - $Ru(phen)_2dppz^{2+}$	4.5 x 10^9	43	20		
Δ - $Ru(phen)_2dppz^{2+}$, poly(dA-dT)	7 x 10^9		70		
Δ - $Ru(phen)_2dppz^{2+}$, poly(dG-dC)	2 x 10^8	50[e]	47[e]		

[a] The k_{rec} and $\%_{rec}$ values were obtained with Δ-$Rh(phi)_2bpy^{3+}$ as the electron acceptor, with λ_{exc} = 400 nm and λ_{obs} = 420 nm. Except where noted, samples contain 20 μM donor complex, 1 mM bp calf thymus DNA, in 5 mM tris, 50 mM NaCl, pH 8.5. Error in rates is estimated to be < 15%. [b] The $\%_{quench}$ represents the amount of total quenching at 3 eq Δ-$Rh(phi)_2bpy^{3+}$. Error in percentages is estimated to be ± 5%. [c] The $\%_{rec}$ values are the fraction of fast ground-state recovery at 3 eq Δ-$Rh(phi)_2bpy^{3+}$, as determined by the preexponential factors of a biexponential fit. Error in percentages is estimated to be < 10%. [d] At 20 μM metal complex, 500 μM base pairs calf thymus DNA, 60 μM quencher. [e] At 4 equiv quencher. k_{rec} and $\%_{rec}$ were measured at 67 μM metal complex, 1675 μM bp calf thymus DNA, 268 μM quencher.

respect to shape, hydrophobicity, and photophysical properties. Each $*M(L)_2dppz^{2+}$ shows emission quenching by Δ-Rh(III) on a < 10 ns timescale, and each donor-acceptor pair shows measurable recovery of ground-state absorption on the picosecond to nanosecond time scale. It is noteworthy that the rate constant for the fast component of ground-state recovery is independent of the donor-acceptor ratio, as was observed for reactions of Δ-$Ru(phen)_2dppz^{2+}$with Δ-$Rh(phi)_2bpy^{3+}$. Fast and efficient reactions between metallointercalators is thus found to be a general reaction; however, Table 2.2 indicates that there are some important differences in rates and efficiencies of ET as a function of donor (Section 2.3.6) and DNA sequence (Section 2.3.7).

Os(II) and Ru(II) show similar ET reactivity towards Δ-Rh(III). The steady-state quenching of Δ-$Os(phen)_2dppz^{2+}$ follows an identical profile[12] to that of its isostructural Ru(II) analog and TCSPC also indicates $k_{et} > 10^{10}\ s^{-1}$; recombination kinetics monitored by transient absorption spectroscopy are similar, but slightly faster ($k_{rec} = 1.1 \times 10^{10}\ s^{-1}$), for Os(III) than for Ru(III). Of the donors shown in Table 2.2, the most significant change in driving force is with Δ-$Os(phen)_2dppz^{2+}$ (~500 mV); this decrease, however, has only a small effect on k_{rec}. Figure 2.6 shows a typical titration of DNA-bound Δ-Os(II) with Δ-Rh(III) monitored by transient absorption spectroscopy. Due to the short excited-state lifetimes of Δ-$Os(phen)_2dppz^{2+}$, a significant fraction of the ground-state recovery is observable in the 3-ns time window. The shapes of the decay curves clearly change as a function of Rh(III); however, this change in curvature indicates an increase in the fraction of k_{rec} and not a change in the values of the intrinsic decay constants given in Table 2.1. Thus, the results with $Os(phen)_2dppz^{2+}$ show that an insensitivity of k_{rec} to loading still occurs when there is not a large difference between the intrinsic rate of excited-state decay and the rate of recombination.

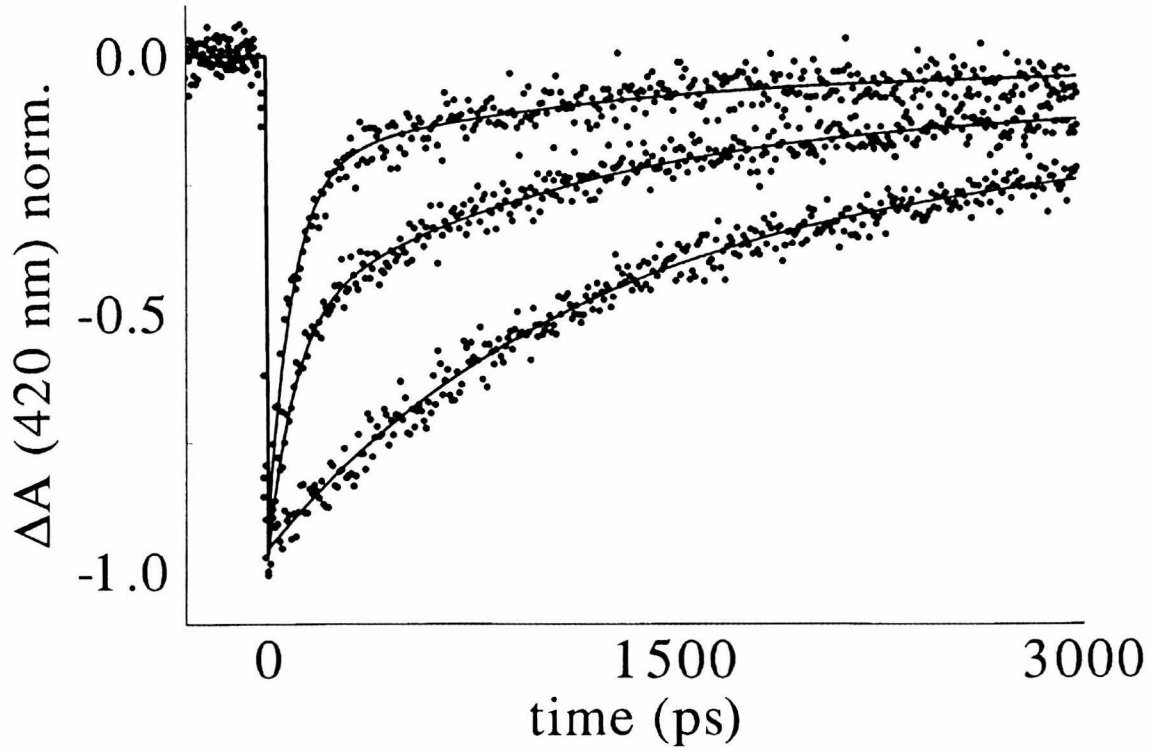

Figure 2.6

Time-resolved transient absorption data monitoring the ground-state recovery kinetics of Δ-Os(phen)$_2$dppz^{2+} (10 μM) bound to mixed-sequence DNA (500 μM bp) in the presence of increasing concentrations of Δ-Rh(phi)$_2$bpy^{3+}. From bottom to top: 0, 10, and 30 μM Rh(III). Fitting was performed analogously to Figure 3, except that k_1 = 1.1 x 10^{10} s^{-1}; again, when k_1 is not set, its value remains constant (± 15%) for each point in the titration. The rate constant k_2 = 7(1) x 10^8 s^{-1}, the shorter intrinsic decay constant of DNA-bound *Os(II); the longer decay constant for unquenched *Os(II), 1 x 10^8 s^{-1}, was incorporated into a constant offset.

Figure 2.7

A) Steady-state emission quenching of Δ-(●) and Λ-(▲) $Ru(phen)_2dppz^{2+}$ (20 μM) by Δ-$Rh(phi)_2bpy^{3+}$ in the presence of mixed-sequence DNA (1 mM bp). B) Time-resolved transient absorption data monitoring the ground-state recovery kinetics of enantiomers of $Ru(phen)_2dppz^{2+}$ bound to mixed-sequence DNA and quenched by enantiomers of $Rh(phi)_2bpy^{3+}$. Shown are Δ-Ru(II) quenched by Δ-Rh(III) (Δ/Δ), Λ-Ru(II) quenched by Δ-Rh(III) (Λ/Δ), and Λ-Ru(II) quenched by Λ-Rh(III) (Λ/Λ) at concentrations of 20 μM Ru(II), 1 mM DNA bp, 60 μM Rh(III).

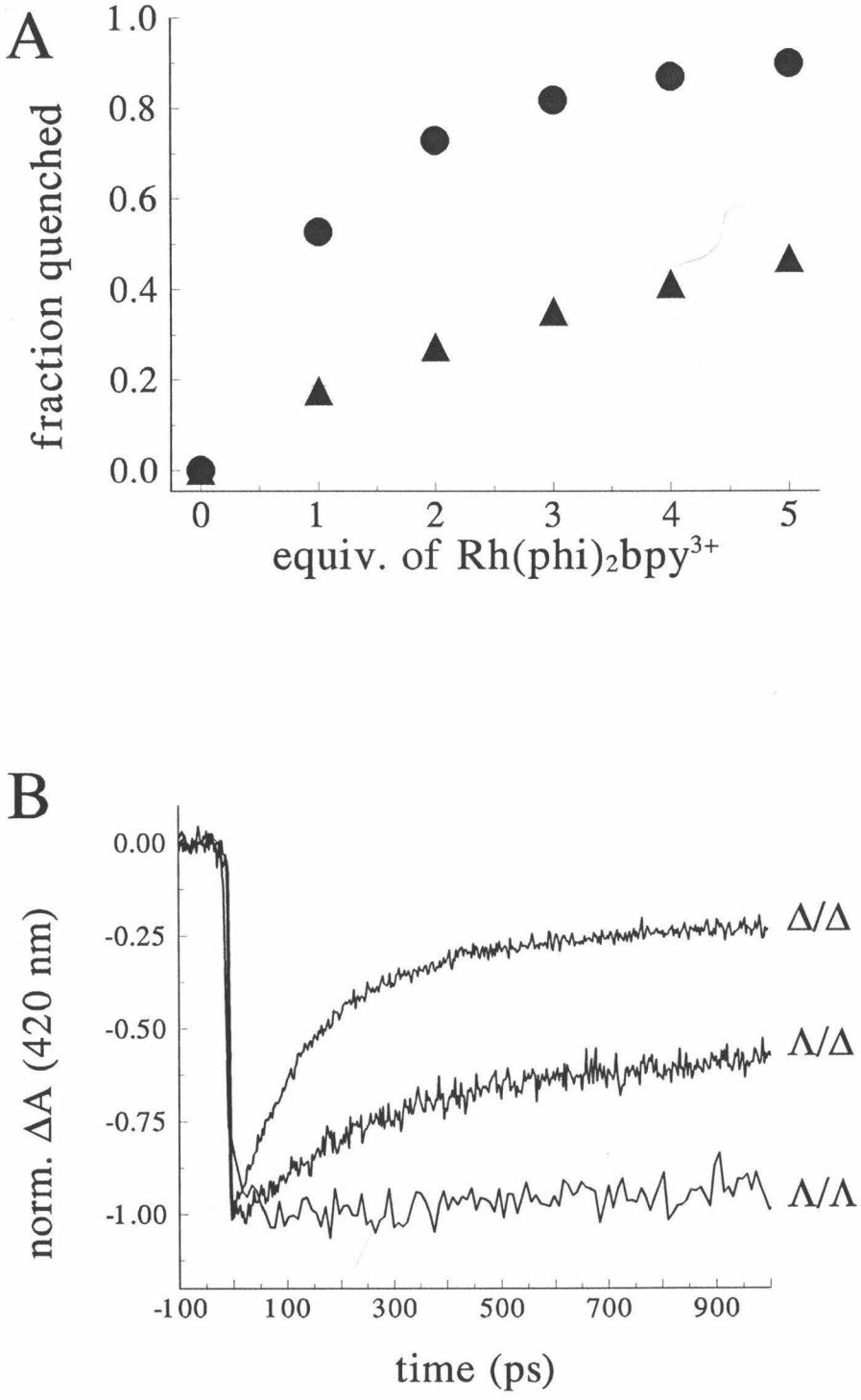
A
fraction quenched
1.0
0.8
0.6
0.4
0.2
0.0
0
1
2
3
4
5
equiv. of Rh(phi)2bpy3+
B
norm. ΔA (420 nm)
0.00
-0.25
-0.50
-0.75
-1.00
-100
100
300
500
700
900
time (ps)
Δ/Δ
Λ/Δ
Λ/Λ

2.3.6 Effect of enantiomers on ET rates

One of the striking results listed in Table 2.2 is the comparison of Δ-$Ru(phen)_2dppz^{2+}$ to Λ-$Ru(phen)_2dppz^{2+}$. Figure 2.7A shows that the Δ isomer bound to DNA is quenched by Δ-$Rh(phi)_2bpy^{3+}$ (3 equiv) twice as effectively as is Λ-$Ru(phen)_2dppz^{2+}$. The quenching profiles have been measured by nanosecond laser flash photolysis for the four diasteriomeric pairs of $Ru(phen)_2dppz^{2+}$ and $Rh(phi)_2bpy^{3+}$ in three DNA sequences [calf thymus, poly(dG-dC), and poly(dA-dT)]. In all cases, reactions between Δ-Ru(II) and Δ-Rh(III) are the most efficient, followed by Λ-Ru(II)/Δ-Rh(III) and Δ-Ru(II)/Λ-Rh(III) (data not shown). The recovery of ground-state absorption has been monitored on the picosecond time scale for Δ-Ru(II)/Δ-Rh(III), Λ-Ru(II)/Δ-Rh(III), Δ-Ru(II)/Λ-Rh(III), and Λ-Ru(II)/Λ-Rh(III). As shown in Table 2.2 and Figure 2.7B, k_{rec} is 9 x 10^9 s^{-1} for Δ-$Ru(phen)_2dppz^{2+}$ and 5 x 10^9 s^{-1} for the Λ isomer; the kinetics of back ET are therefore twice as fast for the Δ isomer. Furthermore, the recovery of ground state absorption of DNA-bound Λ-Ru(II) quenched by Λ-Rh(III) is much slower than for ET reactions with Δ-Rh(III) and thus the kinetics are highly sensitive to the chirality of the Rh(II) donor in the recombination reaction. This potentially important result should be described further by measuring the kinetics of reactions with Λ-Rh(III) on the nanosecond time scale. Importantly, the sensitivity of ET reactions to the Ru(II) and Rh(III) chirality is seen only in the presence of DNA,[38] underscoring the importance of intercalation on rates of DNA-mediated electron transfer.

2.3.7 Binding of Δ-$Rh(phi)_2bpy^{3+}$ in the presence of Ru(II) intercalators

The photocleavage assay developed for phi complexes of Rh(III) was used to determine the effect of Δ-$Ru(phen)_2dppz^{2+}$ and *rac*-$Ru(bpy)_2dppz^{2+}$ on the binding of Δ-$Rh(phi)_2bpy^{3+}$.[19,33] Irradiation of phi complexes of Rh(III) with UV light leads to abstraction of an H atom from the DNA sugar-phosphate backbone, causing direct cleavage of the DNA strand at the site of metal complex binding.[19] Figure 2.8 illustrates the

Figure 2.8

Gel electrophoresis measurements of DNA photocleavage by Δ-Rh(phi)$_2$bpy^{3+} . Shown are phosphorimager scans of a 180 bp, 3'-^{32}P-end-labeled DNA restriction fragment from pUC18 (Eco RI/PVU II). A) Photocleavage of 180 bp fragment with 10 μM Δ-Rh(phi)$_2$bpy^{3+} irradiated at 313 nm for 7 min in the presence and absence of 10 μM Δ-Ru(phen)$_2$dppz^{2+}. A) Photocleavage of 180 bp fragment with 10 μM Δ-Rh(phi)$_2$bpy^{3+} in the presence and absence of 10 μM *rac*-Ru(bpy)$_2$dppz^{2+}. The two sets of histograms represent different regions of the same 180 bp sequence. Data analyzed with ImageQuant software (Molecular Dynamics, Sunnyvale, CA).

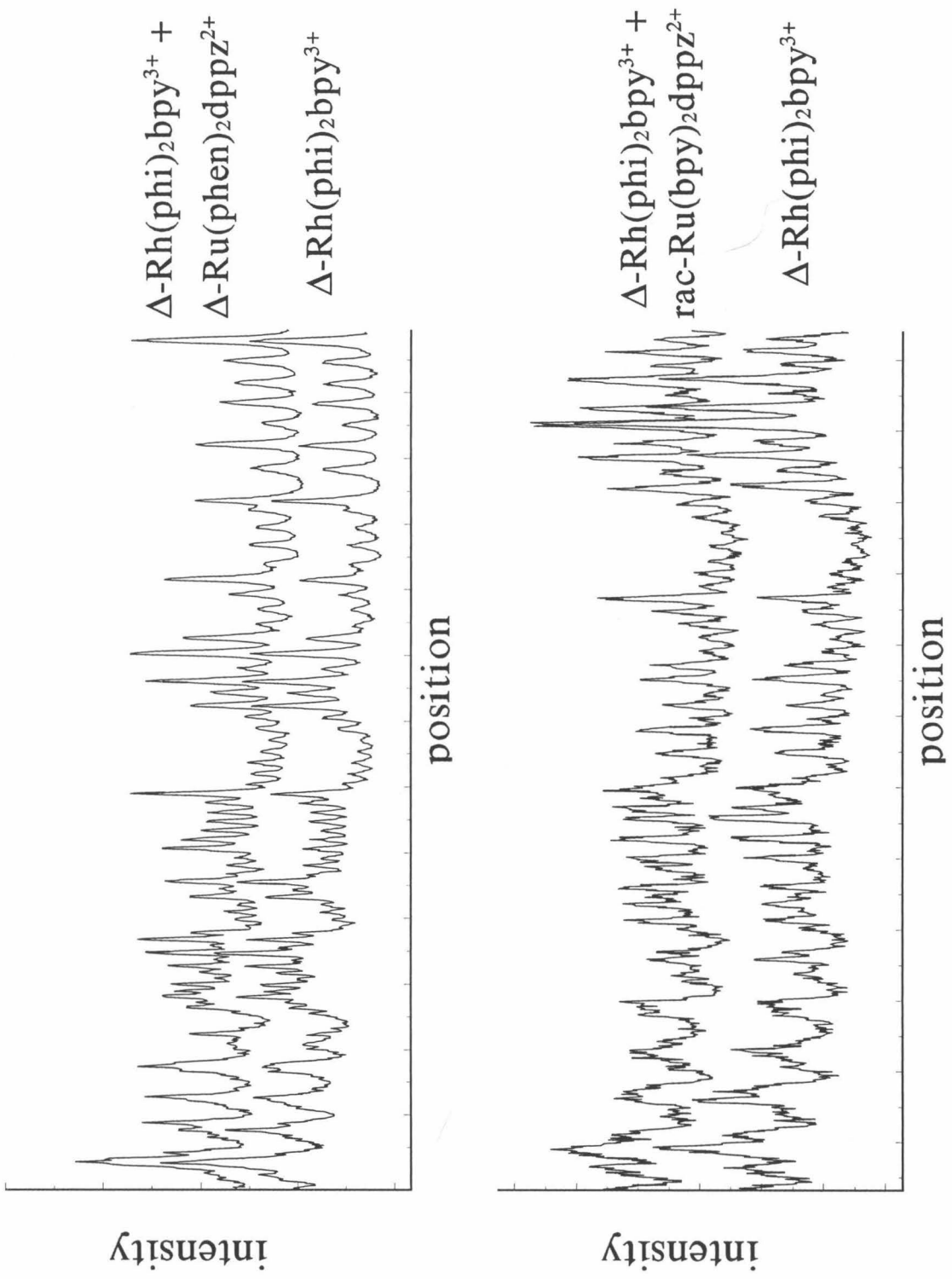
Δ-Rh(phi)2bpy3+ +
Δ-Ru(phen)2dppz2+
Δ-Rh(phi)2bpy3+
intensity
position
Δ-Rh(phi)2bpy3+ +
rac-Ru(bpy)2dppz2+
Δ-Rh(phi)2bpy3+
intensity
position

cleavage of a 180 bp DNA restriction fragment by Δ-Rh(phi)$_2$bpy^{3+}. In the absence of Ru(II) complexes, Δ-Rh(III) binds to this DNA strand at each base pair site, but not with uniform intensity. We expect the sequence selectivity of dppz complexes of Ru(II) also to be fairly low,[12,14] although recent experiments suggest that the binding constant is somewhat higher for Δ-Ru(phen)$_2$dppz^{2+} bound to AT over GC sequences.[39] In the case of nonselective binding by Ru(II), if Ru(II) and Rh(III) complexes bound cooperatively on the DNA, cleavage by Rh(III) at its preferred sites would become still more intense. If Ru(II) binds more selectively than Rh(III), on the other hand, cooperativity would lead to Rh(III)-induced cleavage of the DNA near preferred Ru(II) binding sites. Nevertheless, the characteristic cleavage pattern is unchanged in the presence of Δ-Ru(phen)$_2$dppz^{2+} or *rac*-Ru(bpy)$_2$dppz^{2+} (Figure 2.8), indicating that neither complex perturbs the binding of Δ-Rh(phi)$_2$bpy^{3+} under these conditions. Interestingly, cleavage of the 180 bp fragment by Δ-Rh(III) is sensitive to the salt conditions and shows a different pattern of photocleavage at 50 mM and 500 mM NaCl (data not shown). Light-initiated cleavage of DNA is thus a highly sensitive technique for measuring changes in DNA structure and DNA/metal complex interactions.

2.3.8 Rates of ET between intercalators bound to synthetic DNA polymers

Titrations were also carried out with poly(dA-dT) and poly(dG-dC) to determine the effect of sequence on the efficiency and rate of DNA-mediated ET. Transient bleach decays of Δ-Ru(phen)$_2$dppz^{2+} bound to poly(dA-dT) in the presence of Δ-Rh(phi)$_2$bpy^{3+} (Figure 2.9) show that the kinetics of the recombination reaction are similar (k_{rec} = 7 x 10^9 s^{-1}) to reactions in mixed-sequence DNA, but the amount of emission quenching is greater for the alternating A-T polymer (Table 2.2). In poly(dG-dC), however, k_{rec} is much reduced (2 x 10^8 s^{-1}) and emission quenching is less efficient [16% versus 70% for poly(dA-dT) at 1 equiv Rh]. TCSPC measurements indicate that the quenching reactions are faster than 3 x 10^{10} s^{-1} in both polymers. Thus, poly(dA-dT) serves as the best medium for ET, followed

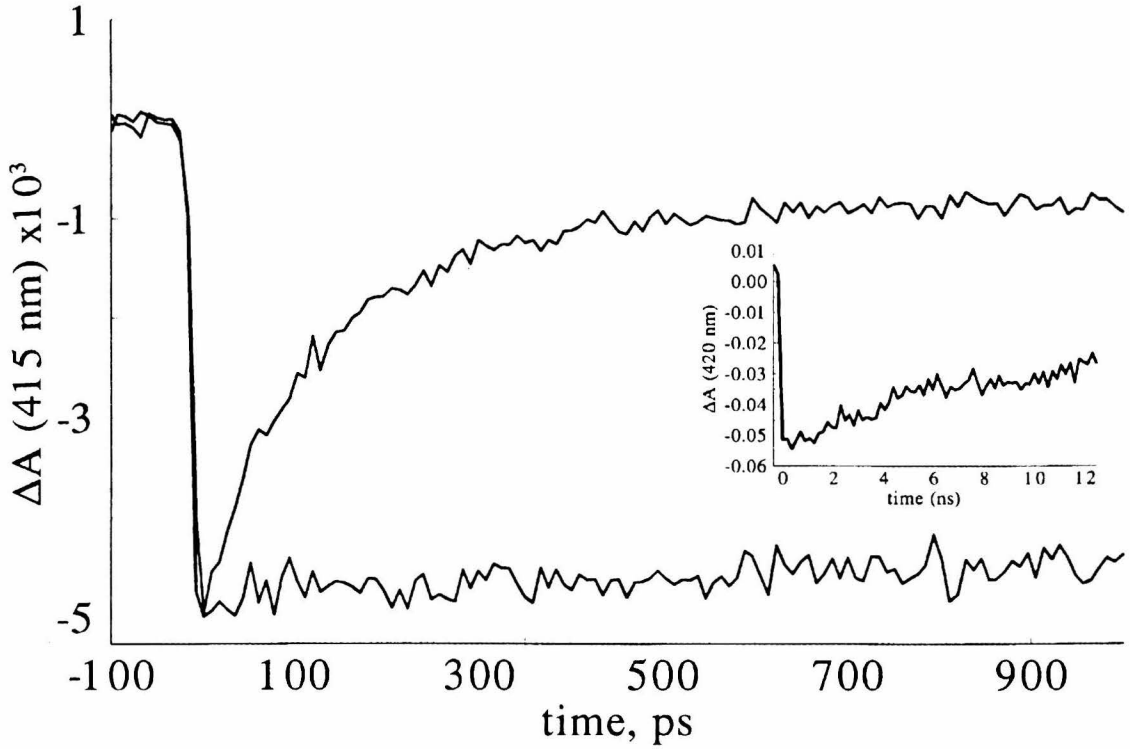

Figure 2.9

Recovery of ground state absorption of Δ-Ru(phen)$_2$dppz^{2+} (20 μM) bound to poly(dA-dT) (top trace) and poly(dG-dC) (bottom trace and inset) in the presence of Δ-Rh(phi)$_2$bpy^{3+}. As described in Table 2.2, for poly(dA-dT), k_{rec} = 7 x 10^9 s^{-1} (70% at 3 equiv); for poly(dG-dC), k_{rec} = 2 x 10^8 s^{-1} (45% at 4 equiv).

by mixed sequences and then poly(dG-dC). Recent studies with other polymers indicate that AT basepairs are necessary to observe high quenching efficiency.[39]

2.3.9 Quenching in an A-form duplex

After noting the strong dependence of B-DNA sequence on ET reactions, we began to investigate the importance of helical conformation. Figure 2.10A illustrates the three major conformations of DNA and RNA duplexes, viewed along the helical axis (InsightII). In B-form DNA, the π–stacked array runs down the center of the helix, with basepairs separated by 3.4 Å and stacked perpendicular to the long axis; this structure is well-suited for intercalation of metal complexes.[14,20,21] By contrast, the basepairs of the A-form helix are displaced from the helix axis by 4.5 Å and are tilted at an angle of 20° with respect to the long axis, resulting in a shallow major groove and deep, narrow minor groove which does not support intercalation of either $Ru(phen)_2dppz^{2+}$ or $Rh(phi)_2bpy^{3+}$.[21] While both arrays of bases are well-stacked, showing similar absorption hypochromicity and thermal stability, the *structure* of the π-stacks differ considerably.[40,41]

Figure 2.10B presents our approach towards studying ET reactions between complexes separated by an A-form duplex. Since RNA-RNA and RNA-DNA hybrids are known to form A-like structures, we constructed a chimeric duplex in which 12 bp of DNA-RNA hybrid is flanked on either end by 4 bp of B-form DNA duplex. Transition metals are expected to intercalate only in the B-form regions,[14,21] and should therefore be separated by the 12 bp of A-like helix (through-space distance ~31 Å).

Time-resolved luminescence measurements and photocleavage experiments indicate that Δ-$Ru(phen)_2dppz^{2+}$ and Δ-$Rh(phi)_2bpy^{3+}$ do indeed bind primarily to the B-form ends of this 20 bp chimera. The emission intensity and lifetimes of chimera-bound Δ-$Ru(phen)_2dppz^{2+}$ [760 ns (35%; 150 ns (65%)] are typical of B-DNA binding and distinct from the weak emission and short lifetimes seen in RNA duplexes [490 ns (20%) 80 ns (80%)].[14a] Binding of Δ-$Rh(phi)_2bpy^{3+}$ is monitored by gel electrophoresis (Figure

Figure 2.10

Schematic representation of ET reactions through an A-form helix. A) Three major conformations of DNA and RNA duplexes. Shown are A-form helix with DNA-RNA hybrid (left), B-form helix with DNA-DNA hybrid (center), and Z-form helix with poly(dG-dC) sequence (right). Helices were drawn in InsightII (MSI/Biosym) using canonical parameters. B) Illustration of DNA strand (top) hybridized to DNA-RNA chimeric strand (bottom) with Ru(II) and Rh(III) intercalated into predicted B-form regions. Bold sequence letters indicate RNA nucleotides; the 12 basepairs containing DNA-RNA hybrids are expected to have and A-like conformation.

A

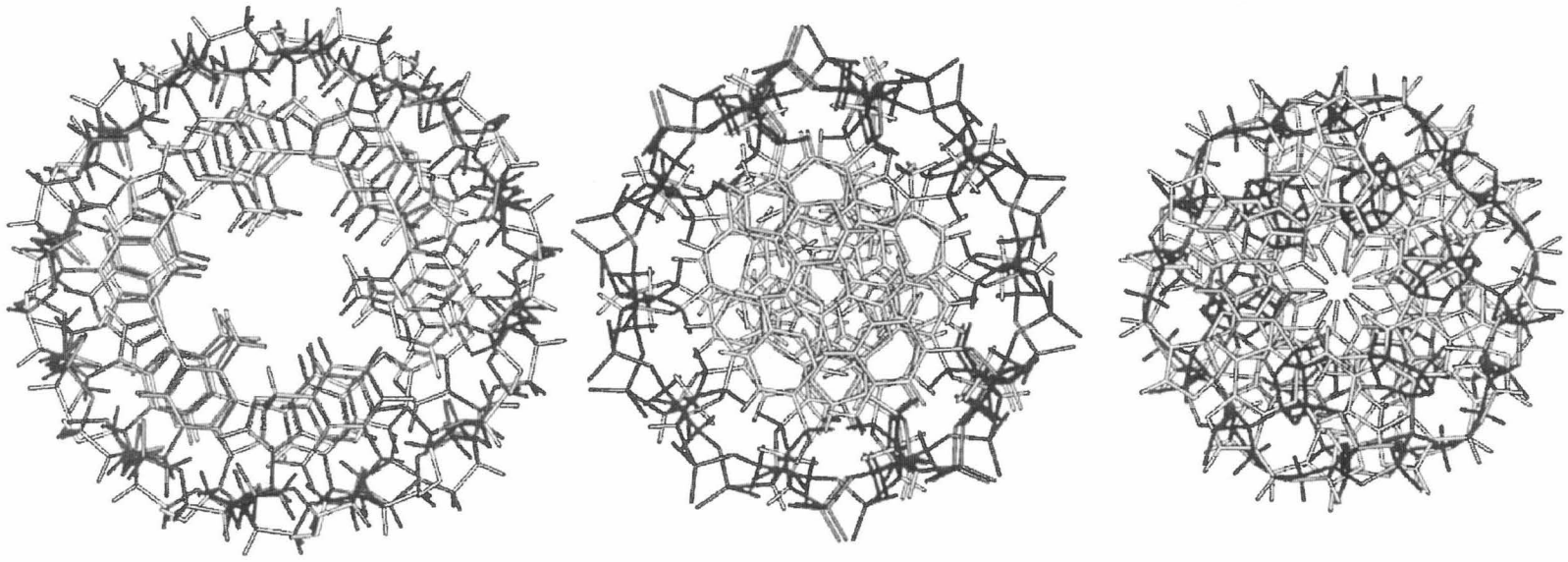

B

Figure 2.11

Autoradiogram after 20% denaturing polyacrylamide gel electrophoresis monitoring the binding sites of Δ-Rh(phi)$_2$bpy^{3+} in a DNA-RNA hybrid duplex. 5'-AGGAACCAGGCCTTCTATCT-^{32}P-3' was hybridized to the DNA-RNA chimeric complement 5'-d(AGAT)r(AGAAGGCCUGGU)d(TCCT)-3' (10 μM duplex), incubated with Δ-Rh(III), and irradiated at 313 nm. Samples shown are as follows: lanes 1 and 2, Maxam-Gilbert sequencing reactions C+T and G, respectively; lane 3, ^{32}P-DNA-RNA + 10 μM Rh(III) without irradiation; lane 4, ^{32}P-DNA-RNA irradiated for 20 min; lanes 5-7, ^{32}P-DNA-RNA + 20 μM Rh(III), irradiated for 20, 10, 5 min, respectively; lanes 8-10, ^{32}P-DNA-RNA + 10 μM Rh(III), irradiated for 20, 10, 5 min, respectively; lanes 11-13, ^{32}P-DNA-RNA + 5 μM Rh(III), irradiated for 20, 10 5 min, respectively.

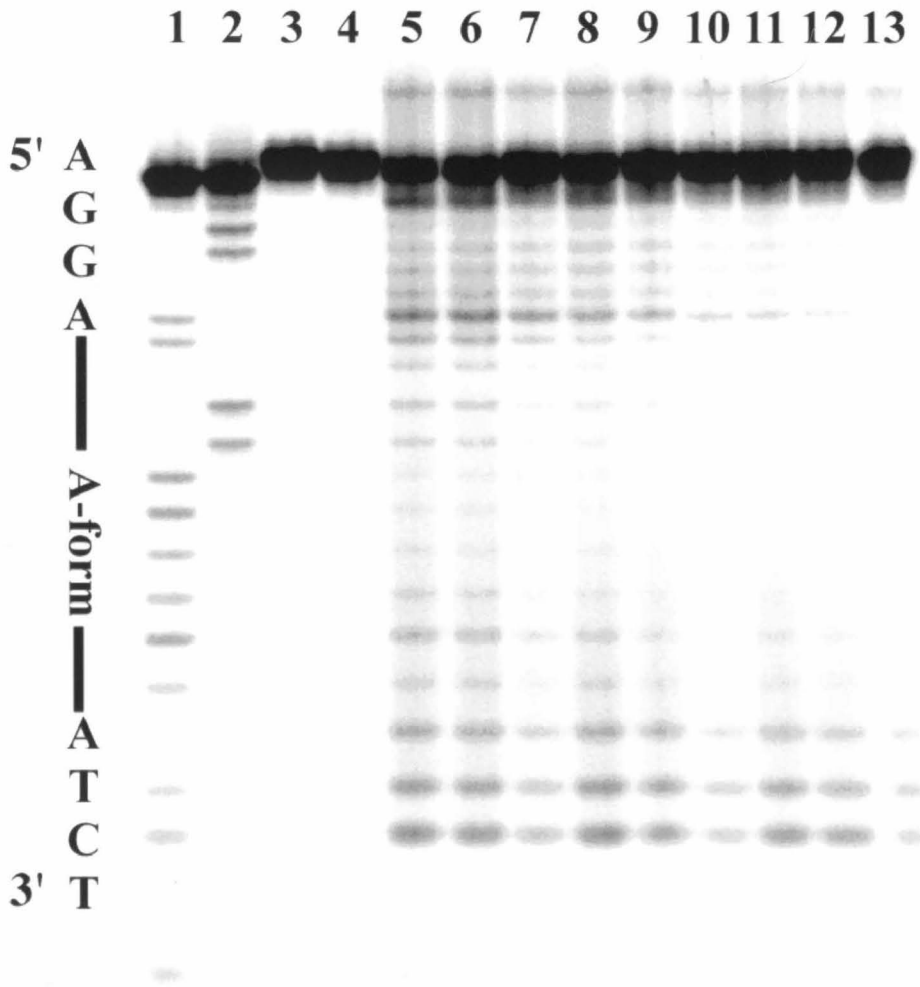
1 2 3 4 5 6 7 8 9 10 11 12 13
5'
A
G
G
A
A-form
A
T
C
T
3'

Figure 2.12

Time-resolved emission quenching of Δ-Ru(phen)$_2$dppz^{2+} bound to the DNA-RNA hybrid duplex shown in Figure 2.10B and quenched by Δ-Rh(phi)$_2$bpy^{3+}. A) Stern-Volmer plot showing steady-state quenching of Δ-Ru(II) (1 equiv) as a function of quencher concentration (0 - 1 equiv) bound to 2 μM (●), 5 μM (▲), and 10 μM (◆) DNA-RNA hybrid duplex. B) Emission lifetimes of Δ-Ru(II) (1 equiv) as a function of quencher concentration (0 - 1 equiv) bound to 2 μM (●), 5 μM (▲), and 10 μM (◆) DNA-RNA hybrid duplex. Quenching is shown to be primarily static by the upward-curving Stern-Volmer plots, small changes in emission lifetimes, and independence of quenching on absolute concentration.

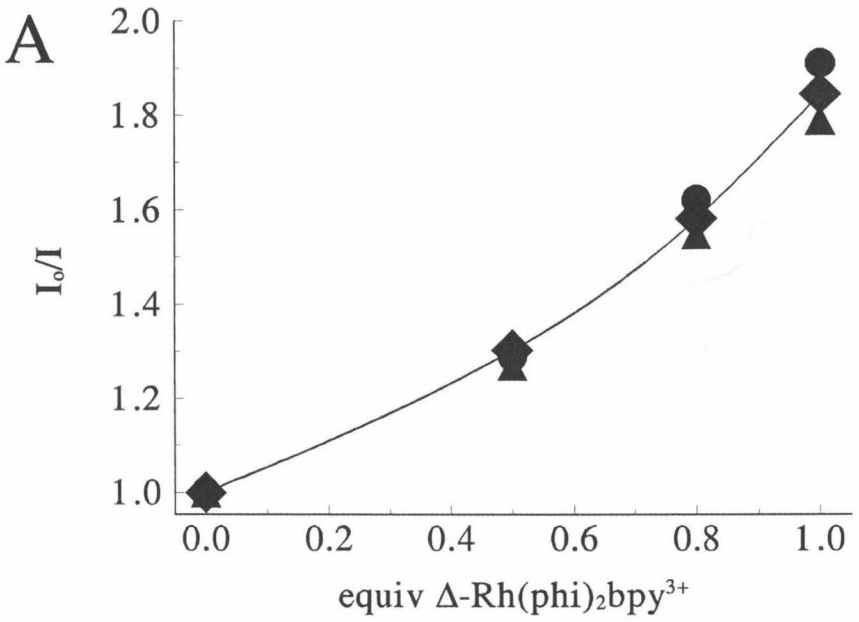
A
2.0
1.8
1.6
1.4
1.2
1.0
I_o/I
0.0
0.2
0.4
0.6
0.8
1.0
equiv Δ-Rh(phi)$_2$bpy^{3+}

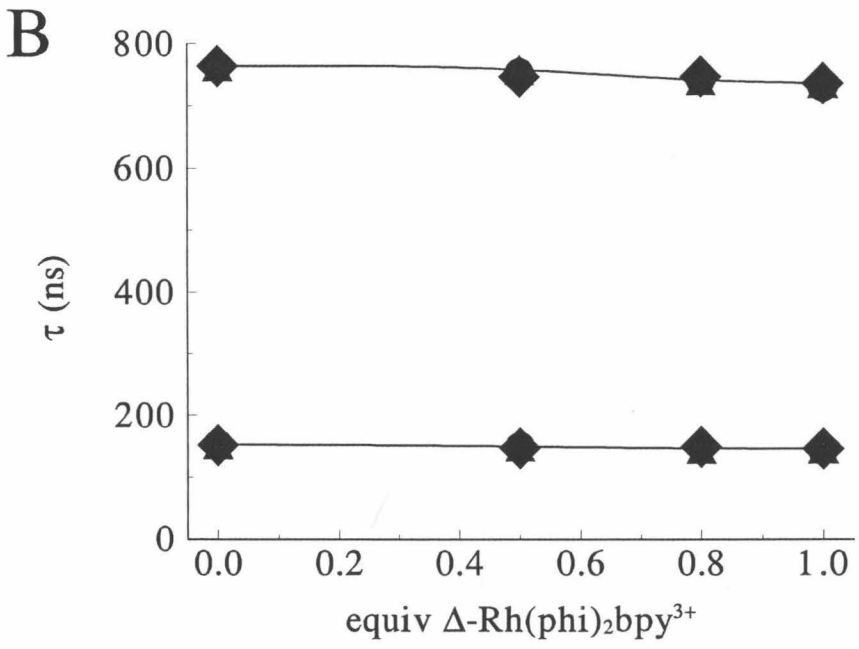
B
800
600
400
200
0
τ (ns)
0.0
0.2
0.4
0.6
0.8
1.0
equiv Δ-Rh(phi)$_2$bpy^{3+}

33% of Δ-Ru(II) emission is quenched; comparing this reaction efficiency to the 50% quenching of Δ-Ru(II) by Δ-Rh(III) seen in calf thymus DNA indicates that a significant amount of ET still occurs in the presence of an A-form helix. Moreover, the binding data suggests that reactions occur over a long distance, through the 12 bp of DNA-RNA hybrid. Finally, preliminary results on ultrafast timescales indicate that the recovery of Ru(II) ground-state absorption is too slow to measure within a 3-ns time window, and is therefore much slower for the chimera than for complexes bound to B-DNA. It will be very interesting to further explore the effect of helical conformation through additional spectroscopic measurements and by preparing tethered systems (Chapter 4)[4] in which intercalators are separated by B- or A-form helices.

2.4 Discussion

2.4.1 Excited-state lifetimes of dppz complexes in H_2O versus DNA

Previous studies have reported that dppz complexes of Ru(II) and Os(II) show no steady-state luminescence in aqueous buffer in the absence of DNA.[11,14] However, the true enhancement in excited-state lifetime afforded by DNA intercalation had not been quantitated. Using ultrafast transient absorption spectroscopy and TCSPC, we have measured the excited-state lifetimes for several complexes in H_2O, D_2O, and DNA (Table 2.1). Emission lifetimes are shown to increase by three orders of magnitude upon the addition of B-form DNA.

Inhibition of excited-state proton transfer has been proposed as the mechanism for this remarkable luminescence enhancement.[34] The kinetics obtained by TCSPC agree with transient absorption data, supporting the notion that both are measuring the fast decay of *M(II). However, the emission maxima for Ru(II) complexes in aqueous solution are red-shifted by > 250 nm compared to emission in organic solvents and DNA. Both observations can be explained by excited-state proton transfer from solvent to $dppz^{\bullet -}$, a strong base generated by excitation of MLCT.[34] This hypothesis is also supported by the

large solvent isotope effect observed in the recovery of ground-state absorption of $Ru(phen)_2dppz^{2+}$ in H_2O *versus* D_2O ($k_H/k_D = 2.2$). Moreover, proton-transfer quenching of $Ru(phen)_2dppz^{2+}$ has been shown to be sensitive to the intercalative binding mode of the complex in DNA.[42] Thus, the remarkable "light switch" property described for dppz complexes of Ru(II) and Os(II) results from the protection of the intercalating dppz ligand from proton transfer. It is not yet clear whether the different excited-state lifetimes for $M(L)_2dppz^{2+}$ in H_2O can be attributed to differences in the basicity of the $dppz^{\bullet-}$ in each complex.

2.4.2 Mechanism of DNA-mediated reactions

Several lines of evidence indicate that quenching occurs by ET. First, the thermodynamics for photoinduced ET are quite favorable, with $\Delta G^0 > 0.5$ V for all donors discussed (Table 2.2). Second, time-resolved transient absorption experiments indicate that the rate of ground state recovery of DNA-bound Δ-$Ru(phen)_2dppz^{2+}$ in the presence of Δ-Rh(III) ($k_{rec} \approx 1 \times 10^{10}$ s^{-1}) is more than twice as fast as that of $Ru(phen)_2dppz^{2+}$ in water ($k_d \approx 4 \times 10^9$ s^{-1}) without DNA (Table 2.1). This result argues against displacement of intercalated Ru(II) complexes by Rh(III) complexes, where the excited state would simply be quenched by water outside of the DNA. The other donors listed in Tables 2.1 and 2.2 show similar differences in transient absorption data in the presence and absence of DNA. Third, the striking similarities of both the quenching efficiencies[12] and recombination kinetics for Δ-$Ru(phen)_2dppz^{2+}$ and Δ-$Os(phen)_2dppz^{2+}$ rules out energy transfer as a quenching mechanism, since the red-shifted emission of Δ-*Os(II) eliminates spectral overlap between donor emission and acceptor absorption.[35] Most importantly, the ~10^{10} s^{-1} phase observed by transient absorption is slower than the quenching (> 3×10^{10} s^{-1}), and both of these processes increase concomitantly with increasing rhodium concentration. These facts strongly indicate that we are monitoring photoinduced ET by

TCSPC and the recombination of electron transfer intermediates by picosecond transient absorption spectroscopy.

Furthermore, comparison of reactions in H_2O and D_2O indicate that ET is mediated by the DNA helix. Steady-state emission measurements show no solvent isotope effect in the efficiency of quenching,[38] whereas a pronounced effect would be expected for a diffusion-controlled reaction. Furthermore, transient absorption data (Figure 2.5) indicate that no solvent-isotope effect is seen in the kinetics of back ET, whereas a strong isotope effect ($k_H/k_D \approx 2.2$) has been observed for quenching of Ru(II) by H_2O in aqueous solution (Figure 2.5), in acetonitrile,[14a] and in DNA.[38] Thus, water does not directly participate in the electron-transfer reaction.

2.4.3 Effect of donor

The difference in quenching and recombination of diasteriomeric pairs of $Ru(phen)_2dppz^{2+}$ and $Rh(phi)_2bpy^{3+}$ is striking. Quenching is twice as efficient for Δ-$Ru(phen)_2dppz^{2+}$ than for the Λ isomer, and the rate of recombination is approximately twice as fast (Figure 2.7). Furthermore, while the quenching profile for Λ-$Ru(phen)_2dppz^{2+}$ and Λ-$Rh(phi)_2bpy^{3+}$ is similar to Λ-Ru(II) quenched by Δ-Rh(III), the rate is much slower for the recombination of Δ-Ru(III) and Λ-Rh(II). These differences are not likely to be due to changes in K_b, as picosecond transient absorption data for all three reactions are inconsistent with displacement of Ru(II) complexes by Rh(III). Additionally, ΔG for reactions should be similar between diasteriomeric pairs. The greater access of H_2O to the DNA-bound Λ enantiomers will have some effect on ET reorganization energies,[37] but these effects are likely smaller than differences in ΔG noted between other donors in Table 2.2.

The changes in ET reaction efficiency and kinetics for Δ- and Λ-Ru(II) mirror the emission intensity of these two DNA-bound donors in the absence of quencher. Proton transfer between the dppz ligand and H_2O is a major pathway for nonradiative decay of

*$Ru(L)_2dppz^{2+}$;[14,34] therefore, the emission lifetimes of DNA-bound $Ru(L)_2dppz^{2+}$ reflect the degree of protection of the intercalated dppz ligand from solvent. The longer lifetimes observed for Δ-$Ru(phen)_2dppz^{2+}$ relative to Λ-$Ru(phen)_2dppz^{2+}$ indicate that the right handed isomer is more deeply stacked between the DNA bases, consistent with the symmetry matching between chiral metallointercalators and the right-handed double helix.[25]

We propose that intercalation of Δ-Ru(II) and Δ-Rh(III) permits electronic coupling between the complex and the DNA π-stack, thereby promoting efficient ET.[38] Futhermore, Figure 2.13 indicates that a correlation between emission lifetime and quenching efficiency is found for several of the donors characterized in Section 2.3.5. The graph in Figure 2.13 includes all $Ru(L)_2dppz^{2+}$ quenching studies listed in Table 2.2 and therefore incorporates the effects of donor structure, chirality, and DNA sequence. Additional work is required to define the relationships among DNA binding, emission decay, and ET chemistry; nevertheless, these general correlations support the hypothesis that intercalation provides electronic access to the DNA π-stack.

2.4.4 Effect of DNA sequence

Poly(dA-dT) is found to be a much more efficient medium for ET than poly(dG-dC). This sensitivity to sequence further indicates that ET proceeds through the DNA and is not a function of van der Waals contact between bound intercalators, since the same ET rates are expected if the donor and acceptor are in physical contact. Thus, even at the nearest available intercalation site, the interaction distance through DNA is 10.2 Å, the neighbor-excluded distance.[43] Neither the integrity of the DNA duplex nor the binding affinity of the metal complexes can account for the difference in quenching rates. From the photocleavage study, Δ-$Rh(phi)_2bpy^{3+}$ binds to all DNA sites with little preference for AT- or GC-rich regions, and is thus bound to both polymers at the concentration range studied. Both alternating polymers are B-form, although poly(dA-dT) is considered more flexible;[44]

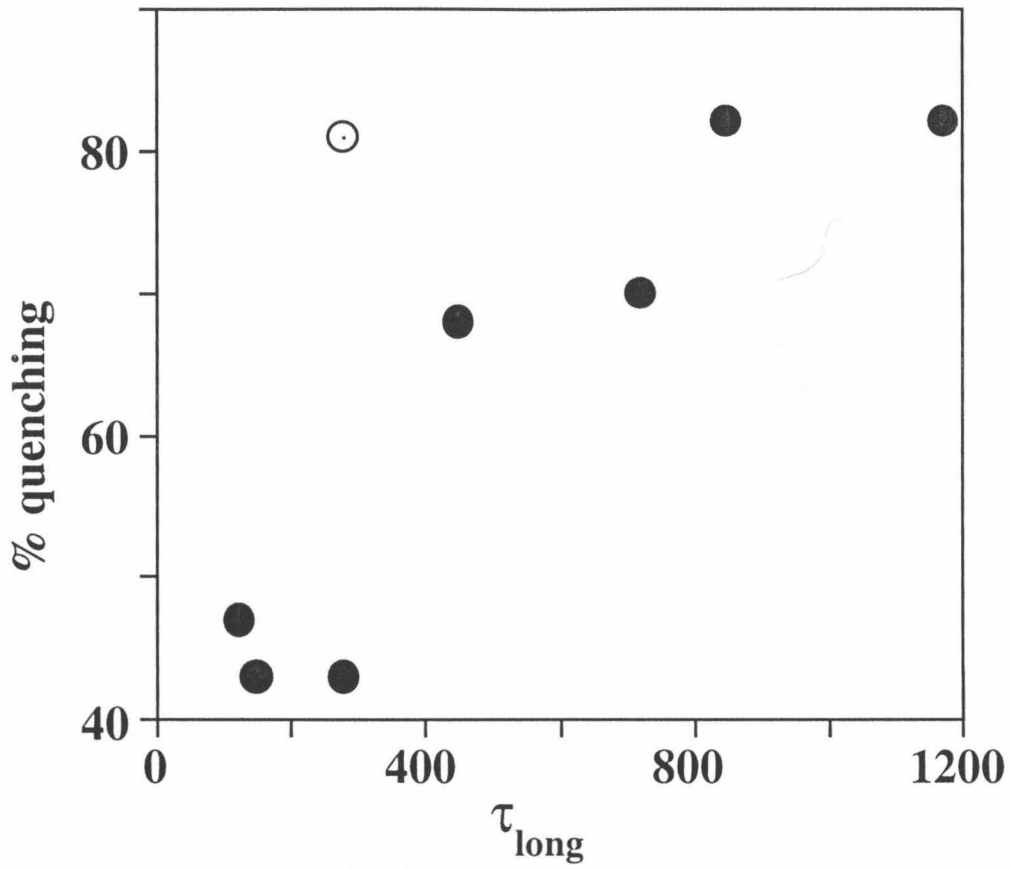

Figure 2.13

Plot showing the correlation between the long excited-state lifetime (t_{long}) of $Ru(L)_2dppz^{2+}$ bound to DNA in the absence of quencher and the efficiency of quenching (% quenching) at 3 equiv Δ-$Rh(phi)_2bpy^{3+}$. Data taken from Tables 2.1 and 2.2. With the exception of Δ-$Ru(phen)_2(F_2\text{-}dppz)^{2+}$ (○), complexes with long luminescence lifetimes are also most efficiently quenched. Note that different enantiomers and DNAs are included in the correlation.

theoretical studies suggest that this flexibility may play a role in facilitating reactions through the π-stack.[45]

It is likely, however, that stacking interactions between metallointercalators and base pairs vary between polymers. For example, the emission lifetimes of Δ-Ru(II) bound to poly(dA-dT) and poly(dG-dC) are very different (Table 2.3), indicating the different environments of the intercalated metal complex. Furthermore, recent data suggests that Δ-Ru(II) binds with higher affinity to poly(dA-dT) than to poly(dG-dC);[39] it is noteworthy that Δ-Ru(II) bound either to poly(dA-dT) or to a mixed-sequence of DNA gives similar excited-state lifetimes, quenching efficiencies, and recombination rates (Table 2.2). These observations could indicate that ET is most efficient when complexes are bound at A-T sites in the mixed sequence, and that the difference in ET efficiencies is due to initial coupling of the donor with the DNA medium.

Finally, it is interesting to consider ET reactions through an A-form duplex in the context of stacking interactions. Quenching in this system is nearly as efficient as in B-form DNA (Figure 2.12), but the recombination reaction seems to be much slower. Reaction rates might be governed by the conformation at the B-A junction, and perhaps changes in sequence and structure constitute "defect boundaries" at which the electronic coupling is altered. It is noteworthy that Baguley and co-workers have also observed more efficient electron-transfer quenching in poly(dA-dT) than in poly(dG-dC) in their studies with ethidium bromide and amsacrine;[5] additionally, a recent theoretical study has found that the electronic coupling factor ß is smaller for A-T sequences than for G-C steps.[8b] Thus, DNA sequence and intercalator/DNA binding interactions are important characteristics of DNA-mediated ET.

2.4.5 Loading independence of k_{rec}: two models

For all donors studied, the rate of recombination of M(III)+Rh(II) is insensitive to the concentration of Rh(III) intercalators on DNA (Figure 2.4). Figure 2.1B emphasizes

that, throughout most of the titration, intercalators are dilute on the double helix and the amounts of photoinduced ET observed are too great to be accounted for by nearest neighbors. For random binding of Ru(II) and Rh(III) complexes, 2% of the Ru(II)-Rh(III) pairs are nearest neighbors at 0.5 equiv Δ-Rh(III), yet 20% of Δ-Ru(III) complexes show rapid ground-state recovery at this loading in mixed-sequence DNA. Similarly, 16% of Ru(II)-Rh(III) pairs are in closest contact at 4 equiv Δ-Rh(III), where 60% of molecules return to the ground state with $k_{rec} = 9 \times 10^9\ s^{-1}$. The fast quenching of *M(II) is also likely simple first order at times < 10 ns. If the early time ET kinetics were not first-order and the rates decayed with an exponential distance dependence,[37] we should have observed some slower components (10^{10} to $10^8\ s^{-1}$). Thus, neither the quenching nor the transient absorption data are consistent with ET over discrete, multiple distances related by an exponential decay with distance.

Two results show conclusively that the single recombination rate observed for ET reactions in the mixed sequence of DNA is not due to oxidation of a proximal base by the oxidized donor M(III). First, since guanine is the most easily oxidized base,[46] the rate of ground-state recovery would have been faster in poly(dG-dC) than in poly(dA-dT); however, the opposite trend is observed. Second, the loading independent rate of $k_{rec} \sim 10^{10}\ s^{-1}$ is also observed for $Os(phen)_2dppz^{3+}$, which has an insufficient reduction potential to react with guanine.[47] Therefore, instead of direct oxidation of the DNA, we will consider two binding models to describe the insensitivity of the recombination rate to Rh(III) concentration: i) clustering of donors and acceptors on the helix and ii) distance-independent ET over a finite distance.

2.4.5.1 Cooperative binding

A cooperative donor-acceptor binding model leading to a high concentration of nearest neighbor pairs could account for the observation of a single recombination rate for the reaction of Δ-Ru(II) with Δ-Rh(III) in a mixed sequence of DNA.[31b] However, this

model would require a cooperative binding energy of 1.5 kcal/mol to predict the efficiency of the ultrafast quenching process at low loading of Rh. The highly cooperative binding of cationic metallointercalators on DNA has been observed thus far only for Δ-Rh(4,4'-diphenylbpy)$_2$phi^{3+} (K = 2.0 kcal/mol).[48] The large and hydrophobic phenyl substituents on this Rh(III) complex allow intermolecular contact of the ancillary ligands. By contrast, the ancillary ligands on the molecules used here do not permit a significant amount of π-overlap or hydrophobic contact between adjacent molecules. We have also done two types of experiments to identify clustering. The data in Chapter 3 indicates that no clustering is seen in the quenching kinetics when Ru(phen)$_2$dppz^{2+} and Rh(phi)$_2$bpy^{3+}are bound to SDS micelles, where clustering has been seen for other donor-acceptor pairs.[38,49] Also, the photocleavage assay (Figure 2.9) provides no evidence for Δ-Ru(phen)$_2$dppz^{2+} or *rac*-Ru(bpy)$_2$dppz^{2+} influencing the binding of Δ-Rh(phi)$_2$bpy^{3+} to DNA. While a cooperative binding model cannot be definitively ruled out in an experiment with noncovalently bound donors and acceptors, these studies provide no evidence for direct contact of these metallointercalators.

Without direct contact, an interaction resulting in one donor-acceptor distance is difficult to rationalize. Structural studies have shown that intercalation of similar Ru(II) and Rh(III) complexes cause only a local unwinding of the double helix.[14,18] Indeed, the observed sequence dependence to ET indicates that recombination does not involve reactants in direct van der Waals contact. Such direct contact could not explain the > 30 fold difference in recombination rate observed for poly(dG-dC) and poly(dA-dT). Thus, even at closest approach, ET proceeds through the DNA over a nonbonded distance of 10.2 Å.

It is also important to note that no modelling has been done for the other titrations described. For example, since the quenching of Λ-Ru(II) by Δ-Rh(III) and reactions in poly(dG-dC) show very different reaction kinetics from the modeled system, it is necessary to understand these experiments in the same context as ET between Δ isomers bound to a

mixed sequence of DNA. Thus, the clustering hypothesis has not been shown to adequately describe the complete set of data presented here.

2.4.5.2 ET mediated by stacking interactions

Alternatively to the clustering hypothesis, it is possible that ET is mediated by the DNA over some distance without a significant decrease in rate. In this context, it is important that a loading-independence in k_{rec} is observed when the ancillary ligands, the intercalating ligand, the metal center, and even the chirality of the donor is varied. While there does not seem to be a relationship between the shape of the donor and the reaction efficiency, as might be expected for cooperative binding, there is a reasonable correlation between the depth of intercalation and ET kinetics.

A model including long-range DNA-mediated ET is consistent with several results obtained in our laboratory. Chapter 1 summarizes the fast quenching of $Ru(phen')_2dppz^{2+}$ by $Rh(phi)_2(phen')^{3+}$ when these intercalators were covalently tethered to opposite ends of a 15 bp oligonucleotide duplex.[4] Recently, ET reactions between tethered ethidium and $Rh(phi)_2(bpy')^{3+}$ were monitored as a function of distance, from 24 to 37 Å; for all distances, a component of fast ET quenching ($> 10^{10}$ s^{-1}) was observed.[50] Furthermore, long-range hole transfer has been detected in three different experiments in which the DNA itself acts an an electron donor.[51-54] Long-range ET in such systems, where 5'-GG-3' and thymine dimers are oxidized by electron-poor metallointercalators, are analogous to the ground-state recombination reaction between electron-rich Δ-$Rh(phi)_2bpy^{2+}$ and the potent oxidant $M(L)_2dppz^{3+}$.

Spectroscopic data do indicate, however, that while the fast *rates* of recovery are independent of loading, the *yields* of ET reactions depend strongly on the concentration of Rh(III) quencher. Thus, rapid long-range ET is precluded for some of the *M(II) population. Importantly, increasing the concentration of acceptor leads to an increase in the subnanosecond component of both the forward and reverse ET reactions. To describe the

increasing yield of ET, we have considered a "sphere-of-action" model in which reactions are static within some donor-acceptor separation and very slow outside this interaction distance. Such a model has been formulated to describe static quenching in two- and three-dimensions by Perrin.[55,56] Considering DNA as a one-dimensional lattice, the Perrin equation can be written

$$I_o/I = e^{VC_A};\ V = 2R_o.$$

The quenching of Δ-Ru(II) by Δ-Rh(phi)$_2$phen^{2+} is well-fit by this model, which gives an interaction distance R_o of 35Å.[1b] We have also attempted to apply a simple statistical model to the fraction of the fast component ($k_{rec} \sim 10^{10}$ s^{-1}) observed by transient absorption spectroscopy. The distribution of donors and acceptors is calculated and the probabilities of donor-acceptor distances are fit to the experimental yields of fast ground-state recovery. For the reaction of Δ-Ru(II) and Δ-Rh(III) in a mixed sequence of DNA, the fraction of the fast component at low concentrations of quencher suggests a reaction range of 20 bp. However, the predicted interaction distance becomes shorter as the loading of Δ-Rh(III) increases. This attenuation of fast ET could be due to increased deformation of the DNA helix as intercalators are added; additionally, the noted sequence-dependence to DNA-mediated ET could indicate that populating G-C sites at higher loadings reduces ET efficiency.

A sphere-of-action model is plausible from a physical standpoint. The stacking interactions responsible for the stability of the helical structure of DNA are weak, noncovalent forces. The π-stack is therefore a dynamic system in which the basepairs open, tilt, and unstack.[44b,57,58] It is possible that the subpopulation of unquenched donors is decoupled from acceptors by such transient defects in base stacking. The probability of this decoupling should increase exponentially with increasing donor-acceptor separation. Recent work with tethered ethidium-DNA-Δ-Rh(phi)$_2$(bpy')$^{3+}$ assemblies has demonstrated excellent agreement with this model over a distance range of 24 to 37 Å.[50]

Thus, if DNA-mediated ET is sensitive to electronic coupling along the base stack, limits to the distance of long-range ET are expected.

2.4.6 Theoretical approaches

Our results suggest that ET through DNA occurs on the picosecond time scale over a through-space distance of >10 Å. These results need to be understood in the context of theory and other experimental observations. Pathway calculations for ET by a superexchange mechanism[59] have been valuable in describing protein-mediated ET (with $0.8\ Å^{-1} < \beta \leq 1.4\ Å^{-1}$).[60] However, an analogy between DNA and σ-bonded pathways for ET could not explain the results obtained here unless one assumes a weak distance dependence ($\beta < 0.2\ Å^{-1}$) for the π-stacked medium. The rate reported for an 8 bp oligonucleotide bearing metal complexes unstacked and coordinated to the sugar-phosphate backbone[8] could be understood by a pathway model in which the σ-system limits access to the π-stack. A hopping model in which the individual bridge elements are transiently oxidized or reduced has been useful in describing conductivity in stacked π-systems in the solid state,[10] and may be applicable for DNA as well.[61] Other theories incorporate a small probability of thermal access of the electron to delocalized bridging states in the DNA,[45,62] thus permitting ET through an adiabatic channel. More experimental data are needed before the distance dependence of ET through DNA will be well understood,[63] and our work indicates that theoretical models must take into account the sensitivity of ET parameters to π-stacking interactions.[7,38,64]

2.4.7 Future work

The spectroscopic studies presented in this chapter suggest several avenues for future investigation. In particular, preliminary transient absorption data indicate that recombination rates depend strongly on the chirality of the Rh(III) acceptor, the sequence of DNA, and the conformation of the oligonucleotide duplex. To characterize these

reactions in detail, a laser apparatus able to monitor reactions between 50 ps and 50 ns is required. The function of helical conformation in DNA-mediated ET reactions is another critical, and very interesting, issue. Future experiments could utilize tethered intercalators to compare B- and A-form oligonucleotides of the same sequence. Finally, we have proposed that stacking interactions permit this fast ET chemistry, yet "stacking" has remained a difficult parameter to quantify. Emission lifetimes of $M(L)_2dppz^{2+}$ complexes and degrees of absorption hypochromicity provide two qualitative handles; thermodynamic descriptions of π-stacking are currently under investigation.[65]

2.5 Conclusions

Electron-transfer reactions between metallointercalators are found to be remarkably sensitive to the DNA bridge which connects the electron donor to the acceptor. Time-resolved experiments monitoring the quenching of intercalated *M(II) by Δ-$Rh(phi)_2bpy^{3+}$ and the subsequent reverse electron transfer indicate rate processes on the picosecond and microsecond timescales for both reactions. The picosecond transient absorption data reveal reactions which follow simple-first-order kinetics on the order of $k_{rec} \sim 10^{10}\ s^{-1}$. This observation could suggest cooperative binding of intercalators on DNA and/or an insensitivity to the distance separating the reactants over the concentration range investigated. Additionally, the increases in quenching and recombination yield with increasing quencher indicate that reactions occur over a finite distance. Importantly, despite the insensitivity of recombination rate to the ratio of acceptor/DNA, both the forward and back electron transfer reactions are remarkably sensitive to the nature of the π-stack and donor/acceptor binding geometry.

2.6 References

1. For recent reviews, see a) Arkin, M. R.; Jenkins, Y.; Turro, N. J.; Barton, J. K. *Adv. Chem. Ser.* **1995**, *246*,449. b) Stemp, E. D. A.; Barton, J. K. *Metal Ions in Biology* **1996**, *33*, 325. b) Meade, T. J. *Metal Ions in Biology* **1996**, *32*, 453.
2. a) Barton, J. K.; Kumar, C. V.; Turro, N. J. *J. Am. Chem. Soc.* **1986**, *108*, 6391. b) Purugganan, M. D.; Kumar, C. V.; Turro, N. J. Barton, J. K. *Science* **1988**, *241*, 1645.
3. Murphy, C. J.; Arkin, M. R.; Ghatlia, N. D.; Bossmann, S.; Turro, N. J.; Barton, J. K. *Proc. Nat. Acad. Sci., USA*, **1994**, *91*, 5315.
4. Murphy, C. J.; Arkin, M. R.; Jenkins, Y. C.; Ghatlia, N. D.; Bossmann, S.; Turro, N. J.; Barton, J. K. *Science*, **1993**, *262*, 1025.
5. a) Baguley, B. C.; Le Bret, M. *Biochemistry* **1984**, *23*, 937. b) Davis, L. M.; Harvey, J. D.; Baguley, B. C. *Chem.-Biol. Interactions* **1987**, *62*, 45.
6. a) Whillans, D. W. *Biochimica et Biophysica Acta* **1975**, *414*, 193. b) Fromhertz, P.; Rieger, B. *J. Am. Chem. Soc.* **1986**, *108*, 5361. c) Atherton, S. J.; Beaumont, P. C. *J. Phys. Chem.* **1987**, *91*, 3993. d) Cullis, P. M.; McClymont, J. D.; Symons, C. R. *J. Chem. Soc. Faraday Trans.* **1990**, *86*, 591. e) Houée-Levin, C.; Gardés-Albert, M.; Rouscilles, A.; Ferradini, C.; Hickel, B. *Biochemistry*, **1991**, *30*, 8216. f) Atherton, S. J.; Beaumont, P. C. *J. Phys. Chem.* **1995**, *99,* 12025.
7. a) Brun, A. M.; Harriman, A. *J. Am. Chem. Soc.* **1992**, *114*, 3656. b) Brun, A. M.; Harriman, A. *J. Am. Chem. Soc.* **1994**, *116*, 10383.
8. a) Meade, T. J.; Kayyem, J. F. *Angew. Chem. Int. Ed. Engl.* **1995**, *34*, 352. b) Risser, S. M.; Beratan, D. N.; Meade, T. J. *J. Am. Chem. Soc.* **1993**, *115*, 2508.
9. a) Szent-Gyorgyi, A.; Isenberg, I.; Baird, Jr., S. L. *Proc. Natl. Acad. Sci. USA* **1960**, *46,* 1444. b) Snart, R. S. *Biopolymers* **1968**, *6*, 293. c) O'Konski, C. T.; Moser, P.; Shirai, M. *Biopol .Symp.* **1964**, *1*, 479. d) Warman, J. M.; de Haas, M. P.; Schouten, P. G. in *Radiation Research: A 20th-Century Perspective Volume II:*

Congress Proceedings, (Dewey, W. C.; Edington, M.; Fry, R. J. M.; Hall, E. J.; Witmore, G. F., Eds.) Academic Press, **1992**, 93. e) Candeias, L. P.; Steenken, S. *J. Am. Chem. Soc.* **1993**, *115*, 2437.

10. For other π-stacked systems, see: a) Marks, T. J. *Angew. Chem. Int. Ed. Engl.* **1990** *29*, 857. b) Quirion, G.; Poirier, M.; Liou, K. K.; Hoffman, B. M. *Synth. Metals* **1991**, *42*, 2653. c) Markovitz, D.; Bengs, H.; Ringsdorf, H. *J. Chem. Soc. Faraday Trans.* **1992**, *88*, 1275. d) Schouten, P. G.; *et al. J. Am. Chem. Soc.* **1994**, *116*, 6880.
11. Stemp, E. D. A.; Arkin, M. R.; Barton, J. K. *J. Am. Chem. Soc.*, **1995**, *117*, 2375.
12. Holmlin, R. E.; Stemp, E. D. A.; Barton, J. K. *J. Am. Chem. Soc.* **1996**, *118*, 5236.
13. Friedman, A. E.; Chambron, J.-C.; Sauvage, J.-P.; Turro, N. J.; Barton, J. K. *J. Am. Chem. Soc.* **1990**, *112*, 4960.
14. a) Jenkins, Y.; Friedman, A. E.; Turro, N. J.; Barton, J. K. *Biochemistry*, **1992**, *31*, 10809. b) Hartshorn, R. M.; Barton, J. K. *J. Am. Chem. Soc.* **1992**, *114*, 5919.
15. Holmlin, R. E.; Barton, J. K. *Inorg. Chem.* **1995**, *34*, 7.
16. a) Dupureur, C. M.; Barton, J. K. *J. Am. Chem. Soc.* **1994**, *116*, 10286. b) Dupureur, C. M.; Barton, J. K. *Inorg. Chem.* **1997**, in press.
17. Hiort, C.; Lincoln, P.; Norden, B. *J. Am. Chem. Soc.* **1993**, *115*, 3448.
18. a) David, S. S.; Barton, J. K. *J. Am. Chem. Soc.* **1993**, *115*, 2984. b) Collins, J. G.; Shields, T. P.; Barton, J. K. *J. Am. Chem. Soc.* **1994**, *116*, 9840. c) Shields, T. P.; Barton, J. K. *Biochemistry*, **1995**, *34*, 15049. d) Shields, T. P.; Barton, J. K. *Biochemistry*, **1995**, *34*, 15037. e) Hudson, B.; Dupureur, C. M.; Barton, J. K. *J. Am. Chem. Soc.*, **1995**, *117*, 9379.
19. Sitlani, A.; Long, E. C.; Pyle, A. M.; Barton, J. K. *J. Am. Chem. Soc.***1992**, *114*, 2303.

20. a) Uchida, K.; Pyle, A. M.; Morii, T.; Barton, J. K. *Nucleic Acids Res.* **1989**, *17*, 10259. b) Sitlani, A.; Barton, J. K. *Biochemistry* **1994**, *33*, 12100.

21. a) Dupureur, C. M.; Barton, J. K. *Comprehensive Supramolecular Chemistry V. 5*, J.-M. Lehn, ed. Pergamon Press, **1995**, 295. b) Johann, T. W.; Barton, J. K. *Trans. Royal Soc. (London) A.* **1996**, *354*, 299.

22. Chambron, J.-C.; Sauvage, J.-P.; Amouyal, E.; Koffi, P. *New. J. Chem.* **1985**, *9*, 527. b) Amouyal, E.; Homsi, A.; Chambron, J. C.; Sauvage, J. P. *J. Chem. Soc. Dalton Trans.* **1990**, *6*, 1841.

23. Creutz, C.; Chou, M; Netzel, T. L.; Okumura, M.; Sutin, N. *J. Am. Chem. Soc.* **1980** *102*, 1309.

24. a) Turro, C.; Evenzahav, A.; Bossmann, S. H.; Barton, J. K.; Turro, N. J. C. *Inorg. Chim. Acta* **1996**, *243*, 101. b) Pyle, A. M.; Chiang, M. Y.; Barton, J. K. *Inorg. Chem.* **1990**, *29*, 4487.

25. Barton, J. K. *Science* **1986**, *233*, 727.

26. Jenkins, Y. C. Ph.D. Thesis, *California Institute of Technology*, 1996.

27. a) Beaucage, S. L.; Caruthers, M. H. *Tet. Lett.* **1981**, *23*, 1859. b) Goodchild, J. *Bioconj. Chem.* **1990**, *1*, 165.

28. Bacharach, M. Ph.D. Thesis, *California Institute of Technology*, 1995.

29. Ramaswamy, M.; Ulman, M; Paye, J.; Fujimoto, J. G. *Optics Lett.* **1993**, *18*, 572.

30. a) Squier, J.; Salin, F.; Mourou, G.; Harter, D. *Optics Lett.* **1991**, *16*, 324. b) Kliner, D. A. V.; Alfano, J. C.; Barbara, P. F. *J. Chem. Phys.* **1993**, *98*, 5375.

31. a) Olson, E. J. C.; Hu, D.; Hörmann, A.; Barbara, P. F. unpublished results. b) For more detailed studies, clustering interactions were modeled in two stages by first determining the equilibrium distribution of donors and acceptors as a function of clustering potential and then calculating the ET kinetics assuming an exponential distance-dependence to the rate of ET.

32. Sambrook, J.; Fritsch, E. F.; Maniatis, T. *Molecular Cloning: A Laboratory Manual*, 2nd ed., NY: Cold Spring Harbor Laboratory, **1989.**

33. Chow, C. S.; Barton, J. K. *Methods Enzymol.* **1992**, *212*, 219.

34. Olson, E. J. C.; Barbara, P. F. unpublished results.

35. Turro, N. J. *Modern Molecular Photochemistry*, Menlo Park, CA: Benjamin/Cummings, **1978**.

36. Kalyanasundaram, K.; *Coord. Chem. Rev.* **1982**, *46*, 159.

37. Marcus, R. A.; Sutin, N. *Biochim. Biophys. Acta* **1985**, *811*, 265.

38. Arkin, M. R.; Stemp, E. D. A.; Turro, C.; Turro, N. J.; Barton, J. K. *J. Am. Chem. Soc.* **1996**, *118*, 2267.

39. Stemp, E. D. A. unpublished results.

40. Saenger, W.; Cantor, C. R., eds. *Principles of Nucleic Acid Structure*, NY: Springer-Verlag, **1984**.

41. Blackburn, G. M.; Gait, M. J. eds. *Nucleic Acids in Chemistry and Biology*, New York: Oxford University Press, **1990**.

42. Turro, C.; Bossmann, S. H.; Jenkins, Y; Barton, J. K.; Turro, N. J. *J. Am. Chem. Soc.* **1995**, *117*, 9026.

43. a) Crothers, D. M. *Biopolymers* **1968**, *6*, 575. b) Schmechel, D. E. V.; Crothers, D. M. *Biopolymers* **1971**, *10*, 465.

44. a) Vorlickova, M.; Kypr, J. *J. Biomolec. Struct. Dyn.* **1985**, *3*, 67. b) Hunter, C. A. *J. Mol. Biol.* **1993**, *230*, 1025. c) Yanagi, K.; Privé, G. G.; Dickerson, R. E. *J. Mol. Biol* **1991**, *217*, 201.

45. Felts, A. K.; Pollard, W. T.; Friesner, R. A. *J. Phys. Chem.* **1995**, *99*, 2929.

46. Sugiyama, H. and Saito, I. *J. Am. Chem. Soc.* **1996**, *118*, 7063.

47. Welch, T. W.; Corbett, A. H.; Thorp, H. H. *J. Phys. Chem.*, **1995**, *99*, 11757.

48. Sitlani, A.; Dupureur, C. M.; Barton, J. K. *J. Am. Chem. Soc.* **1993**, *115*, 12589.

49. Atherton, S. J.; Hubig, S. M; Callan, T. J.; Duncanson, J. A.; Snowden, P. T.; Rodgers, M. A. J. *J. Phys. Chem.* **1987**, *91*, 3137.

50. Kelley, S. O.; Holmlin, R. E.; Stemp, E. D. A.; Barton, J. K. unpublished results.

51. Hall, D. B; Holmlin, R. E.; Barton, J. K. *Nature*, **1996**, *382*, 731.

52. Hall, D. B.; Barton, J. K., unpublished results.

53. Dandliker, P. J.; Holmlin, R. E.; Barton, J. K., *Science*, in press, **1996**.

54. Arkin, M. R.; Stemp, E. D. A.; Barton, J. K. unpublished results.

55. Perrin, F. *Compt. Rend.* **1924**, *178,* 1978.

56. White, W.; Seybold, P. G. *J. Phys. Chem.* **1977**, *81*, 2035.

57. Ornstein, R. L.; Rein, R.; Breen, D. L.; Macelroy, R. D. *Biopolymers* **1978**, *17*, 2341.

58. a) Hogan, M. E.; Jardetzky, O. *Proc. Natl. Acad. Sci. USA* **1979**, *76*, 6341. b) Englander, S. W.; Kallenbach, N. R.; Heeger, A. J.; Krumhansl, J. A.; Litwin, S. *Proc. Natl. Acad. Sci. USA* **1980**, *77*, 7222.

59. McConnell, H. M. *J. Chem. Phys.* **1961**, *35*, 508. b) Naleway, C. A.; Curtiss, L. A.; Miller, J. R. *J. Phys. Chem.* **1991**, *95*, 8434. c) Closs, G. L.; Miller, J. R. *Science* **1988**, *240*, 440.

60. a) Onuchic, J. N.; Beratan, D. N.; Winkler, J. R.; Gray, H. B. *Ann. Rev. Biophys. Biomol. Struct.* **1992**, *21*, 349. b) Wuttke, D. S.; Bjerrum, M. J.; Winkler, J. R.; Gray, H. B. *Science* **1992**, *256*, 1007. c) Moser, C. C.; Keske, J. M.; Warncke, K.; Farid, R. S.; Dutton, P. L. *Nature* **1992**, *355*, 796. d) Langen, R.; Chang, I. J.; Germanas, J. P.; Richards, J. H.; Winkler, J. R.; Gray, H. B. *Science* **1995**, *268*, 1733. e) Ullmann, G. M.; Kostic N. M. *J. Am. Chem. Soc.* **1995**, *117*, 4766.

61. a) Mujica, V.; Kemp, M.; Ratner, M. A. *J. Chem. Phys.* **1994**, *101*, 6856. b) Mujica, V.; Kemp, M.; Ratner, M. A. *J. Chem. Phys.* **1994**, *101*, 6849. c) Kemp, M.; Mujica, V.; Ratner, M. A. *J. Chem. Phys.* **1994**, *101*, 5172.

62. Dee, D.; Baur. M. E. *J. Chem. Phys.* **1974**, *60*, 541.

63. Several authors have determined thermodynamic parameters for the DNA bases, but no consensus has yet emerged. See: a) Steenken, S.; Telo, J. P.; Novais, H. M., Candeias, L. P. *J. Am. Chem. Soc.* **1992**, *114*, 4701. b) Hush, N. S.; Cheung, A. S. *Chem. Phys. Lett.* **1975**, *34*, 11. c) Faraggi, M.; Klapper, M. H. *J. Chim. Phys.* **1994**, *91*, 1054. d) Jovanovic, S. V.; Simic, M. G. *J. Phys. Chem.* **1986**, *90*, 974. e) Kittler, L.; Löber, G.; Gollnick, F. A.; Berg H. *J. Electroanal. Chem.* **1980**, *116*, 503.

64. Lipscomb, L. A.; Zhou, F. X.; Presnell, S. R.; Woo, R. J.; Peek, M. E.; Plaskon, R. R.; Williams, L. D. *Biochemistry* **1996**, *35*, 2818.

65. Colocci, N.; Dervan, P. B. *J. Am. Chem. Soc.* **1995**, *117*, 4781.

Chapter 3

Luminescence Quenching in Supramolecular Systems: A Comparison of DNA- and SDS Micelle-Mediated Photoinduced Electron Transfer Reactions between Metal Complexes*

* Adapted from Arkin, M. R.; Stemp, E. D. A.; C. Turro; N. J. Turro; Barton, J. K. *J. Am. Chem. Soc.*, **1996**, *118*, 2267.

3.1 Introduction

Recent research has focused on electron transfer ET reactions between molecules bound to macromolecular assemblies such as polymers, micelles, and biomolecules.[1-3] Such systems could provide one route to producing long-lived charge separation and, ultimately, artificial photosynthesis. In comparing supramolecular systems, it is important to understand how the host medium manipulates the reactivity of the guest molecules. In this report, we compare and contrast the photoinduced reactions between transition metal complexes which bind tightly both to the DNA helix and to sodium dodecyl sulfate (SDS) micelles. The contrasts in reactions observed in these two media point to the importance of π-stacking within the DNA double helix in mediating ET chemistry.

Several groups have addressed whether the π-stacked bases of the DNA polymer provide an effective pathway for ET reactions.[4-11] Studies in our laboratory (Chapters 1, 2) have focused on reactions between transition metal complexes which bind to DNA by intercalation and/or surface interactions.[4-6] Intercalation, which for metal complexes involves the insertion of one aromatic, heterocyclic ligand between the basepairs of DNA, derives binding stabilization through π-stacking, and thus may serve as a sensitive probe of the DNA π-stack. In fact, studies[5] comparing luminescence quenching of intercalated or groove bound reactants demonstrate that intercalation of both the donor and acceptor is required for rapid and efficient quenching.

Our recent investigations of DNA-mediated ET have taken advantage of derivatives of $Ru(phen)_2dppz^{2+}$ (dppz = dipyridophenazine), shown in Figure 3.1, as a photoexcited donor. Two-dimensional NMR studies[12] of Δ-$Ru(phen)_2dppz^{2+}$ bound to a hexamer duplex have shown that the dppz ligand intercalates into B-form DNA from the major groove, and emission titrations[13] have indicated a DNA binding affinity of $6x10^7\ M^{-1}$. In aqueous solutions, the excited state of $Ru(phen)_2dppz^{2+}$ is highly quenched due to proton transfer from the solvent to the dipyridophenazine ligand (τ = 250 ps).[14-20] When the ligand is protected from water, as by intercalation into DNA[15-19] or binding to anionic

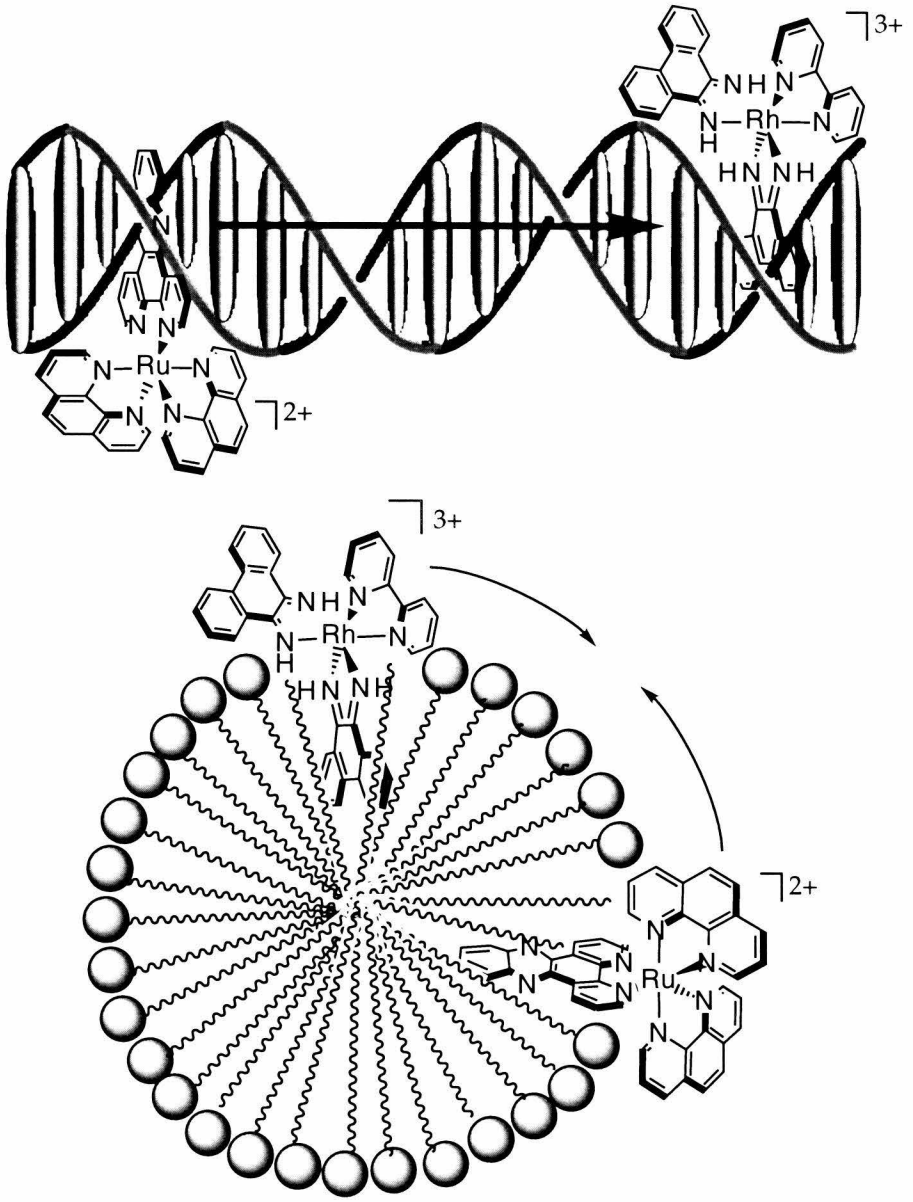

Figure 3.1

Schematic pictures of $Ru(phen)_2dppz^{2+}$ and $Rh(phi)_2bpy^{3+}$ bound to DNA by intercalation (top) and to SDS micelles in the Stern layer (bottom). Both environments provide binding energy by electrostatic and hydrophobic interactions. The hydrophobic interaction varies, however, in that B-form DNA contains a highly ordered stack of aromatic heterocycles, while SDS micelles form a disordered array of aliphatic chains. Arrows indicate that ET proceeds through the DNA π-stack between spatially fixed reactants, whereas ET in micelles requires diffusion of reactants.

micelles,[20] luminescence is observed on the nanosecond timescale. Emission for the metal complex bound to DNA is characterized by a biexponential decay which is sensitive to the sequence of the DNA and to the structure of the ligand environment.[15-19]

The DNA-bound acceptor $Rh(phi)_2bpy^{3+}$ (phi = phenanthrenequinone diimine) is also shown in Figure 3.1. For several phi complexes of Rh(III), two-dimensional NMR studies have indicated that the phi ligand intercalates into B-form DNA from the major groove.[21-23] The depth of intercalation has been shown to depend upon the shape of the ancillary ligands. Rh(III) complexes containing the phi ligand are useful probes of DNA structure, since irradiation with ultraviolet light leads to cleavage of the DNA strand at the site of complex binding.[24-29] For example, $Rh(phen)_2phi^{3+}$ binds preferentially to sites on the DNA which are opened in the major groove ($K_b \approx 10^6\ M^{-1}$), due to steric clashes between the nonintercalated phen ligands and major-groove substituents.[24,25,28,29] $Rh(phi)_2bpy^{3+}$, on the other hand, binds to DNA with low sequence-selectivity,[24,25,27] with an average association constant of $10^7\ M^{-1}$.

The reaction cycle of interest is depicted below. In the presence of B-form DNA, complexes of the formula $Rh(phi)_2L^{3+}$, where L = bpy or phen, quench the emission of dppz complexes of Ru(II) and Os(II) on a subnanosecond timescale.[5,30] Experiments utilizing intercalated complexes covalently tethered to a 15-mer oligonucleotide have established that these quenching reactions can occur efficiently over long distances (>40 Å).[6] For the photoexcited donors $Ru(DMP)_2dppz^{2+}$ (DMP = 4,7 dimethyl-1,10-phenanthroline) and $Os(phen)_2dppz^{2+}$ quenched by $Rh(phi)_2bpy^{3+}$, ET intermediates have been observed by transient absorption spectroscopy.[30,31] Finally, recent work on picosecond timescales has yielded rate constants on the order of $10^{10}\ s^{-1}$ for DNA-mediated reactions between a variety of noncovalently bound metallointercalators.[14] What are the characteristics of the DNA duplex that serve to mediate fast, efficient, long-range reactions?

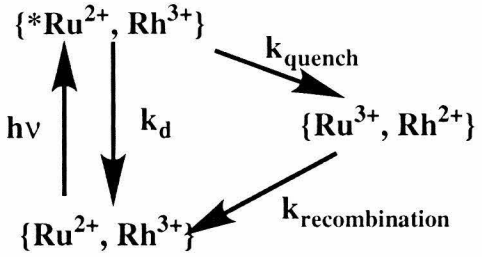

In this chapter, we compare the quenching of photoexcited $Ru(phen)_2dppz^{2+}$ [*Ru(II)] by two intercalators, $Rh(phi)_2bpy^{3+}$ and $Rh(phen)_2phi^{3+}$, mediated through binding to DNA or to SDS micelles (Figure 3.1). SDS micelles provide a particularly useful environment to compare the quenching of *Ru(II) by tris chelate complexes of Rh(III). Like DNA, SDS brings the molecules together in a supramolecular system which is both hydrophobic and negatively charged. Unlike DNA, however, SDS contains no highly organized pathway, such as the DNA π-stack, which might mediate reactions over a long distance. Thus, micelle-mediated reactions are expected to rely on molecular collisions.

Many analogous studies of ET reactions have utilized $Ru(bpy)_3^{2+}$ as a photoexcited donor bound to SDS micelles.[32-38] Several groups have shown that cationic complexes such as RuL_3^{2+} [35,36,39-41] and $Co(phen)_3^{3+}$ [42] containing hydrophobic ligands bind to micelles in the Stern layer. This mode of interaction is similar to intercalation in that it maximizes electrostatic interactions with the charged head groups and nestles the hydrophobic portions of the molecules in the organic portion of the supramolecular structure. The kinetics of quenching of $*Ru(bpy)_3^{2+}$ emission in SDS micelles have been shown to vary dramatically, depending on the location of the bound quencher. Therefore, dynamic quenching is observed when both donor and acceptor are able to diffuse within the micelle[37] or when the acceptor is dissolved in aqueous solution.[36] In contrast, static quenching, which occurs on a timescale that is fast relative to the excited-state lifetime, has been seen when a hydrophobic quencher is bound deeply within the micellar interior.[32]

In the nanosecond flash photolysis experiments presented here, $Rh(phi)_2bpy^{3+}$ is found to quench Ru(II) emission statically in DNA but in a dynamic fashion in anionic

micelles. Furthermore, $Rh(phen)_2phi^{3+}$ is seen to quench the emission of $*Ru(phen)_2dppz^{2+}$ in micelles but no quenching is evident in DNA. We propose that the differences observed depend on the unique features of the DNA π-stack which facilitate ET between intercalators. Differences observed in quenching between $Rh(phen)_2phi^{3+}$ and $Rh(phi)_2bpy^{3+}$ must be related to differences in the intercalation of these two quenchers. Therefore, DNA-mediated ET reactions between metallointercalators are found to be sensitive not only to the mode of binding, but also to the nature of the intercalator/DNA stacking interaction.

3.2 Experimental

Materials. $[Ru(phen)_2dppz]Cl_2$ and $[Rh(phi)_2bpy]Cl_3$ were prepared according to literature procedures[43,44] and further purified by high pressure liquid chromatography. Enantiomers were resolved using standard protocols[12,21,45] and analyzed by circular dichroism spectroscopy. $[Rh(phen)_2phi]Cl_3$ was prepared as described earlier.[44] Sodium dodecyl sulfate (Pierce) was used as received. Sonicated calf thymus DNA was purchased from Sigma and exchanged into with 5 mM tris, 50 mM NaCl, pH 8.5 by ultrafiltration (Amicon). For titrations in deuterated solvent, stock solutions were prepared by repeatedly dissolving the complex in D_2O and drying. Deuterated buffer was prepared from 1M tris-d_{11} in D_2O (Cambridge Isotope Labs).

Instrumentation. Steady-state emission experiments were performed with an SLM 8000 fluorimeter using a xenon arc lamp as the light source. Time-resolved measurements utilized the laser facilities in the Beckman Institute Laser Resource Center, as has been described.[16] Experiments with DNA were accomplished using an excimer-pumped dye laser containing Coumarin 480 (Exciton). Laser powers were 1.0 - 1.5 mJ at 10 Hz and the pulse width was ca. 20 ns. For SDS systems, excitation at 532 nm was provided by a Nd:YAG laser; the power at the sample was 10 - 15 mJ at 10 Hz and the laser pulse width was 8 ns. Reasonable fits to time-resolved measurements on micelle

samples were obtained by defining single-exponential decays without deconvolution or by assuming biexponential fits with deconvolution. For the latter algorithm, one decay rate was always faster than the pulse width, and was not considered to be important in describing the actual emission lifetime of the *Ru(II) complex. Both fitting procedures give similar results. Steady-state intensities were measured by integrating time-resolved decay traces.

Methods. All experiments were performed in aerated solution. For titrations with sonicated calf thymus DNA, concentrated stocks of metal complexes were added to DNA solutions, followed by extensive shaking. The ratio of basepairs/Ru(II) was 50. When micelles were used, samples were prepared by adding concentrated solutions of detergent to dilute metal complexes to avoid precipitation. The concentration of micelles was determined by the equation [mic] = ([SDS] - cmc)/ñ, where cmc is the critical micelle concentration and ñ is the aggregation number (62 in water).[32,46,47] The cmc is not expected to change dramatically upon addition of metal complex, and has been reported to drop from 8 mM to 7 mM when 200 μM $Ru(bpy)_3^{2+}$ is added.[38a]

Electrochemistry. Reduction potentials for $Ru(phen)_2dppz^{2+}$ and Rh(III) complexes were measured using instrumentation described previously[5] at a scan rate of 100 mV/s. Complexes were dissolved in dry DMF (Fluka) with 100 mM tetrabutylammonium hexafluorophosphate as supporting electrolyte. $Ru(phen)_2dppz^{2+}$ and $Rh(phi)_2bpy^{3+}$ gave reversible and quasi-reversible voltammagrams, respectively. $Rh(phen)_2phi^{3+}$ showed complex and irreversible electrochemistry and, therefore, reduction potentials are not reported.

3.3 Results

3.3.1 Quenching in the presence of DNA

3.3.1.1 Variations in acceptor

Figure 3.2A indicates the quenching of *Ru(phen)$_2$dppz^{2+} by three Rh(III) complexes bound to DNA. As has been discussed in Chapter 2, Rh(phi)$_2$bpy^{3+} serves as a remarkably efficient quencher of Ru(II) emission, yielding Stern-Volmer quenching curves which are upward-curving and indicative of quenching by a primarily static mechanism.[5] Figure 3.2B presents the time-resolved decays of *Ru(II) in the presence of increasing concentration of Rh(phi)$_2$bpy^{3+}; the large static component to quenching is manifested by a large loss in initial intensity with only a small change in curve shape. Also shown in Figure 3.2A, and contrasting the titration with Rh(phi)$_2$bpy^{3+}, no luminescence quenching is observed in the presence of Rh(phen)$_2$phi^{3+}, and the emission lifetimes actually increase slightly, from 160 ns/860 ns to 170 ns/915 ns at 5 equivalents of Rh(III). Similar behavior has been seen when a variety of intercalators which cannot quench *Ru(phen)$_2$dppz^{2+} are added to Ru(phen)$_2$dppz^{2+} bound to DNA; one interpretation of this effect is that binding of intercalators rigidifies the DNA helix, which secondarily, serves to increase the luminescence of DNA-bound Ru(phen)$_2$dppz^{2+}. In addition, no reaction is observed between *Ru(phen)$_2$dppz^{2+} and Rh(phen)$_3^{3+}$. This lack of reactivity is expected, due to the weaker binding of Rh(phen)$_3^{3+}$ to DNA and its lower reduction potential [$E^{1/2}$ (Rh^{III}/Rh^{II}) ≈ -0.67 V vs NHE].[48] The driving force for ET between *Ru(II) + Rh(phen)$_3^{3+}$ is close to 0 mV, compared to 560 mV for the reaction of Ru(phen)$_2$dppz^{2+} and Rh(phi)$_2$bpy^{3+} [$E^{1/2}(Ru^{III}/*Ru^{II})$ = -0.61 V vs NHE, $E^{1/2}(Rh^{III}/Rh^{II})$ = -0.05 V vs NHE].

3.3.1.2 Effects of solvent deuteration

Table 3.1 describes the effect of deuterated solvent on reactions between intercalated donor and acceptor. Experiments on fast timescales (Chapter 2) have shown

Figure 3.2

A) Stern-Volmer plot describing luminescence quenching of $Ru(phen)_2dppz^{2+}$ by complexes of Rh(III). Quenching of lifetimes and emission intensity of 10 μM $Ru(phen)_2dppz^{2+}$ by $Rh(phi)_2bpy^{3+}$ (intensity, ▲; lifetimes, ▼), $Rh(phen)_2phi^{3+}$ (intensity, ●), and $Rh(phen)_3^{3+}$ (intensity, ◆) in the presence of 1 mM nucleotides of sonicated calf thymus DNA in 5 mM tris, 50 mM NaCl, pH 8.5. B) Time-resolved emission decays of $*Ru(phen)_2dppz^{2+}$ in DNA as a function of added quencher. 10 μM $Ru(phen)_2dppz^{2+}$, 0, 10, 20, 50 μM $Rh(phi)_2bpy^{3+}$, 1 mM DNA nucleotides, 5 mM tris, 50 mM NaCl, pH 8.5.

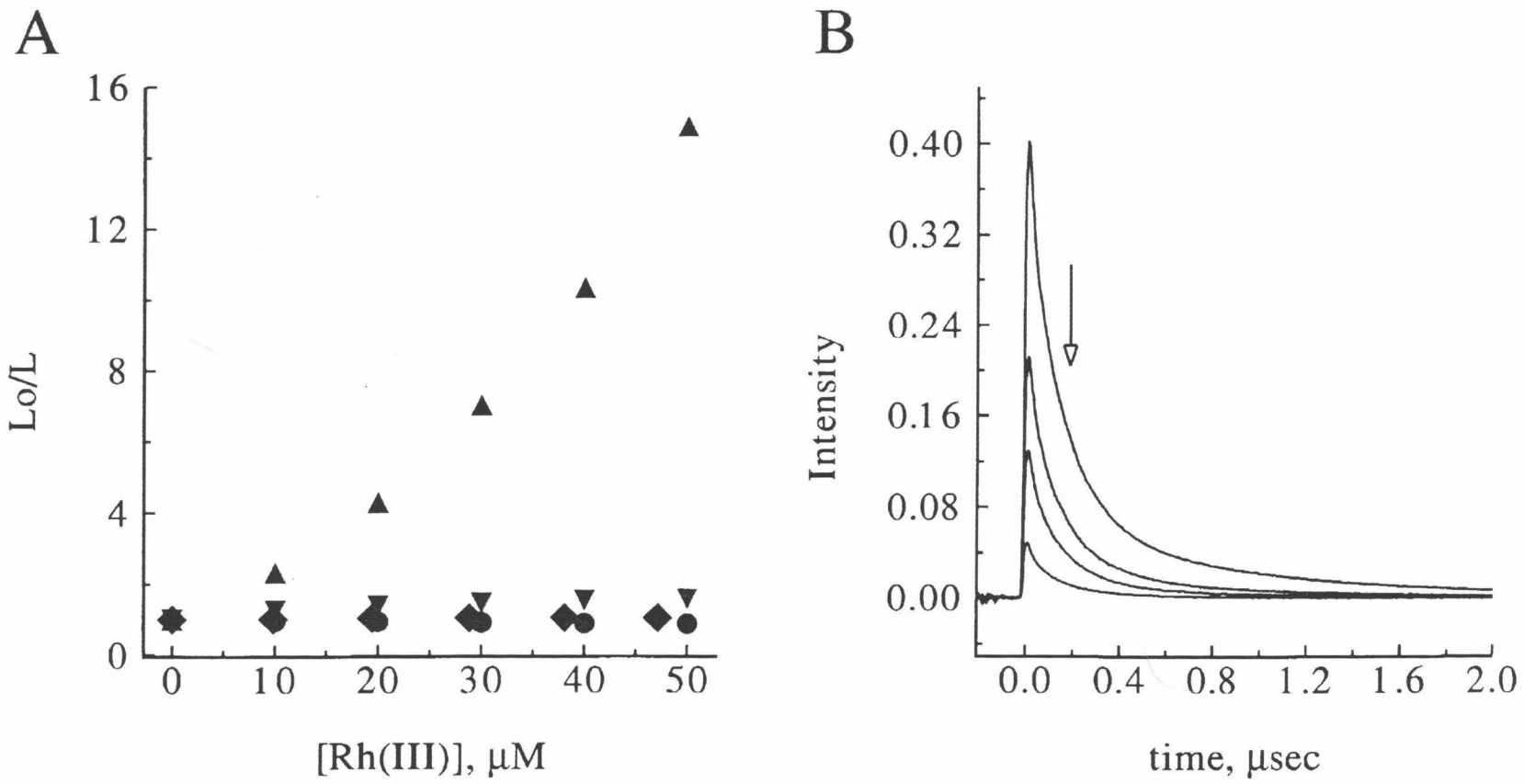
A
16
12
8
4
0
Lo/L
0
10
20
30
40
50
[Rh(III)], μM
B
0.40
0.32
0.24
0.16
0.08
0.00
Intensity
0.0
0.4
0.8
1.2
1.6
2.0
time, μsec

Table 3.1: Emission lifetimes of $Ru(phen)_2dppz^{2+}$ in supramolecular environments.

		H_2O		D_2O		quenching in
Sample	medium	τ (ns)	%	τ (ns)	%	H_2O vs D_2O
Δ-$Ru(phen)_2dppz^{2+}$	DNA[a]	150	80	385	75	0.95[c]
		850	20	1260	25	
Λ-$Ru(phen)_2dppz^{2+}$	DNA[a]	40	80	74	70	
		150	20	290	30	
$Ru(phen)_2dppz^{2+}$	SDS[b]	80		220		1.12[d]

[a]10 μM Ru(II), 1 mM sonicated calf thymus DNA, 5 mM tris (or tris-d_{11}), 50 mM NaCl, pH 8.5. [b]40 μM Ru(II), 13 mM SDS monomers. [c]ratio of Io/I in H_2O and D_2O at 3 equivalents of $Rh(phi)_2bpy^{3+}$. [d]ratio of k_{obs} in H_2O and D_2O.

that the lifetime of the excited state of $Ru(phen)_2dppz^{2+}$ is 250 ps in water and 550 ps in D_2O, giving an isotope effect of 2.3.[14] Similar solvent-isotope effects are seen in the emission lifetimes of $Ru(phen)_2dppz^{2+}$ bound to DNA. Table 3.1 presents the lifetimes of Δ- and Λ-$Ru(phen)_2dppz^{2+}$ in calf thymus DNA, where the two intercalative binding geometries of Δ-Ru(II) show k_H/k_D ratios of 2.6 for the short lifetime and 1.5 for the long; similar isotope effects are evident with the Λ-isomer bound to DNA. The emission lifetimes in the absence of quencher show large isotope effects because proton transfer from solvent provides a major pathway for excited-state decay.[19]

In contrast to quenching by solvent, no strong isotope effects are observed in the fraction of quenching of $*Ru(phen)_2dppz^{2+}$ by $Rh(phi)_2bpy^{3+}$ in DNA (Table 3.1). Picosecond transient absorption measurements also show a $k_H/k_D \approx 1$ for the rate of ground-state recovery of Ru(II).[14] The absence of a solvent-isotope effect indicates that quenching of *Ru(II) by $Rh(phi)_2bpy^{3+}$ in the presence of DNA is not mediated by water, but rather involves metallointercalators bound to the DNA polymer. Furthermore, the slow dissociation of intercalators from DNA[12,21,22] ensures that the metal complexes are fixed during the timescale of the reaction.

3.3.1.3 Effects of a change in donor chirality

Since both the donor and acceptor are chiral, their enantiomers might be expected to behave differently in the environment of right-handed DNA. Indeed, the photophysical properties of $Ru(phen)_2dppz^{2+}$ and its derivatives are sensitive to the twist of the double-helix; the left-handed Λ isomer has shorter luminescence lifetimes (Table 3.1) and, therefore, greater accessibility to water[12,13] than does the right-handed Δ enantiomer. Table 3.2 shows that the reaction between these metallointercalators bound to DNA is also affected by their chirality.[14] The most efficient quenching occurs between Δ-$Ru(phen)_2dppz^{2+}$ and Δ-$Rh(phi)_2bpy^{3+}$, with 75% being quenched at 2 equivalents of

Table 3.2: Intensity quenching of the enantiomers of $Ru(phen)_2dppz^{2+}$ by the enantiomers of $Rh(phi)_2bpy^{3+}$.

Ru/Rh	I_o/I, SDS[a]	I_o/I, DNA[b]
Δ/Δ	1.52	3.90
Λ/Δ	1.56	1.50
Λ/Λ	1.50	1.27

[a] 84 μM Ru(II), 168 μM Rh(III), 13 mM SDS in water. [b] 10 μM Ru(II), 20 μM Rh(III), 1 mM nucleotides DNA in 5 mM tris, 50 mM NaCl, pH 8.5.

Rh(III). However, the other pairs of enantiomers do react and quenching in each case is primarily static (Table 3.2).

3.3.2 Quenching in the presence of SDS micelles

3.3.2.1 Association of metal complexes with micelles

Many earlier studies have established that cationic metal complexes containing hydrophobic ligands bind to anionic micelles in the Stern layer, and binding affinities near 10^5 M^{-1} have been suggested.[40,42] Binding of the Rh(III) acceptors is established by UV-visible spectroscopy. In the presence of DNA, the ultraviolet spectra of phi complexes of Rh(III) are known to undergo hypochromic, red shifts in the phi transitions centered near 360 nm ($\Delta\lambda_{max} \approx 13$ nm).[25] Upon the addition of SDS above the cmc, both $Rh(phi)_2bpy^{3+}$ and $Rh(phen)_2phi^{3+}$ show 10 nm shifts in these bands to lower energies, but without significant hypochromicity (Figure 3.3). Binding of $Ru(phen)_2dppz^{2+}$ to SDS micelles is indicated by the onset of emission above the cmc.[20] These complexes are expected to remain bound to the micelle during the lifetime of the experiment, with a lower limit for the residence time of $Ru(phen)_2dppz^{2+}$ being provided by the excited-state lifetime in D_2O/SDS (~220 ns).

The emission of $Ru(phen)_2dppz^{2+}$ is sensitive to the micellar environment. The decrease in lifetime relative to $Ru(phen)_2dppz^{2+}$ bound to DNA indicates a greater water accessibility in the micelle. As in DNA, emission in micelles also shows a large solvent isotope effect (Table 3.1, $k_H/k_D = 2.8$). The time-resolved luminescence decay can reasonably be fit to a single exponential in SDS/water. The rate of emission decay decreases slightly as the ratio of Ru/SDS increases, from $1.3x10^7$ s^{-1} at 0.1 Ru/micelle to $1.7x10^7$ s^{-1} at 1.0 Ru/micelle. This dynamic quenching of $*Ru(phen)_2dppz^{2+}$ could arise from binding competition as well as self-quenching, e.g., triplet-triplet annihilation.[49]

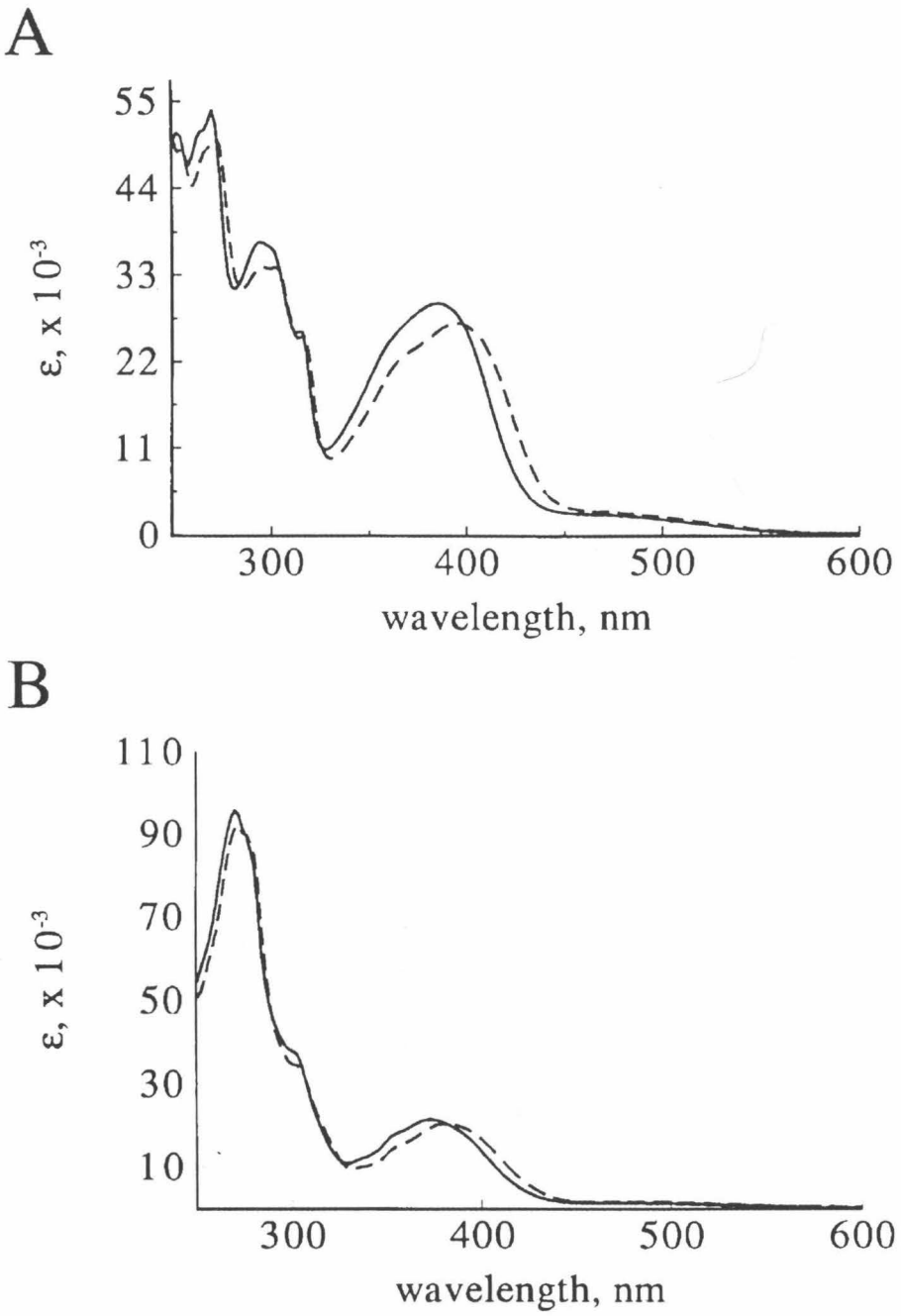

Figure 3.3

Ultraviolet-visible spectra of $Rh(phi)_2bpy^{3+}$ (A) and $Rh(phen)_2phi^{3+}$ (B) in water (solid) and in SDS micelles (dashes). 10 nm red-shifts in absorbance bands of the phi ligand are indicative of binding in a hydrophobic environment.

3.3.2.2 Effects of variation in acceptor

In contrast to the *static* quenching of *$Ru(phen)_2dppz^{2+}$ by $Rh(phi)_2bpy^{3+}$ in DNA, $Rh(phi)_2bpy^{3+}$ quenches *Ru(II) emission in SDS by a primarily *dynamic* mechanism, as indicated by the similarity in Stern-Volmer plots of I_o/I or τ_o/τ vs [Q] in Figure 3.4A. The emission decay, presented in Figure 3.4B, emphasizes the change in the shape of the decay curve with little loss in initial intensity.

There is additionally a dramatic difference in the quenching behavior of $Rh(phen)_2phi^{3+}$ in the two systems. When bound to SDS micelles in water, both $Rh(phi)_2bpy^{3+}$ and $Rh(phen)_2phi^{3+}$ quench $Ru(phen)_2dppz^{2+}$ emission to similar extents (Figure 3.4A), whereas $Rh(phen)_2phi^{3+}$ does not serve as a quencher of *$Ru(phen)_2dppz^{2+}$ emission when bound to DNA (Figure 3.2A). This interesting result suggests that there are important differences between how the DNA polymer and the SDS micelles participate in this chemisty. As in DNA, $Rh(phen)_3^{3+}$ does not quench the excited state of $Ru(phen)_2dppz^{2+}$, presumably as a result of the low driving force for ET (*vide supra*).

3.3.2.3 Variation in micellar concentration

For a range of Ru/SDS ratios, quenching by both $Rh(phi)_2bpy^{3+}$ and $Rh(phen)_2phi^{3+}$ yields linear Stern-Volmer plots (Figure 3.4A). Application of the Stern-Volmer equation

$$I_o/I = \tau_o/\tau = 1 + K_{sv}[Q];\ K_{sv} = k_{obs}/k_o$$

(where k_o = the intrinsic decay constant of the unquenched donor) to time-resolved quenching data yields Stern-Volmer constants (K_{SV}) of 8700 M^{-1} and 9000 M^{-1} for $Rh(phi)_2bpy^{3+}$and $Rh(phen)_2phi^{3+}$, respectively, at 84 μM Ru, 13 mM SDS monomers. Between Ru/micelle ratios of 0.1 - 1.0, plots of $\tau o/\tau$ vs Rh/SDS yield similar values for K_{SV} (Figure 3.5), indicating that quenching is determined by the distribution of donors and acceptors among micelles[50] and not by their absolute concentration.

Figure 3.4

A) Stern-Volmer plot describing luminescence quenching in SDS micelles of photoexcited $Ru(phen)_2dppz^{2+}$ (84 μM) by $Rh(phi)_2bpy^{3+}$ (intensity, ▲; lifetimes, ▼), $Rh(phen)_2phi^{3+}$ (intensity, ●; lifetimes, ■), and $Rh(phen)_3^{3+}$ (intensity, ◆). [SDS] = 13 mM monomer in water. B) Time-resolved emission decays of $*Ru(phen)_2dppz^{2+}$ in DNA as a function of added quencher. 84 μM $Ru(phen)_2dppz^{2+}$, 0, 40, 80, 160 μM $Rh(phi)_2bpy^{3+}$, 13 mM SDS monomers. In contrast to quenching in DNA, both $Rh(phi)_2bpy^{3+}$ and $Rh(phen)_2phi^{3+}$ cause a similar reduction in $*Ru(phen)_2dppz^{2+}$ emission lifetime. Additionally, quenching is primarily dynamic in nature, compared to the large static component observed for $Ru(phen)_2dppz^{2+}$ and $Rh(phi)_2bpy^{3+}$ bound to DNA.

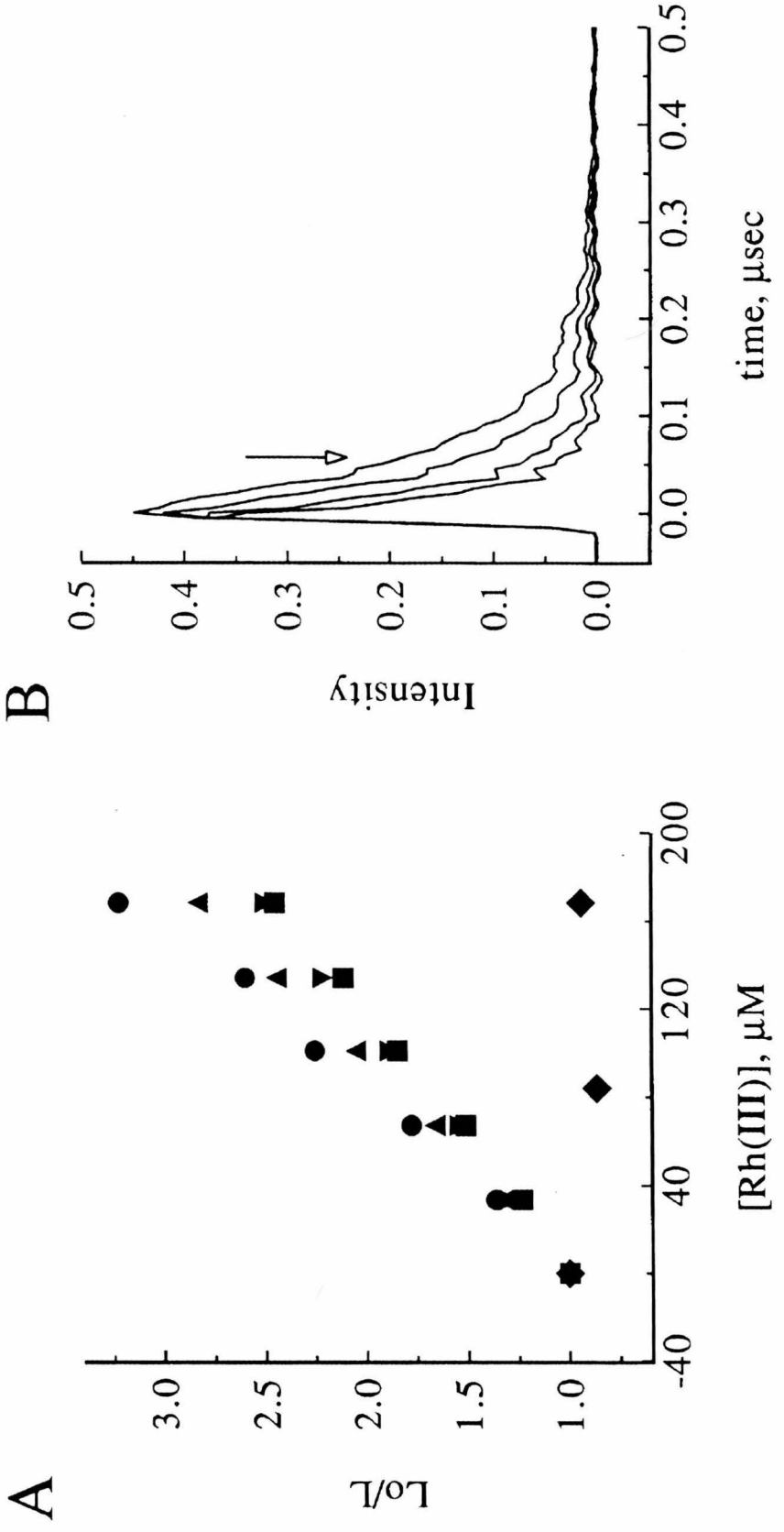
A
Lo/L
3.0
2.5
2.0
1.5
1.0
-40
40
120
200
[Rh(III)], μM
B
Intensity
0.5
0.4
0.3
0.2
0.1
0.0
0.0
0.1
0.2
0.3
0.4
0.5
time, μsec

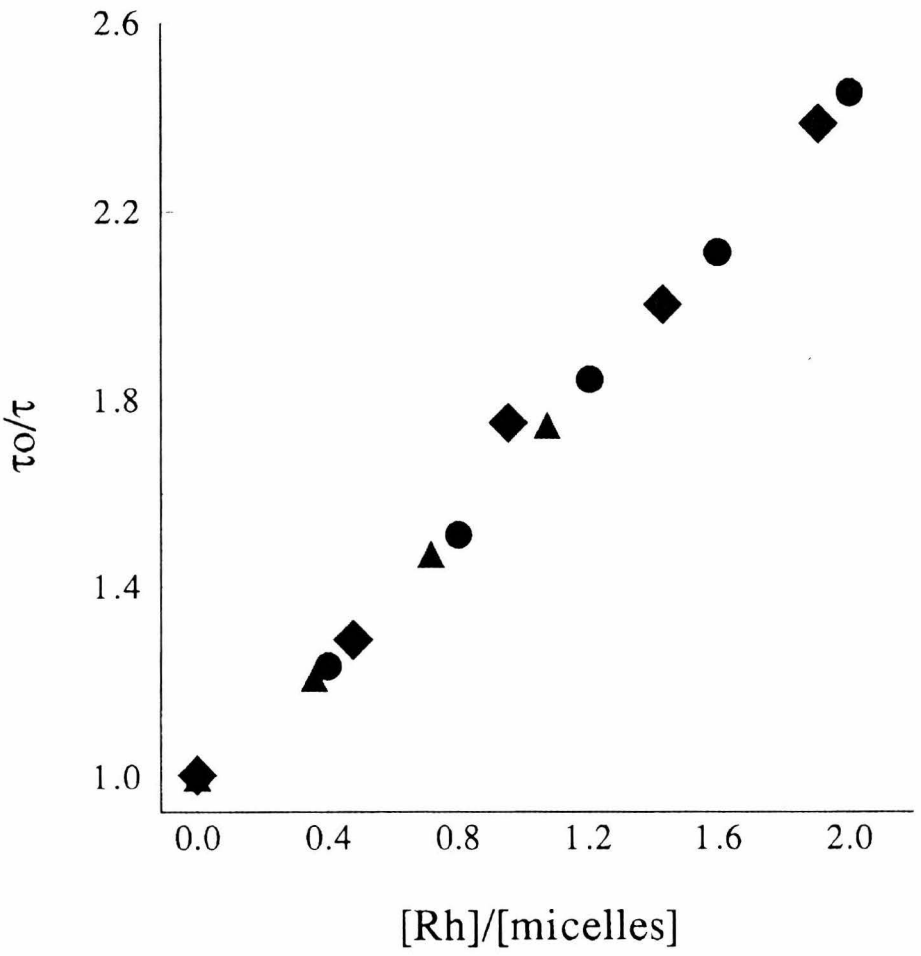

Figure 3.5

Stern-Volmer analysis of quenching of $Ru(phen)_2dppz^{2+}$ by $Rh(phen)_2phi^{3+}$ at three ratios of Ru/SDS. Slopes of quenching plots are the same for Ru:SDS ratios of 0.1 (▲), 0.5 (◆), and 1.0 (●). Quenching therefore depends on the distribution of acceptors among micelles, rather than the absolute concentration of donors and acceptors.

If quenching of a molecule of *Ru(phen)$_2$dppz^{2+} by a Rh(III) complex involves diffusion within a micelle (as opposed to diffusion of an unbound quencher through the solvent),[36] then increasing the number of micelles should reduce the amount of quenching by sequestering acceptors in donorless micelles. The following kinetic model has been derived by Berezin and coworkers[51] in describing reactions which follow Stern-Volmer kinetics and in which the reactants are bound tightly to the micelle:

$$k_{obs} = (k_m/V)K_aK_b/[(K_a+K_b)+K_aK_bC]$$

where k_m is the micellar quenching rate, V is the partial molar volume of SDS in the micelle, C = [SDS]-cmc, and K_a and K_b are the equilibrium dissociation constants for reactants a and b, respectively. This model predicts that the inverse of the observed quenching rate k_{obs} will be proportional to C. Figure 3.6 shows such a plot for quenching of *Ru(phen)$_2$dppz^{2+} by Rh(phen)$_2$phi^{3+} and by Rh(phi)$_2$bpy^{3+} as the concentration of detergent varies from 10 - 30 mM. The plot of $1/k_{obs}$ vs C is linear over a 10-fold range of micelle concentration, from approximately 32 – 350 μM, supporting the notion that quenching occurs by diffusion within a micelle. From the slope (V/k_m) the true bimolecular rate constant (k_m) can be determined, assuming a value for the partial volume V. V is 0.25 M^{-1} for donor/acceptor residing in the volume of the micelle and 0.14 M^{-1} for complexes restricted to the Stern layer.[42] Given a value for V of 0.14 M^{-1}, true bimolecular rate constants are found from the slope to be 1.1 x 10^8 $M^{-1}s^{-1}$ and 1.2 x 10^8 $M^{-1}s^{-1}$ for Rh(phi)$_2$bpy^{3+}and Rh(phen)$_2$phi^{3+}, respectively. Additionally, the slope/intercept ratio suggests association constants for donor and acceptor on the order of 5 x 10^4 M^{-1}, assuming $K_a = K_b$ and cmc = 8 mM[52] (values for the intercept are negative for cmc < 7.8 mM). Although the small value for the intercept (10^{-13} Ms) implies a large uncertainty in the binding constants, this value is similar to earlier estimates of binding constants for less hydrophobic tris chelate complexes of Ru(II),[40] Co(II),[41] and Co(III).

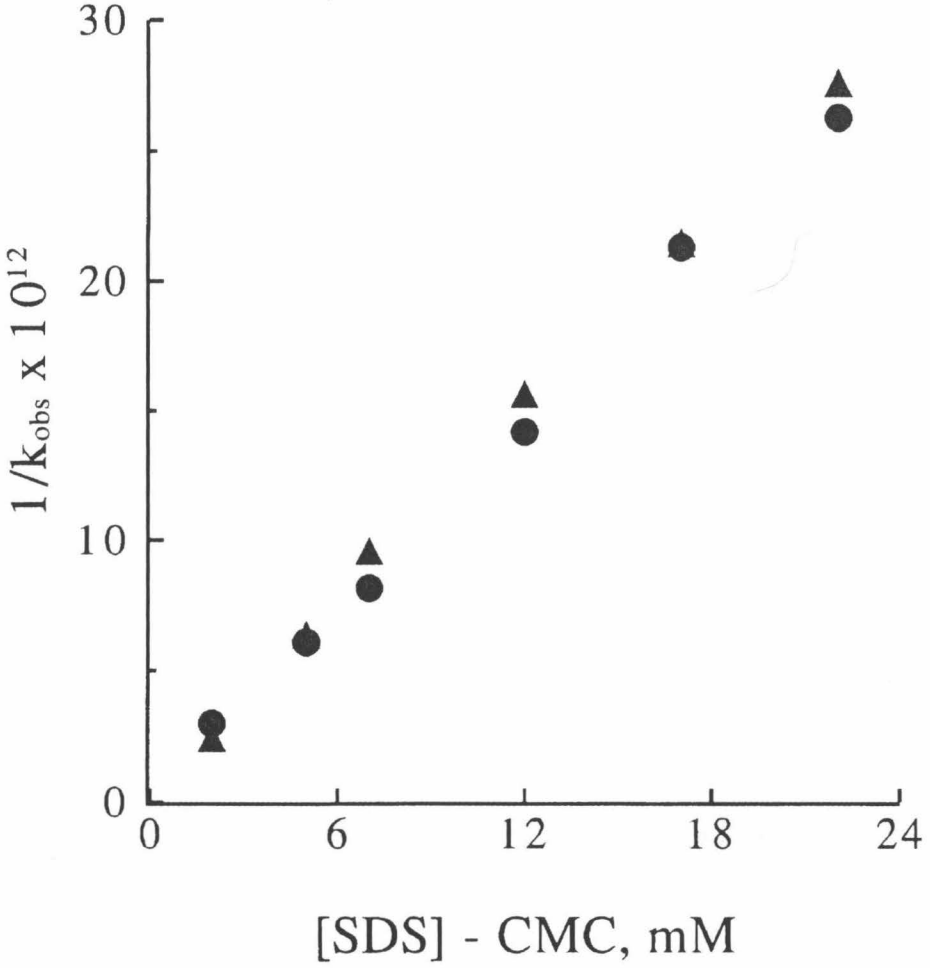

Figure 3.6

Plots of $1/k_{obs}$ versus concentration of detergent-cmc for the quenching of $Ru(phen)_2dppz^{2+}$ by $Rh(phen)_2phi^{3+}$ (●) and $Rh(phi)_2bpy^{3+}$ (▲).

3.3.2.4 Mechanism of quenching in the micelle

Photoinduced ET is the most likely mechanism of quenching of *$Ru(phen)_2dppz^{2+}$ by $Rh(phi)_2bpy^{3+}$ and $Rh(phen)_2phi^{3+}$ in SDS micelles. Evidence for ET is provided by transient absorption spectroscopy with a related donor, $Ru(DMP)_2dppz^{2+}$. Previously we observed a long-lived Ru(III) species generated by reaction of *$Ru(DMP)_2dppz^{2+}$ and $Rh(phi)_2bpy^{3+}$ bound to DNA.[31] Compared to $Ru(phen)_2dppz^{n+}$ ($E^{3+/2+}$ = 1.61 V), $Ru(DMP)_2dppz^{n+}$ ($E^{3+/2+}$ = 1.54 V) is less unstable in the 3+ oxidation state and has a shorter excited state lifetime; both properties improve detection of the transient intermediate. The intrinsic lifetime of *$Ru(DMP)_2dppz^{2+}$ in SDS is too short to be determined accurately with the time resolution of our instrument. However, quenching of the emission intensity occurs upon addition of Rh(III), with the concomitant increase of a transient signal which decays with a rate constant of 3.7 x 10^6 s^{-1} (Figure 3.7). This rate constant is significantly longer than the excited-state decay of the *$Ru(DMP)_2dppz^{2+}$ complex, and is consistent with transient formation of Ru(III). It is noteworthy that *Rh(III) is generated by laser excitation at 532 nm (ε_{532} = 1230 $M^{-1}cm^{-1}$), and the transient signals for the *Rh(III)-Rh(III) difference spectrum are, in general, large. Therefore, full spectral characterization of transient absorption spectra is not possible, and transient intermediates have been identified primarily at the 422 nm isobestic point in the *Rh(III)-Rh(III) difference spectrum. Interestingly, ET intermediates are sometimes not seen for reactions in micelles, presumably due to reduced cage-escape yield;[33,36,38a,38d] it is therefore likely that the transient signals observed in Figure 3.7 arise from only a fraction of the ET intermediate formed.

Other plausible mechanisms for quenching, including energy transfer and excited-state proton transfer, do not account for the dynamic quenching observed. Energy transfer is unlikely, due to the very small amount of spectral overlap between the absorption spectra of the acceptors and the emission profile of the donor. Excited-state proton transfer[19] has been ruled out by the experiments shown in Figure 3.8 and summarized in Table 3.3. Four

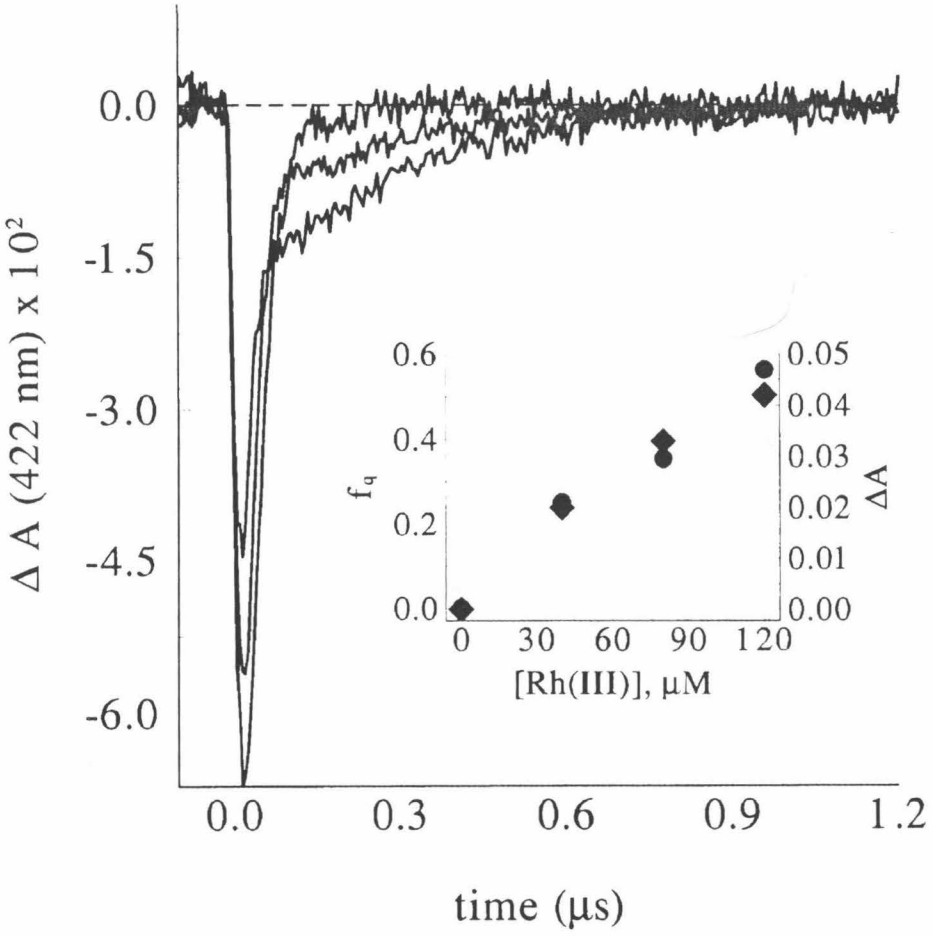

Figure 3.7

Transients observed at 422 nm formed by 532 nm excitation of $Ru(DMP)_2dppz^{2+}$ during titration with $Rh(phi)_2bpy^{3+}$ in SDS micelles. Addition of $Rh(phi)_2bpy^{3+}$ produces a long-lived signal which decays with a rate constant of $3.7 \times 10^6\ s^{-1}$. Conditions are 10 μM Ru(II), 13 mM SDS, 0, 30, 90 μM Rh(III). Data are uncorrected for inner filter effects due to Rh(III) absorption. Inset: comparison of emission quenching (●) and yield of transient intermediate at 422 nm (◆). 40 μM Ru(II), 13 mM SDS, λ_{exc} = 480 nm. $f_q = 1-I/I_o$.

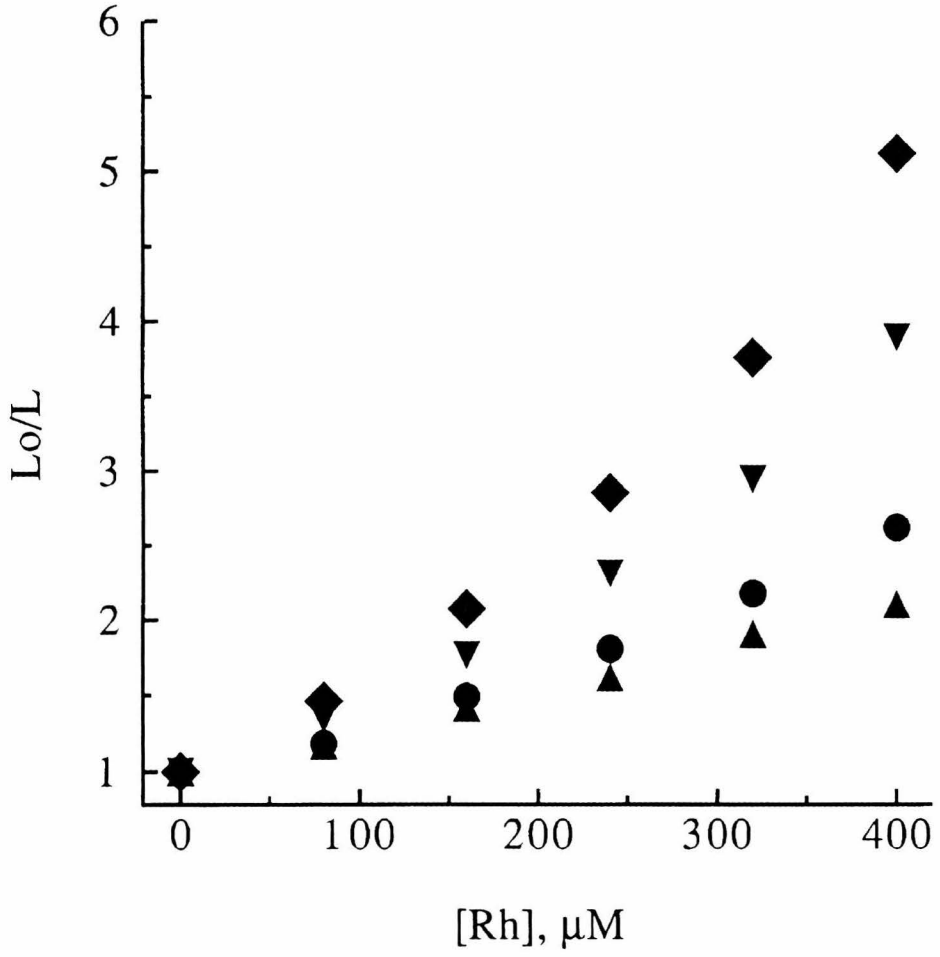

Figure 3.8

Stern-Volmer plots showing the quenching of $Ru(phen)_2dppz^{2+}$ by $Rh(phi)_2bpy^{3+}$ and $Rh(phen)_2phi^{3+}$ in basic solution. 40 μM $Ru(phen)_2dppz^{2+}$, 13 mM SDS, 10 mM tris buffered to pH 8.5. Quenching by $Rh(phi)_2bpy^{3+}$ of emission intensity (◆) and lifetime (▼); quenching by $Rh(phen)_2phi^{3+}$ of emission intensity (●) and lifetimes (▲). Above the pK_a of Rh(III) complexes, Stern-Volmer plots become upward-curving, and $Rh(Hphi)_2bpy^{+}$ reacts more than $Rh(phen)_2(Hphi)^{2+}$.

Table 3.3: Parameters for quenching of $Ru(phen)_2dppz^{2+}$ by phi complexes of Rh(III).

			4 eq quencher		
Quencher[a]	**solvent**	**pK_a**	**K_{SV} (M^{-1})[b]**	**Io/I**	**$\tau o/\tau$**
$Rh(phi)_2bpy^{3+}$	water	6.7	7300		
$Rh(phi)_2bpy^{3+}$	pH 8.5 tris		upward-curving	2.13	1.8
$Rh(phen)_2phi^{3+}$	water	6.3	8700	2.48	2.4
$Rh(phen)_2phi^{3+}$	pH 8.5 tris		2750	1.5	1.4
$Rh([12]S_4ane)phi^{3+}$[c]	water	2.3	upward-curving	2.0	1.8
$Rh(NH_3)_4phi^{3+}$	water	9.5	---	0.93	---

[a] 40 μM Ru, 13 mM SDS. [b] from $\tau_o/\tau = 1 + K_{SV}[Q]$. [c] $[12]S_4ane$ = 1,4,7,10-tetrathiacyclododecane.

phi complexes of Rh(III), spanning a broad range of pK_a, were tested for reaction with *$Ru(phen)_2dppz^{2+}$; no correlation between pK_a and quenching was found. Additionally, the presence of 10 mM tris buffer at pH 8.5 did not eliminate quenching of *$Ru(phen)_2dppz^{2+}$ by either $Rh(phi)_2bpy^{3+}$ (pK_a = 6.7) or $Rh(phen)_2phi^{3+}$ (pK_a = 6.3).

A few interesting differences are noteworthy, however, in comparing protonated and deprotonated quenchers. First, the amount of luminescence quenching is less in pH 8.5 buffer than in water. Second, Stern-Volmer plots are now upward-curving and, in the case of $Rh(phi)_2bpy^{3+}$, show a greater proportion of static quenching. These changes are not due to the addition of 10 mM salt, since 10 mM tris buffered to pH 5.7 did not affect the quenching (data not shown). It is also noteworthy that no significant pH effects are seen in the quenching of $Ru(phen)_2dppz^{2+}$ by $Rh(phi)_2bpy^{3+}$ bound to DNA.

3.3.2.5 Effects with enantiomers

In order to compare the effects of enantiomers in the chiral environment of DNA and the achiral medium of SDS micelles, quenching of the pure enantiomers of *$Ru(phen)_2dppz^{2+}$ was also considered. Table 3.2 shows that, unlike the large effects in quenching efficiency between diasteriomeric pairs bound to DNA, differences in quenching in micelles were within the experimental error of the measurements.

3.4 Discussion

3.4.1 Quenching in the presence of DNA

3.4.1.1 Reaction environment

Reactions between *Ru(II) and Rh(III) bound to DNA are best described as occurring in a DNA medium. There are no solvent-isotope effects in ET efficiencies or rates, indicating that the solvent does not play a role in the quenching reaction (Table 3.1). One would expect a correlation between quenching in DNA and changes in the DNA medium and the binding of the donor/acceptor to the double helix. In fact, we have shown

here that the binding of $Ru(phen)_2dppz^{2+}$ to DNA strongly influences quenching, since there is a relationship between the chirality of the metal complex and its reaction with intercalated $Rh(phi)_2bpy^{3+}$. Importantly, Figures 3.2 and 3.4 indicate that the medium itself plays a critical role in the rates of quenching of $*Ru(phen)_2dppz^{2+}$ by $Rh(phi)_2bpy^{3+}$. In the disordered environment of the micelle, quenching occurs with diffusion-controlled rates. In contrast, unimolecular, subnanosecond quenching is observed when these metallointercalators are bound in the highly ordered medium of the DNA helix. Quenching depends on the supramolecular environment.

3.4.1.2 Effect of acceptor

Quenching of *Ru(II) bound to DNA is highly sensitive to the choice of DNA-bound electron acceptor. $Rh(phi)_2bpy^{3+}$ quenches the emission of *Ru(II) by a static mechanism, as shown by large changes in emission intensity and small changes in lifetime (Figure 3.2a, 3.3a). By contrast, the seemingly similar $Rh(phen)_2phi^{3+}$ does not quench *Ru(II) emission at all, despite a comparably high binding constant for intercalation to B-form DNA. This interesting result is compared to quenching in SDS micelles below.

3.4.1.3 DNA as a mediator for long-range reaction

Although experiments between randomly bound intercalators do not directly address the distance-dependence of ET, reactions between $*Ru(phen)_2dppz^{2+}$ and $Rh(phi)_2bpy^{3+}$ noncovalently bound to DNA appear to occur over a long distance (Chapter 2). Assuming random binding, at 1 equiv Δ-$Rh(phi)_2bpy^{3+}$, donor/acceptor pairs are an average of 25 basepairs apart, and 4 % of pairs are in closest contact. However, at this concentration, we observe that 30% of Δ-$*Ru(phen)_2dppz^{2+}$ is quenched and thus propose that reactions occur at long range. This analysis is consistent with experiments between metallointercalators covalently bound to an oligonucleotide, where quenching was found to occur rapidly over 40 Å.[6]

3.4.1.4 Diastereomeric effects on quenching

Varying the chirality of both donor and acceptor dramatically effects the quenching of *Ru(II) bound to DNA (Table 3.2), and the effects are correlated with the stacking of the complex into the DNA helix. In the case of the donor, 30% of the Δ enantiomer is quenched at 1 equiv Δ-Rh(phi)$_2$bpy^{3+}, compared to only 15% quenching of the Λ-isomer. The excited-state lifetimes in the absence of quencher are longer for the right-handed isomer (150/850 ns) than for the left-handed one (40/150 ns). Since water quenches the excited state ($k_H/k_D \approx 2.3$), longer emission lifetimes imply decreased solvent accessibility and increased stacking with the DNA bases. Thus, deeper intercalation results in better quenching. These results can be contrasted to reactions between isomers in SDS micelles, where no significant differences between diastereomeric pairs are observed.[53] The correlation between excited-state lifetime and quenching efficiency points to the importance of stacking interactions in mediating ET between DNA-bound molecules.

3.4.2 Quenching in SDS micelles

3.4.2.1 Reaction environment

Both donor and acceptor are tightly bound to SDS micelles, and thus ET reactions between them occur within the restricted space of the micelle. Emission and absorption spectroscopies provide information on micellar binding of donor and acceptor. The donor Ru(phen)$_2$dppz^{2+} displays an emission lifetime of ~80 ns in SDS micelles compared to a lifetime of 250 ps in aqueous solution.[14] This 320-fold increase in excited-state lifetime is indicative of removal of the dppz ligand from water. The absorption spectra of the acceptor complexes are red-shifted by 10 nm in the presence of SDS micelles (Figure 3.3), similar to changes seen for phi complexes of Rh(III) when the solvent hydrophobicity is increased.[44]

3.4.2.2 Effects of Acceptors

Both $Rh(phen)_2phi^{3+}$ and $Rh(phi)_2bpy^{3+}$ quench the emission of $*Ru(phen)_2dppz^{2+}$ when the complexes are bound to SDS micelles. Quenching is not observed when *Ru(II) is titrated with $Rh(phen)_3^{3+}$. The lack of reactivity of $Rh(phen)_3^{3+}$ is not surprising, based on the absence of thermodynamic driving force, but it is an important control since the size and shape of micelles are known to be sensitive to the addition of ions. $Rh(phen)_3^{3+}$ is similar to $Rh(phi)_2bpy^{3+}$ and $Rh(phen)_2phi^{3+}$ in terms of charge and shape, and would therefore have a similar effect on micellar structure. The quenching of $*Ru(L)_2dppz^{2+}$ by Rh(III) complexes is not due to a perturbation of the environment around the lumophore.

3.4.2.3 Kinetic description of quenching in SDS

For both $Rh(phi)_2bpy^{3+}$ and $Rh(phen)_2phi^{3+}$, Stern-Volmer plots based on intensity and lifetime quenching are linear and have comparable slopes; thus, quenching is dynamic for both acceptors. Berezin plots of $1/k_{obs}$ vs C are linear (Figure 3.6), indicating that the quenching reaction is intramicellar. The micellar quenching rate constant, extracted from the slope of the Berezin plot, is $1.1 \times 10^8\ M^{-1}s^{-1}$ for quenching by $Rh(phi)_2bpy^{3+}$ and $1.2 \times 10^8\ M^{-1}s^{-1}$ for $Rh(phen)_2phi^{3+}$. Intramicellar quenching occurs with rates close to the rate of diffusion within a micelle,[37,38b] and rates are similar for quenching by both phi complexes.

3.4.2.4 Effect of pH

Table 3.3 indicates that the quenching of $*Ru(phen)_2dppz^{2+}$ by Rh(III) complexes decreases when the pH is raised above the pK_a of the phi ligand;[54] furthermore, $Rh(phi)_2bpy^{3+}$ is a more efficient quencher than $Rh(phen)_2phi^{3+}$ and yields nonlinear Stern-Volmer plots. The differences between quenching by the protonated and deprotonated forms of the acceptors may be explained by both binding and electronic

factors. For $Co(phen)_3^{3+/2+}$, Davies *et al.*[42] find that the binding constant for Co(III) is lower than for Co(II), and suggest that divalent metal complexes bound to SDS micelles are stabilized by hydrophobic interactions, whereas electrostatic attraction accounts for ca. 50% of binding stabilization for 3+ ions. Thus, the protonation state of phi complexes could be important in determining the nature of their binding and diffusion in SDS micelles. Additionally, the stronger binding of $Rh(Hphi)_2bpy^+$ to the micelle could result in greater competition, resulting in the ejection of some $Ru(phen)_2dppz^{2+}$ from the micelle. Lastly, preliminary results suggest that the protonated and deprotonated forms of $Rh^{III}(phi)_2bpy^{3+/+}$ have different electron-transfer reactivities, and so the reduction potential might change with pH.[55]

3.4.3 Comparison of quenching in DNA and SDS

We have shown that $Ru(phen)_2dppz^{2+}$, $Rh(phen)_2phi^{3+}$, and $Rh(phi)_2bpy^{3+}$ bind strongly both to DNA and to SDS micelles and that quenching of *Ru(II) can occur in both environments. However, electron-transfer reactions between *Ru(II) and Rh(III) complexes display some striking differences depending on the nature of the medium. The quenching of $*Ru(phen)_2dppz^{2+}$ by $Rh(phi)_2bpy^{3+}$ is static in DNA, but dynamic in SDS micelles. This interesting result demonstrates that *the structure of DNA plays a central role in mediating the electron transfer reaction.* Furthermore, the two quenchers $Rh(phi)_2bpy^{3+}$ and $Rh(phen)_2phi^{3+}$ behave differently in DNA; $Rh(phi)_2bpy^{3+}$ is a highly efficient quencher of *Ru(II) emission, while $Rh(phen)_2phi^{3+}$ does not react. In SDS micelles, by contrast, emission is quenched by a dynamic mechanism by both phi complexes with similar efficiencies.

There are several possible explanations for the differences between $Rh(phi)_2bpy^{3+}$ and $Rh(phen)_2phi^{3+}$ bound to DNA, including i) insufficient thermodynamic driving force for $Rh(phen)_2phi^{3+}$ to oxidize *Ru(II), ii) cooperative binding in the $Rh(phi)_2bpy^{3+}$/Ru(II) pair that is missing with $Rh(phen)_2phi^{3+}$/Ru(II), iii) long Rh/Ru distances generated by the

greater sequence-selectivity of $Rh(phen)_2phi^{3+}$, iv) differential binding of the acceptors to the helix, causing $Rh(phi)_2bpy^{3+}$ to be reactive while $Rh(phen)_2phi^{3+}$ is not. The experiments described here suggest that differences in stacking of the Rh(III) complexes with the DNA bases account for the quenching effects observed.

The similarity of quenching rates for the two acceptors in SDS micelles is incompatible with the first two propositions listed above. If $Rh(phen)_2phi^{3+}$ lacked the thermodynamic driving force for ET, then no quenching would have occurred between $*Ru(phen)_2dppz^{2+}$ and $Rh(phen)_2phi^{3+}$. If cooperative binding were important, then quenching would be different for the two acceptors and likely would be static; in other words, no changes in Ru(II) emission lifetime would be observed. While it is known that $Rh(phen)_2phi^{3+}$ binds to DNA with greater sequence-selectivity than $Rh(phi)_2bpy^{3+}$ (iii), differences in binding affinity between sites is small compared to the concentrations used in these experiments, and therefore all sites on the DNA should be sampled. Additionally, there is no evidence for large sequence preferences for $Ru(phen)_2dppz^{2+}$ binding to B-form DNA.[12]

Photocleavage and binding studies[21-29] provide an explanation for the lack of DNA-mediated quenching by $Rh(phen)_2phi^{3+}$. Figure 3.9 illustrates a thoroughly investigated model for the intercalation of $Rh(phen)_2phi^{3+}$ and $Rh(phi)_2bpy^{3+}$ into B-form DNA.[25,29] Comparisons of photocleavage and crystal structures of several DNA oligonucleotides indicate that there is a strong correlation between the binding of $Rh(phen)_2phi^{3+}$ and the degree of opening in the major groove. This opening of the major groove results in a destacking of the basepairs and, presumably, separation of the base step from the electronically well-coupled π-stack. The shape-selective binding of $Rh(phen)_2phi^{3+}$ but not $Rh(phi)_2bpy^{3+}$ is also responsible for the increased sequence-selectivity of $Rh(phen)_2phi^{3+}$ compared to $Rh(phi)_2bpy^{3+}$. Finally, the notion that $Rh(phen)_2phi^{3+}$ and $Rh(phi)_2bpy^{3+}$ are stacked differently is consistent with the observed hypochromicity of the phi ligands upon binding to DNA; $Rh(phen)_2phi^{3+}$ shows 40%

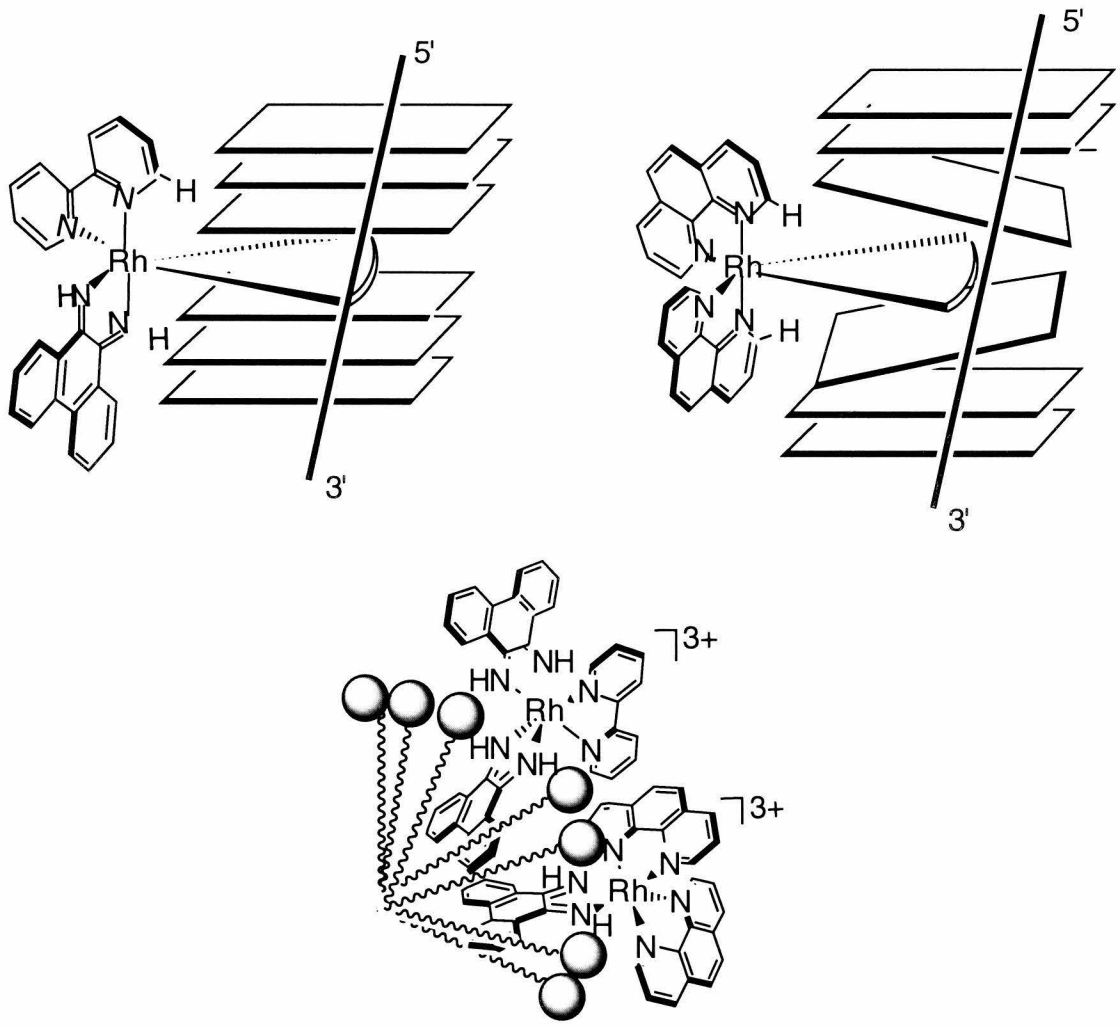

Figure 3.9

Models for binding of $Rh(phi)_2bpy^{3+}$ (left) and $Rh(phen)_2phi^{3+}$ (right) to DNA and SDS micelles (center). Due to steric clashes of the 2,9 phen protons with major groove substituents, intercalation of $Rh(phen)_2phi^{3+}$ into DNA occurs preferentially at basesteps which are opened in the major groove, resulting in reduced basestacking at the binding site. No such steric interactions inhibit binding of $Rh(phi)_2bpy^{3+}$, and thus binding is largely sequence-neutral and the basepairs are well-stacked with the intercalating phi ligand.[24,25,29] The more disordered binding of Rh(III) complexes to SDS micelles suggests that the two acceptors will bind equivalently.

hypochromicity in the phi bands, while $Rh(phi)_2bpy^{3+}$ shows 60% for the intercalated ligand (30% for the complex).[25]

We therefore propose a model whereby intercalative binding affords access to the purported DNA π-way, and this intimate coupling of the donor and acceptor into the DNA helix depends sensitively on stacking of the intercalator. Poor stacking of the intercalating guest with the DNA host limits DNA-mediated quenching, as in the case of Λ-$Ru(phen)_2dppz^{2+}$, or abolishes such quenching, as for $Rh(phen)_2phi^{3+}$. The SDS micelle affords a medium for dynamic quenching through collision, but offers no comparable π-stacked array, as in a DNA duplex, to mediate fast electron-transfer chemistry.

3.5 References

1. a) Jones, W. E.; Baxter, S. M.; Strouse, G. F. Meyer, T. J. *J. Am. Chem. Soc.* **1993**, *115*, 7363. b) Fox, M. A. *Accts. Chem. Res.* **1992**, *25*, 569. c) Lehn, J. M. *Angew. Chem. Int. Ed. Engl.* **1990**, *29*, 1304, d) Bowler, B. D.; Raphael, A. L.; Gray, H. B. *Prog. Inorg. Chem.* **1990**, *38*, 259.
2. a) Fendler, J. H. *Membrane Mimetic Chemistry,* New York: Wiley, **1982**. b) Turro, N. J.; Barton, J. K.; Tomalia, D. A. *Accts. Chem. Res.* **1991**, *11*, 332.
3. a) Onuchic, J. N.; Beratan, D. N.; Winkler, J. R.; Gray, H. B. *Ann. Rev. Biophys. Biomol. Struct.* **1992**, *21*, 349. b) Boxer, S. G. *Ann. Rev. Biophys. and Biophys. Chem.* **1990**, *19*, 267. c) Arkin, M. R.; Jenkins, Y. C.; Barton, J. K. *Adv. Chem. Ser.* **1995**, *246*,449. d) Stemp, E. D. A.; Barton, J. K. *Metal Ions in Biology* **1996**, *33*, 325. e) Meade, T. J. *Metal Ions in Biology* **1996**, *32*, 453.
4. a) Barton, J. K.; Kumar, C. V.; Turro, N. J. *J. Am. Chem. Soc.* **1986**, *108*, 6391. b) Purugganan, M. D.; Kumar, C. V.; Turro, N. J.; Barton, J. K. *Science* **1988**, *241*, 1645.
5. Murphy, C. J.; Arkin, M. R.; Ghatlia, N. D.; Bossmann, S. H.; Turro, N. J.; Barton, J. K. *Proc. Natl. Acad. Sci. USA* **1994**, *91*, 5315.
6. Murphy, C. J.; Arkin, M. R.; Jenkins, Y.; Ghatlia, N. D.; Bossmann, S. H.; Turro, N. J.; Barton, J. K. *Science* **1993**, *262*, 1025.
7. a) Brun, A. M.; Harriman, A. *J. Am. Chem. Soc.* **1994**, *116*, 10383. b) Brun, A. M.; Harriman, A. *J. Am. Chem. Soc.* **1992**, *114*, 3656.
8. a) Meade, T. J.; Kayyem, J. F. *Angew. Chem. Int. Ed. Engl.* **1995**, *34*, 352. b) Risser, S. M.; Beratan, D. N.; Meade, T. J. *J. Am. Chem. Soc.* **1993**, *115*, 2508.
9. a) Snart, R. S. *Biopolymers* **1968**, *6*, 293. b) Hoffmann, T. A.; Ladik, J. *Adv. Chem. Phys.* **1964**, *7*, 84. c) Miller, J. H.; Swenberg, C. E. *Can. J. Phys.* **1990**, *68*, 962. d) Dee, D.; Baur, M. E. *J. Chem. Phys.* **1974**, *60*, 541.

10. a) Warman, J. M.; de Haas, M. P.; Schouten, P. G. in *Radiation Research: A 20th-Century Perspective Volume II: Congress Proceedings*, (Dewey, W. C.; Edington, M.; Fry, R. J. M.; Hall, E. J.; Witmore, G. F., Eds.) Academic Press, **1992**, 93. b) Candeias, L. P.; Steenken, S. *J. Am. Chem. Soc.* **1993**, *115*, 2437.

11. a) Whillans, D. W. *Biochimica et Biophysica Acta* **1975**, *414*, 193. b) Fromhertz, P.; Rieger, B. *J. Am. Chem. Soc.* **1986**, *108*, 5361. c) Atherton, S. J.; Beaumont, P. C. *J. Phys. Chem.* **1987**, *91*, 3993. c) Baguley, B. C.; Lt Bret, M. *Biochemistry* **1984**, *23*, 937. d) Houée-Levin, C.; Gardés-Albert, M.; Rouscilles, A.; Ferradini, C.; Hickel, B. *Biochemistry*, **1991**, *30*, 8216. e) Cullis, P. M.; McClymont, J. D.; Symons, C. R. *J. Chem. Soc. Faraday Trans.* **1990**, *86*, 591.

12. a) Dupureur, C. M.; Barton, J. K. *J. Am. Chem. Soc.* **1994**, *116*, 10286. b) Dupureur, C. M.; Barton, J. K. submitted for publication.

13. Hiort, C.; Lincoln, P.; Norden, B. *J. Am. Chem. Soc.* **1993**, *115*, 3448.

14. Arkin, M. R.; Stemp, E. D. A.; Holmlin, R. E.; Barton, J. K.; Hoermann, A.; Olson, E.; Barbara, P. *Science* **1996**, *273*, 475.

15. Friedman, A. E.; Chambron, J.-C.; Sauvage, J.-P.; Turro, N. J.; Barton, J. K. *J. Am. Chem. Soc.* **1990**, *112*, 4960.

16. Friedman, A. E.; Kumar, C. V.; Turro, N. J.; Barton, J. K. *Nucleic Acids Res.* **1991**, *19*, 2595.

17. Jenkins, Y.; Friedman, A. E.; Turro, N. J.; Barton, J. K. *Biochemistry* **1992**, *31*, 10809.

18. Hartshorn, R. M.; Barton, J. K. *J. Am. Chem. Soc.* **1992**, *114*, 5919.

19. Turro, C.; Bossmann S. H.; Jenkins, Y.; Barton, J. K.; Turro, N. J. *J. Amer. Chem. Soc.* **1995**, *117*, 9026.

20. Chambron, J.-C.; Sauvage, J.-P. *Chem. Phys. Lett.* **1991**, *182*, 603.

21. David, S. S.; Barton, J. K. *J. Am. Chem. Soc.* **1993**, *115*, 2984.

22. a) Collins, J. G.; Shields, T. P.; Barton, J. K. *J. Am. Chem. Soc.* **1994**, *116*, 9840.

b) Shields, T. P.; Barton, J. K. *Biochemistry*, **1995**, *34*, 15049.

23. Hudson, B.; Dupureur, C. M.; Barton, J. K. *J. Am. Chem. Soc.*, **1995**, *117*, 9379.
24. a) Pyle, A. M.; Long, E. C.; Barton, J. K. *J. Am. Chem. Soc.* **1989**, *111*, 4520. b) Pyle, A. M.; Morii, T.; Barton, J. K. *J. Am. Chem. Soc.* **1990**, *112*, 9432.
25. Sitlani, A.; Long, E. C.; Pyle, A. M.; Barton, J. K. *J. Am. Chem. Soc.* **1992**, *114*, 2302.
26. Sitlani, A.; Barton, J. K. *Biochemistry* **1994**, *33*, 12100.
27. Uchida, K.; Pyle, A. M.; Morii, T.; Barton, J. K. *Nucleic Acids Res.* **1989**, *17*, 10259.
28. Chow, C. S.; Behlen, L. S.; Uhlenbeck, O. C.; Barton, J. K. *Biochemistry* **1992**, *31*, 972.
29. Campisi, D.; Morii, T.; Barton, J. K. *Biochemistry*, **1994**, *33*, 4130.
30. a) Holmlin, R. E.; Barton, J. K. *Inorg. Chem.* **1995**, *34*, 7. b) Holmlin, R. E.; Stemp, E. D. A.; Barton, J. K. *J. Am. Chem. Soc.* **1996**, *118*, 5236.
31. Stemp, E. D. A.; Arkin, M. R.; Barton, J. K. *J. Am. Chem. Soc.* **1995**, *117*, 2375.
32. Turro, N. J.; Yekta, A. *J. Am. Chem. Soc.* **1978**, *100*, 5951.
33. Turro, N. J.; Khudyakov, I. V.; Gopidas, K. R. *Chem. Phys.* **1992**, *162*, 131.
34. Gopidas, K. R.; Leheny, A. R.; Caminati, G.; Turro, N. J.; Tomalia, D. A. *J. Am. Chem. Soc.* **1991**, *113*, 7335.
35. Kunjappu, J. T.; Somasundaran, P.; Turro, N. J. *J. Phys. Chem.* **1990**, *94*, 8464.
36. Dressick, W. J.; Hauenstein, B. L. Jr.; Demas, J. N.; DeGraff, B. A. *Inorg. Chem.* **1984**, *23*, 1107.
37. Kuzmin, M. G.; Soboleva, I. V. *J. Photochem. Photobiol. A: Chemistry* **1995**, *87*, 43.
38. a) Meisel, D.; Matheson, M. S.; Rabini, J. *J. Am. Chem. Soc.* **1978**, *100*, 117. b) Miyashita, T.; Murakata, T.; Matsuda, M. *J. Phys. Chem.* **1989**, *93*, 1426. c) Miyashita, T.; Murakata, T.; Matsuda, M. *J. Phys. Chem.* **1983**, *87,* 4529. d)

Wolszczak, M.; Thomas, J. K. *Radiat. Phys. Chem.* **1991**, *38*, 155. e) el Torki, F. M.; Schmehl, R. H.; Reed, W. F. *J. Chem. Soc. Faraday Trans. 1* **1989**, *85*, 349.

39. Ottaviani, M. F.; Ghatlia, N. D.; Turro, N. J. *J. Phys. Chem.* **1992**, *96*, 6075.

40. Snyder, S. W.; Buell, S. L.; Demas, J. N.; DeGraff, B. A. *J. Phys. Chem.* **1989**, *93*, 5265.

41. Hauenstein, B. L. Jr.; Dressick, W. J.; Buell, S. L.; Demas, J. N.; DeGraff, B. A.; *J. Am. Chem. Soc.* **1983**, *105*, 4251.

42. a) Davies, K.; Hussam, A. *Langmuir* **1993**, *9*, 3270. b) Davies, K. M.; Hussam, A.; Rector, B. R. Jr.; Owen, I. M.; King, P. *Inorg. Chem.* **1994**, *33*, 1741.

43. Amouyal, E.; Homsi, A.; Chambron, J.-C.; Sauvage, J.-P. *J. Chem. Soc. Dalton Trans.* **1990**, *6*, 1841.

44. Pyle, A. M.; Chiang, M. Y.; Barton, J. K. *Inorg. Chem.* **1990**, *29*, 4487.

45. Yoshikawa, Y.; Yamasaki, K. *Coord. Chem. Rev.* **1979**, *28*, 205.

46. Granath, K. *Acta Chem. Scand.* **1953**, *7*, 297.

47. Coll, H. *J. Phys. Chem.* **1970**, *74*, 520.

48. Chan, S. F.; Chow, M.; Creutz, C.; Matsubara, T.; Sutin, N. *J. Am. Chem. Soc.* **1981**, *103*, 369.

49. Lachish, U.; Ottolenghi, M.; Rabani, J. *J. Am. Chem. Soc.* **1977**, *99*, 8062.

50. Gehlen, M. H.; De Schryver, F. C. *Chem. Rev.* **1993**, *93*, 199.

51. Berezin, I. V.; Martinek, K.; Yatsimirskii, A. K. *Russian Chem. Rev.* **1973**, *42*, 787.

52. Mukerjee, P.; Mysels, K. J. "Critical Micelle Concentration of Aqueous Surfactant Systems," NSRDS-NBS 36, U. S. Government Printing Office, Washington, D.C., 1971.

53. Diastereomeric effects in ET between tris chelate complexes of Co(III/II) in solution have been observed in some cases. See a) Warren, R. M. L., Tatehata, A.; Lappin, A. G. *J. Chem. Soc. Dalton Trans.* **1994**, *11*, 1655. b) Warren, R. M. L.; Lappin, A.

G.; Mehta, B. D.; Neumann, H. M. *Inorg. Chem.* **1990**, *29*, 4185.

54. Krotz, A. H.; Kuo, L. Y.; Barton, J. K. *Inorg. Chem.* **1993**, *32*, 5963.

55. Turro, C.; Evenzahav, A.; Bossmann, S. H.; Barton, J. K.; Turro, N. J. C. *Inorg. Chim. Acta* **1996**, *243*, 101.

Chapter 4

Synthesis and Characterization of Metallointercalator-Oligonucleotide Conjugates

4.1 Introduction

A number of laboratories have developed syntheses for the covalent attachment of lumophores, cleavage reagents, and cross-linking reagents to DNA oligonucleotides.[1-20] Our laboratory has been especially active in designing metal complexes which bind to DNA by intercalation, and the tethering of such molecules to DNA could lead to a new class of sequence-specific DNA probes.[12-14,21,22] In particular, phenanthrenequinone diimine (phi) complexes of rhodium(III) and iridium(III) have been used as photocleavage reagents of nucleic acids[23,24] and polypyridyl complexes of ruthenium(II) and osmium(II) have been developed as sensitive luminescence probes.[21,22,25-29] Additionally, we have utilized covalently tethered metallointercalators of Ru(II) and Rh(III) to study long-range electron transfer (ET) through the DNA double helix.[30]

Our studies of DNA-mediated ET reactions have led to several interesting observations which may be best investigated using covalently modified oligonucleotide duplexes (M-DNA).[31-35] Chapter 2 describes the kinetics of ET reactions between a series of metallointercalators noncovalently bound to DNA.[35] These experiments indicated that DNA-mediated ET occurred on the picosecond time scale with rates that were independent of the loading of acceptors on the double helix. Furthermore, ET was found to be highly sensitive to DNA sequence and to the close contact of intercalators with the stacked base pairs of DNA. The comparison of luminesence quenching of Ru(II) by Rh(III) in DNA and SDS micelles (Chapter 3) further emphasized the requirement of the π-stacked bases in mediating fast and efficient electron transfer reactions.[33] Based on these studies, we suggested that DNA-mediated ET reactions are higly sensitive to the stacking of metallointercalator with the DNA base stack but not strongly dependent on the distance separating well-bound intercalators. In order to test this hypothesis, we have been working to prepare donor-DNA-acceptor assemblies with well-defined duplex structures and nucleic acid sequences.[21,22]

In addition to donor-acceptor assemblies in which DNA serves as a bridge for electron transfer reactions, our laboratory has investigated long-range reactions where the DNA itself acts as an electron donor. Chapter 1 described two sets of studies which demonstrated that oxidative damage of 5'-GG-3' sequences[36] and repair of thymine dimers[37] can be effected by a photoexcited Rh(III) acceptor placed up to 37Å away from the reactive DNA site. The synthesis of covalent Rh(III)-oligonucleotides was critical to these measurements, since the distances between DNA donor and intercalating acceptor could be defined. In Chapter 5, we describe another metal-DNA conjugate which enables further study of DNA-mediated hole transfer. In this case, a flash-quench methodology is used to generate an oxidizing Ru(III) intercalator *in situ*.[38] By tethering this novel metal complex to a DNA oligonucleotide, we have been able to demonstrate long-range ET between 5'-GG-3' sequences and Ru(III) over 37Å.[39] For these studies, the binding of Ru(II) is defined by *Ru-sensitized, $^1O_2$ damage of guanine residues near the intercalation site.

The development of metallointercalator-oligonucleotide conjugates may also lead to a novel class of sequence-specific nucleic acid probes. For example, phi complexes of Rh(III) have been shown to cleave DNA and RNA upon photoexcitation.[40] Rh(III)-oligonucleotide chimeras could therefore serve as sequence-specific photocleavage reagents, complementing other studies in which oligonucleotides labeled with fluorophores or cleavage reagents are targeted to single- or double-stranded nucleic acids.[16-20] Furthermore, as discussed in Chapters 1 and 2, polypyridyl complexes of Ru(II) and Os(II) containing the dppz ligand are "molecular light switches" for DNA.[25-29,35] These complexes show no steady-state luminescence in aqueous solvent due to interactions between the solvent and the phenazine nitrogens of the dppz ligand; when complexes containing dppz are intercalated into B-form DNA, however, the ligand is protected from H_2O and ~10^3-fold increases in excited-state lifetimes are observed. The excited-state lifetimes of Ru(II) and Os(II) complexes can be modulated by changes in ligand structure;

additionally, the emission properties are highly sensitive to DNA structure and sequence. One could envision combining the sensitivity of these emission properties with the sequence-specificity of DNA hybridization to create novel biosensors for DNA structure and sequence detection.[21]

Here, we report the preparation of Ru(II)-oligonucleotide chimeras containing novel trisheteroleptic complexes of ruthenium. The synthesis of Ru(II) complexes containing three different ligands, described by Strouse *et al.*[41] and Anderson *et. al.*,[42] will allow us to tune the emission, redox, and DNA-binding properties of these complexes. The trisheteroleptic complexes of Ru(II) which have been prepared are shown in Figure 4.1; of these, $Ru(phen)(bpy')(Me_2dppz)^{2+}$ has been especially useful in quenching experiments and in studies of long-range G oxidation.[39] The synthesis and characterization of analogous complexes of Os(II) have also been explored.[43]

While covalent metal-oligonucleotide chimeras have several important advantages over noncovalent assemblies, they also represent a new class of DNA-binding molecules and thus require extensive characterization. Towards this end, we have developed synthetic strategies which are high-yielding and flexible, so that a series of conjugates can be prepared which systematically vary the ligands of the metal complex, the length and conformation of the tether, and the sequence of the DNA. Most of the work described here utilizes an alkylamine-terminated oligonucleotide prepared by a solid-phase synthetic strategy. Additionally, a solution-phase scheme is described in which the metal and oligonucleotide are joined by a disulfide bond. We have also described some of the structural and spectroscopic features of metallated oligonucleotides. By studying the properties of chimeras by spectroscopy (UV-visible absorption, circular dichroism, emission intensity, and emission quenching) and biophysical methods (mass spectrometry, enzymatic digestion, gel electrophoresis, and thermal denaturation), we have begun to build a detailed picture of the structure and reactivity of metallointercalator-DNA conjugates.

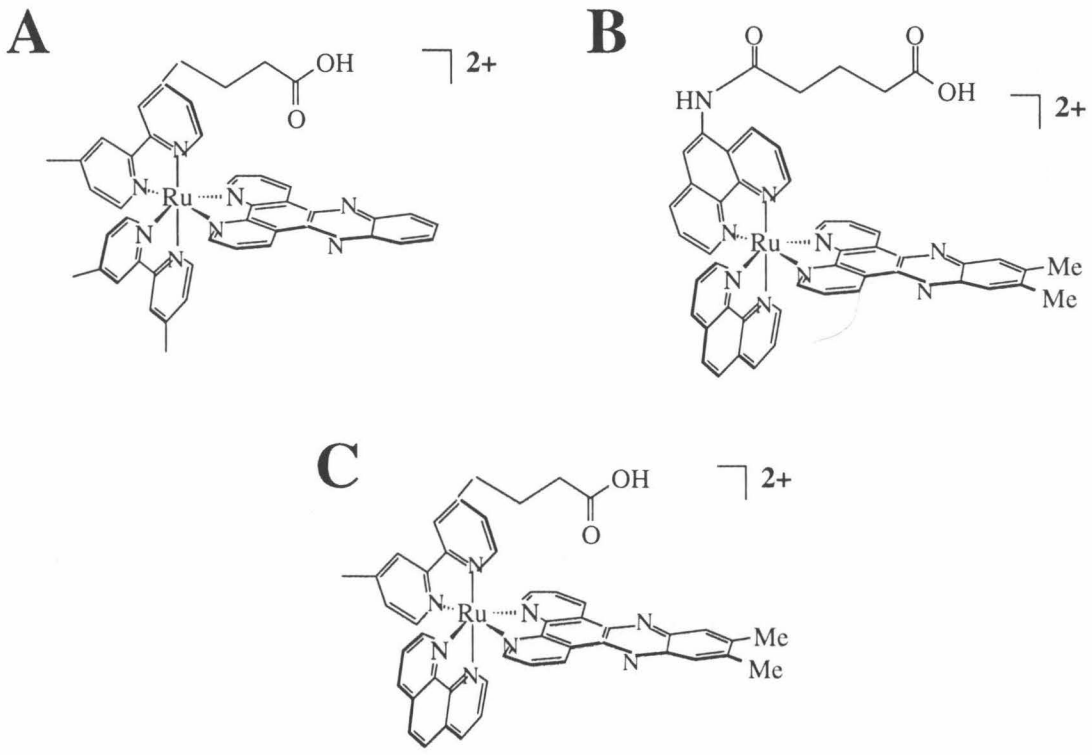

Figure 4.1

Structures of three trisheteroleptic complexes Ru(dmb)(bpy')$(dppz)^{2+}$ (A); Ru(phen)(phen')$(Me_2dppz)^{2+}$ (B); Ru(phen)(bpy')$(Me_2dppz)^{2+}$ (C). Ligand abbreviations are as follows: dmb = 4,4'-dimethyl-2,2'-bipyridine; bpy' = 4-(4-carboxybutyl)-4'-methyl-2,2'-bipyridine; dppz = dipyridophenazine; phen = 1,10-phenanthroline; phen' = 5-amidoglutaric-1,10-phenanthroline; Me_2dppz = 7,8-dimethyl-dipyridophenazine.

The work discussed herein is best described as "ongoing." Rather than treat these experiments as a complete study, we have instead chosen to describe the synthesis and characterization of metallated oligonucleotides generally, presenting the various techniques with appropriate examples. Our characterization and discussion of metal duplexes then focuses on one sequence, with the goal of highlighting methods of charcterization and addressing possible problems. Chapter 5 further presents the utilization of well-behaved Ru(II)-DNA chimeras in the study of long-range guanine oxidation chemistry.

4.2 Experimental

4.2.1 Instrumentation

High performance liquid chromatography (HPLC) purification was performed on a Hewlett-Packard 1050 system with diode array detection. Enzymatic digestions of oligonucleotides were analyzed with a Hewlett-Packard 1090 system with diode array detection and oven-regulated column cabinet. UV-visible spectroscopy and thermal denaturation studies were performed on a Hewlett-Packard 8452A diode arrray spectrometer equipped with a Peltier heating unit (Hewlett-Packard); variable temperature data were analyzed with software supplied by the manufacturer (Tempco). Steady-state emission measurements utilized an SLM 8000 fluorimeter equipped with a controlled-temperature bath; data were analyzed using SLM software. Circular dichroism (CD) spectroscopic measurements were performed on a Jasco 500 CD spectrometer. Time-resolved emission measurements were performed with instrumentation provided by the Beckman Institute Laser Resource Center as described previously.[34] Fast atom bombardment mass spectrometry (FAB-MS) was performed at the Chemistry and Chemical Engineering Mass Spectrometry Laboratory at Caltech. Electrospray ionization mass spectrometry (ESI-MS) was performed at the Battelle Institute, Pacific Northwest Laboratories, by Dr. Amy Harms under the direction of Professor Richard Smith, and at Schering-Plough by Dr. Larry Heimark. Matrix-assisted laser desorption ionization-time

of flight mass spectrometry (MALDI-TOF) was performed at the Protein and Peptide Microanalytical Facility at Caltech.

4.2.2 Synthesis of Ligands and metal complexes

$RuCl_3 \cdot 3H_2O$ and $RhCl_3 \cdot H_2O$ were purchased from Johnson & Mathey/AESAR. 5-amino-1,10-phenanthroline (5-NH_2phen) was purchased from Polysciences. Hydroxyazobenzotriazole (HATU) was purchased from Millipore. Anhydrous solvents were purchased from Fluka. All other materials were purchased from Aldrich. 4-(4-Hydroxybutyl)-4'-methyl-2,2'-bipyridine and 4-(4-Carboxybutyl)-4'-methyl-2,2'-bipyridine (bpy') were prepared by the method of Della Ciana *et al.*[44] The ligands dppz (dipyrido[3,2-; 2',3'-c]phenazine) and Me_2dppz (7,8-dimethyl dipyridophenazine) were prepared as described previously.[27,45] $[Rh(phi)_2(bpy')]Cl_3$, $[Rh(phi)_2(phen')]Cl_3$, and Δ-$[Rh(phi)_2dmb]Cl_3$ were prepared from $[Rh(phi)_2Cl_2]Cl$[46] according to published procedures.[47]

5-amidoglutaryl-1,10-phenanthroline (phen').[48] Glutaric anhydride (0.6 g) was dissolved in 20 ml hot ethanol (absolute). 5-NH_2phen (0.1 g) was added and the mixture heated to 70 °C for 2 hrs; another 0.44 g glutaric anhydride was added and the reaction heated overnight. Reaction was followed by TLC (3:1 CH_2Cl2_2:MeOH on silica, no F_{254}). Solution was then dried to yellow oil and the product precipitated with 200 ml cold, dry acetonitrile. The cloudy solution was concetrated to 100 ml *in vacuo*; the flask was chilled at -20 °C and the pale solid product collected by vacuum filtration. Yield = 0.097 g.

4-(4-carboxybutyl)-4'-methyl-2,2'-bipyridine, methyl ester (bpy'^{Me}). Bpy'^{Me} was formed by refluxing bpy' in methanol containing concentrated H_2SO_4 (5 drops). After 1 hour, the mixture was dried, the product extracted into CH_2Cl_2, and the organic layer dried *in vacuo* to an oil. The oil slowly crystallized *in vacuo* to a waxy solid or was recrystallized from diethyl ether/hexane.

4-(4-thioacetylbutyl)-4'-methyl-2,2'-bipyridine (1).[49,50] Triphenyl phosphine (2.1 g) and THF (20 ml) were chilled to 0 °C. Diisopropyl azodicarboxylate (DEAD) (1.67 g; 1.78 ml) was then added and the reaction stirred at 0 °C for 30 min, during which time a yellow solution and white precipitate formed. A solution of 4-(4-hydroxybutyl)-4'-methyl-2,2'-bipyridine[ref] (1 g) and thioacetic acid (0.608 g 0.57 ml) was then added dropwise to the phosphine/DEAD mixture. The green, cloudy reaction was stirred for 1 hr at 0 °C and then warmed to room temperature and stirred for a further 1.5 hrs. The resulting clear orange solution was concentrated to an oil and purified by silica colmun (4 x 26 cm) in 1:1 hexanes:ethyl acetate. Yield = 1.25 g (55%) of pale, waxy solid. ^{1}H NMR ($CDCl_3$, 300 MHz) ∂: 8.7 (t); 8.4 (d); 7.1 (m); 3.0 (t); 2.8 (t); 2.6 (s); 2.4 (s); 1.9 (m); 1.7 (q).

4-[4-(2-pyridyldisulfidyl)butyl]-4'-methyl-2,2'-bipyridine (2).[50,51] In an argon atmosphere, 830 µmol (0.25 g) of **1** and 1.67 mmol 2,2'-dipyridyldisulfide (2,2'-Aldrithiol) (0.37 g) were dissolved into 3 ml CH_3CH_2OH and 1 ml THF. 1 ml degassed 1 M LiOH was then added dropwise over the course of 1 hr, during which time the reaction became dark orange. After 6 hrs, the mixture was concentrated to a biphasic oil and purified by column chromatography using basic alumina (3 x 25 cm) and 20% ethyl acetate in hexanes. Yield = 186 mg (0.5 mmol, 63%). ^{1}H NMR ($CDCl_3$, 300 MHz) ∂: 8.6 (d, bpy); 8.4 (d, S-pyridine); 7.7-7.6 (m, bpy, S-pyridine); 7.1 (m, bpy, S-pyridine); 2.8 (t, CH_2); 2.7 (t, CH_2); 2.4 (s, CH_3); 1.8 (2d, $2CH_2$).

[Rh(phi)$_2$(SO$_3$CF$_3$)$_2$](SO$_3$CF$_3$). An addition funnel, condenser, and universal adapter fit with a glass pipet were fit onto a three-neck flask to which 0.2 g $[Rh(phi)_2Cl_2]Cl$ was added. Under argon flow, 5 g trifluoromethanesulfonic acid (triflic acid) was placed in the addition funnel and then added dropwise with stirring. The reaction mixture, which turned blue, was heated at 100 °C for 1.5 hrs (until HCl vapors are no longer visible). The orange/red product was precipitated by cooling and adding 20-30 ml

of dry diethyl ether rapidly to solution. The product was then collected by filtration, washed thoroughly with water and dried with diethyl ether.

Trisheteroleptic complexes of Ru(II). $Ru(dmb)(bpy')(dppz)Cl_2$, $Ru(phen)(phen')(Me_2dppz)Cl_2$, and $Ru(phen)(bpy')(Me_2dppz)^{2+}$ were prepared according to published methods;[41,42,52,53] details of $Ru(phen)(bpy')(Me_2dppz)^{2+}$ are given as an example. Intermediates in the synthesis of $Ru(dmb)(bpy')(dppz)Cl_2$ have been extensively characterized by mass spectrometry, elemental analysis, and infrared spectroscopy (Appendix 4.1).

$[Ru(CO)_2Cl_2]_n$ (3). Formic acid (50 ml) was sparged with argon in a three necked-flask fit with a universal adapter/pipet and a condenser. Paraformaldehyde (1.0 g) and $RuCl_3 \cdot 3H_2O$ (3.02 g) were added and the solution heated under reflux for 6-20 hours. The color changed from dark red to green to dark yellow over several hours. After color changes were complete, the solution was concentrated to an orange oil and triturated (precipitated from an oil) by adding CH_2Cl_2 or hexanes.[ref] The orange-yellow solid may be collected by evaporation or filtration. IR (Nujol): 2077, 2020 cm^{-1}. The impurity $[Ru(CO)_2Cl_3]_2$ was identified by IR absorption at 2148 cm^{-1}. Yield = 2.5 g (90%).

$Ru(CO)_2Cl_2phen$ (4). Compound **3** (0.52 g) and 1,10-phenanthroline (phen) (0.50 g) were combined in a three-neck flask with methanol (10 ml) in an argon atmosphere. The reaction was heated under reflux for 1 hr, during which time the yellow-orange product precipitated. The reaction was cooled to room temperature and the product collected by filtration. Purity was analyzed by ^1H NMR, which indicated that the complex was symmetric with respect to the ligand. If necessary, $Ru(CO)_2Cl_2L$ complexes may be recrystallized from hot solutions of chloroform, methanol, or methanol/acetone. ^1H NMR (CH_2Cl_2, 300 MHz) ∂: 9.8 (d); 9.0 (d); 8.4 (s); 8.2 (dd). Yield = 0.47 g (50%).

$Ru(CO)_2(SO_3CF_3)_2phen$ (5). An addition funnel, condenser, and universal adapter fit with a glass pipet were fit onto a three-neck flask to which **4** (0.20 g) was added. Under argon flow, 5 g triflic acid was added to the addition funnel and then added

to **4** dropwise with stirring. The reaction was heated at 100 °C for 1.5 hrs (until HCl vapors are no longer visible). The color of the reaction varied from khaki-green to burgundy. White/gray product was precipitated by cooling and adding 20-30 ml of dry diethyl ether rapidly to solution. The flask was chilled at -20 °C to complete precipitation. The precipitate was then collected by vacuum filtration, washed with water and dried with ether. Although it has been reported that **5** should not be stored,[42] we have found that this solid is stable for months if care has been taken to wash all residual acid from the filtrate. Yield = 0.26 g (85%).

[Ru(CO)$_2$(phen)(bpy'^{Me})] (PF$_6$)$_2$ (6). Compound **5** (0.13 g), bpy'^{Me} (0.065 g), and 2-methoxyethanol (2 ml) were combined in the three-neck flask under argon flow and heated for 2 hrs. The resulting orange solution was then cooled and excess NH_4PF_6 (aq) was added to precipitate product. Flask was chilled at -20 °C to complete precipitation and the pale pink or tan product collected by vacuum filtration. Solid was washed with water and diethyl ether. Yield = (0.15 g) 85%.

[Ru(phen)(bpy'^{Me})(Me$_2$dppz] Cl$_2$ (7). Me_2dppz (0.048 g), **6** (0.070 g), and 2-methoxyethanol (4 ml) were added to a three-neck flask under argon flow and warmed for 15 min to dissolve the ligand. Trimethylamine N-oxide (0.018 g) were added and the solution heated for 90 min, during which time reaction darkened to a deep red color. The solution was cooled to room temperature and loaded directly onto a Sephadex QAE column, Cl^- form, and eluted with CH_3CN/H_2O. The red solution was then dried *in vacuo*, redissolved into acetonitrile, and purified by column chromatography (neutral alumina; CH_3CN/H_2O gradient). After the elution of excess ligand and minor amounts of Ru(II) complexes, the product eluted at 2-3% H_2O; complexes bearing carboxylic acids were found to require higher concentrations of water (5 - 10%) or low concentrations of acetic acid (5%).

[Ru(phen)(bpy')(Me$_2$dppz] Cl$_2$ (8). The methyl ester **7** was deprotected by stirring in 2 ml LiOH (1 M) overnight. The reaction was neutralized with 1M HCl and

desalted on a C18 seppak column (5 g; Waters) as described in the product literature. Careful washing of the column-bound complex with H_2O was critical, since excess salt was found to interfere with the DNA-coupling reaction. If desired, the two coordination isomers of **8**, in which the carboxylate arm of bpy' is axial or equatorial to the Me_2dppz ligand, may be separated by HPLC [C18, 300 Å column material; gradient of 15-85% CH_3CN, 85-15% NH_4OAc (100 mM) over 35 min]. For the syntheses described here, the isomers were not separated and the two products **8** were characterized by mass spectrometry, UV-visible spectroscopy, and HPLC. Absorption: 272 nm, $\varepsilon \sim 120{,}000\ M^{-1}cm^{-1}$ (ligands, π-π^*); 380 nm, $\varepsilon \sim 25{,}000\ M^{-1}cm^{-1}$ (Me_2dppz, π-π^*); 440 nm, $\varepsilon \sim 21{,}000\ M^{-1}cm^{-1}$ (MLCT). FAB-MS (m/z): 993 {[Ru(phen)(bpy')(Me_2dppz)](PF_6)}; 847 [Ru(phen)(bpy')(Me_2dppz)]; 592 [Ru(phen)(Me_2dppz)H]; 538 [Ru(phen)(bpy')H]. Yield = 0.056 g (78%).

UV-visible spectroscopy. Metal complexes were quantitated by absorption spectroscopy using the following extinction coefficients (ε_{nm}): $\varepsilon_{350} = 23{,}600\ M^{-1}cm^{-1}$ [$Rh(phi)_2(phen')^{3+}$; $Rh(phi)_2(bpy')^{3+}$; $Rh(phi)_2(dmb)^{3+}$];[46] $\varepsilon_{440} = 21{,}000\ M^{-1}cm^{-1}$ [Ru(phen)(phen')($Me_2dppz)^{2+}$; Ru(phen)(bpy')($Me_2dppz)^{2+}$; Ru(dmb)(bpy')(dppz)$^{2+}$].[27]

4.2.3 Synthesis and characterization of metallated oligonucleotides

Preparation of nucleic acids. Synthetic oligonucleotides were prepared on 2000Å controlled pore glass resin (CPG) by standard phosphoramidite chemistry[54] (ABI 394 DNA synthesizer) using starting materials purchased from Glen Research. Trityl-protected alkylamine $PO_4(CH_2)_6NH$-MMT (MMT = 4-monomethoxytrityl) and disulfide-protected alkylthiol $PO_4(CH_2)_6S$-$S(CH_2)_6OC(C_5H_5)_3$ were added to the 5'-terminus of resin-bound DNA during solid-phase synthesis. The MMT protecting group on the alkylamine was removed by trichloroacetic acid, as described by the manufacturer, to generate the free amine linker (N6P).

The linkers $NH_2(CH_2)_xNHCO$- were added to the 5'-ribose of resin-bound DNA using chemistry described by Wachter *et al.*[55] Briefly, 0.5 g carbonyl diimidazole in dry dioxane was added to CPG-bound oligonucleotides immediately following automated synthesis. The reaction was agitated for 20 min in a glass-fritted reaction vessel, the solution drained, and the resin rinsed with dioxane. 0.5 g alkyl diammine [$NH_2(CH_2)_6NH_2$, $NH_2(CH_2)_9NH_2$, or $NH_2C_2H_4OC_2H_4OC_2H_4NH_2$] in 9:1 dioxane:$H_2O$ was added to CPG-DNA and agitated for 30 min. The solution was then drained, rinsed with 40 ml dioxane, 10 ml H_2O, and 20 ml MeOH, and dried *in vacuo* to generate the tethered amine linker (N6C, N9C, or NO8). This synthesis has been automated for the ABI 394 DNA synthesizer; the procedures and cycles (MICHELLEC1; LINKCLEAN) are included in Appendix 4.2.

Formation of M-DNA conjugates via N,N,N',N'-tetramethyl-O-(N-succinimidyl)-uronium tetrafluoroborate (TSTU).[13] This procedure has been reported for synthesis of $Rh(phi)_2(bpy')^{3+}$-oligonucleotide conjugates,[36] and has not yet been successful for coupling of complexes containing the phen' ligand. To summarize, $[Rh(phi)_2bpy']Cl_3$ (10 μmol) was combined with TSTU (30 μmol) and 30 μmol N,N'-diisopropylethylamine (DIEA) and dissolved into 600 μl of 1:1:1 methanol:acetonitrile:methylene chloride. The reaction was stirred at room temperature to form the succinimide ester of the metal complex (TLC: alumina; CH_3OH). Another 100 μmol DIEA and amine-derivatized CPG-DNA (2 μmol) were then added to the solution and the slurry stirred vigorously at room temperature. After 12 hrs, the resin was rinsed and the Rh(III)-oligonucleotide conjugate cleaved and deprotected by treatment with 2 ml NH_4OH at 55 °C for 6 hours.

Formation of M-DNA conjugates via hydroxyazobenxotriazole (HATU).[56,57] This procedure has been found to be general for coupling of Ru(II) and Rh(III) complexes containing both bpy' and phen' ligands to amino-modified DNAs. As an example, $Ru(phen)(bpy')(Me_2\text{-}dppz)Cl_2$ (7 μmol), HATU (14 μmol), DIEA (14

μmol), and amine-derivatized CPG-DNA (2 μmol) were vigorously stirred in 400 μl dimethylformamide (DMF) at room temperature.[angel] After 12 hrs, the resin was rinsed and the Ru(II)-oligonucleotide conjugate cleaved and deprotected by treatment with 2 ml NH_4OH at 55 °C for 6 hours.

Synthesis of Rh(phi)$_2$[4-methylbpy-(CH$_2$)$_4$-S]-S-(CH$_2$)$_6$-5'-GGCCTTCGCACT-3' (Rh-SS-DNA). CPG-bound oligonucleotide containing the disulfide-protected, 5'-thiol linker (1 μmol) was cleaved and deprotected by treatment with NH_4OH (2 ml) + dithiothreitol (50 mM) at 55 °C for 6 hours. The reaction mixture was filtered, dried *in vacuo* and the thiol-oligonucleotide purified by HPLC [Dynamax C18 resin, 300 Å, 1.0 x 25 cm column (Rainin); gradient: 5 - 25% CH_3CN, 95-75% NH_4OAc (100 mM) over 40 min]. A concentrated solution of the activated disulfide ligand **2** (10 μmol) was immediately added to $HS(CH_2)_6PO_4$-DNA after collection from the HPLC and the cloudy mixture agitated for 12 hrs. The reaction was then dried *in vacuo*, dissolved in buffer (100 mM NH_4OAc) and extracted with an equal volume of ethyl acetate to remove yellow pyridyl-2-thione. The aqueous layer was separated and the product isolated by HPLC [Dynamax C18 resin, 300 Å, 1.0 x 25 cm column (Rainin); gradient: 5 - 50% CH_3CN, 95-50% NH_4OAc (100 mM)/EDTA (1 mM) over 45 min]. The bpy-DNA conjugate was desalted by seppak (Waters), using the directions provided by the manufacturer, and concentrated. The yield of bpy-DNA conjugate was estimated by UV absorption to be 85 nmol (8.5% yield from DNA synthesis); a concentrated solution of 85 nmol $[Rh(phi)_2(SO_3CF_3)_2](SO_3CF_3)$ in DMF was then added and the reaction agitated at 60 °C for 24 hrs.

Purification of metallated oligonucleotides by HPLC. Purification of metal-oligonucleotide chimeras was achieved by reverse-phase HPLC (column materials: C4, C18; CH_3CN/NH_4OAc eluent). Conditions of separation varied with the metal complex, sequence, and linker; examples are presented in Section 4.3.2. Coupling of the two coordination isomers of trisheteroleptic complexes of Ru(II) to DNA led to formation

of Δ- and Λ- diastereomeric conjugates. In most cases, the four diastereomers of Ru(II)-oligonucleotide conjugate were isolated by HPLC. Similarly, coupling of $Rh(phi)_2(bpy')^{3+}$ or $Rh(phi)_2(phen')^{3+}$ yielded two diastereomeric products.

UV-visible spectroscopy. Yields of metallated oligonucleotides were quantitated by absorption spectroscopy using the following ε_{nm}: ε_{390} = 19,500 $M^{-1}cm^{-1}$ for Rh(III)-modified oligonucleotides and ε_{440} = 19,000 $M^{-1}cm^{-1}$ for Ru(II)-modified oligonucleotides (Section 4.3.2).

Enzymatic digestion of oligonucleotides with snake venom phosphodiesterase (SVP)/alkaline phosphatase (AP).[58] Each metallated oligonucleotide (0.25 nmol) was incubated for 3 hrs in the following cocktail: H_2O (70 μl), 1 M $MgCl_2$ (10 μl), AP buffer (10 μl), AP (Boehringer Mannheim) (5 μl), SVP (Sigma) (5 μl). The reaction was then filtered and analyzed by HPLC [Microsorb MV, C18 100 Å, 0.46 x 25 cm column; 0-5% CH_3CN, 100-95% NH_4OAc (250 mM; pH 5); oven temperature: 40 °C]. For quantitation of nucleosides, moles of products were calculated from peak integrals (A•s) by the following formula:

$$\text{mol} = (\text{peak integral})/(\text{flow rate})(\varepsilon_{nm}),$$

where [flow rate] = liters/sec and $[\varepsilon_{nm}] = M^{-1}cm^{-1}$ at the wavelength measured. Nucleosides were identified by comparison of retention times and UV spectra to authentic standards (Sigma). Ratios were quantitated by dividing peak areas by ε_{260} ($M^{-1}cm^{-1}$) for each nucleoside (ε_{dC} = 7,400; ε_{dG} = 11,700; ε_{dT} = 8,800; ε_{dA} = 15,400).

Phosphate analysis of DNA. The yield of oligonucleotides was quantitated by a colorimetric test for phosphate.[59] 100 μl samples in H_2O were prepared as well as standard solutions of phosphate (5, 10, 15 μM) in glass test tubes. 30 μl perchloric acid was added and the samples heated to 200 °C for 20 min. Solutions were cooled to room temperature, 80 μl Na_2SO_3 (M) was added, and the samples were heated for 5 min at 100 °C. Solutions were cooled to room temperature, 40 μl N_2H_4, 100 μl Na_2MoO_4, and 500 μl H_2O added and the samples heated for 15 min at 100 °C. Concentrations of phosphate

in each sample was then determined by the absorption at 820 nm compared to standard phosphate solutions.

Sample preparation. Metallated oligonucleotide duplexes were prepared as follows: equimolar amounts of single-stranded oligonucleotides were combined in a buffer of 5 mM phosphate, 50 mM NaCl, pH 7 ($[strands]_{final}$ = 10 μM, typically). Stranded were hybridized by slow cooling on a thermal cycler (Perkin Elmer) (preheat at 90 °C, 15 min; 90 - 20 °C over 3 hrs).

Analysis of Ru(II) and Rh(III) binding sites. Oligonucleotides were radioactively labeled with ^{32}P at either the 5' or 3' termini by standard techniques;[60] oligonucleotides labeled at the 5' end with Ru(II) complexes were labeled with ^{32}P at the 3'-terminus without procedural modifications. To monitor the sites of binding of Ru(II), Ru(II)-modified duplexes and unmodified duplexes + Ru(II) were either irradiated i) at 435 nm with a 1000 W Hg/Xe lamp equipped with a monochrometer (13 mW at 435 nm) or ii) at 442 with a CW He-Cd laser (17 mW) for 60 minutes. After irradiation, samples were treated with 100 μl of 1 M piperidine at 90 °C for 30 min, dried, and electrophoresed through a 20% denaturing polyacrylamide gel. To monitor the sites of binding of Rh(III), Rh(III)-modified duplexes were irradiated for 20 min at 313 nm with a 1000 W Hg-Xe lamp (~2mW). After irradiation, samples were electrophoresed through a 20% denaturing polyacrylamide gel. The extent of damage was quantitated by phosphorimagery (Imagequant).

Nondenaturing gel electrophoresis. ^{32}P-labeled oligonculeotide duplexes were compared to ^{32}P-labeled single-stranded oligonucleotides by nondenaturing gel electrophoresis (12% polyacrylamide; 4 °C). The extent of hybridization was quantitated by phosphorimagery (Imagequant).

Thermal denaturation of DNA duplexes. Melting of DNA duplexes was monitored by the characteristic hyperchromicity in UV absorption. Typical temperature

gradients started at 80 °C (15 min), decreased to 25 °C in 2 °C intervals (3 min/measurement), then increased to 80 °C in 2 °C intervals (3 min/measurement).

Steady-state emission. For emission measurements, 100-200 μl samples were placed in 0.5 cm cuvettes and thermally equilibrated for 5 min at 25 °C in a thermostated sample chamber. For variable-temperature measurements, samples were equilibrated at each temperature for 15 min. Results were similar when several samples were monitored in parallel or when temperature cycles were run consecutively.

4.3 Results

4.3.1 Synthesis of functionalized ligands and complexes

4.3.1.1 Substituted 4,4'-dimethyl-2,2'-bipyridine ligands

Hydroxyalkyl-substituted bpy ligands have served versatile starting points for the synthesis of metal complexes containing reactive linkers.[44] Scheme 4.1 illustrates the preparation of an activated disulfide derived from this ligand. The first step in the synthesis[49] of **2** is a variation of the Mistunobu synthesis for substituting alcohols with complete inversion of configuration; the second step of this reaction is simply a base-catalyzed deprotection of the thioester followed by *in situ* disulfide exchange. Disulfides of 2-thiopyridine are known to undergo disulfide exchange readily; the reaction equilibrium is shifted towards the alkyl disulfide by the tautomerization of 2-thiopyridine to 2-pyridyl thione.[51] A similar synthesis has been used to prepare a series of terpyridine-peptide chimeras to which Fe^{2+} was then coordinated.[50] We have used a similar coordination method to form Rh(III)-oligonucleotide conjugates by adding the ligand-DNA conjugate to coordinatively unsaturated $[Rh(phi)_2(SO_3CF_3)_2]^+$. Alternatively, the thioactetate intermediate **1** can be coordinated to this Rh(III) intermediate and the stable complex $[Rh(phi)_2\mathbf{1}]^{3+}$ further reacted to form the thiol or mixed disulfide.

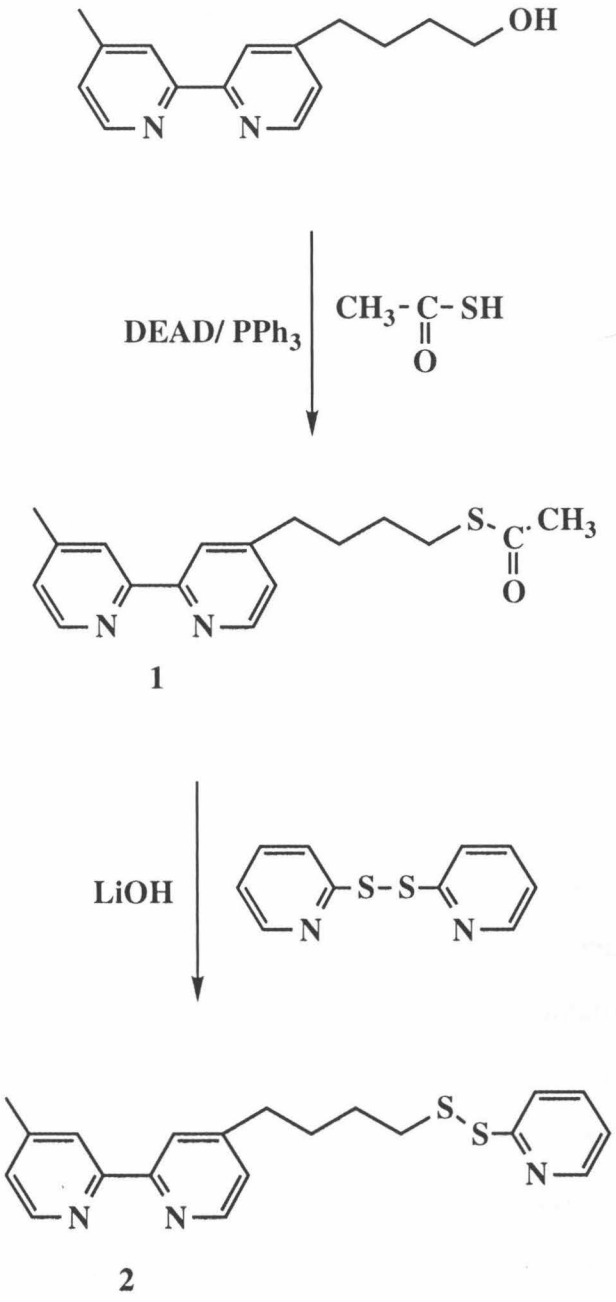

Scheme 4.1. Synthesis of 4-[4-(2-pyridyl disulfide)butyl]-4-methyl-2,2'-bipyridine

4.3.1.2 Trisheteroleptic complexes

Scheme 4.2 illustrates the steps in the synthesis of trisheteroleptic complexes of Ru(II).[41,42] This method has been shown to be generally applicable for diimine ligands, and the optimum order of coordination depends on the solubility of each ligand. For example, Scheme 4.2 shows the most successful preparation of Ru(phen)(bpy')-(Me_2dppz)Cl_2. Adding the Me_2dppz ligand in the last step was found to be most suitable due to its insolubility in H_2O; when added as the second ligand, excess Me_2dppz was not easily separated from [$Ru(CO)_2$(phen)(Me_2dppz)]$(PF_6)_2$. It was also found that the coordination of bpy' as the second ligand was facilitated by using the bpy' methyl ester; in this case, [$Ru(CO)_2$(phen)(bpy'^{Me})]$(PF_6)_2$ was found to be less soluble than the corresponding acid, and excess ligand was easily removed by H_2O. The synthesis of Ru(phen)(phen')-(Me_2dppz)Cl_2, on the other hand, was accomplished in high yield without preparing the methyl ester of phen'. Finally, it is noteworthy that the intermediate coordination compounds of Ru(II) are stable for months at room temperature when stored as solids.

The purification of these trisheteroleptic complexes was straightforward. The crude reaction mixture was eluted through a Sephadex QAE anion exchange column, Cl^--form, in order i) to remove the sparingly soluble Me_2dppz ligand, ii) to improve complex solubility, and ii) to exchange unreacted coordination sites with chloride ion. The reaction was then dried *in vacuo*, redissolved in acetonitrile, and purified on neutral alumina. The product tended to smear on the column, and the most reliable test for purity was found to be analytical HPLC (C18 column; gradient of 30 - 100% CH_3CN over 35 min). The methyl ester of $Ru(CO)_2$(phen)(bpy'^{Me})$^{2+}$ was then cleaved in aqueous base, the solution neutralized, and the product desalted.

Table 4.1 compares the emission properties of three trisheteroleptic complexes of Ru(II) to related complexes bearing two different ligands. As has been shown previously (Chapter 2), all bisheteroleptic complexes of Ru(II) containing dppz and Me_2dppz ligands

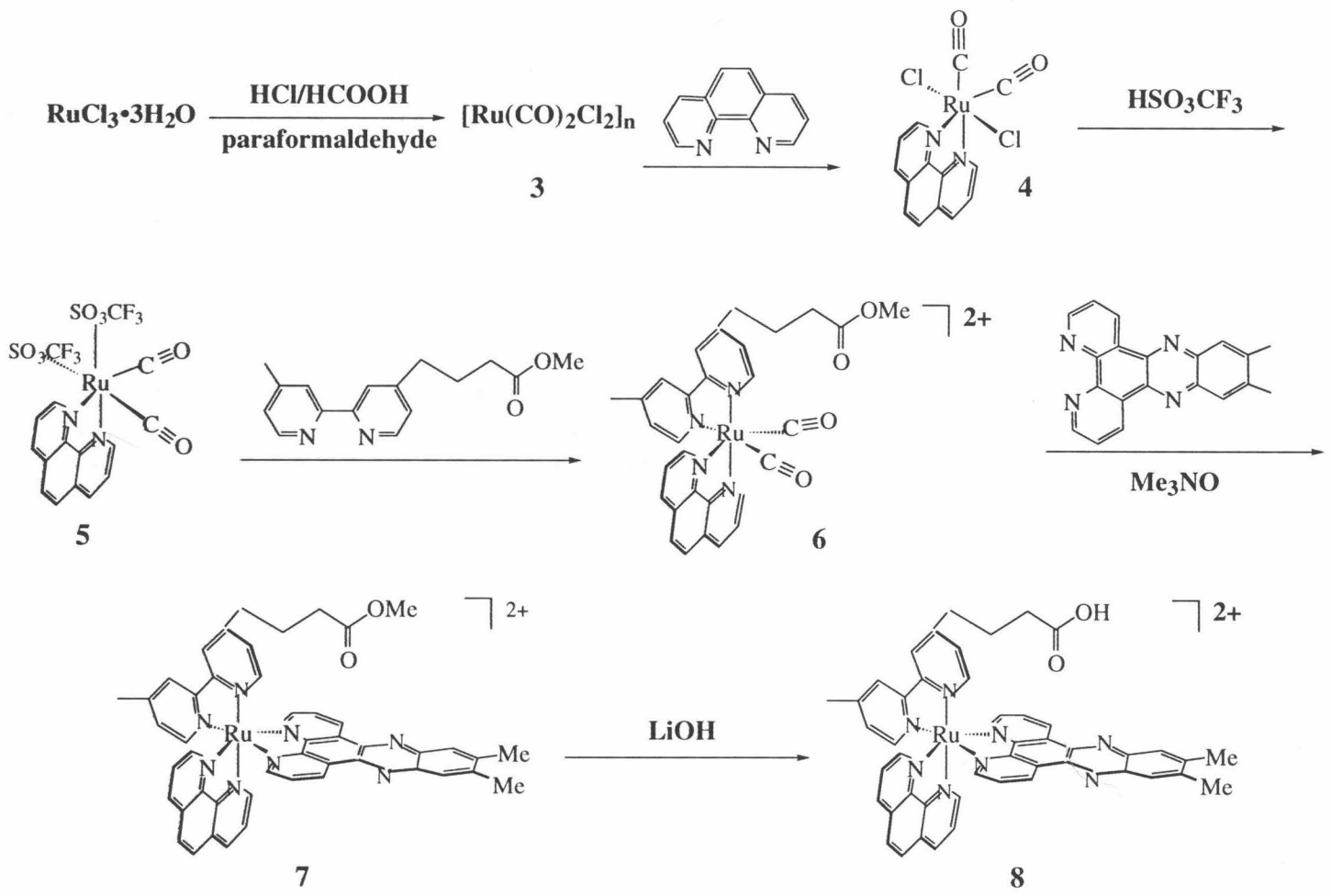

Scheme 4.2. Synthesis of trisheteroleptic complex Ru(phen)(bpy')(Me_2dppz)$^{2+}$

Table 4.1. Emission properties of Ru(II) complexes in presence of B-form DNA.[a]

Complex	Rel. Intensity[b]	excited-state lifetimes[c] τ_1 (ns)	%	τ_2 (ns)	%	emission maxima (nm)
$Ru(bpy)_2dppz^{2+}$	0.23	100	90	450	10	619
$Ru(phen)_2dppz^{2+}$	0.8	115	70	660	30	618
$Ru(dmb)(bpy')(dppz)^{2+}$	0.1	32	80	155	20	630
$Ru(phen)_2(Me_2dppz)^{2+}$	3.0	280	55	1070	45	609
$Ru(phen)(phen')(Me_2dppz)^{2+}$	4.3	445	61	1250	40	608
$Ru(phen)(bpy')(Me_2dppz)^{2+}$	1.6	180[d]	55[d]	630[d]	45[d]	619

[a] Samples were 10 μM Ru(II) bound to 500 μM bp calf thymus DNA in an aerated buffer of 5 mM tris, 50 mM NaCl, pH 8.5. [b] Intensity given relative to $Ru(bpy)_3^{2+}$ (10 μM) in H_2O; steady-state emission measurements were taken with an SLM 8000 with λ_{exc} = 440 nm. [c] Conditions for time-resolved emission measurements were λ_{exc} = 480 nm; λ_{obs} = 610 nm. Lifetimes were determined by fitting time-resolved emission data to a biexponential function; ratios were calculated from the magnitutes of the pre-exponential factors. [d] Sample was 10 μM Ru(II) bound to 10 μM duplex (sequence 16 merA/B; Table 4.2).

luminesce brightly in the presence of DNA but show no steady-state emission in buffered solutions in the absence of DNA.[35] The emission intensity and lifetimes of DNA-bound complexes increases with the hydrophobicity of the ligands; thus, the steady-state intensity increases in the order $Ru(bpy)_2dppz^{2+} < Ru(phen)_2dppz^{2+} < Ru(bpy)_2(Me_2dppz)^{2+}$. Similarly, trisheteroleptic complexes bearing one dppz-type ligand and one carboxylate ligand are "molecular light switches" for DNA and show increased luminescence intensity in the order $Ru(dmb)(bpy')(dppz)^{2+} < Ru(phen)(bpy')(Me_2dppz)^{2+} < Ru(phen)(phen')(Me_2dppz)^{2+}$ (Table 4.1). Interestingly, the emission of trisheteroleptic complexes containing phen and one carboxylate ligand show longer excited-state lifetimes than the corresponding bisheteroleptic complexes, presumably because the hydrophobic linker arm further protects the intercalated complex from H_2O.[30]

4.3.2 Synthesis of metal-DNA chimeras

4.3.2.1 DNA synthesis

Oligonucleotides containing alkyl linkers at the 5' terminus were prepared by automated techniques in high yield. Identification and, if necessary, purification was readily accomplished by HPLC, since the presence of alkyl linkers increased the retention time of oligonucleotides by ~1-4 min (~2 % CH_3CN). As expected, the difference in retention times between modified and unmodified oligonucleotides varied as a function of oligonucleotide sequence and length and with the hydrophobicity of the alkyl linker. The greatest peak separations were obtained for linkers with 9 methylene groups and short DNA sequences. The four linkers used in the experiments below are pictured in Figure 4.2, along with the notation used to describe them. The three letter abbreviation identifies the terminal functional group (S = thiol; N = amine), the length of methylene chain (6 or 9), and the structure of the linkage between the alkyl chain and the 5'-terminus of the DNA (P = phosphate; C = carbamate). The notation NO8 defines the polyether linker, which has a

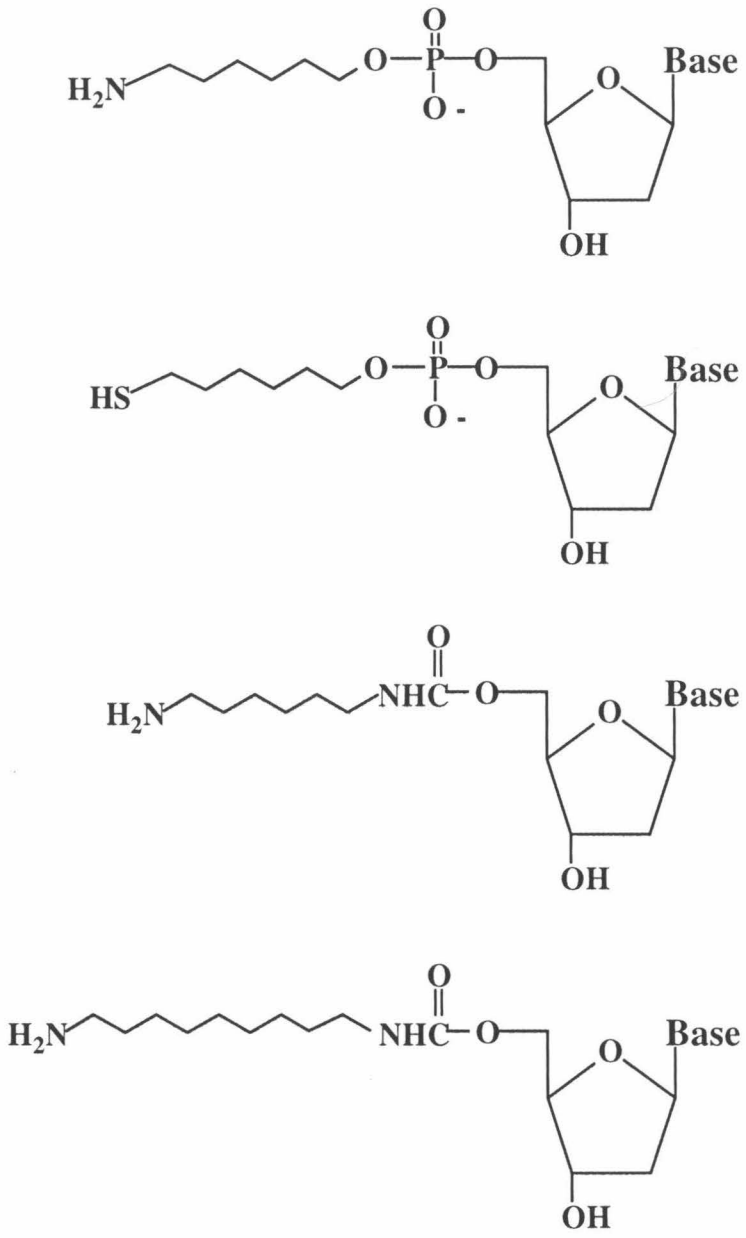

Figure 4.2

5'-DNA linkers used for synthesis of metal-oligonucleotide chimeras. From top: 5'-N6P, 5'-S6P, 5'-N6C, 5'-N9C. Linker abbreviations are a follows: N = amino terminus; S = thiol terminus; 6, 9 = $(CH_2)_6$ and $(CH_2)_9$, respectively; P = phosphate bond to DNA; C = carbamate bond to DNA.

terminal amine, 8 atoms between in the alkyl chain, and a carbamate linkage to the 5' terminus of DNA.

The formation of a carbamate bond between the alkyl diammine and the 5'-OH of a resin-bound oligonucleotide is illustrated in Scheme 4.3.[55] Greater than 90% yields were regularly obtained for this two-step reaction, as monitored by HPLC. In addition to changes in retention times, the alkylamine-oligonucleotide has been characterized by enzymatic digestion and mass spectrometry, as described below for metallated oligonucleotides. The products generated in both manual and automated syntheses of N9C-oligonucleotides were identical and showed the same reactivity. Use of the ABI DNA synthesizer, however, permitted the simultaneous synthesis of up to four different DNA sequences.

4.3.2.2 Solution-phase synthesis of disulfide-linked chimeras

Scheme 4.4 illustrates the solution-phase synthesis of Rh(III)-oligonucleotide conjugates linked by a disulfide bond. This preparation, while reproducible and high-yielding, requires three HPLC purification steps to isolate the S6P-oligonucleotide, the bpy-SS-oligonucleotide, and the Rh(III)-coupled product. The crude reaction of S6P-5'-GGCCTTCGCACT-3' with the activated disulfide ligand **2** is shown in Figure 4.3A. The four main products are identified as follows: 8 min, 2-pyridyl thione; 12 min, excess **2**; 14.5 min, S6P-5'-GGCCTTCGCACT-3'; 28 min, bpy-SS-5'-GGCCTTCGCACT-3'. Based on the relative peak areas, the yield of disulfide exchange was ~100%. Figure 4.3B shows the reaction of the 26 min product with $Rh(phi)_2(SO_3CF_3)_2^+$. The two primary products, with retention times of 18 and 23 min, were identified as the Rh(III)-oligonucleotide chimeras by mass spectrometry, absorption and CD spectroscopies, and enzymatic digestion (*vide infra*).

Because transition metals with open coordination sites have been shown to bind covalently to the endocyclic amines on DNA,[61,62] it was necessary to demonstrate that the

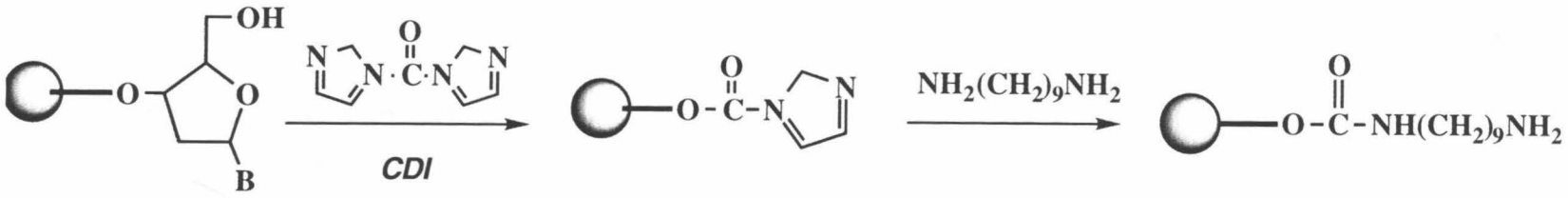

Scheme 4.3. Synthesis of N9C-oligonucleotide

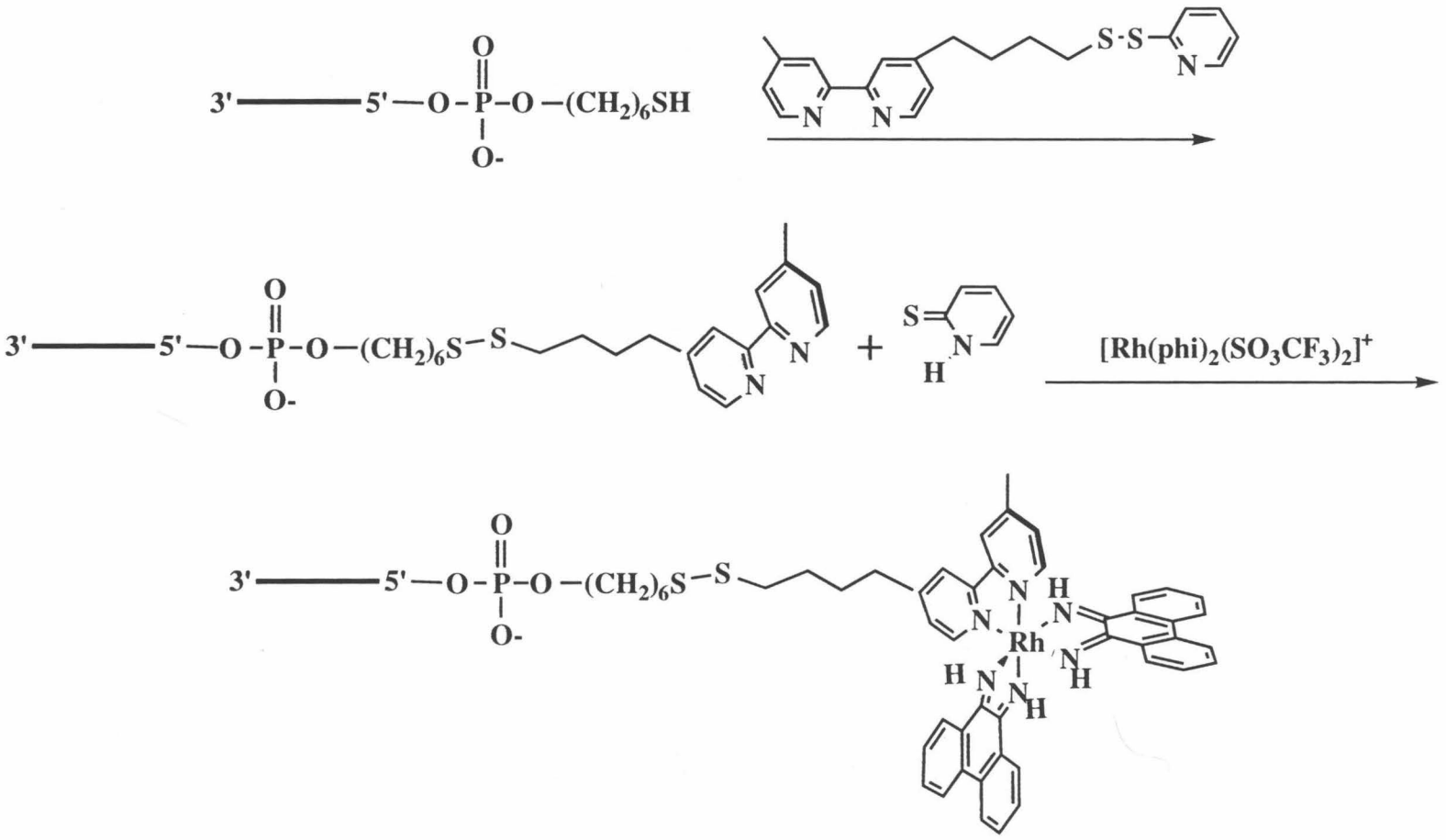

Scheme 4.4. Solution-phase synthesis of $Rh(phi)_2bpy$-S6P-oligonucleotide conjugate

Figure 4.3

HPLC chromatograms showing crude reaction mixtures in the synthesis of $Rh(phi)_2$bpy-S-S6P-5'-GGCCTTCGCACT-3'. A) Reaction of **2** with S6P-5'-GGCCTTCGCACT-3' in CH_2CN. Peaks are identified as follows: 8 min, 2-pyridyl thione; 11 min, excess **2**; 14.5 min, S6P-5'-GGCCTTCGCACT-3'; 28 min, bpy-SS-5'-GGCCTTCGCACT-3'. HPLC conditions were: Dynamax C18 resin, 300 Å, 1.0 x 25 cm column (Rainin); gradient: 5 - 50% CH_3CN, 95-50% NH_4OAc (100 mM)/EDTA (1 mM) over 45 min. B) Reaction of the 28 min product in (A) with $[Rh(phi)_2(SO_3CF_3)_2]$-(SO_3CF_3). Peaks are identified as follows: 18 min, Λ-$Rh(phi)_2$bpy-S-S6P-5'-GGCCTTCGCACT-3'; 22 min, Δ-$Rh(phi)_2$bpy-S-S6P-5'-GGCCTTCGCACT-3'. HPLC conditions were: Dynamax C18 resin, 300 Å, 1.0 x 25 cm column (Rainin); gradient: 5 - 60% CH_3CN, 95-40% NH_4OAc (100 mM) over 55 min.

A

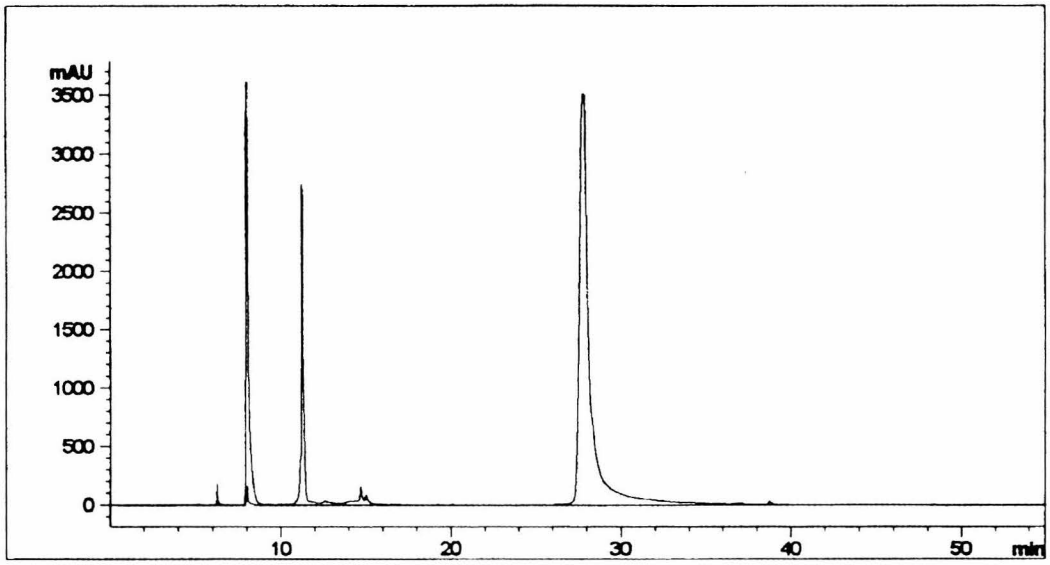
mAU
3500
3000
2500
2000
1500
1000
500
0
10
20
30
40
50
min

B

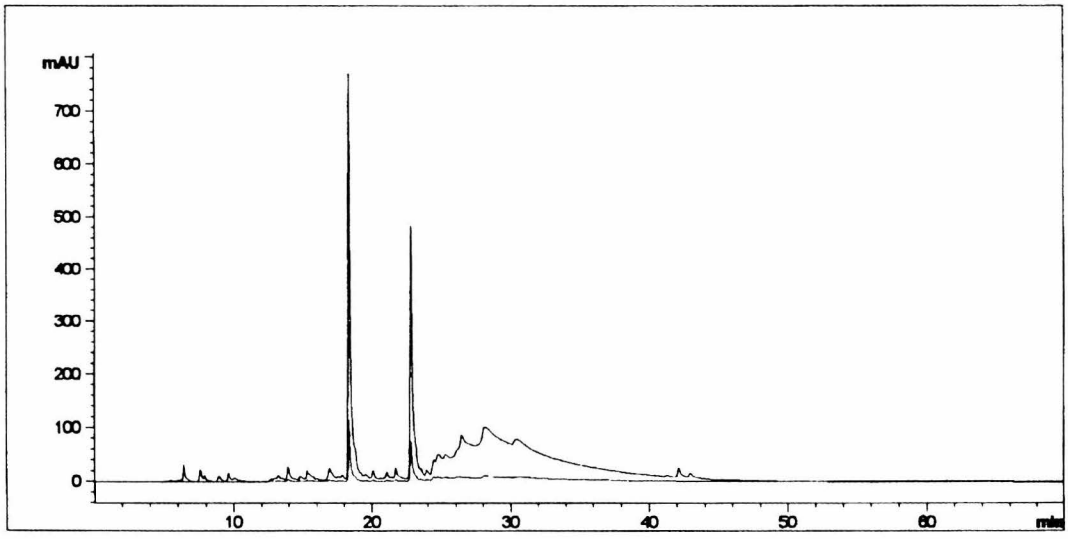
mAU
700
600
500
400
300
200
100
0
10
20
30
40
50
60

two products contained $Rh(phi)_2$-coordination only at the tethered bpy ligand. Control experiments with S6P-5'-GGCCTTCGCACT-3' indicated that, in the absence of a chelating ligand, a small amount of $Rh(phi)_2(SO_3CF_3)_2^+$ did coordinate to the DNA. However, retention times (13-15 min) and UV-visible absorption were significantly different from the products obtained in Figure 4.3B. Furthermore, ~9 poorly resolved products were obtained in the control experiment, compared to the two main products isolated in the presence of bpy-SS-GGCCTTCGCACT-3'.

4.3.2.3 Solid-phase synthesis of amide-linked chimeras

The solid-phase synthetic methods shown in Scheme 4.5 have permitted the facile and reproducible preparation of metal-oligonucleotide conjugates. Both TSTU and HATU assist with amide bond formation by generating an activated ester intermediate; HATU forms an HOAt ester, while TSTU gives the more stable N-hydroxysuccinimide ester. Coupling reactions with the two alternative coupling reagents were found to procede with similar rates, yields, and purities for both Ru(II) and Rh(III) complexes containing the bpy' ligand. Figure 4.4 shows representative HPLC traces of the crude coupling reactions of $Ru(phen)(bpy')(Me_2dppz)$-N9C-5'-AGTCTTAGTATATCGT-3' and $Rh(phi)_2$bpy'-N6P-5'-ACGATATACTAAGACT-3'. Peaks with retention times from 5 - 14 min are due to failure sequences during DNA synthesis, while materials eluting at 12 min (Figure 4.4A) and 11 min (Figure 4.4B) are unmodified, full length oligonucleotides. Products containing only 260 nm absorbance at 15.5 min (Figure 4.4A) and 12 min (Figure 4.4B) are alkyl-modified oligonucleotides, and products containing both 260 and 390 nm absorbance are metal-oligonucleotide conjugates. In both examples shown, metalated oligonucleotides gave two [Rh(III)] or four [Ru(II)] peaks with identical spectral properties (*vide infra*). These peaks were well-separated by HPLC and could be isolated in high purity.

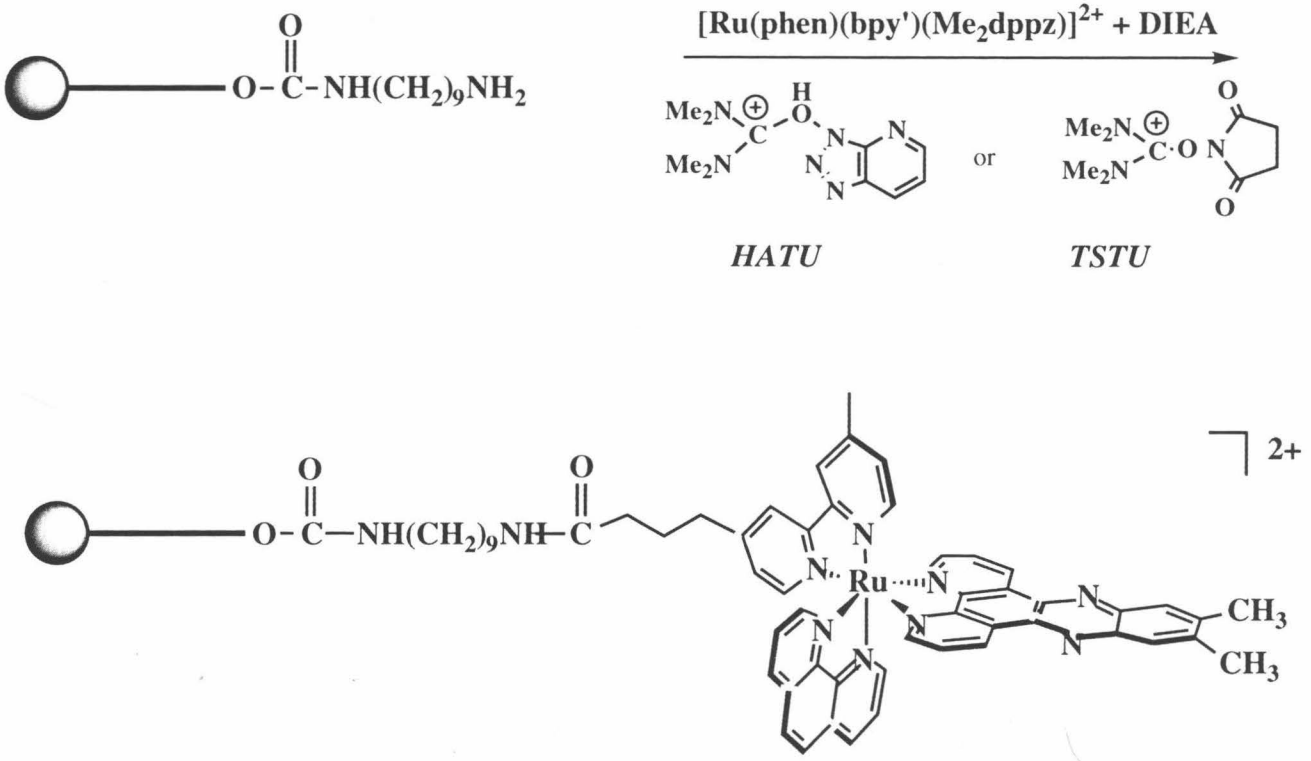

Scheme 4.5. Solid-phase synthesis of Ru(phen)(bpy')(Me_2dppz)-oligonucleotide conjugate

Figure 4.4

HPLC chromatograms showing crude reaction mixtures of metallated oligonucleotides after cleavage from CPG resin. A) Reaction of *rac*-[Ru(phen)(bpy')-(Me_2dppz)]Cl_2 with 5'-N9C-16 merA (Table 4.1). Peaks are identified as follows: 12 min, 16 merA; 15.5 min, N9C-16 merA; 31 min, 1-Λ-Ru(II)-N9C-16 merA; 33 min, 2-Δ-Ru(II)-N9C-16 merA; 36.5 min, 2-Λ-Ru(II)-N9C-16 merA; 39.5 min, 4-Δ-Ru(II)-N9C-16 merA; 56 - 60 min, unreacted Ru(II) complexes. HPLC conditions were: Vydac C4 resin, 300 Å, 1.0 x 25 cm column; gradient: 5 - 25% CH_3CN, 95-75 % NH_4OAc (100 mM) over 45 min, 25 - 80 % CH_3CN over 25 min. B) Reaction of *rac*-[Rh(phi)$_2$(bpy')]Cl_2 with N6P-16 merB. Peaks are identified as follows: 11 min, 16 merB; 12 min, N6P-16 merB; 19.5 min, Λ-Rh(III)-N6P-16 merB; 20 min, Δ-Rh(III)-N6P-16 merB. HPLC conditions were: Vydac C4 resin, 300 Å, 1.0 x 25 cm column; gradient: 5 - 20% CH_3CN, 95-80% NH_4OAc (100 mM) over 45 min.

A

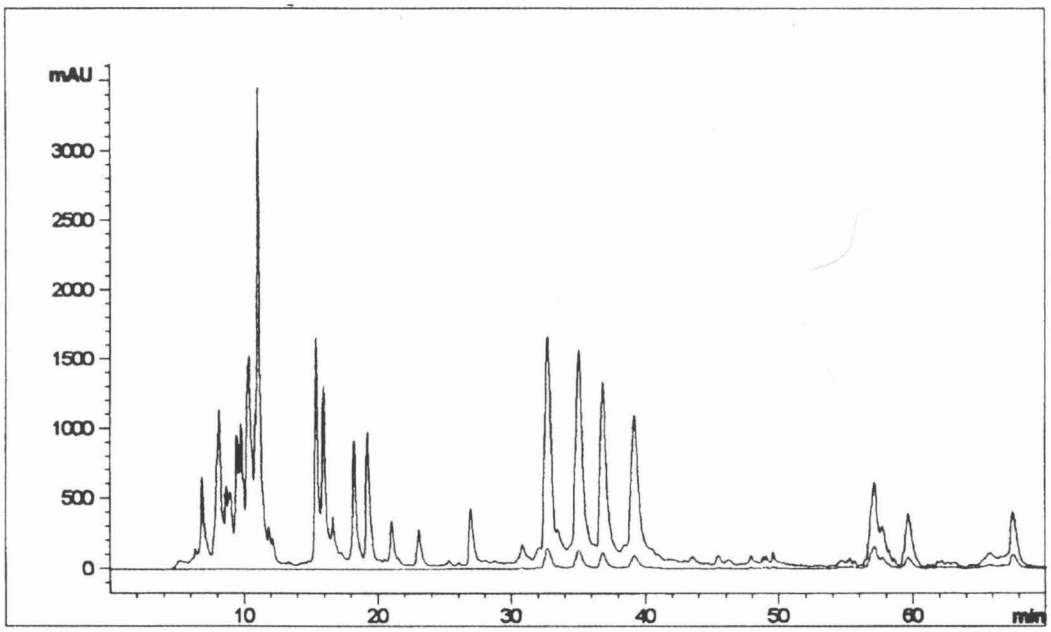
mAU
3000
2500
2000
1500
1000
500
0
10
20
30
40
50
60
min

B

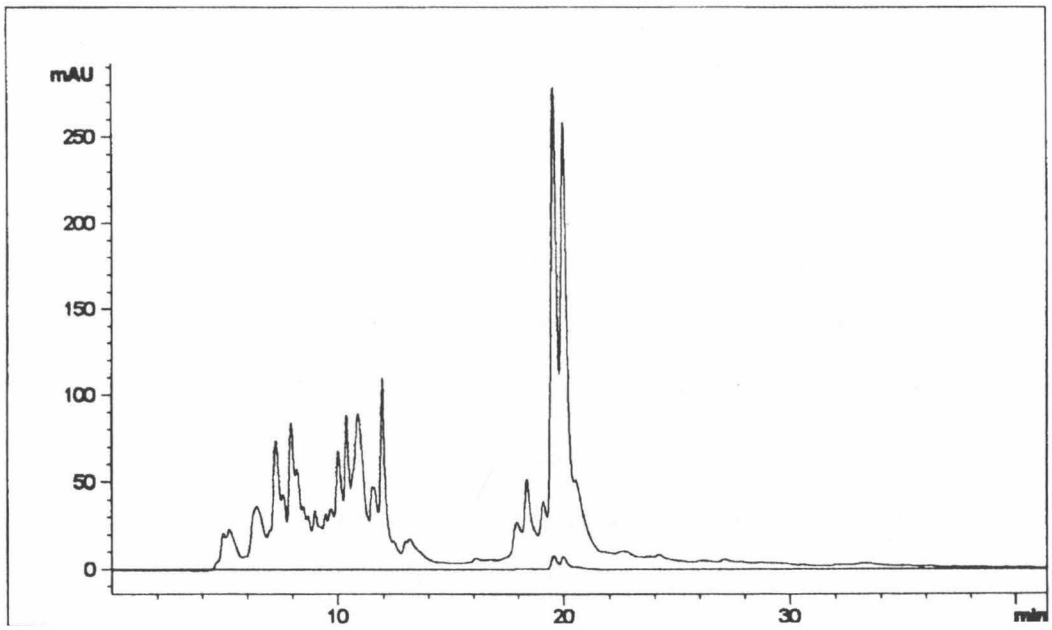
mAU
250
200
150
100
50
0
10
20
30
min

Both HATU and TSTU required 1 equiv non-nucleophilic base (such as DIEA) for coupling of Ru(II) complexes and 3 equiv of base for coupling Rh(III) complexes, presumably because the phi ligands acted as a buffer. Perhaps due to this buffering effect, reactions with Rh(III) complexes were less sensitive to the concentration of base than reactions with Ru(II) trisheteroleptic complexes; excess base dramatically inhibited amide bond formation between Ru(II) and amine-linked oligonucleotides. In all cases, reactions were stopped within 24 hrs, since longer reactions times resulted in base-catalyzed cleavage of the oligonucleotide from the resin. A number of non-nucleophilic bases have been used to effect coupling in the presence of HATU, including DIEA, n-methyl morpholine, and proton sponge (Aldrich). While the choice of base significantly affects the yields of peptide coupling with sterically-hindered amino acids and for coupling of $Rh(phi)_2(phen')^{3+}$ to resin-bound peptides, the base did not seem to alter the yield of metal-oligonucleotide conjugation.[57,63] Additionally, it is noteworthy that Rh(III) complexes have been reported to inhibit the cleavage of Rh(III)-peptide from polystyrene resin.[47] By contrast, yields of metallated oligonucleotides were on the order of 100 nmol/1μmol scale synthesis, comparable to the yield of underivatized DNA following HPLC purification.

Whereas the yields of coupling reactions between bpy'-containing complexes were similar for TSTU and HATU coupling reagents, reactions with phen'-containing complexes gave very different results. Neither $Ru(phen)(phen')(Me_2dppz)^{2+}$ nor $Rh(phi)_2(phen')^{3+}$ were reactive under the experimental conditions used to couple $Rh(phi)_2(bpy')^{3+}$ via TSTU. The procedure developed for coupling bpy' complexes of Ru(II) and Rh(III) via HATU, however, could also be used for $Ru(phen)(phen')(Me_2dppz)^{2+}$ and $Rh(phi)_2(phen')^{3+}$. In this context, it is noteworthy that the yield of reactions between $Rh(phi)_2(phen')^{3+}$ and peptides was also increased in the presence of HATU over DCC/HOBt.[63] Thus, HATU has been found to be a highly versatile reagent for coupling metal complexes to biopolymers in solid-phase reactions.

Other coupling reagents, including DCC/HOBt, DCC/HOAt, and DSC, have given variable results. DCC (dicyclohexyl carbodiimide) with HOBt (hydroxybenzotriazole) or HOAt (hydroxyazobenzotriazole) have been used successfully to couple Rh(III) complexes to peptides, and have also given low yields of Ru(II)-oligonucleotide conjugates in solid-phase preparations. DSC (disuccinimydyl carbonate) has been used to reproducibly couple $Ru(phen')_2dppz^{2+}$ to amino-linked oligonucleotides, but the method was found to be difficult and time-consuming.[22] At least part of the synthetic difficulty was caused by the presence of two carboxylate arms on the complex, since a number of spectroscopically identical products were obtained.

4.3.3 Characterization of chimeras

Table 4.2 lists the sequences discussed below and their abbreviations. In addition to identifying the sequence and linker, these notations describe the chirality of the metal complex (4.3.3.1). Rh(III)-oligonucleotides are simply characterized by Λ and Δ, to designate left-handed and right-handed chiralities, respectively. Due to the two isomers of trisheteroleptic complexes of Ru(II), Ru(II)-oligonucleotides are characterized by both the chirality of the complex and by the order of elution of conjugates; thus, the two right-handed Ru(II)-16 merA chimeras are identified by 2-Δ-Ru(II)-N9C-16 merA and 4-Δ-Ru(II)-N9C-16 merA. Each conjugate given in Table 4.2 was prepared at least twice by solid-phase synthesis using TSTU and/or HATU as coupling reagents.

4.3.3.1 Spectroscopy of metal-oligonucleotides

The UV-visible absorption spectra for metal-oligonucleotide conjugates clearly show properties from both the metal complex and the DNA strand. Figure 4.5 compares the UV-visible absorption spectra for $Ru(phen)(bpy')(Me_2dppz)^{2+}$, sequence 16 merA and 2-Δ-Ru(phen)(bpy')(Me_2dppz)-N9C-16 merA. The Ru(II)-oligonucleotide conjugate has a maximum absorption at 260 nm, due to π-π* transitions in both the aromatic bases and the

Table 4.2. Sequences used.

Abbreviation[a,b]	sequence	Δ isomers (peak #)[c]
N9C-20 merA	5'-AGTCTCAGACGCACCGATCA-3'	1, 3
20 merB	5'-TGATCGGTGCGTCTGAGACT-3'	N/D[d]
N9C-16 merA	5'-AGTCTTAGTATATCGT-3'	2, 4
N6P-16 merA	5'-AGTCTTAGTATATCGT-3'	2, 4
NO8-16 merA	5'-AGTCTTAGTATATCGT-3'	3, 4
N9C-16 merB	5'-ACGATATACTAAGACT-3'	2
N9C-14 merA	5'-AGTCTTAGTATCGT-3'	2, 4
N9C-14 merB	5'-ACGATACTAAGACT-3'	1
N9C-12 merA	5'-AGTCTTGATCGT-3'	2, 4
N9C-12 merB	5'-ACGATCAAGACT-3'	2

[a] oligonucleotides labeled A and were prepared for conjugation to Ru(II) and Rh(III) complexes, respectively. [b] These abbreviations are related to laboratory notebook references as follows: 20 merA/B = seq. 15/16; 16 merA/B = seq. 9/10; 14 mer A/B = seq. 11/12; 12 merA/B = seq. 13/14. [c] numbers refer to the relative HPLC retention times of the metal-oligonucleotide chimeras. [d] N/D = not determined.

Figure 4.5

UV-visible absorption spectra comparing a metallated oligonucleotide to the unconjugated metal complex. A) Complete UV-visible spectra for *rac*-Ru(phen)(bpy')(Me_2dppz)$^{2+}$ (a), 2-Δ-Ru(phen)(bpy')(Me_2dppz)-N9C-16 merA (b), and N9C-16 merA (c). Spectra are normalized at the maximum absorbance (272 nm for a; 260 nm for b, c). B) Spectra of Ru(II) absorption for *rac*-Ru(phen)(bpy')(Me_2dppz)$^{2+}$ (a) and 2-Δ-Ru(phen)(bpy')(Me_2dppz)-N9C-16 merA (b). Spectra are normalized at 440 nm.

A

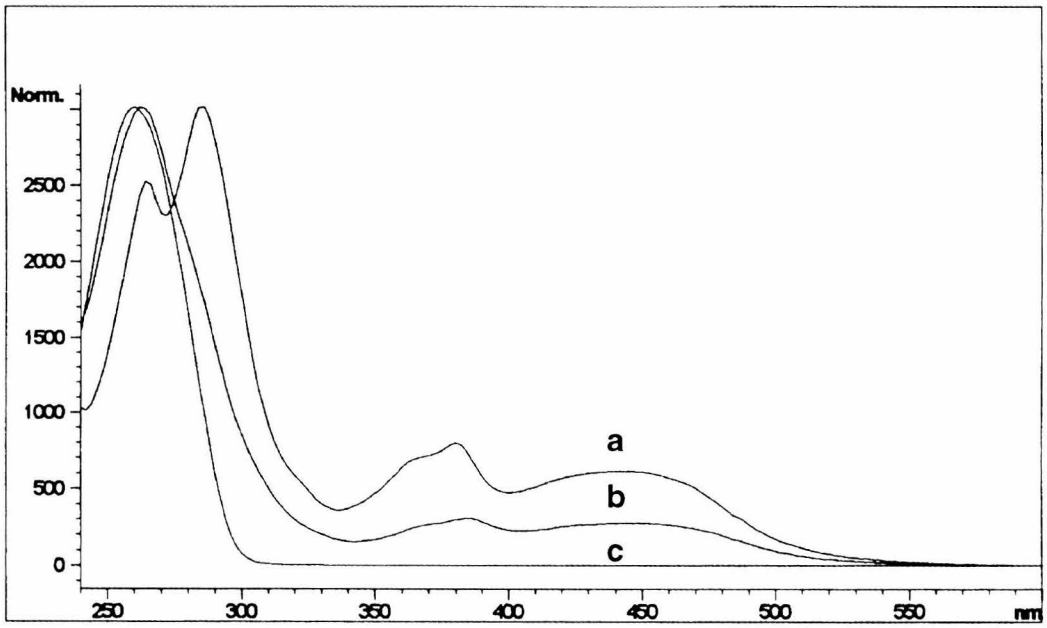
Norm.
2500
2000
1500
1000
500
0
250
300
350
400
450
500
550
nm
a
b
c

B

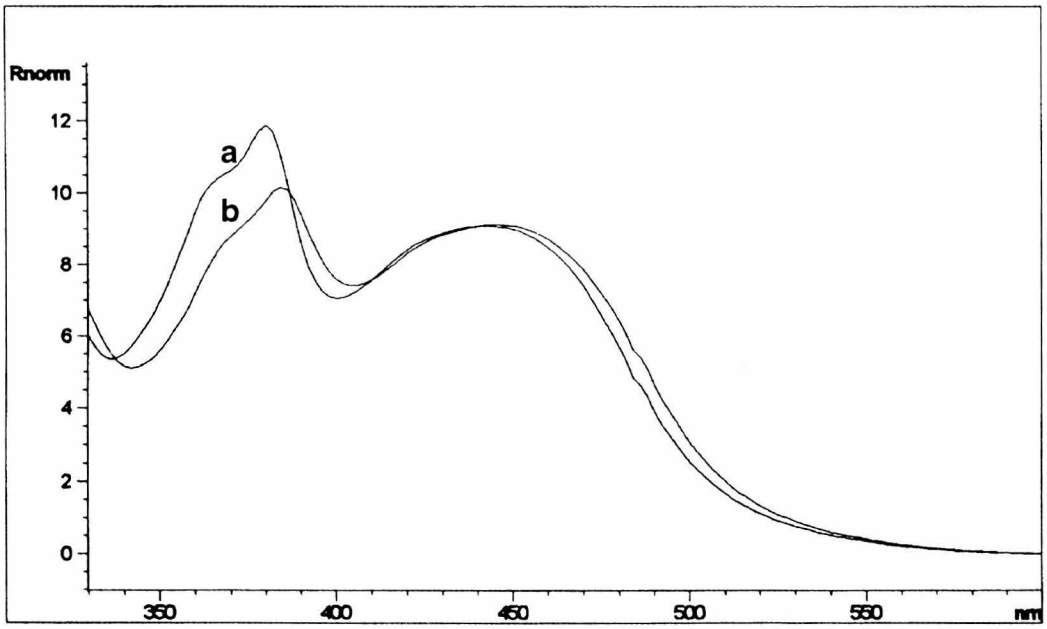
Rnorm
12
10
8
6
4
2
0
350
400
450
500
550
nm
a
b

polypyridyl ligands; the absorption intensity is ~2-fold enhanced in the conjugate over the DNA ($\varepsilon_{260,strand}$ ~ 138,000 $M^{-1}cm^{-1}$) or the metal complex itself (ε_{272} ~ 120,000 $M^{-1}cm^{-1}$). Absorption bands at 372 and 385 nm in the conjugate are due to π-π^* transitions in the Me_2dppz ligand, and are somewhat hypochromic and red-shifted (~2 and 5 nm, respectively) compared to the free metal complex (Figure 4.5B). MLCT absorption centered at 446 nm is similarly red shifted by ~6 nm compared to Ru(phen)(bpy')-$(Me_2dppz)^{2+}$, but these transitions show less hypochromicity than the Me_2dppz-centered transitions. The spectral changes observed upon covalent attachment of Ru(II) are similar to those seen for noncovalently bound complex intercalated into B-form DNA. The UV-visible absorption spectrum of $Rh(phi)_2$(bpy')-N9C-16 merB also indicates absorption due to both DNA and the metal complex. For this metallointercalator, the phi transitions are ~30% hypochromic and red-shifted by 11 nm; both the hypochromicity and red-shift are comparable to those seen for $Rh(phi)_2bpy^{3+}$ intercalated into DNA (Section 1.5.2).[40] Therefore, UV-visible spectra indicate that the molecular structures of both DNA and metal complex are preserved in the chimera; additionally, spectral changes offer evidence that the two parts of the metal-oligonucleotide conjugate interact with each other.

As noted in Section 4.3.2.3, reactions of $Rh(phi)_2(bpy')^{3+}$ with S6P-12 merB or aminoterminated DNA yield two products with identical UV-visible absorption properties; these two peaks also have the same nucleoside ratios (Section 4.3.3.2) and mass spectra (Section 4.3.3.3). CD spectroscopy (Figure 4.6A) identifies these two products as diastereomers in which the Rh(III) complex is either Λ or Δ. In this instance, the first peak to elute from the HPLC is identified as the Λ-isomer, while the slower eluting product is the Δ-isomer. Similarly, reactions with the two isomers of Ru(phen)(bpy')-$(Me_2dppz)^{2+}$ with aminoterminated DNA yield four products with comparable physical properties. Again, CD spectroscopy identifies these products as two sets of diastereomers (Figure 4.6B). When the isomers of Ru(phen)(bpy')$(Me_2dppz)^{2+}$ were separated prior to conjugation with N9C-16 merA, each isomer yielded two diastereomeric Ru-

Figure 4.6

Circular dichroism spectra comparing diastereomers of metallated oligonucleotides. A) CD spectra of Δ- (solid line) and Λ- (dotted line) $Rh(phi)_2(bpy')$-N9C-16 merB. B) CD spectra of 1-Λ- (solid line) and 2-Δ- (dotted line) $Ru(phen)(bpy')(Me_2dppz)$-N9C-16 merA.

A

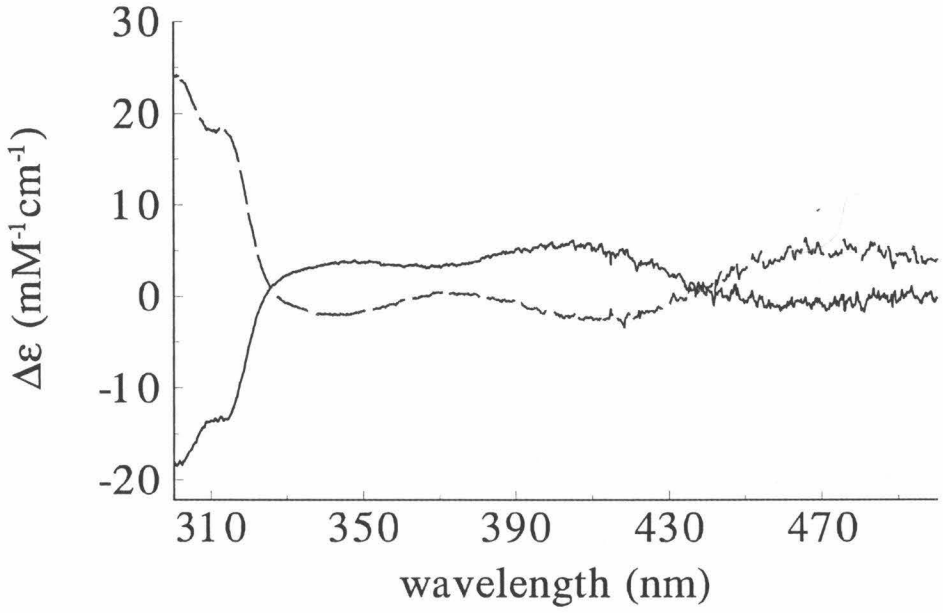
30
20
10
0
-10
-20
Δε (mM-1cm-1)
310
350
390
430
470
wavelength (nm)

B

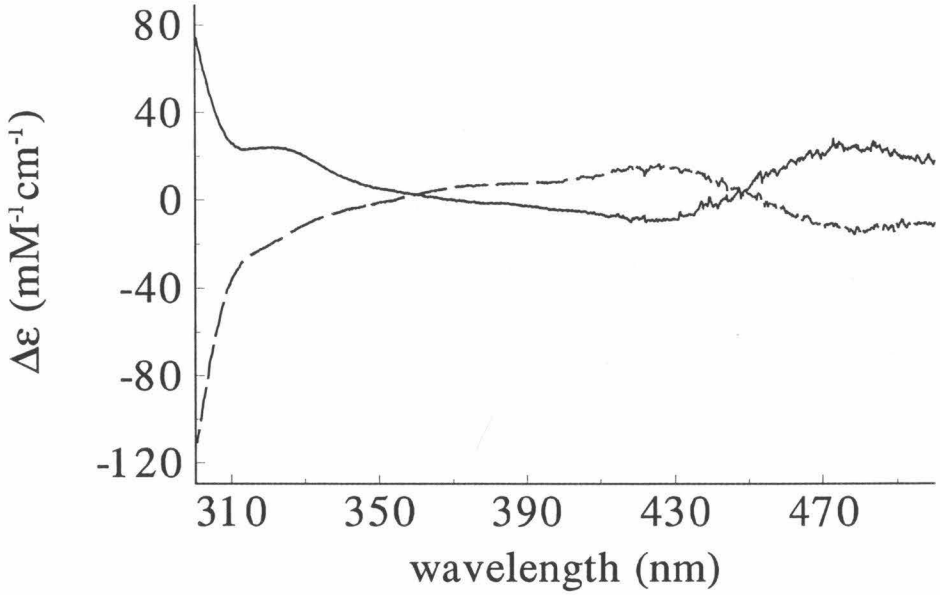
80
40
0
-40
-80
-120
Δε (mM-1cm-1)
310
350
390
430
470
wavelength (nm)

oligonucleotide conjugates. As noted in Table 4.2, the relative retention times of diastereomers vary for both Ru(II) and Rh(III) chimeras as a function of sequence; thus, it is necessary to characterize each new system by CD spectroscopy. Furthermore, since ET reactivity has been shown to vary substantially between enantiomers of both $Ru(phen)_2dppz^{2+}$ and $Rh(phi)_2bpy^{3+}$, it is fortunate that we are able to characterize the enantiomers of DNA-tethered metal complexes as well.

Previous studies of Ru(II)-oligonucleotide conjugates reported that the single-stranded Ru(phen')$_2$dppz-N6P-5'-AGTCGGAAGCTTGCA-3' did not luminesce in aqueous solution.[21,30] Single-stranded oligonucleotides bearing Ru(phen)(bpy')-$(Me_2dppz)^{2+}$, however, have all shown significant steady-state luminescence. For example, 4-Δ-Ru(II)-N9C-16 merA has an emission intensity of 1.8 relative to $Ru(bpy)_3^{2+}$ (10 μM, H_2O). Time-resolved luminescence indicates two excited-state lifetimes of 280 ns and 915 ns for this single-stranded chimera. By comparison, the luminescence of the Δ-Ru(phen)(bpy')$(Me_2dppz)^{2+}$ + 16 merA/B duplex is 1.3 relative to $Ru(bpy)_3^{2+}$ (10 μM, H_2O) and shows emission lifetimes of 180 ns and 630 ns. The relative intensities of a series of Ru(II)-16 merA strands and Ru(II)-16A/B duplexes with varying linkers are discussed in detail in Section 4.3.4.4.

Figure 4.7 shows the steady-state emission as a function of temperature for 4-Δ-Ru(II)-N9C-16 merA and 4-Δ-Ru(II)-N6P-16 merA. Importantly, the luminescence of both chimeras decreases exponentially with temperature. This temperature-dependence varies dramatically from the behavior of Ru(II)-DNA duplexes (Section 4.3.4.4.4), and may be very useful for the differential detection of single-stranded and duplex DNA in hybridization probes.[22]

4.3.3.2 DNA analysis

Enzymatic digestion of metallated oligonucleotides provides quantitative information about the nucleoside composition of DNA and can be used to estimate the ratio

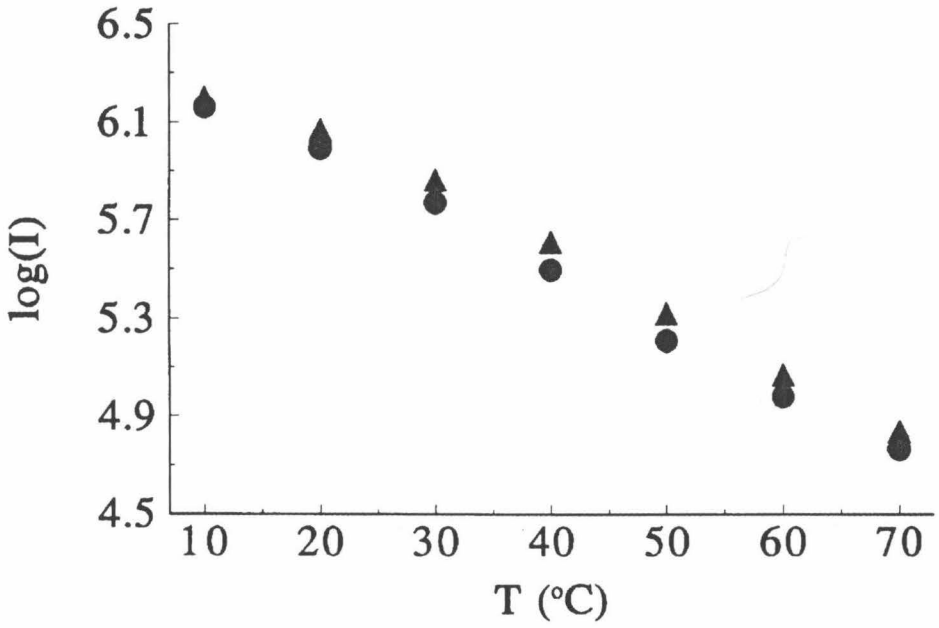

Figure 4.7

Plot showing the log of steady-state emission intensity as a function of temperature for single-stranded Ru(II)-oligonucleotides. Temperature-dependent behavior is similar for both 4-Δ-Ru(phen)(bpy')(Me_2dppz)-N9C-16 merA (▲) and 4-Δ-Ru(phen)(bpy')(Me_2dppz)-N6P-16 merA (●). Sample conditions were 10 μM conjugate in a buffer of 5 mM phosphate, 50 mM NaCl, pH 7. Samples were equilibrated for 15 min at each temperature prior to measurement.

of metal complex:oligonucleotide. A typical digestion is shown in Figure 4.8 for the conjugate 1-*rac*-Ru(phen)(bpy')(Me_2dppz)-N9C-5'-AGTCTAGGCCTATCGT-3'. From the areas of each nucleoside peak, the composition of the DNA strand was found to be 4.1 (dC): 4.1 (dG):5.0 (dT):1.6 (dA). This ratio indicates the loss of the 5' deoxyadenosine, indicating that the carbamate bond between the 5' nucleoside and the alkylamine tether is not severed by the phosphodiesterase. For ruthenated oligonucleotides, the derivatized metal complex can be identified at long retention times (~50% CH_3CN); Rh(III) complexes, however, seem to be unstable in the enzyme buffer and are not typically isolable. The ratio of DNA:metal complex can be determined by quantitation of the nucleosides directly from the HPLC chromatogram (Section 4.2.3) or by comparison of the peak areas to a calibration curve. The yield of dC in Figure 4.8 is 1.37 nmol, indicating 243 pmol of DNA strands (4 dC/strand). The same sample was found to contain 320 pmol of metal complex by UV-visible absorption spectroscopy (ε_{440} = 19,000 $M^{-1}cm^{-1}$). This assay therefore supports the results of other spectroscopies which indicate that a single Ru(II) complex is tethered to an oligonucleotide.

4.3.3.3 Mass spectrometry

Figure 4.9 compares the mass spectra of 1-Δ-Ru(phen)(bpy')(Me_2dppz)-N9C-20 merA obtained by two different ionization techniques. MALDI-TOF (Figure 4.9A) shows one material with a charge/mass ratio (m/z) of 7085.1 amu; this m/z corresponds closely to the calculated mass of 7085 amu with a single charge. ESI-MS provides an analogous result from which a mass of 7083.0 amu is determined; furthermore, the ESI-MS data show several ionization states of the Ru(II)-oligonucleotide conjugate and the mass resolution is higher than for the MALDI-TOF spectrum. While both MS methods are highly sensitive, the two techniques do require different amounts of material. MALDI-TOF typically uses 2-5 pmol of conjugate, while ESI-MS requires 250 - 500 pmol of product (Battelle Institute).

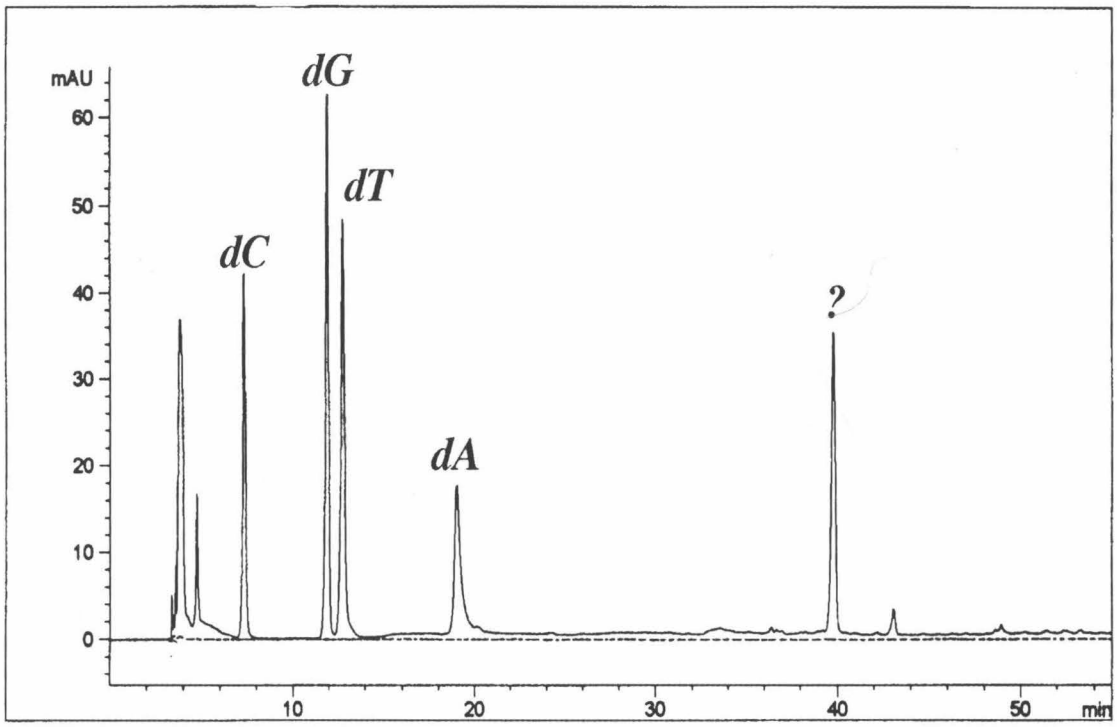

Figure 4.8

HPLC trace of 1-*rac*-Ru(phen)(bpy')(Me_2dppz)-N9C-5'-AGTCTAGGC-CTATCGT-3' following enzymatic digestion. Ratios of each nucleoside were: dC = 4.1; dG = 4.1; dT = 5.0; dA = 1.6. Yield of oligonucleotide was determined from dC = 1.38 nmol to be 342 pmol. UV-visible absorption spectroscopy indicated 320 pmol Ru(II) in this sample. HPLC conditions were: Microsorb MV, C18 100 Å column, 0.46 x 25 cm column; 0-5% CH_3CN, 100-95% NH_4OAc (250 mM; pH 5); oven temperature: 40 °C.

A

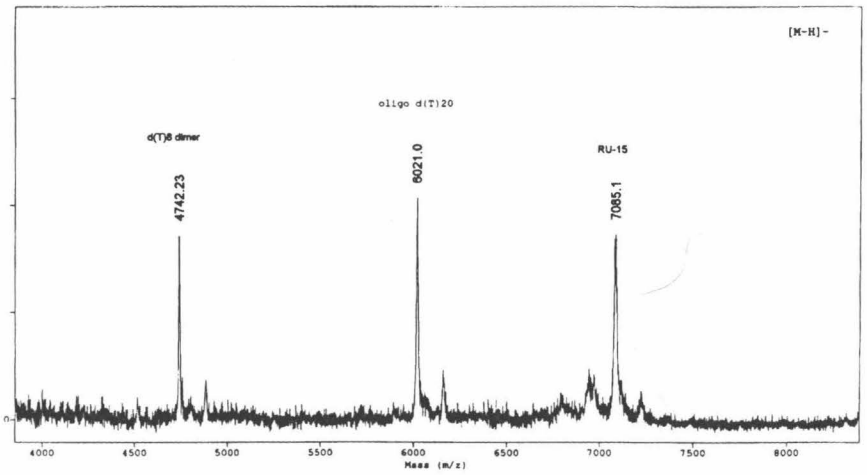

B

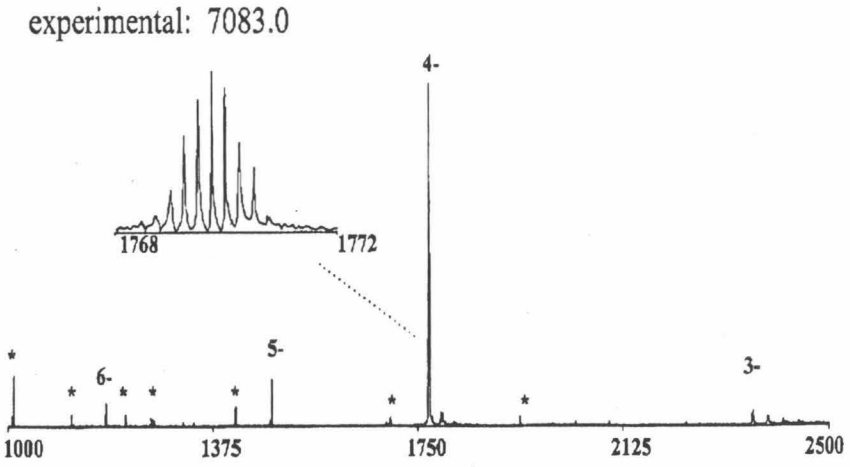

Figure 4.9

MALDI-TOF (A) and ESI (B) mass spectra of 1-Δ-Ru(phen)(bpy')(Me_2dppz)-N9C-20 merA. Predicted mass = 7085 amu; experimental masses = 7085.1 amu (A) and 7083.0 amu (B).

The "gentle" electrospray ionization technique has made ESI-MS the preferred method for DNA samples; in fact, recent studies have shown that noncovalent interactions between biomolecules such as proteins and DNA are maintained during ESI-MS detection.[64] In collaboration between our laboratory, the research group of Dr. Richard Smith has found that $Ru(phen)_2dppz^{2+}$ remains intercalated into duplex DNA when aqueous solutions are vaporized by ESI.[65] Furthermore, when a solution containing $Rh(phi)_2bpyCl_3$ and a 12 bp single-stranded oligonucleotide was analyzed, ESI-MS detected two products in negative ion mode. In addition to a peak whose mass corresponded to the 12 bp DNA strand, a larger peak with a mass equal to the 12 bp strand + $Rh(phi)_2bpy^{3+}$ was identified. Further experiments are needed to determine whether this gas-phase interaction depends on the length and sequence of the DNA and on the structure of the metal complex.

4.3.4 Properties of metal-DNA duplexes

4.3.4.1 Determination of Rh(II) and Ru(III) binding sites

4.3.4.1.1 Photocleavage by Rh(III)

The binding of $Rh(phi)_2(bpy')^{3+}$ to Rh(III)-modified DNA has been investigated by photocleavage followed by gel electrophoresis. Figure 4.10 shows a 20% denaturing polyacrylamide gel in which 5'-AGTCGGAAGCTTGCT-3'-^{32}P was hybridized to 5'-Rh(III)-modified complement. The damage seen in lanes 7 and 8 indicates that Δ-$Rh(phi)_2(bpy')^{3+}$ is intercalated at several base steps near the end of the duplex to which it is tethered. Lanes 9 and 10 show that the damage caused by Λ-$Rh(phi)_2(bpy')^{3+}$ does not extend beyond the third base step, suggesting that the tethered left-handed isomer is more contrained than the Δ-isomer. In contrast to cleavage by tethered Rh(III), photocleavage of duplex DNA by noncovalently bound Δ-$Rh(phi)_2(bpy)^{3+}$ is primarily sequence-neutral (lane 6); the data even suggest that the 5'-TTGCT-3' terminus of the labeled strand is a poor binding site for freely intercalated Δ-Rh(III). Lastly, the cleavage of duplex DNA is

Figure 4.10

Autoradiogram after 20% denaturing polyacrylamide gel electrophoresis showing photocleavage of Rh(III)-oligonucleotide duplex. Top: The oligonucleotide 5'-AGTCGGAAGCTTGCT-3' was 3'-^{3}P-end-labeled, hybridized to Rh(phi)$_2$bpy'-N9C-modified complement or unmodified complement (2 μM duplex), and irradiated at 313 nm for 20 min as described in Section 4.2.3. Samples shown are as follows: lanes 1 and 2, Maxam-Gilbert reactions C+T and G, respectively; lane 3, unmodified duplex; lane 4, Δ-Rh(phi)$_2$bpy^{3+} + unmodified duplex without irradiation; lane 5, Δ-Rh(III) + single-stranded oligonucleotide; lane 6, Δ-Rh(III) + unmodified duplex; lane 7, Δ-Rh(III)-DNA; lane 8, Δ-Rh(III)-DNA + 0.5 μM excess Δ-Rh(III)-oligonucleotide; lane 9, Λ-Rh(III)-DNA; lane 10, Λ-Rh(III)-DNA + 0.5 μM excess Λ-Rh(III)-oligonucleotide. Bottom: Histogram illustrating light-induced cleavage of Δ-Rh(III)-DNA. The intercalation site shown is one of ~4 sites suggested by photocleavage result.

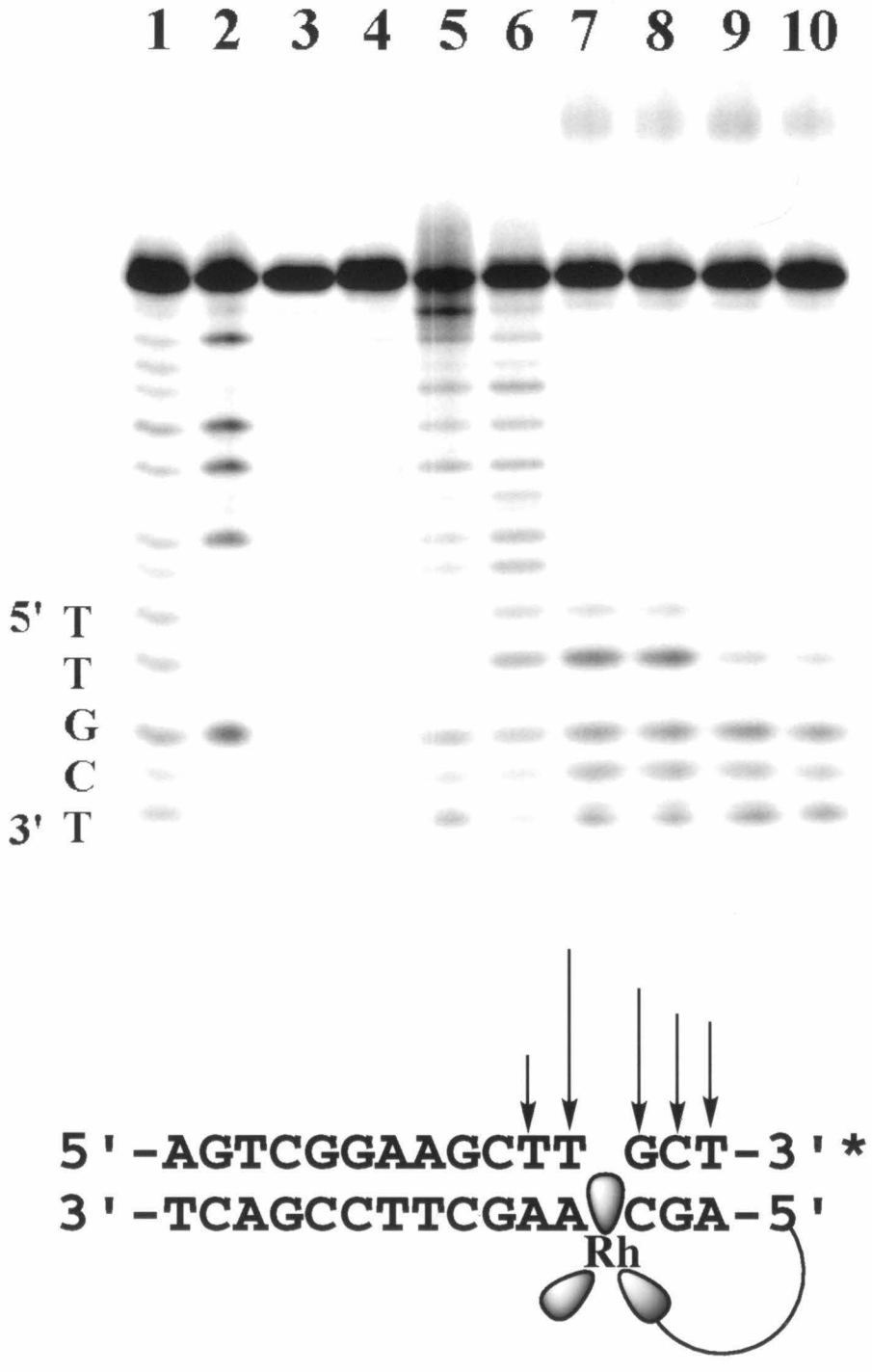
1 2 3 4 5 6 7 8 9 10
5' T
T
G
C
3' T
5'-AGTCGGAAGCTT GCT-3'*
3'-TCAGCCTTCGAA CGA-5'
Rh

compared to damage caused by Rh(III) in solution with single-stranded DNA (lane 5). Even though the metal complex cannot intercalate into the single-stranded oligonucleotide, photoinitiated damage indicates that these two molecules somehow interact in solution. In summary, the regiospecific binding of tethered Rh(III) complexes to the 15 bp duplex indicates that $Rh(phi)_2bpy'^{3+}$ is covalently bound to the 5' terminus of 15 merB and that intercalation of Rh(III) is primarily intramolecular.

4.3.4.2 Sensitization of $^1O_2$ by *Ru(II)

No such direct cleavage assay exists for Ru(II) complexes. However, photoexcited Ru(II) complexes have been shown to sensitize formation of $^1O_2$; this reactive radical then oxidizes guanine bases in DNA.[66] Therefore, by irradiation of Ru(II) polypyridyl complexes in the presence of DNA, piperidine-sensitive G damage is generated in *regions* near Ru(II) binding sites.[22,67,68] In comparing yields of damage, it is important to note that the formation of $^1O_2$ depends on the excited-state of Ru(II); thus, complexes with higher luminescence intensities, such as $Ru(phen)(phen')(Me_2dppz)^{2+}$, will cause more efficient G damage throughout the DNA strand.

We have used this assay to identify preferred sequences on a 20 bp DNA duplex for the binding of *rac*-$Ru(phen)(bpy')(Me_2dppz)^{2+}$, *rac*-$Ru(phen)(phen')(Me_2dppz)^{2+}$, and Δ-$Ru(phen)_2dppz^{2+}$ (Figure 4.11). Lane 7 shows that $Ru(phen)_3^{2+}$ yields damage throughout the DNA strand with little preference for different G residues. In contrast, the data indicate that racemic trisheteroleptic complexes do show some sequence selectivity. For example, binding of $Ru(phen)(bpy')(Me_2dppz)^{2+}$ leads to damage primarily at 5'-TGA-3' sequences (62% of total strand scission) and AGA-3' (25%). Ru(phen)(phen')-$(Me_2dppz)^{2+}$ shows even greater selectivity, with 58% of damage occurring at 5'-TGAGA-3' sequence located at the 3' end of the labeled strand. Δ-$Ru(phen)_2dppz^{2+}$ seems to show much weaker sequence preference than the trisheteroleptic complexes; however, one striking exception is the low yield of strand scission at the guanine in the 3'-terminal sequence 5'-AGACT-3'.

Figure 4.11

Autoradiogram after 20% denaturing polyacrylamide gel electrophoresis showing *Ru(II) sensitized damage. The oligonucleotide 5'-TGATCGGTGCGGTCTGAGACT-3' was 5'-^{32}P end labeled, hybridized to its complementary strand (8 μM duplex), and irradiated at 435 nm in the presence of Ru(II) complexes (8 μM) as described in Section 4.2.3. Following irradiation, samples were treated with piperidine (1M) for 30 min. Samples shown are as follows: lanes 1 and 2, Ru(phen)(bpy')(Me_2dppz)$^{2+}$ + DNA; lanes 3 and 4, Ru(phen)(phen')(Me_2dppz)$^{2+}$ + DNA; lanes 5 and 6, Δ-Ru(phen)$_2$dppz^{2+} + DNA; lane 7, Ru(phen)$_3^{2+}$ + DNA; lane 8, DNA without irradiation; lane 9, DNA without irradiation or treatment with piperidine; lanes 10 and 11, Maxam-Gilber sequencing reactions G and C+T, respectively. Lanes 1, 3, 5 were irradiated in airtight glass vials (Hewlett Packard), while lanes 2, 4, 6 were irradiated in 1.7 ml eppendorf tubes.

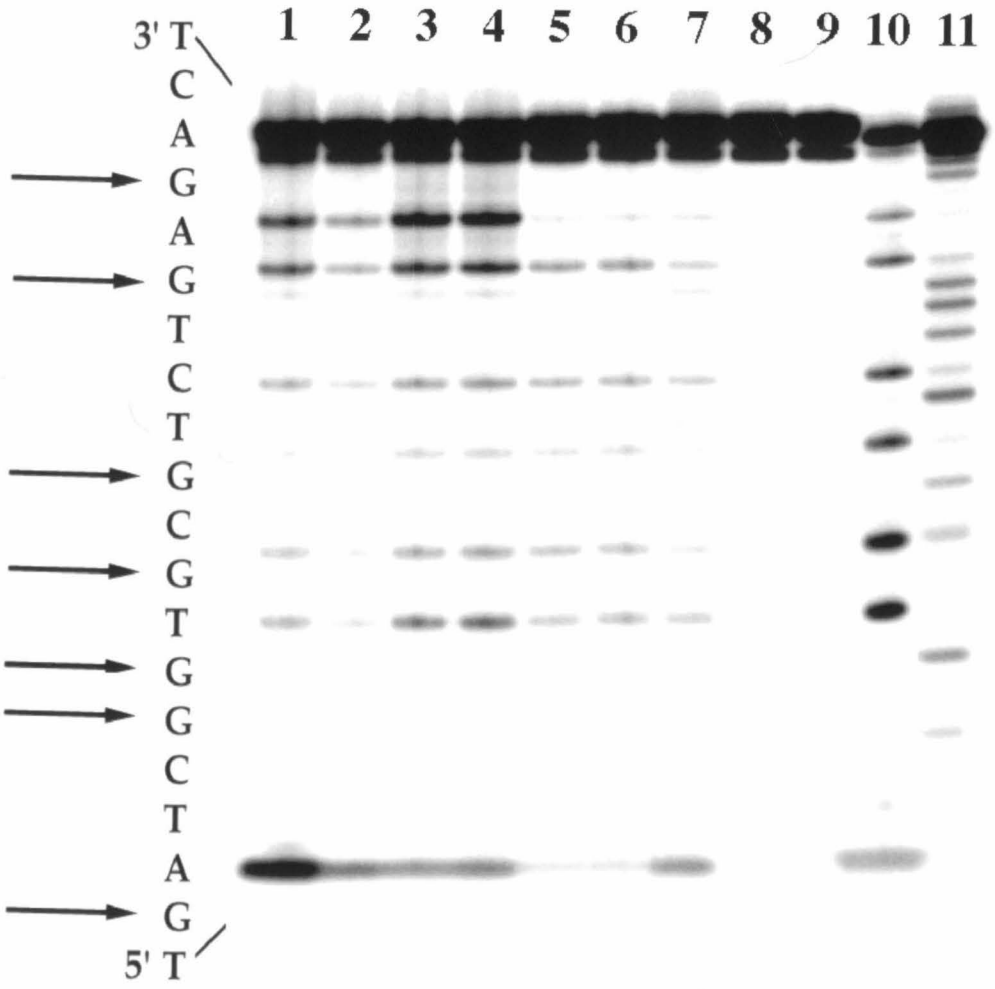
1 2 3 4 5 6 7 8 9 10 11
3' T
C
A
G
A
G
T
C
T
G
C
G
T
G
G
C
T
A
G
5' T

4.3.4.3 Choosing binding sites for covalent DNA assemblies

Oligonucleotides designed for DNA-mediated ET experiments have incorporated information gained from DNA cleavage studies. Binding of metallointercalators to the DNA assembly should affect duplex hybridization, Ru(II) luminescence, and efficiency of electron transfer (Chapter 2). Photocleavage experiments have identified preferred DNA sequences for noncovalently bound analogs of Rh(III), and thus these sites (5'-ACGA-3', 5'-ACGT-3') have been placed at the 5' end of Rh(III)-tethered oligonucleotides (Table 4.2). Figure 4.12 schematically illustrates the cleavage of ^{32}P-3'-labeled 16 merA hybridized to Rh(III)-N9C-16 merB. Intercalation of the Δ-Rh(III) complex, probed by irradiation at 313 nm, occurs primarily at bases 2-4 from the site of attachment (A), as expected from previous work with this 5' sequence. As observed in Section 4.3.4.1, the cleavage pattern generated by tethered Λ-Rh(III) is shifted one base closer to the linker (B), indicating that this isomer is intercalated primarily at the second and third base steps.

Based on the results of *Ru(II) sensitized damage (Figure 4.11) and ^{1}H NMR measurements,[28] the sequence 5'-AGTC-3' has been placed at the 5' end of Ru(II)-tethered oligonucleotides. Figure 4.12 shows the sites and relative intensities of G damage following irradiation of ^{32}P-3'-labeled 4-Δ-Ru(phen)(bpy')(Me_2dppz)-N9C-16 merA alone (C) or hybridized to unmodified 16 merB (D). When the Ru(II)-oligonucleotide is irradiated in the absence of the complementary strand, piperidine-labile G damage is seen throughout the oligonucleotide and is only slightly more intense at the 5'-G. When the metallated strand is hybridized to 16 merB, however, G oxidation is strongly preferred at the 5'-G near the putative intercalation site. It is possible that the damage observed at the 3'-G far from the Ru(II) tether is due to alternate, poorly hybridized structures; in general, these data support the notion that Ru(II) is primarily, but not completely, intercalated intramolecularly near the site of covalent attachment.

Figure 4.12

Histograms illustrating the results of an autoradiogram after 20% denaturing polyacrylamide gel electrophoresis. A) The oligonucleotide 16 merA was 3'-^{32}P end-labeled, hybridized to Δ-Rh(phi)$_2$bpy'-N9C-labeled complement (8 μM duplex), and irradiated for 20 min at 313 nm as described in Section 4.2.3. Arrows indicate the relative efficiencies of cleavage; these data suggest intercalation at the first, second, and third base steps. B) The oligonucleotide 16 merA was 3'-^{32}P end-labeled, hybridized to Λ-Rh(phi)$_2$bpy'-N9C-labeled complement (8 μM duplex), and irradiated for 20 min at 313 nm as described in Section 4.2.3. Arrows indicate the relative efficiencies of cleavage; these data suggest intercalation at the second, and third base steps. C) The oligonucleotide 2-Δ-Ru(phen)(bpy')(Me$_2$dppz)-16 merA (8 μM) was 3'-^{32}P end-labeled and irradiated for 60 min at 442 nm as described in Section 4.2.3. Following irradiation, samples were treated with piperidine (1M) for 30 min. Arrows indicate the relative efficiencies of $^1O_2$-mediated damage. D) The oligonucleotide 2-Δ-Ru(phen)(bpy')(Me$_2$dppz)-16 merA was 3'-^{32}P end-labeled, hybridized to unmodified complement (8 μM) and irradiated for 60 min at 442 nm as described in Section 4.2.3. Following irradiation, samples were treated with piperidine (1M) for 30 min. Arrows indicate the relative efficiencies of $^1O_2$-mediated damage; these data suggest intercalation near the 5'-terminus of the labeled strand. Both C and D are corrected for G damage revealed by piperidine treatment of unirradiated DNA.

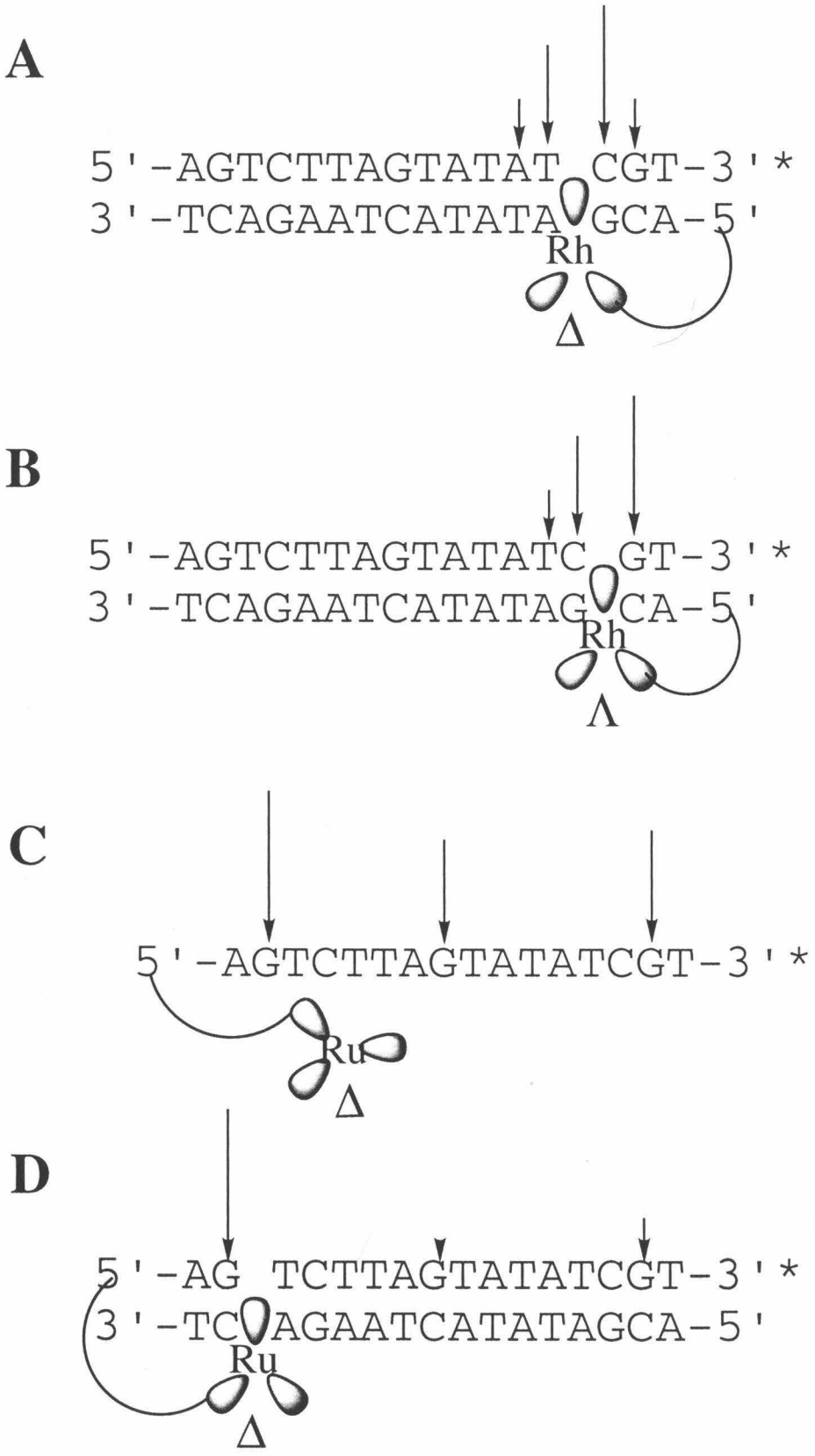
A
5'-AGTCTTAGTATAT CGT-3'*
3'-TCAGAATCATATA GCA-5'
Rh
Δ
B
5'-AGTCTTAGTATATC GT-3'*
3'-TCAGAATCATATAG CA-5'
Rh
Λ
C
5'-AGTCTTAGTATATCGT-3'*
Ru
Δ
D
5'-AG TCTTAGTATATCGT-3'*
3'-TC AGAATCATATAGCA-5'
Ru
Δ

4.3.4.2 Nondenaturing gel electrophoresis

The integrity of metallated duplexes has been assayed by nondenaturing gel electrophoresis. Figure 4.13 shows a 12% polyacrylamide gel in which ^{32}P labeled 2-Δ-Ru(phen)(bpy')(Me_2dppz)-N9C-16 merA (lanes 1, 4) has been hybridized to unmodified 16 merB (lanes 2,5) and to Δ-Rh(phi)$_2$(bpy')-N9C-16 merB (lanes 3,6). Clearly, the Ru(II)-DNA duplex runs through the gel more slowly than its single-stranded counterpart; furthermore, doubly metallated DNA is further retarded due to the additional positive charge and mass of the metal complex. The samples shown in lanes 1-3 were hybridized by slow cooling on a heat block in which the temperature was not carefully regulated. The samples in lanes 4-6, on the other hand, were hybridized on a thermal cycler so that the cooling procedure was tightly controlled. Quantitation of the two sets of experiments indicates that ~85% of Ru(II)-N9C-16 merA is found in the main bands for lanes 1 and 4; similarly, 87% of Ru(II)-DNA duplex runs as a single, tight band for both temperature cycles. On the other hand, using the thermal cycler does seem to improve hybridization of the doubly-metallated duplex, since the main bands of lane 3 and 6 contain 77% and 90% of radioactivity, respectively. The band shape is also somewhat improved in lane 6, but it is still not as distinct as the main product in lane 5. Unless otherwise stated, emission measurements described in Section 4.3.4.4 utilized samples hybridized on the thermal cycler (temperature gradient: 90 - 20 °C over 3 hrs).

4.3.4.3 Thermal denaturation of metallated duplexes

UV-visible absorption spectroscopy can be used to measure the temperature-dependent melting of the DNA duplex. Stacking interactions between adjacent DNA bases causes a 20-30% decrease in absorption,[69] and this hypochromicity is diminished as the double helical structure cooperatively dissociates into single strands. In the presence of intercalators, the melting temperature (T_m) of oligonucleotide duplexes typically increases 5-10 °C due to thermodynamic stabilization of the π-stack. Thus, the strength of

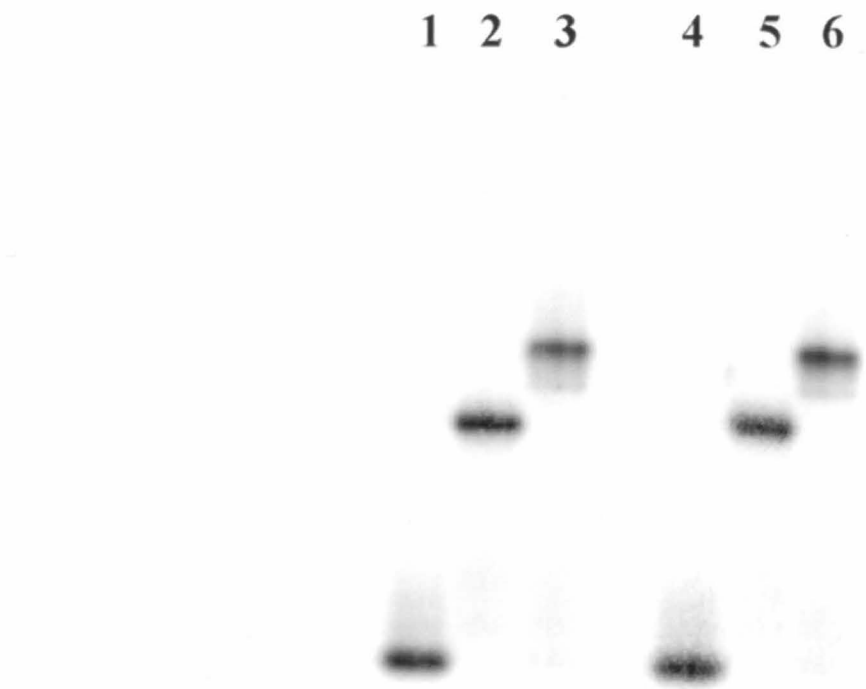

Figure 4.13

Autoradiogram following 12 % nondenaturing polyacrylamide gel electrophoresis. The oligonucleotide 2-Δ-Ru(phen)(bpy')(Me_2dppz)-16 merA (8 μM) was 3'-^{32}P end-labeled and hybridized to unmodified or Δ-Rh(III)-modified complement as described in Section 4.2.3. Samples contained 5 μM duplex in a buffer of 5 mM phosphate, 50 mM NaCl, pH 7, and were hybridized on a heat block (lanes 1-3) or on a thermal cycler (lanes 4-6). Samples shown are as follows: lanes 1 and 4, single-stranded Ru(II)-oligonucleotide, "annealed" on heat block; lanes 2 and 5, Ru(II)-DNA duplex, lanes 3 and 6, Ru(II)-DNA-Rh(II) duplex.

intercalation can be estimated by the T_m. Intercalated ligands themselves show hypochromicity, and therefore the binding of intercalators such as Ru(phen)(bpy')-$(Me_2dppz)^{2+}$ can also be interogated by thermal denaturation. In principle, binding of Rh(phi)2(bpy')$^{3+}$ to DNA may also be studied; however, measurement of hyperchromicity is made technically difficult by red-shifting of the phi absorption bands between ~350-500 nm.

Table 4.3 describes the melting of a series of metallated 16 merA/B duplexes. The unmodified duplex melts at 41 °C; this T_m is lower than a typical 16 bp duplex due to the high percentage of AT base pairs in the sequence. Binding of either *rac*-Ru(phen)(bpy')$(Me_2dppz)^{2+}$ or tethered Δ-Rh(phi)$_2$(bpy')$^{3+}$ to 16 merA/B raises the T_m by 11 °C, indicating strong intercalation of these two metal complexes. In contrast, tethered 2-Δ-Ru(phen)(bpy')$(Me_2dppz)^{2+}$ does not cause an increase in the thermal stability of the DNA duplex. Furthermore, the binding of the metal complex, monitored at 382 - 384 nm, seems to be weaker for tethered Ru(II) than for the noncovalently bound complex. As shown in Figure 4.14A, intercalated Ru(II) dissociates from the DNA duplex when most of the DNA is melted, indicating that the complex stabilizes the base stack preferentially at the Ru(II) binding site. Covalently modified 2-Δ-Ru(II)-N9C-16 merA/B, on the other hand, shows the same melting temperature for both the metal complex and the DNA. The difference between Figures 4.14A and B could suggest that the tethered Ru(II) complex is not well-intercalated. In this context, it is noteworthy that single-stranded 2-Δ-Ru(II)-N9C-16 merA does not show sigmoidal melting, and thus does not seem to hybridize into a discrete secondary structure.

4.3.4.4 Emission properties of Ru-DNA and Ru-DNA-Rh assemblies

4.3.4.4.1 Reproducibility of quenching efficiencies

We have measured the emission properties of 4-Δ-Ru(phen)(bpy')(Me_2dppz)-N9C-16 merA in several, independent experiments so that we may determine the reproducibility

Sample[b]	T_m (°C)[c]	λ_{abs} (nm)	% hypochromicity
16 merA/B	41	260	14
rac-Ru(II) + 16 merA/B	52 62	260 384	10
2-Δ-Ru(II)-N9C-16 merA/B	45 46	260 382	14 15
Δ-Rh(III)-N9C-16 merA/B	52	260	17
2-Δ-Ru(II)-N9C-16 merA/B-Δ-Rh(III)	51	260	15
2-Δ-Ru(II)-N9C-16 merA	N/A N/A	260 382	7 10

[a] Thermal denaturation was monitored by UV hyprochromicity using a diode array spectrophotometer (HP 8452A) and Tempco software supplied by the manufacturer. [b] Sample conditions were 2.5 μM duplex in an aqueous buffer of 5 mM phosphate, 50 mM NaCl, pH 7. Ru(II) = Ru(phen)(bpy')$(Me_2dppz)^{2+}$, Rh(III) = $Rh(phi)_2(bpy')^{3+}$. [d] N/A = hypochromicity increased linearly with temperature.

Figure 4.14

Plots showing thermal denaturation of 16 merA/B duplex (2.5 μM duplex) with bound Ru(phen)(bpy')(Me_2dppz)$^{2+}$ (2.5 μM). Temperature gradients were as described in Section 4.2.3. A) 16 merA/B + noncovalently bound Ru(II), monitored at 260 nm and 384 nm. B) Δ-Ru(II)-N9C-16 merA/B, monitored at 260 nm and 382 nm.

A

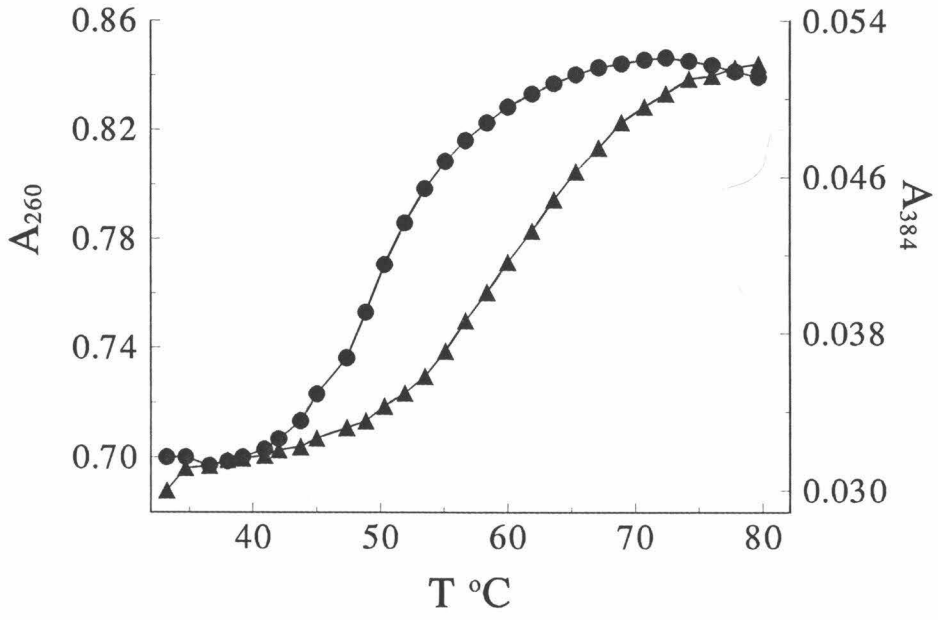
0.86
0.82
0.78
0.74
0.70
A260
0.054
0.046
0.038
0.030
A384
40
50
60
70
80
T °C

B

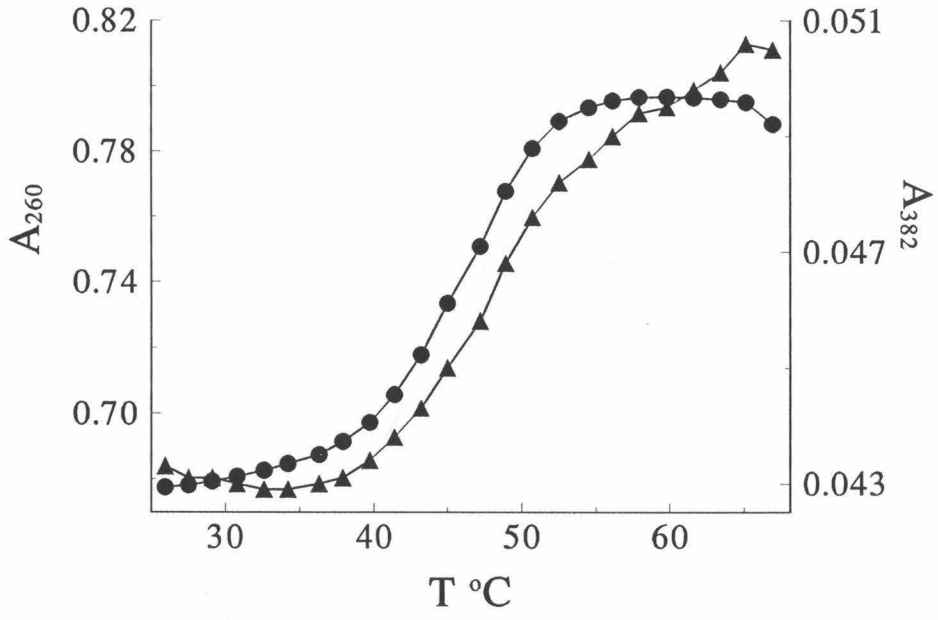
0.82
0.78
0.74
0.70
A260
0.051
0.047
0.043
A382
30
40
50
60
T °C

of quenching experiments. Table 4.4 lists relative emission intensities for five measurements in which each set of samples were prepared together. The luminescence of both the single-stranded chimera and the metal complex noncovalently bound to the DNA duplex are shown to be stable across experiments, and indicate an inherent error in the measurement of < 10%. On the other hand, the emission intensities of the two metallated duplexes vary considerably across experiments, and no clear correlation is found among the intensity of Ru(II)-DNA, the method of hybridization, or the amount of quenching. It is noteworthy that other metallated assemblies do not seem to show this large margin of error. For example, quenching of tethered ethidium by tethered Δ-$Rh(phi)_2(bpy')^{3+}$ is reproducible within 5%;[70] additionally, the Ru(II)-modified oligonucleotide duplexes discussed in Chapter 5 give highly reproducible yields of oxidative damage resulting from long-range hole migration.

It is clearly important to understand the origin of the marked instability in emission quenching, especially since the amount of quenching is determined by comparing the luminescence of two, independent samples. If the changes in intensity vary between samples, and not as a function of the *set* of samples, e.g., buffer or hybridization conditions, then the error in the relative intensities (quenching) may be quite large. However, to minimize the uncertainties between experiments, the Tables 4.5 - 4.7 compare samples which were prepared and measured on the same day.

4.3.4.4.2 Comparison of tethered and noncovalently bound complexes

Table 4.5 summarizes the emission quenching of $Ru(phen)(bpy')(Me_2dppz)^{2+}$ by $Rh(phi)_2(bpy')^{3+}$ in the sequence 16 merA/B; the 67% quenching observed for noncovalently bound complexes provides a point of comparison for quenching between tethered complexes. The emission titration with "hemicovalent" assemblies serves as a measurement of the coupling of the tethered metallointercalator into the DNA. For example, when noncovalently bound Ru(II) is added to Δ-Rh(III)-N9C-16 merB/A duplex,

Table 4.4. Reproducibility of relative emission of 4-Δ-Ru(phen)(bpy')(Me$_2$dppz)-N9C-16merA.[a]

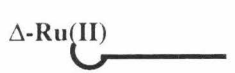	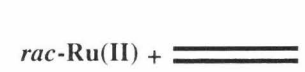			Quenching (%)[b]
1.81	1.28	1.76	1.04	**41**[c]
1.80	1.27	1.17	0.85	**28**[c]
1.76	N/D	1.16	0.69	**40**[d]
N/D	1.18	0.81	0.58	**28**[e]
N/D	1.14	1.24	0.82	**35**[c]

[a] All luminescence measurements taken with SLM 8000 fluorimeter with the following parameters: λ_{exc} = 440 nm; slit width = 8 mm; polarizers = 0/0. Samples were 10 μM duplex in a buffer of 5 mM phosphate, 50 mM NaCl, pH 7. [b] Intensities are given relative to $Ru(bpy)_3^{2+}$ (10 μM) in H_2O. [c] Samples were hybridized by slow cooling on a Perkin Elmer thermal cycler (preheat 90 °C, 15 min; 90 - 20 °C over 3 hrs). [d] Samples were hybridized at 50 μM duplex by slow cooling on a Perkin Elmer thermal cycler (preheat 90 °C, 15 min; 90 - 20 °C over 3 hrs) and diluted to 10 μM duplex. [e] Samples were hybridized by slow cooling on a heat block (preheat 90 °C, 20 min; 90 - 25 °C over ~1.5 hrs).

Table 4.5. Steady-state quenching of Ru(phen)(bpy')(Me_2dppz)$^{2+}$ by Δ, Λ-Rh(phi)$_2$(bpy)$^{3+}$ in sequence 16 merA/B.[a]

Sample	quenching (%)
rac-Ru(II) + ═══ + Δ-Rh(III)	67
rac-Ru(II) + ═══ Δ-Rh(II)	78
Δ-Ru(II)═══ + Δ-Rh(II)	65
Λ-Ru(II)═══ + Δ-Rh(II)	44
Δ-Ru(II)═══ Δ-Rh(II)	30
Δ-Ru(II)═══ Λ-Rh(II)	20
Λ-Ru(II)═══ Δ-Rh(II)	17
Λ-Ru(II)═══ Λ-Rh(II)	11

[a] All luminescence measurements taken with SLM 8000 fluorimeter with the following parameters: λ_{exc} = 440 nm; slit width = 8 mm; polarizers = 0/0. Samples were 10 μM oligonucleotide or duplex in a buffer of 5 mM phosphate, 50 mM NaCl, pH 7. Samples were hybridized by slow cooling on a heat block (preheat 90 °C, 20 min; 90 - 25 °C over ~1.5 hrs).

emission is quenched by 78% relative to Ru(II) intercalated into the unmodified 16 mer duplex. Comparable experiments with other oligonucleotide duplexes have shown similar or less quenching by tethered $Rh(phi)_2(bpy')^{3+}$. This high yield of quenching therefore suggests that the Rh(III) complex is well-intercalated into the 16 merA/B duplex. Quenching of tethered Ru(II) complexes by noncovalently bound Δ-$Rh(phi)_2bpy^{3+}$ is less efficient, yielding 65 % efficiency for the Δ-Ru(II) isomer. Again, this amount of quenching is typical or better than analogous experiments with different Ru(II) complexes and different sequences.

A number of studies in our laboratory have indicated that the chirality of intercalating donors and acceptors has significant effects on the rates and efficiencies of electron transfer through DNA (Chapter 2).[35] We therefore considered whether the chirality of tethered complexes was important in the emission properties of $Ru(phen)(bpy')(Me_2dppz)^{2+}$-modified duplexes. Table 4.5 shows that, in all cases, the Δ-isomers of both Ru(II) and Rh(III) yield higher quenching efficiencies than the corresponding Λ-isomer. Because of these results, experiments have focused on the properties of the Δ-isomers of both donor and acceptor.

4.3.4.4.3 Effect of alkyl linker on emission of Ru(II)

Three chimeras have been prepared in which $Ru(phen)(bpy')(Me_2dppz)^{2+}$ is tethered to 16 merA via different alkyl amine linkers. The emission properties of the two Δ-isomers of each chimera were measured for i) Ru(II)-16 merA, ii) Ru(II)-16 merA hybridized to unmodified complement, and iii) for Ru(II)-16 merA hybridized to Δ-$Rh(phi)_2(bpy')$-N9C-16 merB (Table 4.6). All six single-stranded conjugates showed high steady-state emission, and the intensity of emission was lower for the duplex Ru(II)-DNA in all cases; additionally, the emission maximum between single- and double-stranded forms blue-shifts ~ 5 nm for all three linkers. Two features of the double-stranded emission are particularly noteworthy. First, the emission intensity varies dramatically as a

Table 4.6. Emission intensity and quenching of Ru(phen)(bpy')(Me_2dppz)-16 merA as a function of linker.[a]

Ru(II)-oligonucleotide	I_{ds}/I_{ss}[b]	$I_{rel,ds}$[c,d]	quenching (%)[d,e]
2-Δ-Ru(II)-N9C-16 merA	0.75[e]	1.0 defined	26
2-Δ-Ru(II)-N6P-16 merA	0.86	0.49	22
3-Δ-Ru(II)-NO8-16 merA	0.87	0.63	30
4-Δ-Ru(II)-N9C-16 merA	0.65	0.84	30
4-Δ-Ru(II)-N6P-16 merA	0.54[d]	0.32	28
4-Δ-Ru(II)-NO8-16 merA	N/D[g]	0.53	33

[a] All luminescence measurements taken with SLM 8000 fluorimeter with the following parameters: l_{exc} = 440 nm; slit width = 8 mm; polarizers = 0/0. Samples were 10 μM oligonucleotide or duplex in a buffer of 5 mM phosphate, 50 mM NaCl, pH 7. Samples were hybridized by slow cooling on a Perkin Elmer thermal cycler (preheat 90 °C for 15 min; 90 °C - 20 °C over 180 min). [b] I_{ds}/I_{ss} = ratio of steady-state emission intensity for the Ru(II)-16 merA single-stranded oligonucleotide versus the emission of the Ru(II)-16 merA/B duplex. [c] Steady-state emission intensity relative to 2-Δ-Ru(phen)(bpy')(Me_2dppz)-N9C-16 merA/B. [d] determined July 11, 1996. [e] quenching = ratio of steady-state emission intensity for Ru(II)-16 merA hybridized to unmodified 16 merB versus emission of Ru(II)-16 merA hybridized to Δ-Rh(phi)$_2$(bpy')-N9C-16 merB. [f] determined May 11, 1996. [g] N/D = not determined.

function of the linker; for example, the emission of Ru(phen)(bpy')(Me_2dppz)$^{2+}$ is half as intense when the liner is N6P as when the same complex is linked to N9C. The emission intensity also varies between the two coordination isomers bound to the same alkyl linker. Second, the quenching of the Δ-Ru(II) complexes by tethered Δ-Rh(phi)$_2$(bpy')-N9C-16 merB varies as a function of the linker. However, these differences are smaller than the differences between emission intensities for Ru(II)-DNAs, and could be within the error of the emission experiments.

4.3.4.4.4 Variations in oligonucleotide length

To test the effect of oligonucleotide length on the emission properties of Ru(II), we prepared 14 and 12 bp duplexes based on the sequence 16 merA/B described above. Table 4.7 compares the time-resolved emission data and the steady-state quenching of these three DNA sequences. Inspection of the excited-state lifetimes and quenching efficiencies suggests that the 12 bp sequence is different from both the 14 and 16 bp duplexes. The excited-state lifetimes are similar for Ru(II)-16 merA/B and Ru(II)-14 merA/B while the short lifetime is much shorter for Ru(II)-12 merA/B. Interestingly, of the tethered complexes, the excited-state lifetimes of Ru(II)-12 merA/B are closest to those of the freely intercalated *rac*-Ru(phen)(bpy')(Me_2dppz)$^{2+}$. The most striking comparisons are in the quenching of Δ-Ru(II) as a function of oligonucleotide length. Quenching of 2-Δ-Ru(phen)(bpy')(Me_2dppz)$^{2+}$ increases from 26 to 32% between 16 merA/B and 14 merA/B but then drops to 5% in the shortest duplex. Importantly, quenching in the 16 and 14 bp duplexes is largely due to changes in the excited-state lifetimes and is therefore mostly dynamic. This data may be contrasted with the primarily fast, static quenching observed for noncovalently bound Ru(II) and Rh(III) intercalators (Chapter 2,3).[33,35] Taken together, these emission data could suggest that metallated oligonucleotides are incompletely hybridized and/or intercalated, and that the shortest duplexes are most affected by the binding characteristics of the Ru(II) complex.

Table 4.7. Excited-state lifetimes and emission quenching of 2-Δ-Ru(phen)(bpy')(Me$_2$dppz)-N9C-DNA for three DNA lengths.[a]

	excited-state lifetimes[b]				
Sample	τ_1 (ns)	%	τ_2 (ns)	%	**quenching (%)**[c]
Δ-Ru-16 merA/B	310	30	715	70	
Δ-Ru-16 merA/B-Δ-Rh	310	50	715	50	**26**
Δ-Ru-14 merA/B	290	30	715	70	
Δ-Ru-14 merA/B-Δ-Rh	260	40	590	60	**32**
Δ-Ru-12 merA/B	180	40	715	60	
Δ-Ru-12 merA/B-Δ-Rh	185	40	715	60	**5**
rac-Ru(II) + 16merA/B	180	55	630	45	

[a] Samples were 10 μM duplex in a buffer of 5 mM phosphate, 50 mM NaCl, pH 7. Samples were hybridized by slow cooling on a Perkin Elmer thermal cycler (preheat 90 °C, 15 min; 90 - 20 °C over 3 hrs). [b] Conditions for time-resolved emission measurements were as follows: λ_{exc} = 480 nm, λ_{obs} = 616 nm. [c] Quenching measured by steady-state luminescence. Measurements taken with SLM 8000 fluorimeter with the following parameters: λ_{exc} = 440 nm; slit width = 8 mm; polarizers = 0/0.

4.3.4.4.5 Temperature-dependence of emission

The emission intensity of intercalated complexes of Ru(II) containing dppz have been shown to be stable with increasing temperature until the T_m of the duplex is reached. Since emission is dictated by the protection of the intercalated dppz ligand from solvent, the loss of Ru(II) emission intensity is a measure of the dissociation of Ru(II) from the DNA. We have therefore compared the temperature-dependence of emission for ruthenated DNA and doubly metallated DNA assemblies to that of the noncovalently bound *rac*-Ru(phen)(bpy')$(Me_2dppz)^{2+}$. These curves, shown in Figure 4.15, indicate that the emission of tethered Ru(II) is stable at low temperatures, suggesting that the Ru(II)/DNA complex is well-behaved below 40 °C in the presence and absence of tethered Rh(III). Importantly, after the duplex has melted, the emission intensities of both Ru-DNA and Ru-DNA-Rh are identical, indicating that the hybridized structure is required for quenching to occur. However, the emission of tethered Ru(II) begins to decrease after 40 °C; by comparison, the emission of noncovalently bound Ru(II) does not decrease until ~60 °C. These emission melting curves are in close agreement with UV melting curves shown in Figure 4.14 (Section 4.3.4.3), indicating that the DNA and the metal complex dissociate at 40 °C for tethered Ru(II) duplex whereas Ru(II) bound to unmodified 16 merA/B remains associated for another 20 °C.

4.4.3.4.6 Concentration-dependence of emission

If the emission quenching of tethered Ru(II) by tethered Rh(III) were intraduplex, then the efficiency of quenching should be independent of concentration. However, Figure 4.16 shows that the quenching of Δ-Ru(phen)(bpy')(Me_2dppz)-N9C-16 merA hybridized to Δ-Rh$(phi)_2$(bpy')-N9C-16 merB decreases markedly at low duplex concentrations. Interestingly, the "loss" of quenching is due to the nonlinear decrease in the emission of Ru-DNA-Rh. In other words, the emission of Ru-DNA decreases 2-fold each time the concentration is halved; in contrast, the emission of Ru-DNA-Rh drops only ~1.8-fold for

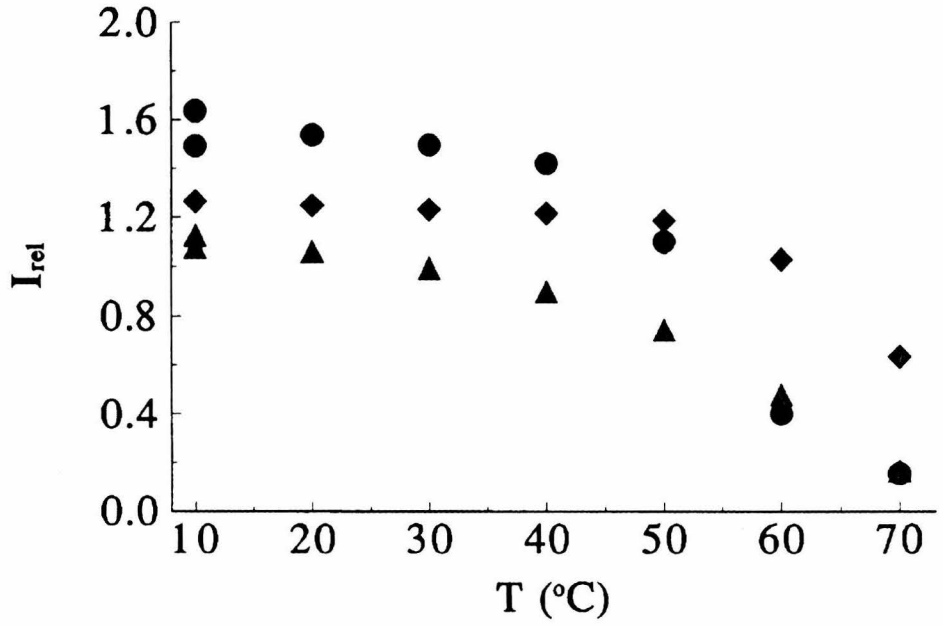

Figure 4.15

Plot comparing the emission of Ru(II) as a function of temperature. Samples (10 μM duplex) were hybridized at 10 μM duplex in a buffer of 5 mM phosphate, 50 mM NaCl, pH 7, as described in Section 4.2.3. Samples include 2-Δ-Ru(phen)(bpy')(Me_2dppz)-N9C-16 merA/B duplex (●), 2-Δ-Ru(phen)(bpy')(Me_2dppz)-N9C-16 merA hybridized to Δ-Rh(phi)$_2$bpy'-N9C-16 merB (▲), and unmodified 16 merA/B + noncovalently bound *rac*-Ru(phen)(bpy')(Me_2dppz)$^{2+}$ (◆).

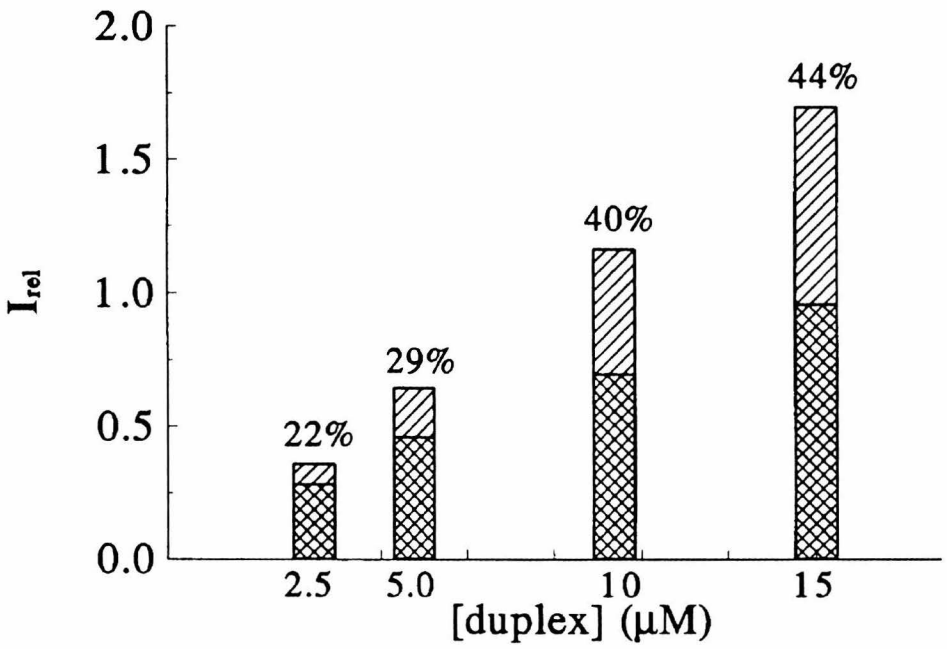

Figure 4.16

Bar graph comparing the emission of 4-Δ-Ru(phen)(bpy')(Me_2dppz)-N9C-16 merA hybridized to unmodified complement or to Δ-Rh(phi)$_2$bpy'-N9C-modified complement (Table 4.2) as a function of concentration of duplex. Samples were hybridized at 50 μM duplex (Section 4.2.3) in a buffer of 5 mM phosphate, 50 mM NaCl, pH 7 and diluted to 15 μM with buffer. Each concentration was then obtained by further addition of buffer. Numbers given above bars indicate the percentage difference between Ru-DNA (taller bars) and Ru-DNA-Rh (shorter bars). Intensities are given relative to 10 μM $Ru(bpy_3)^{2+}$ in H_2O at 20 °C.

the same change in concentration. The observation that quenching is reduced at 2 and 5 μM duplex suggests that the loss of emission is not due solely to long-range electron transfer quenching. Instead, some quenching could arise from intermolecular ET or from concentration-dependent structural changes in the metallated assemblies.

4.4 Discussion

4.4.1 Trisheteroleptic complexes of Ru(II)

Evidence for the synthesis of pure, trisheteroleptic complexes of Ru(II) has been provided by HPLC and mass spectometry. Analytical HPLC has identified two spectroscopically identical Ru(II) products. FAB-MS identifies the trisheteroleptic parent ion as well as several of the mixed bisheteroleptic fragments. Thus, the sequential addition of three ligands yields one mixed-ligand complex rather than three homoleptic complexes of Ru(II).

Trisheteroleptic complexes of Ru(II) and Os(II) have been used to prepare a series of metallointercalator-oligonucleotide conjugates. These coordination compounds offer several synthetic advantages over $Ru(phen')_2dppz^{2+}$, which has previously been used to form Ru(II)-DNA.[21,22,30] The synthesis of $Ru(phen')_2dppz^{2+}$ leads to formation of three isomers which must be separated by HPLC; it is thus difficult to generate large amounts of complex for subsequent reactions. In contrast, the synthesis of trisheteroleptic complexes gives two coordination isomers which do not need to be separated prior to coupling of the complex to DNA. Instead, the metal-oligonucleotide chimeras themselves are separated by HPLC and the effect of linker position on the complex can therefore be assessed from one conjugation reaction. The presence of only one linker ligand thus simplifies the synthesis and characterization of tethered metal-oligonucleotides.

We have used this synthetic methodology to tune the emission properties of Ru(II) intercalators. For example, the three Ru(II) complexes listed in Table 4.1 show a 40-fold range of steady-state emission intensities in the presence of DNA. These complexes also

seem to show different DNA-binding properties. $Ru(dmb)(bpy')(dppz)^{2+}$ binds poorly to DNA, based on the low luminescence intensity compared to $Ru(bpy)_2dppz^{2+}$ and on the small degree of hypochromicity seen in dppz absorption (data not shown). Substituting dppz and dmb for more hydrophobic ligands Me_2dppz and phen raised the emission intensity by an order of magnitude; however, the emission measurements described in Section 4.3.4.4 indicate that the more hydrophobic complex $Ru(phen)(bpy')(Me_2dppz)^{2+}$ interacts strongly with single-stranded DNA. Perhaps new ligands should be designed so that Ru(II) complexes show strong intercalation but weaker nonspecific interactions with single-stranded DNA. For example, it might be helpful to add anionic functional groups to the third ligand, reducing the electrostatic attraction of the complex for the DNA polymer.

Multi-ligand complexes such as those shown in Figure 4.1 will also permit the effect of linker conformation to be studied. The alkyl linkers of both phen' and bpy' vary in length, rigidity, and conformation; these structural differences could dramatically affect the properties of metal-oligonucleotide conjugates.[71] In addition to these two carboxylate-linked ligands, other linkers have been designed,[72] and these might further improve the luminescence and binding properties of tethered Ru(II) complexes. Notably, Os(II) trisheteroleptic complexes have also been prepared, and these expand the range of photophysical properties of tethered intercalators.[43] Given the complexity and utility of M(II)-oligonucleotide conjugates, the flexible synthetic routes to trisheteroleptic complexes of Ru(II) and Os(II) will surely be very valuable.

4.4.2 Syntheses of metal-oligonucleotide chimeras

4.4.2.1 Comparison of amide linkages

Prior to the development of solid-phase syntheses with TSTU and HATU, conjugates of $Rh(phi)_2(phen')^{3+}$ and $Ru(phen')_2dppz^{2+}$ had been prepared by three alternate coupling methods. The first procedure utilized a two-phase reaction in which purified DNA was mixed with an anhydrous solution of the metal complex, DCC, HOBt,

dioxane, and DMF.[30] This preparation proved difficult to reproduce, presumably due to the insolubility of the oligonucleotide in anhydrous solvents and the sensitivity of DCC/HOBt to H_2O in the solid DNA. The first solid-phase preparation of Ru(II)-oligonucleotide chimeras utilized resin-bound DNA mixed with an anhydrous solution of Ru(II), DSC, and LiOH in dioxane and DMF.[22] This synthesis was advantageous in that the fully-protected oligonucleotides bound to CPG support were solvated by anhydrous solvent. However, the yields of these reactions were low, likely due to the high sensitivity of DSC to H_2O and the reactivity of phen' linker towards cyclization to form a diamide. The third synthesis to be developed for Ru(II)-oligonucleotides used the water soluble carbodiimide EDC.[22] This coupling reagent is highly reactive, and has been shown to couple carboxylate groups to the usually unreactive exocyclic amines on the DNA bases.[73] In order to protect these amines from reacting with $Ru(phen')_2dppz^{2+}$, the procedure called for the hybridization of the amino-terminated oligonucleotide with its unmodified complement prior to reaction;[15] after solution-phase coupling, the complementray strand was removed by gel electrophoresis or high-temperature HPLC. While high yielding and reproducible, these reactions were thus complicated by several purification steps. Additionally, reactions with EDC also yielded several Ru(II)-oligonucleotide products for each isomer of $Ru(phen')_2dppz^{2+}$.[22] These multiple products could have resulted from i) conformational isomers of Ru(II)-DNA due to the rigidity of linkers, ii) coordination isomers and diastereomers arising from the presence of two phen' ligands, iii) coordination to the amine groups of the oligonucleotide bases. The EDC reagent was also successful at coupling $Rh(phi)_2(phen')^{3+}$; importantly, these reactions yielded only the two diastereomeric products (data not shown). It therefore seems likely that interactions between the Ru(II) complex and DNA were responsible for product complexity.

Reactions of metal complexes with CPG-bound oligonucleotides have several advantages over solution-phase methods. Because the CPG-oligonucleotide is used directly after automated synthesis, conjugation reactions can be completed rapidly and with

minimal purification steps. Additionally, the use of fully protected DNA reduces the possibility of side reactions and improves the solubility of the oligonucleotide in organic solvents. Four important synthetic advances led to the development of these methods. First, the solid-phase preparation of carbamate-linked alkyl amine-oligonucleotides permitted the use of a number of different linkers, including N6C, N9C, and NO8.[55] Second, we realized that phi complexes of Rh(III), which had previously been thought to degrade in aqueous base, were actually very stable to the DNA cleavage conditions (NH_4OH, 55 °C). Third, the uronium compound TSTU was found to have the optimal degree of reactivity to form an amide bond between bpy'-containing metal complexes and alkylamine-oligonucleotides;[13,36] in contrast, other reagents either yielded no reaction or multiple side reactions. Finally, the more reactive HATU was identified as a more general coupling reagent, permitting the conjugation of both bpy'- and phen'-containing metal complexes.[56,57] The methods described for TSTU and HATU-mediated coupling have been shown to be both high-yielding and highly reproducible, and reactivities of analogous Ru(II) and Rh(III) complexes have been shown to be very similar.

4.4.2.2 Preparation of disulfide-linked chimeras

As probes of nucleic acid structure and reactivity, disulfide-linked conjugates are complementary to amide-linked chimeras. The chemistry of disulfide exchange is distinct from that of amide-bond formation; thus, these two techniques are largely orthogonal, and may be used for preparing complex chimeras such as oligonucleotides bearing both Ru(II) and Rh(III) complexes.[7] Additionally, these conjugates provide alternative lengths and conformations of the flexible tether; these variations could be important in determining the intramolecular binding of intercalator-DNA assemblies.

The final step in the synthesis of Rh(III)-SS-oligonucleotides described in 4.3.2.1 is a coordination reaction of $Rh(phi)_2(SO_3CF_3)_2^+$ with bpy-linked oligonucleotide. While Rh(III) complexes have been shown to coordinate to the bases of oligonucleotides in the

absence of chelating ligands such as bpy,[61] characterization by HPLC, CD, UV, ESI-MS, and enzymatic digestion indicates that the product formed in this reaction is $Rh(phi)_2(bpy)$-SS-oligonucleotide. As noted above, solid-phase reactions have synthetic advantages over solution-phase reactions; it would therefore be useful, and straightforward, to adapt the preparation of disulfide-linked conjugates to solid-phase techniques. Furthermore, coupling methods in which the fully coordinated metal complex is tethered to the oligonucleotide may be advantageous to the "coordination method" described here. Therefore, activated disulfide complex $Rh(phi)_2(bpy)$-SS-pyr could be prepared and then coupled to thiol-linked oligonucleotide. In studying this chemistry, we have found that the coordination of thiol-containing ligands to Rh(III) seems to be more successful when the thiol is protected (e.g., as thiolacetate). Further synthesis and characterization are required to determine the utility of these novel chimeras; again, it will be valuable to have an arsenal of different synthetic schemes for the full characterization of metal-DNA chimeras.

4.4.3 Characterization of conjugates

4.4.3.1 Interactions of intercalators with single-stranded DNA

Several experiments indicate that Ru(II) and Rh(III) metallointercalators bind to single-stranded DNA. Mass spectrometry and photocleavage measurements indicate that untethered metal complexes associate with single-stranded oligonucleotides, while UV-visible absorption and luminescence spectroscopies also provide evidence for interactions of metal complex-oligoncleotide chimeras. Characterizing these binding interactions is likely to be critical to understanding the structure(s) and luminescence properties of metal-DNA chimeras.

Mass spectrometry and photocleavage experiments both identify binding of $Rh(phi)_2bpy^{3+}$ to single-stranded DNA. ESI-MS of the metallointercalator and a 12 bp DNA oligonucleotide clearly illustrates that these two molecules interact in the gas phase. Similar results have been obtained by ESI-MS for intercalators and proteins bound to short

DNA duplexes; in these studies, it was argued that the electrospray ionization technique permitted weak, noncovalent interactions present in solution to persist during vaporization.[64] Analysis of DNA damage by gel electrophoresis also demonstrates that the Rh(III) complex undergoes photochemical reactions with single-stranded DNA (Figure 2.10); however, the mechanism of the chemical reaction is uncertain. Thus, while DNA damage and mass spectroscopy both indicate that $Rh(phi)_2bpy^{3+}$ binds to single-stranded DNA, neither technique addresses the structure of this interaction.

Metalated oligonucleotides show some of the spectroscopic features of intercalated metal complexes. The UV-visible absorption of the metal complexes are hypochromic, as has been observed for intercalated complexes, and also show lower energy absorption maxima compared to the water-solvated complexes (Figure 4.5). These red-shifts are indicative of an increasingly hydrophobic environment for the chromophores; similar changes have been previously identified for complexes bound to DNA[22,40] and to SDS micelles.[33] The long excited-state lifetimes observed for single-stranded Ru(II)-oligonucleotides also indicate that the Me_2dppz ligand of $Ru(phen)(bpy')(Me_2dppz)^{2+}$ is somehow protected from solvent by the covalently attached DNA. Importantly, the temperature-dependence of emission (Figure 4.7) varies dramatically from the stable luminescence found for Ru-DNA duplexes (Figure 4.15); it is therefore unlikely that the single-stranded oligonucleotide and the metal complex maintain a stable, intercalated interaction. Instead, the exponential dependence on temperature could indicate that the metal complex is loosely associated with the poorly-structured single-stranded oligonucleotide, and that this weak structure "melts" smoothly with increasing temperature.

4.4.3.2 Binding of intercalators in Ru-DNA and Rh-DNA assemblies

The emission measurements described in Section 4.3.4.4 have focused on the luminescent complex $Ru(phen)(bpy')(Me_2dppz)^{2+}$ tethered to the sequence 16 merA. This particular trisheteroleptic complex was chosen because it showed strong emission in the

presence of DNA and gave high yields of Ru(II)-oligonucleotide conjugates, thus permitting extensive characterization. The oligonucleotide duplex 16 merA/B was designed based on the results of gel electrophoresis studies, ^{1}H NMR measurements, and earlier ET experiments with different DNA sequences. Gel electrophoresis measurements of DNA damage caused by *Ru(II)-sensitized $^1O_2$ showed that Ru(phen)(bpy')$(Me_2dppz)^{2+}$ tended to bind at 5'-TGAGACT-'3 sequences (Figure 4.11); a subset of this binding site (5'-GACT-3') was also determined from ^{1}H NMR measurements of Δ-Ru$(phen)_2dppz^{2+}$ bound to a hexamer oligonucleotide duplex.[28] The complementary sequence 5'-AGTC-3' was therefore placed at the 5' end of the ruthenated strand. Previously, photocleavage of DNA restriction fragments by Δ-Rh$(phi)_2dmb^{3+}$ has shown that this complex bound preferentially at 5'-ACGA-3' sequences;[36] thus, this sequence was designed into the 5' end of the Rh(III)-oligonucleotide sequence. The intervening sequence was synthesized to contain a high percentage of A•T base pairs, since time-resolved photophysical measurements indicated that A•T-rich sequences facilitate electron transfer reactions more efficiently than G•C-rich duplexes.[35]

The results of DNA cleavage, gel electrophoresis, and some quenching experiments with 16 merA/B supported the notion that this sequence provides adequate intercalation sites for both Ru(phen)(bpy')$(Me_2dppz)^{2+}$ and Rh$(phi)_2(bpy')^{3+}$. As Figure 4.12 summarizes, *Δ-Ru(II)-sensitization of $^1O_2$ yielded damage primarily near the putative Ru(II) binding site in the duplex but not in the single-stranded form. It is noteworthy that such regiospecific cleavage has not been observed in cases in which the Ru(II) binding site contained a 5'-AGCA-3' sequence (Chapter 5). Similarly, photoactivated Δ-Rh(III) caused direct strand scission primarily near the second base step from the site of covalent attachment (Figure 4.12); less specific cleavage has been obtained in some cases in which either the linker or the Rh(III) binding site was changed. Furthermore, electrophoresis of singly- and doubly metallated oligonucleotide duplexes through a nondenaturing polyacrylamide gel suggested that hybridization yielded one primary product with the

characteristics of double-stranded DNA (Figure 4.13). The steady-state emission quenching experiments listed in Table 4.5 offered promising data as well. For instance, reactions between Δ-Ru(II) and Δ-Rh(III) intercalators was more efficient than other diastereomeric pairs, as had been observed for noncovalently bound intercalators. Additionally, when noncovalently bound Ru(II) was added to the Δ-Rh(III)-N9C-16 merA/B duplex, efficient quenching of the lumophore was observed, suggesting that the tethered Rh(III) complex was well-coupled into the DNA duplex. Tethered Ru(II) was also significantly quenched by added $Rh(phi)_2bpy^{3+}$. The ~15% difference in quenching between these two reactions could indicate that the Ru(II) complex was not intercalated as well when it was tethered to the oligonucleotide as when it was noncovalently bound to the 16 mer duplex.

Other spectroscopic experiments suggested that Ru(II) was *not* tightly bound to its tethered DNA duplex. The temperature-dependence of both emission (Figure 4.15) and absorption (Table 4.3) spectra indicated that binding of tethered Ru(II) did not stabilize the DNA duplex, whereas intercalation of both noncovalently bound Ru(II) and tethered Rh(III) increased the T_m of the 16 merA/B duplex by ≥ 10 °C. Furthermore, steady-state and time-resolved emission measurements were highly sensitive to the sample preparation, the concentration of metallated duplex, the chemical structure of the alkyl linker, and the length of the DNA sequence. The marked irreproducibility in both absolute emission intensities and quenching efficiencies for these particular Ru-DNA and Ru-DNA-Rh assemblies (Table 4.4) seems to imply that these chimeras could adopt a number of energetically similar structures. The absence of a clear thermodynamic minimum could explain the sensitivity of emission properties to the sample preparation. The observation that emission quenching in these Ru-DNA-Rh depended on duplex concentration could further suggest that metallated oligonucleotides were aggregated (Figure 4.16). In this case, the apparent quenching would occur either by intermolecular ET or by structural changes upon the addition of the Rh(III)-oligonucleotide. It is noteworthy that the T_m of

the 16 merA/B was found to be 40 °C at 2.5 μM; therefore, melting of the duplex at low concentrations does not account for the anomalous concentration-dependence. The photocleavage results indicate that the Rh(III) complex is mostly bound intramolecularly, and therefore suggest that intermolecular quenching via intercalation is unlikely; additional experiments with $^1O_2$-sensitized cleavage by Ru(II) would address the possibility of intermolecular intercalation for the photoexcited donor.

The sensitivity of the steady-state emission intensity to the structure of the alkyl linker further suggests that the Ru(II)-16 merA/B duplexes were on the edge of providing the conformational requirements for hybridization and intercalation of Ru(phen)(bpy')-$(Me_2dppz)^{2+}$ (Table 4.6). If the complex were able to intercalate completely in each instance, then the hydrophobicity of the linker would have had only a minor effect on the excited-state lifetimes. Most studies subsequent to these measurements have used the N9C and NO8 tethers since chimeras containing these linkers show higher yields of emission and emission quenching than chimeras containing N6C and N6P. Finally, both the emission of Ru(II)-DNA and the efficiency of quenching in Ru-DNA-Rh decrease markedly between 14 merA/B and 12 merA/B (Table 4.7). A decreased yield of quenching is inconsistent with ET theory and other DNA-mediated ET experiments, and indicates that structural changes in the metallated assemblies have overshadowed the properties of quenching caused by electron transfer.

If Ru-DNA and Ru-DNA-Rh chimeras containing the sequence 16 merA/B were not properly hybridized, then the actual structure of these assemblies needs to be understood. Some evidence suggests that there were only a small set of chimeric duplex structures; for instance, nondenaturing gel electrophoresis shows a reasonably narrow band of material with the expected mobility (Figure 4.13). Dilution studies with both single-stranded Ru(II)-oligonucleotide[22] and Ru(II)-DNA duplexes (Section 4.4.3.4.5) indicate that the emission of Ru(II) decreased linearly with concentration, consistent with the presence of unique structures. On the other hand, the emission properties of single-

stranded Ru(II)-oligonucleotide conjugates indicate a significant interaction of the metal complex with the DNA strand. Since the emission lifetimes of Ru(II) were not dramatically altered by hybridization to the complementary strand, it is possible that annealing of the two strands was incomplete. Current studies using HPLC could serve as an additional sensitive method for analyzing the number of annealed structures.

It must be emphasized that the issues discussed here are not general for all intercalator-oligonucleotide conjugates. Notably, ethidium-DNA-Rh(phi)$_2$(bpy')$^{3+}$ assemblies have shown reproducible efficiencies of quenching for a range of distances, sequences, and concentrations.[70] Perhaps the large size and hydrophobicity of the trisheteroleptic Ru(II) complex create additional structural obstacles to the formation of well-hybridized metallated assemblies. On the other hand, predictable results have been observed for other oligonucleotide sequences containing Ru(phen)(bpy')(Me$_2$dppz)$^{2+}$ tethered by an NO8 linker.[74] Thus, it is possible that the DNA length, sequence, and tether require further modification.

As noted, Ru(phen)(bpy')(Me$_2$dppz)-N9C-20 merA/B shows reproducible DNA damage by long-range G oxidation (Chapter 5).[39] In comparing the present studies to measurements of oxidative damage, it is important to note that Ru(II) emission arises from a number of processes involving the environment of the Me$_2$dppz ligand and thus may be highly sensitive to even subtle changes in DNA structure and binding. Furthermore, emission quenching in these covalently-modified duplexes relies on the *difference* between the luminescence of two, independent samples. In contrast, oxidative chemistry arises from a specific chemical reaction, and is thus much less sensitive to the details of the chromophore environment. This readily characterized oxidation reaction has recently served as a very sensitive tool for probing the sequence- and structure-dependence of long-range DNA-mediated ET reactions.[36,37,39,74]

4.5 Future directions

The synthetic strategies for preparing metal complexes and metal-oligonucleotides are highly flexible; thus, it should be possible to design chimeras which form well-structured duplexes with predictable luminescence properties. Several synthetic approaches are worth exploring, such as varying the metal complex, the linkers, or the hybridization conditions. Trisheteroleptic complexes can be prepared to contain more hydrophilic or negatively charged ligands, thereby reducing the binding of Ru(II) complexes to single-stranded DNA. The conformational flexibility of the aliphatic linker is found to have a strong effect on the emission and photocleavage characteristics of Ru(II) and Rh(III) intercalators, suggesting that the tethers may not orient the complexes properly. Thus, several linkers may be prepared to optimize intramolecular binding of the metallointercalator to DNA. Lastly, the hybridization conditions could dictate the structure of Ru-DNA and Ru-DNA-Rh chimeras, particularly if several structural variations are thermodynamically accessible. By varying temperature gradients, duplex concentrations, salts and other additives, it may be possible to isolate a single well-hybridized, intramolecularly intercalated metal-duplex assembly.

It is important to note that these methodologies have only been recently developed and that major strides have been made in the characterization of metal-DNA chimeras. Using a diverse set of tools, including temperature-dependent emission and absorption spectroscopies, mass spectrometry, and gel electrophoresis, we may predict the behavior of Ru(II) and Rh(III) conjugates. For example, since intercalation has been shown to stabilize the DNA double helix, increases in T_m are expected for tethered metal-DNA assemblies. Similarly, the characteristic temperature-dependence of emission of Ru(II) complexes predicts that well-intercalated Ru(II)-DNA conjugates should show stable emission intensities with increasing temperature until the melting temperature of the duplex is reached. Mass spectrometry has dramatically increased our confidence in the identification of metal-oligonucleotide conjugates, and results have underscored the accuracy of other

characterization methods such as HPLC and UV-visible spectroscopy. Finally, the emission and photocleavage properties of Ru(II)/Os(II) and Rh(III) complexes offer highly sensitive measurements of the sequence- and structure-dependent binding of these intercalators to DNA.

Already, these chimeras have been instrumental in a number of interesting and important studies in nucleic acid chemistry. For example, Rh(III)-DNA and Ru(II)-DNA chimeras have been used to study DNA damage[36,39] and repair as well as structural defects in DNA such as mismatches and bulges.[36,37,74] Current projects in our laboratory have expanded the scope of DNA-mediated ET studies by i) describing the distance dependence of reactions between intercalated ethidium and Rh(III),[70] ii) developing the synthesis of single-stranded oligonucleotides bearing intercalators at the 3'- and 5'-termini,[75] and iii) investigating the effects of DNA binding proteins on the structure of the DNA base stack.[74]

4.6 References

1. Goodchild, J. *Bioconjugate Chem.* **1990**, *1*, 165.
2. Englisch, U.; Gauss, D. H. *Angew. Chem. Int. Ed. Engl.* **1991**, *30*, 613.
3. Beaucage, S. L.; Iyer, R. P. *Tetrahedron* **1993**, *49*, 1925.
4. Thuong, N. T.; Hélène, C. *Angew. Chem. Int. Ed. Engl.* **1993**, *32*, 666.
5. a) Mergny, J. L.; Boutorine, S.; Garestier, T.; Belloc, F.; Rougee, M.; Bulychev, N. V.; Koshkin, A. A.; Bourson, J.; Levedev, A. V.; Valeur, B.; Thuorn, N. T.; Hélène, C. *Nuc. Acids. Res.* **1994**, *22*, 920. b) Cooper, J. P.; Hagerman, P. J. *Biochemistry*, **1990**, *29*, 9261. c) Cardullo, R. A.; Agrawal, S.; Flores, C.; Zamecnik, P. C.; Wolf, D. E. *Proc. Natl. Acad. Sci. USA* **1988**, *85*, 8790.
6. Tesler, J.; Cruickshank, K. A.; Morrison, L. E.; Netzel, T. L.; Chan, C. *J. Am. Chem. Soc.* **1989**, *111*, 7221.
7. Zuckermann, R.; Corey, D.; Schultz, P. *Nuc. Acids. Res.* **1987**, *15*, 5305-5321.
8. Spaltenstein, A.; Robinson, B. H.; Hopkins, P. B. *J. Am. Chem. Soc.* **1989**, *111*, 2303.
9. Allen, D. J.; Darke, P. L.; Benkovic, S. J. *Biochemistry*, **1989**, *28*, 4601.
10. Aurup, H.; Tuscgi, T.; Benseler, F.; Ludwig, J.; Eckstein, *Nuc. Acids. Res.* **1994**, *22*, 20.
11. Lee, B. L.; Murakami, A.; Blake, K. R.; Lin, S.-B.; Miller, P. S. *Biochemistry* **1988**, *27*, 3197.
12. Kenten, J. H.; Gudibande, S.; Link, J.; Willey, J. J.; Curfman, B.; Major, E. O.; Massey, R. J. *Clin. Chem.* **1992**, *38*, 873.
13. Bannwarth, W.; Schmidt, D.; Stallard, R. L.; Hornung, C.; Knorr, R.; Müller, F. *Helv. Chim. Acta* **1988**, *71*, 2085.
14. Bannwarth, W.; Schmidt, D. *Tet. Lett.* **1989**, *30*, 1513.
15 Meade, T. J.; Kayyem J. F. *Angew. Chem. Int. Ed. Engl.* **1995**, *34*, 352.
16. Chen, C.-H. B.; Sigman, D. S. *Proc. Natl. Acad. Sci. USA* **1986**, *83*, 7147.

17. Chu, B. C. F.; Orgel, L. E. *Proc. Natl. Acad. Sci. USA* **1985**, *82*, 963.

18. Francois, J.-C.; Saison-Behmoaras, T.; Barbier, C.; Chassignol, M.; Thuong, N. T.; Hélène, C. *Proc. Natl. Acad. Sci. USA*, **1989**, *86*, 9702.

19. Praseuth, D.; Chassignol, M.; Takasugi, M.; Doan, T. L.; Thuong, N. T.; Helene, C. *J. Mol. Biol.* **1987**, *196*, 939.

20. Singleton, S. F.; Dervan, P. B. *J. Am. Chem. Soc.* **1992**, *114*, 6957.

21. Jenkins, Y.; Barton, J. K. *J. Am. Chem. Soc.* **1992**, *114*, 8737.

22. Jenkins, Y. Ph.D. Thesis, *California Institute of Technology*, **1996**.

23. a) Dupureur, C. M.; Barton, J. K. *Comprehensive Supramolecular Chemistry V. 5*, J.-M. Lehn, ed. Pergamon Press, **1995**, 295. b) Johann, T. W.; Barton, J. K. *Trans. Royal Soc. (London) A.* **1996**, *354*, 299.

24. Erkkila, K. E. unpublished results.

25. Friedman, A. E.; Chambron, J.-C.; Sauvage, J.-P.; Turro, N. J.; Barton, J. K. *J. Am. Chem. Soc.* **1990**, *112*, 4960.

26. Jenkins, Y.; Friedman, A. E.; Turro, N. J.; Barton, J. K. *Biochemistry* **1992**, *31*, 10811.

27. Hartshorn, R. M.; Barton, J. K. *J Am. Chem. Soc*, **1992**, *114*, 5925.

28. a) Dupureur, C. M.; Barton, J. K. *J. Am. Chem. Soc.* **1994**, *116*, 10286. b) Dupureur, C. M.; Barton, J. K. submitted for publication.

29. Holmlin, R. E.; Barton, J. K. *Inorg. Chem.* **1995**, *34*, 7.

30. Murphy, C. J.; Arkin, M. R.; Jenkins, Y.; Ghatlia, N. D.; Bossman, S.; Turro, N. J.; Barton, J. K. *Science* **262**, 1025 (1993).

31. Murphy, C. J.; Arkin, M. R.; Ghatlia, N. D.; Bossmann, S.; Turro, N. J.; Barton, J. K. *Proc. Nat. Acad. Sci., USA*, **1994**, *91*, 5315.

32. Stemp, E. D. A.; Arkin, M. R.; Barton, J. K. *J. Am. Chem. Soc.* **1995**, *117*, 2375.

33. Arkin, M. R.; Stemp, E. D. A.; Turro, C.; Turro, N. J.; Barton, J. K. *J. Am. Chem. Soc.* **1996**, *118*, 2267.

34. Holmlin, R. E.; Stemp, E. D. A.; Barton, J. K. *J. Am. Chem. Soc.* **1996**, *118*, 5236.

35. Arkin, M. R.; Stemp, E. D. A.; Holmlin, R. E.; Barton, J. K.; Hörmann, A.; Olson, E. J. C.; Barbara, P. F. *Science*, **1996**, *273*, 475.

36. a) Hall, D. B.; Holmlin, R. E.; Barton, J. K. *Nature*, **1996**, *382*, 731. b) Hall, D. B. and Barton, J. K., unpublished results.

37. Dandliker, P. J.; Holmlin, R. E.; Barton, J. K., *Science*, in press, **1996**.

38. Stemp, E. D. A., Arkin, M. R.; Barton, J. K. unpublished results.

39. Arkin, M. R.; Stemp, E. D. A.; Barton, J. K. unpublished results.

40. Sitlani, A.; Long, E. C.; Pyle, A. M.; Barton, J. K. *J. Am. Chem. Soc.* **1992,** *14*, 2303.

41. Strouse, G. F.; Anderson, P. A.; Schoonover, J. R.; Meyer, T. J.; Keene, F. R. *Inorg. Chem.* **1992**, *31*, 3004.

42. Anderson, P. A.; Deacon, G. B.; Haarmann, K. H.; Keene, F. R.; Meyer, T. J.; Reitsma, D. A.; Skelton, B. W.; Strouse, G. F.; Thomas, N. C.; Treadway, J. A.; White, A. H. *Inorg. Chem.* **1995**, *34*, 6145.

43. Holmlin, R. E. unpublished results.

44. Della Chiana, L.; Hamachi, I.; Meyer, T. J. *J. Org. chem.* **1989**, *54*, 1731.

45. a) Chambron, J.-C.; Sauvage, J.-P.; Amouyal, E.; Koffi, P. *New J. Chem.* **1985**, *9*, 527. b) E. Amouyal, A. Homsi, J.-C. Chambron and J.-P. Sauvage, *J. Chem. Soc. Dalton Trans.* **1990**, 1841 (1990).

46. Pyle, A. M.; Chiang, M. Y.; Barton, J. K. *Inorg. Chem.* **1990**, *29*, 4487.

47. Sardesai, N. Y.; Lin, S. C.; Zimmerman, K.; Barton, J. K.; *Biochonj. Chem.* **1995**, *6*, 302.

48. Kelley, S. O. unpublished results.

49. Volante, R. P. *Tet. Lett.* **1981**, *22*, 3319.

50. a) Cuenoud, B.; Shepartz, A. *Tet. Lett.* **1991**, *28*, 3325. b) Cuenoud, B.; Schepartz, A. *Proc. Natl. Acad. Sci. USA* **1993**, *90*, 1154.

51. a) Brocklehurst, K.; Little, G. *Biochem. J.* **1973**, *133*, 67. b) Carlsson, J.; Drevin, H.; Axén, R. *Biochem. J.* **1978**, *173*, 723.

52. Thomas, N. C.; Deacon, G. B. *Inorg. Synth.* **1989**, *25*, 107.

53. Black, D. St.C.; Deacon, G. B.; Thomas, N. C. *Aust. J. Chem.* **1982**, *35*, 2445.

54. Beaucage, S. L.; Caruthers, M. H. *Tet. Lett.* **1981**, *23*, 1859.

55. Wachter, L.; Jablonski, J.-A.; Ramachandran, K. L. *Nucl. Acids Res.* **1986**, *14*, 7985.

56. Angell, Y. M.; Garcia-Echeverria, C.; Rich, D. H. *Tet. Lett.* **1994**, *35*, 5981.

57. a) Carpino, L. A.; El-Faham, A. *J. Org. Chem.* **1994**, *59*, 695. b) Carpino, L. A.; El-Faham, A.; Albericio, F. *Tet. Lett.* **1994**, *35*, 2279.

58. Eritja, R.; Horowitz, D. M.; Walker, P. A.; Ziehler-Martin, J. P.; Boosalis, M. S.; Goodman, M. F.; Itakura, K.; Kaplan, B. E. *Nucl. Acids. Res.;* **1986**, *14*, 8135.

59. Lindberg, O.; Ernsten, L. in *Methods of Biochemical Analysis, Vol. 3* (Glick, D. Ed.), Interscience: New York, **1954**.

60. Sambrook, J.; Fritsch, E. F.; Maniatis, T. *Molecular Clonins: a Laboratory Manual* 2nd ed., NY: Cold Spring Harbor Laboratory, **1989.**

61. Mahnken, R. E.; Billadeau, M. A.; Nikonowicz, E. P.; Morrison, H. *J. Am. Chem. Soc.* **1992**, *114*, 9253.

62. a) Barton, J. K.; Lolis, E. *J. Am. Chem. Soc.* **1985**, *107*, 708. b) Grover, N.; Welch, T. W.; Fairley, T. A.; Corey, M.; Thorp, H. H. *Inorg. Chem.* **1994**, *33*, 3544.

63. Franklin, S. J., unpublished results.

64. a) Smith, R. D.; Cheng, X.; Chen, R. D.; Hofstadler, S. A. *Am. Chem. Soc. Symp. Ser.* **1996**, *619*, 294. b) Cheng, X.; Harms, A. C.; Goudreau, P. N.; Terwilliger, T. C.; Smith, R. D. *Proc. Natl. Acad. Sci. USA* **1996**, *93*, 7022.

65. Harms, A.; Jenkins, Y.; Barton, J. K.; Smith, R., unpublished results.

66. Rodgers, M. A. J.; Snowden, P. T. *J. Am. Chem. Soc.* **1982**, *104*, 5543.

67. a) Mei, H.-Y.; Barton, J. K. *J. Am. Chem. Soc.* **1986**, *108*, 7414. b) Mei, H.-Y.; Barton, J. K. *Proc. Natl. Acad. Sci. USA* **1988**, *85*, 1339.

68. Chung, M.-H.; Kiyosawa, H.; Nishimura, S.; Kasai, H. *Biochem. Biophys. Res. Comm.* **1992**, *188*, 1.

69. Saenger, W.; Cantor, C. R., eds. *Principles of Nucleic Acid Structure*, NY: Springer-Verlag, **1984**.

70. Kelley, S. O.; Holmlin, R. E.; Stemp, E. D. A.; Barton, J. K. unpublished results.

71. Sardesai, N. Y.; Zimmermann, K.; Barton, J. K. *J. Am. Chem. Soc.* **1994**, *116*, 7502.

72. Zimmermann, K.; Lin, S. C.; Hall, D. B., unpublished results.

73. Ghosh, S. S.; Musso, G. F. *Nuc. Acids Res.* **1987**, *15*, 5353.

74. Coates, S., unpublished results.

75. Holmlin, R. E.; Dandliker, P. J., unpublished results.

4.7 Appendices

4.7.1 Characterization of intermediates in synthesis of Ru(dmb)(bpy')-(dppz)Cl_2

Table A.4.1. Infrared spectra of carbonyl complexes of Ru(II).*

complex	experimental (cm^{-1})	identification
$[Ru(CO)_2Cl_2]_n$	2147	CO $[Ru(CO)_3Cl_2]$
	2080	CO
	2025	CO
$[Ru(CO)_2(dmb)Cl_2]$	2054	CO
	1987	CO
$[Ru(CO)_2(dmb)(trif)_2]$	2101	CO
	2027	CO
	1325	SO_3
	1236	CF
	1173	SO_3+CF
	1009	SO_3
$[Ru(CO)_2(dmb)(dppz)](PF_6)_2$	2091	CO
	2039	CO
	841	PF_6
	2361/2341	dppz
	1618	dppz

* Infrared spectra obtained on a Mattson Galaxy 3000 FTIR at Occidental College.

Table A.4.2. Mass spectral characterization of complexes of Ru(II).*

complex	mass	identification
$[Ru(CO)_2(dmb)Cl_2]$	412	$[Ru(CO)_2(dmb)Cl_2]+$
	377	$[Ru(CO)_2(dmb)Cl]+$
	349	[Ru(CO)(dmb)Cl]+
	321	[Ru(dmb)Cl]+
$[Ru(CO)_2(dmb)(SO_3CF_3)_2]$	633	$[Ru(CO)_2(dmb)(SO_3CF_3)_2]Na+$
	491	$[Ru(CO)_2(dmb)(SO_3CF_3)]+$
	463	$[Ru(CO)(dmb)(SO_3CF_3)]+$
	435	$[Ru(dmb)(SO_3CF_3)]+$
	377	$[Ru(CO)_2(dmb)Cl]+$
	342	$[Ru(CO)_2(dmb)]H+$
$[Ru(CO)_2(dmb)(dppz)](PF_6)_2$	769	$[Ru(CO)_2(dmb)(dppz)](PF_6)+$
	567	[Ru(dmb)(dppz)]H+
	283	dppzH+
[Ru(dmb)(dppz)(bpy')]$(OAc)_2$	823	[Ru(dmb)(bpy')(dppz)]H+
	640	[Ru(bpy')(dppz)]H+
	568	[Ru(dmb)(dppz)]H+
	542	[Ru(dmb)(bpy')]H+ (tiny)

* FAB-MS data obtained at the Chemistry and Chemical Engineering Mass Spectrometry Laboratory (Caltech).

Table A.4.3. Elemental analysis of carbonyl complexes of Ru(II).*

complex	element	expected %	experimental %
$[Ru(CO)_2(dmb)Cl_2]$	C	40.8	40.81
	H	2.9	3.07
	N	6.8	6.81
$[Ru(CO)_2(dmb)(SO_3CF_3)_2]$	C	30.0	29.97
	H	1.9	2.07
	N	4.4	4.27
$[Ru(CO)_2(dmb)(dppz)](PF_6)_2$	C	42.1	38.12
	H	2.4	2.65
	N	9.2	9.39

* Elemental Analysis performed by Dr. Fenton Harvey at Caltech.

4.7.2 Procedures for automated incorporation of amine linkers

4.7.2.1. Making 4 x 1 μmol of carbamate linked DNA on 394 ABI synthesizer

note: This worksheet assumes you are familiar with the DNA synthesizer.

1) Preparation of reagents

note: Bottles that fit on synthesizer can be obtained by cleaning out used 1g phosphoramidite bottles. I suggest that you keep three of your own for CDI, linker, and CH_2Cl_2 and use three others for leaving on the instrument when you are finished.

a) Dissolve 1g carbonyl diimidazole (CDI)/10 ml dry CH_2Cl_2. Sonicate and decant into 12 ml brown, ABI bottle. This will go onto port 5 (see below).

b) Dissolve 1g linker (e.g., diaminononane)/10 ml CH_2Cl_2. Filter through paper by gravity filtration into 12 ml brown, ABI bottle. This bottle with go onto port 6 (see below).

c) Fill another ABI bottle with 12 ml CH_2Cl_2 for port 7.

2) Preparing synthesizer

a) Run bottle change procedures (not auto dilution) for ports 5, 6, 7 (CDI on 5; linker on 6; solvent on 7).

b) Check rest of reagents as usual, including 18 (acetonitrile), Argon (gas tank on east wall, labeled "west"), and waste.

3) Edit sequence

Type in sequence as usual, adding 6 and 5 to the 5' end, e.g.:

5'> 65X XXX >3'

4) Configure synthesis

a) Start synthesis.

b) Put in sequence #s as usual.

c) Cycle: scroll cycle to "MICHELLEC1"

d) Use **Trityl off**; cleave as desired (either MANUAL or END CE).

e) Start synthesis as usual, do run ABI BEGIN.

5) After synthesis

a) Go to "bottle change procedure"
dilute 1-8
procedure: LINK CLEAN
"yes" to bottles 5,6,7

b) At first interrupt, empty bottles 5, 6 and refill with CH_2Cl_2.

c) At second interrupt, empty bottles 5, 6, 7 and replace empty (they will fill with MeCN).

6) Optional: Rinse synthesis colums with 10 ml methanol with a disposable syringe.

4.7.2.2 "MICHELLEC1" ABI 394 cycle

- 394 Cycle Listing - (Version 1.01)

Name : MICHELLEC1 1:30:30P, 1/19/97
Steps: 151

Step Number	Function #	Name	Step Time	Step Active for Bases A	G	C	T	5	6	7	8	Safe Step
1	106	Begin										Yes
2	64	18 to Waste	3.0									Yes
3	42	18 to Column	10.0	Yes	Yes	Yes	Yes	Yes	Yes	Yes	Yes	Yes
4	2	Reverse Flush	10.0	Yes	Yes	Yes	Yes	Yes	Yes	Yes	Yes	Yes
5	1	Block Flush	4.0	Yes	Yes	Yes	Yes	Yes	Yes	Yes	Yes	Yes
6	101	Phos Prep	3.0									Yes
7	140	Column 1 On										Yes
8	111	Block Vent	2.0	Yes	Yes	Yes	Yes	Yes	Yes	Yes	Yes	Yes
9	58	Tet to Waste	1.7									Yes
10	33	B+Tet to Column	2.5	Yes	Yes	Yes	Yes	No	No	Yes	Yes	Yes
11	34	Tet to Column	1.0	Yes	Yes	Yes	Yes	No	No	Yes	Yes	Yes
12	33	B+Tet to Column	2.5	Yes	Yes	Yes	Yes	No	No	Yes	Yes	Yes
13	1	Block Flush	2.0	No	No	No	No	Yes	Yes	No	No	Yes
14	29	5 to Column	20.0	No	No	No	No	Yes	No	No	No	Yes
15	30	6 to Column	20.0	No	No	No	No	No	Yes	No	No	Yes
16	103	Wait	60.0	No	No	No	No	Yes	Yes	No	No	Yes
17	29	5 to Column	10.0	No	No	No	No	Yes	No	No	No	Yes
18	30	6 to Column	10.0	No	No	No	No	No	Yes	No	No	Yes
19	103	Wait	30.0	No	No	No	No	Yes	Yes	No	No	Yes
20	29	5 to Column	10.0	No	No	No	No	Yes	No	No	No	Yes
21	30	6 to Column	10.0	No	No	No	No	No	Yes	No	No	Yes
22	103	Wait	30.0	No	No	No	No	Yes	Yes	No	No	Yes
23	29	5 to Column	5.0	No	No	No	No	Yes	No	No	No	Yes
24	30	6 to Column	5.0	No	No	No	No	No	Yes	No	No	Yes
25	43	Push to Column										Yes
26	141	Column 1 Off										Yes
27	142	Column 2 On										Yes
28	64	18 to Waste	4.0									Yes
29	1	Block Flush	3.0	Yes	Yes	Yes	Yes	Yes	Yes	Yes	Yes	Yes
30	111	Block Vent	2.0	Yes	Yes	Yes	Yes	Yes	Yes	Yes	Yes	Yes
31	58	Tet to Waste	1.7									Yes
32	33	B+Tet to Column	2.5	Yes	Yes	Yes	Yes	No	No	Yes	Yes	Yes
33	34	Tet to Column	1.0	Yes	Yes	Yes	Yes	No	No	Yes	Yes	Yes
34	33	B+Tet to Column	2.5	Yes	Yes	Yes	Yes	No	No	Yes	Yes	Yes
35	1	Block Flush	2.0	No	No	No	No	Yes	Yes	No	No	Yes
36	29	5 to Column	20.0	No	No	No	No	Yes	No	No	No	Yes
37	30	6 to Column	20.0	No	No	No	No	No	Yes	No	No	Yes
38	103	Wait	60.0	No	No	No	No	Yes	Yes	No	No	Yes
39	29	5 to Column	10.0	No	No	No	No	Yes	No	No	No	Yes
40	30	6 to Column	10.0	No	No	No	No	No	Yes	No	No	Yes
41	103	Wait	30.0	No	No	No	No	Yes	Yes	No	No	Yes
42	29	5 to Column	10.0	No	No	No	No	Yes	No	No	No	Yes

43	30	5 to Column	10.0	No	No	No	No	No	Yes	No	No	Yes
44	103	Wait	30.0	No	No	No	No	Yes	Yes	No	No	Yes
45	29	5 to Column	5.0	No	No	No	No	Yes	No	No	No	Yes
46	30	6 to Column	5.0	No	No	No	No	No	Yes	No	No	Yes
47	43	Push to Column										Yes
48	143	Column 2 Off										Yes
49	144	Column 3 On										Yes
50	64	18 to Waste	4.0									Yes
51	1	Block Flush	3.0	Yes	Yes	Yes	Yes	Yes	Yes	Yes	Yes	Yes
52	111	Block Vent	2.0	Yes	Yes	Yes	Yes	Yes	Yes	Yes	Yes	Yes
53	59	Tet to Waste	1.7									Yes
54	33	B+Tet to Column	2.5	Yes	Yes	Yes	Yes	No	No	Yes	Yes	Yes
55	34	Tet to Column	1.0	Yes	Yes	Yes	Yes	No	No	Yes	Yes	Yes
56	33	B+Tet to Column	2.5	Yes	Yes	Yes	Yes	No	No	Yes	Yes	Yes
57	1	Block Flush	2.0	No	No	No	No	Yes	Yes	No	No	Yes
58	29	5 to Column	20.0	No	No	No	No	Yes	No	No	No	Yes
59	30	6 to Column	20.0	No	No	No	No	No	Yes	No	No	Yes
60	103	Wait	60.0	No	No	No	No	Yes	Yes	No	No	Yes
61	29	5 to Column	10.0	No	No	No	No	Yes	No	No	No	Yes
62	30	6 to Column	10.0	No	No	No	No	No	Yes	No	No	Yes
63	103	Wait	30.0	No	No	No	No	Yes	Yes	No	No	Yes
64	29	5 to Column	10.0	No	No	No	No	Yes	No	No	No	Yes
65	30	6 to Column	10.0	No	No	No	No	No	Yes	No	No	Yes
66	103	Wait	30.0	No	No	No	No	Yes	Yes	No	No	Yes
67	29	5 to Column	5.0	No	No	No	No	Yes	No	No	No	Yes
68	30	6 to Column	5.0	No	No	No	No	No	Yes	No	No	Yes
69	43	Push to Column										Yes
70	145	Column 3 Off										Yes
71	146	Column 4 On										Yes
72	64	18 to Waste	4.0									Yes
73	1	Block Flush	3.0	Yes	Yes	Yes	Yes	Yes	Yes	Yes	Yes	Yes
74	111	Block Vent	2.0	Yes	Yes	Yes	Yes	Yes	Yes	Yes	Yes	Yes
75	59	Tet to Waste	1.7									Yes
76	33	B+Tet to Column	2.5	Yes	Yes	Yes	Yes	No	No	Yes	Yes	Yes
77	34	Tet to Column	1.0	Yes	Yes	Yes	Yes	No	No	Yes	Yes	Yes
78	33	B+Tet to Column	2.5	Yes	Yes	Yes	Yes	No	No	Yes	Yes	Yes
79	1	Block Flush	2.0	No	No	No	No	Yes	Yes	No	No	Yes
80	29	5 to Column	20.0	No	No	No	No	Yes	No	No	No	Yes
81	30	6 to Column	20.0	No	No	No	No	No	Yes	No	No	Yes
82	103	Wait	60.0	No	No	No	No	Yes	Yes	No	No	Yes
83	29	5 to Column	10.0	No	No	No	No	Yes	No	No	No	Yes
84	30	6 to Column	10.0	No	No	No	No	No	Yes	No	No	Yes
85	103	Wait	30.0	No	No	No	No	Yes	Yes	No	No	Yes
86	29	5 to Column	10.0	No	No	No	No	Yes	No	No	No	Yes
87	30	6 to Column	10.0	No	No	No	No	No	Yes	No	No	Yes
88	103	Wait	30.0	No	No	No	No	Yes	Yes	No	No	Yes
89	29	5 to Column	5.0	No	No	No	No	Yes	No	No	No	Yes
90	30	6 to Column	5.0	No	No	No	No	No	Yes	No	No	Yes
91	43	Push to Column										Yes
92	147	Column 4 Off										Yes
93	103	Wait	25.0	Yes	Yes	Yes	Yes	No	No	Yes	Yes	Yes
94	103	Wait	999.0	No	No	No	No	Yes	Yes	No	No	Yes
95	102	Cap Prep	3.0									Yes
96	64	18 to Waste	4.0									Yes
97	2	Reverse Flush	7.0	Yes	Yes	Yes	Yes	No	No	Yes	Yes	Yes
98	1	Block Flush	3.0	Yes	Yes	Yes	Yes	No	No	Yes	Yes	Yes
99	39	Cap to Column	10.0	Yes	Yes	Yes	Yes	No	No	Yes	Yes	Yes

100	103	Wait	5.0	Yes	Yes	Yes	Yes	No	No	Yes	Yes	Yes
101	64	18 to Waste	4.0								Yes
102	2	Reverse Flush	7.0	Yes	Yes	Yes	Yes	No	No	Yes	Yes	Yes
103	1	Block Flush	3.0	Yes	Yes	Yes	Yes	No	No	Yes	Yes	Yes
104	41	15 to Column	8.0	Yes	Yes	Yes	Yes	No	No	Yes	Yes	Yes
105	64	18 to Waste	4.0								Yes
106	1	Block Flush	3.0	Yes	Yes	Yes	Yes	No	No	Yes	Yes	Yes
107	103	Wait	15.0	Yes	Yes	Yes	Yes	No	No	Yes	Yes	Yes
108	42	18 to Column	10.0	Yes	Yes	Yes	Yes	No	No	Yes	Yes	Yes
109	31	7 to Column	10.0	No	No	No	No	Yes	Yes	No	No	Yes
110	4	Flush to Waste	6.0	Yes	Yes	Yes	Yes	Yes	Yes	Yes	Yes	Yes
111	42	18 to Column	10.0	Yes	Yes	Yes	Yes	No	No	Yes	Yes	Yes
112	31	7 to Column	20.0	No	No	No	No	Yes	Yes	No	No	Yes
113	2	Reverse Flush	7.0	Yes	Yes	Yes	Yes	Yes	Yes	Yes	Yes	Yes
114	1	Block Flush	3.0	Yes	Yes	Yes	Yes	Yes	Yes	Yes	Yes	Yes
115	105	Start Detrityl										Yes
116	64	18 to Waste	4.0									Yes
117	42	18 to Column	10.0	Yes	Yes	Yes	Yes	No	No	Yes	Yes	Yes
118	31	7 to Column	10.0	No	No	No	No	Yes	Yes	No	No	Yes
119	2	Reverse Flush	7.0	Yes	Yes	Yes	Yes	Yes	Yes	Yes	Yes	Yes
120	1	Block Flush	3.0	Yes	Yes	Yes	Yes	Yes	Yes	Yes	Yes	Yes
121	112	Trityl Advance										Yes
122	109	Waste - Port										Yes
123	120	Advance FC										Yes
124	120	Advance FC										Yes
125	120	Advance FC										Yes
126	120	Advance FC										Yes
127	113	End Advance										Yes
128	40	14 to Column	6.0	No	No	Yes	Yes	No	No	Yes	Yes	No
129	3	Trityl Flush	5.0	No	No	Yes	Yes	No	No	Yes	Yes	No
130	40	14 to Column	6.0	Yes	Yes	Yes	Yes	No	No	Yes	Yes	No
131	103	Wait	5.0	Yes	Yes	Yes	Yes	No	No	Yes	Yes	No
132	3	Trityl Flush	5.0	Yes	Yes	Yes	Yes	No	No	Yes	Yes	No
133	40	14 to Column	6.0	Yes	Yes	Yes	Yes	No	No	Yes	Yes	No
134	103	Wait	5.0	Yes	Yes	Yes	Yes	No	No	Yes	Yes	No
135	3	Trityl Flush	5.0	Yes	Yes	Yes	Yes	No	No	Yes	Yes	No
136	40	14 to Column	6.0	Yes	Yes	Yes	Yes	No	No	Yes	Yes	No
137	103	Wait	5.0	Yes	Yes	Yes	Yes	No	No	Yes	Yes	No
138	3	Trityl Flush	5.0	Yes	Yes	Yes	Yes	No	No	Yes	Yes	No
139	42	18 to Column	10.0	Yes	Yes	Yes	Yes	No	No	Yes	Yes	No
140	31	7 to Column	10.0	No	No	No	No	Yes	Yes	No	No	Yes
141	3	Trityl Flush	8.0	Yes	Yes	Yes	Yes	Yes	Yes	Yes	Yes	No
142	110	Waste - Bottle										Yes
143	42	18 to Column	8.0	Yes	Yes	Yes	Yes	No	No	Yes	Yes	Yes
144	31	7 to Column	8.0	No	No	No	No	Yes	Yes	No	No	Yes
145	2	Reverse Flush	7.0	Yes	Yes	Yes	Yes	Yes	Yes	Yes	Yes	Yes
146	31	7 to Column	10.0	No	No	No	No	Yes	Yes	No	No	Yes
147	2	Reverse Flush	7.0	No	No	No	No	Yes	Yes	No	No	Yes
148	42	18 to Column	60.0	No	No	No	No	Yes	Yes	No	No	Yes
149	2	Reverse Flush	7.0	No	No	No	No	Yes	Yes	No	No	Yes
150	1	Block Flush	4.0	Yes	Yes	Yes	Yes	Yes	Yes	Yes	Yes	Yes
151	107	End										Yes

4.7.2.3 "LINKCLEAN" ABI 394 procedure

- 394 Bottle Change Listing - (Version 1.01)

Name : LINK CLEAN 1:35:09P, 1/19/87
Steps: 23

Step Number	Function #	Name	Step Time	Step Active for Bases	Safe Step
1	105	Begin			Yes
2	1	Block Flush	5.0		Yes
3	10	Flush to 5	4.0		Yes
4	11	Flush to 6	4.0		Yes
5	12	Flush to 7	4.0		Yes
6	104	Interrupt			Yes
7	158	Bottle05 On			Yes
8	54	5 to Waste	30.0		Yes
9	159	Bottle05 Off			Yes
10	160	Bottle06 On			Yes
11	55	6 to Waste	30.0		Yes
12	161	Bottle06 Off			Yes
13	104	Interrupt			Yes
14	158	Bottle05 On			Yes
15	74	10 to 5	30.0		Yes
16	159	Bottle05 Off			Yes
17	160	Bottle06 On			Yes
18	75	10 to 6	30.0		Yes
19	161	Bottle06 Off			Yes
20	162	Bottle07 On			Yes
21	76	10 to 7	30.0		Yes
22	163	Bottle07 Off			Yes
23	107	End			Yes

Chapter 5

Long-Range Oxidation of Guanine in DNA Using the Flash-Quench Technique

5.1 Introduction

It is important to consider radical migration through the DNA double helix in delineating routes to mutagenesis and carcinogenesis.[1] We have therefore explored whether DNA can mediate electron transfer (ET) reactions over a long molecular distance. Photoinduced electron transfer reactions with the DNA double helix as a bridge between bound donors and acceptors have been probed via luminescence and transient absorption spectroscopies.[2-5] Studies in our laboratory have indicated that DNA-mediated ET is sensitive to π-stacking (Chapter 2, 3),[2] can occur on the picosecond timescale with metallointercalators (Chapter 3),[4] and, with tethered intercalators, can result in luminescence quenching over long range (Chapter 1).[5] ET chemistry can also occur over long range with DNA as a reactant;[6,7] such reactions between intercalators and the DNA bases have been probed primarily through the chemical analyses of the resultant DNA lesions.[6-11] Here, we apply the flash-quench technique,[9] developed to characterize ET reactions in proteins,[12] to probe damage to DNA both spectroscopically and through analysis of ET products.

Several laboratories have investigated the oxidative damage of DNA.[6,8-11,13-16] Damage is observed primarily at guanine (G), as predicted by theoretical and experimental studies which have determined that G is the most easily oxidized base. Anthraquinones,[8] napthalimides,[11] riboflavin,[10] and rhodium(III) intercalators[6] have been shown to cause oxidative damage selectively at 5'-GG-3' sequences. The sites of damage are correlated with the oxidation potentials of G in different sequence contexts;[11] thus, the extended electronic structure of the DNA base stack may determine the extent and sequence-specificity of oxidative damage. Externally bound Ru(III) polypyridyl complexes, generated electrochemically, also have sufficient oxidation potential to react with guanines within the base stack.[13] Recently, in our laboratory, the potent photooxidant and intercalator, $Rh(phi)_2(bpy')^{3+}$, was tethered to a DNA oligonucleotide duplex.[6] With this assembly, it was demonstrated that these oxidation reactions could also proceed from a

remote position through the DNA π-stack over a distance of ~37 Å. Work with tethered Rh(III) photooxidants[6,7] thus indicates that the π-stack can mediate chemistry at a distance.

These studies suggested to us that we could oxidize G within the DNA duplex by generating a Ru(III) intercalator *in situ*. Ru(II) polypyridyl chemistry offers the opportunity to tune ET reactions and follow them spectroscopically; furthermore, there is precedence for initiating ET by a flash-quench experiment in proteins and in DNA. Gray and coworkers have pioneered the use of derivatives of $Ru(bpy)_3^{2+}$, generated from oxidation of *Ru(II) *in situ*, in the spectroscopic study of protein-mediated ET.[12] Kochevar and coworkers have used the flash-quench experiment in DNA with ethidium as an intercalated donor and methyl viologen (MV^{2+}) as a quencher; using gel electrophoresis, these authors demonstrated a net reaction at guanines.[9]

Scheme 5.1 describes the series of ET reactions in our version of the flash-quench experiment. The cycle is initiated by visible light, which excites intercalated $Ru(phen)_2(dppz)^{2+}$ [Ru(II); dppz = dipyridophenazine].[17] The excited ruthenium(II) complex, *Ru(II), is then quenched by a nonintercalating electron acceptor (Q) to form Ru(III); this species can be reduced back to Ru(II) either through bimolecular recombination with reduced quencher Q^{red} or by electron transfer with a nearby guanine base (G). The oxidized guanine radical can then return to its resting state by reaction with the reduced quencher or undergo further reaction to form the oxidation product(s) G^{ox}.

In this chapter, we describe the oxidation reaction in DNA generated through the flash-quench experiment. Using transient absorption spectroscopy, we characterize the formation and decay of the guanine radical in poly(dG-dC) and in a mixed sequence of DNA. We also show that the flash-quench methodology yields permanent damage at 5'-GG-3' and 5'-GGG-3' sequences. Enzymatic digestion indicates the formation of 8-oxo-2'deoxyguanosine (8-oxo-G) when $Ru(NH_3)_6^{3+}$ serves as quencher. Furthermore, the quantum yield of oxidative damage is modulated by the choice of quencher.

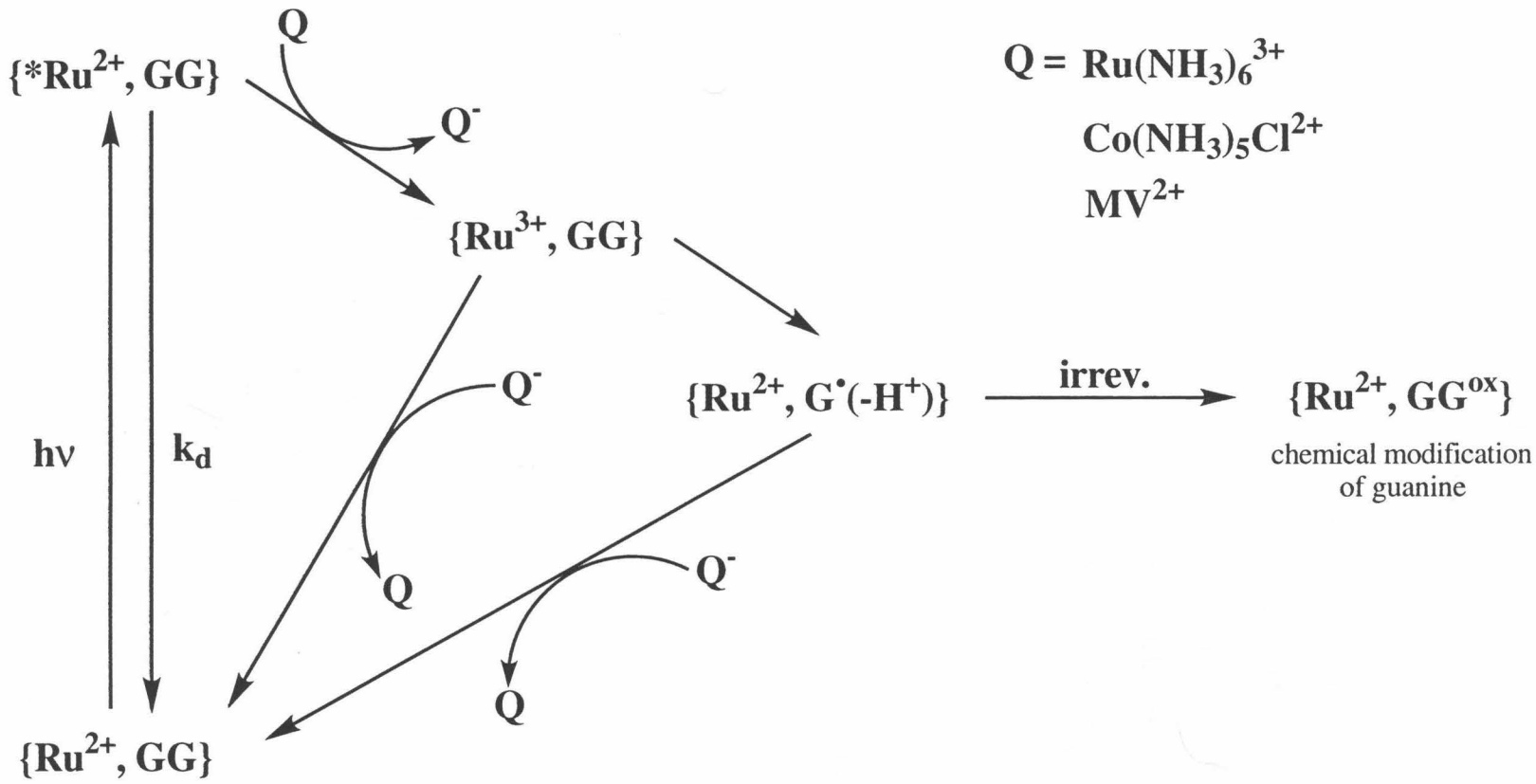

Scheme 5.1: Flash-quench electron transfer cycle

Using a Ru(II)-DNA conjugate (Chapter 4), we will also show that the Ru(III) intercalator can oxidize 5'-GG-3' sequences when the two are separated by 11 basepairs (37 Å) of duplex DNA. In this system, the site of Ru(II) intercalation is determined by $^1O_2$-sensitized damage of guanine residues. We find that oxidative damage caused in the flash-quench experiment is similar for tethered- and noncovalently bound-Ru(II) intercalators in terms of quantum yield, sequence selectivity, and the effect of quencher. Finally, the flash-quench and photooxidation systems are compared and future directions for flash-quench experiments are suggested. The flash-quench methodology expands the scope of ET reactions in DNA by using a ground-state oxidant to produce long-range oxidative damage over a well-defined distance.

5.2 Experimental

Materials. DNA polymers were purchased from Pharmacia and were dialyzed against a buffer of 5 mM phosphate, 50 mM NaCl, pH 8.5 prior to use. Oligonucleotides were prepared on an Applied Biosystems 394 DNA synthesizer, using standard phosphoramidite chemistry.[18] Duplexes were formed by slow cooling of equal concentrations of complementary strands. $Ru(phen)_2(dppz)^{2+}$ was prepared[19] and enantiomers were separated[20] as described previously. Racemic metallointercalator was employed for gel electrophoresis measurements of damage yield; pure enantiomers were used for spectroscopic experiments. The quenchers $[Ru(NH_3)_6]Cl_3$, methyl viologen dichloride, and $[Co(NH_3)_5Cl]Cl_2$ were purchased from Aldrich and used as received.

$Ru(phen)(bpy')(Me_2dppz)^{2+}$-modified oligonucleotides (Me_2dppz = 7,8-dimethyl pyridophenazine) were prepared from *rac*-$[Ru(phen)(bpy')(Me_2dppz)]Cl_2$ as described in Chapter 4. Previous synthetic work with Ru(II) complexes bearing two phen' carboxylate ligands[21] indicated that trisheteroleptic complexes containing a single bpy' ligand would be much simpler to conjugate to DNA and to characterize (Chapter 4). Coupling of the two coordination isomers of $Ru(phen)(bpy')(Me_2dppz)^{2+}$ to DNA led to formation of Δ- and Λ-

diastereomeric conjugates which were separated by high performance liquid chromatography [HPLC; Hewlett Packard HP1050, Dynamax C4 or C18, 300 Å column (Rainin)]. HPLC conditions were as follows: solvent A = NH_4OAc buffer, pH 6.5; solvent B = CH_3CN; gradient = 5 - 25% B over 40 min to elute DNA and Ru-DNA, 25 - 50% B over 10 min to elute unconjugated metal complex. The first Δ-isomer which elutes was used in all studies. Ru-DNA conjugates were characterized by UV-visible spectroscopy ($\varepsilon_{440} \approx 19{,}000\ M^{-1}\ s^{-1}$), circular dichroism spectroscopy, electrospray mass spectrometry, and enzymatic digestion.

Laser spectroscopy. Time-resolved emission and transient absorption measurements used an excimer-pumped dye laser (Coumarin 480), as described previously.[2c] Laser powers at λ_{exc} = 480 nm ranged from 1.0 - 1.5 mJ @ 10 Hz. To generate the transient absorption spectrum, individual data traces at a given wavelength were fit to an exponential function at times > 5 μsec, and the absorbance changes were obtained by extrapolation of the fits back to time zero. Samples containing DNA polymers used 40 μM Δ-$Ru(phen)_2(dppz)^{2+}$, 0.4 mM $Ru(NH_3)_6^{3+}$, 4 mM nucleotides polymer [e.g., poly(dG-dC)] in an aerated, aqueous buffer of 5 mM phosphate, 50 mM NaCl, pH 8.5. Transient absorption measurements of a mixed-sequence of DNA utilized the sequence 5'-TGATC**GG**TGCGTCTGAGACT-3' hybridized to its complement; samples contained 30 μM duplex, 30 μM $Ru(phen)_2(dppz)^{2+}$, and 0.6 mM $Ru(NH_3)_6^{3+}$ in phosphate buffer at pH 7. For most spectroscopic studies of ruthenium(II)-modified DNA, samples contained Ru-DNA (8 μM duplex) and quencher (0-160 μM) in phosphate buffer at pH 7. The measurements discussed in Section 5.3.2.5, however, utilized samples containing 20 μM Ru-DNA and 0.4 mM $Ru(NH_3)_6^{3+}$ in a phosphate buffer at pH 7.

Assays of oxidative products. Strands were 5'-^{32}P-end-labeled (*) by standard protocols[22] and hybridized to either the Ru(II)-modified or unmodified complementary strands in an aerated buffer of 5 mM phosphate, 50 mM NaCl, pH 7. Oligonucleotide duplexes (8 μM; ~ 150,000 cpm) containing 8 μM $Ru(phen)_2(dppz)^{2+}$ and

10-20 equivalents of quencher were irradiated at 436 nm with a 1000 W Hg/Xe lamp equipped with a monochrometer (~6 mW at 442 nm). Irradiation with a CW He-Cd laser (~25 mW @ 442 nm) yielded similar results. Irradiation times varied from 10 seconds to 60 minutes. After irradiation, samples were treated with 100 µl of 1 M piperidine at 90 °C for 30 min., dried, and electrophoresed through a 20% denaturing polyacrylamide gel (15,000 cpm/lane). The extent of damage was quantitated by phosphorimagery (Imagequant).

To investigate the oxygen dependence of piperidine-labile damage caused by the flash-quench experiment, 100 µl samples containing oligonucleotide (8 µM), $Ru(phen)_2dppz^{2+}$ (8 µM), and $Ru(NH_3)_6^{3+}$ (160 µM) were added to quartz cuvettes (1 cm path length, 1 ml volume). Cuvettes were sealed with rubber septa and parafilm and gases were exchanged by three freeze-pump-thaw cycles (15 min/cycle). The specific activity of radioactive samples was ~ 10^6 cpm/sample; ~5 x 10^5 cpm were treated with piperidine and dried, and 20,000 cpm were loaded onto a 20% denaturing polyacrylamide gel.

To characterize the products of oxidative damage, samples (200 µl) containing oligonucleotide (10 µM), Ru(II) complex (10 µM) and quencher (200 µM) were irradiated as described above. DNA was then digested (2 hours each) with nuclease P_1 (Boehringer Mannheim) and then alkaline phosphatase (Boehringer Mannheim).[6,10] The resultant ucleosides were separated by HPLC [Hewlett Packard HP1090, Microsorb MV C18, 100 Å column (Rainin)] and identified by coelution with authentic standards (Caymen Chemicals). HPLC conditions were as follows:[10] oven temperature = 40 °C; solvent A = citric acid, NH_4OAc buffer, pH 5; solvent B = MeOH; gradient = 1 - 4% B over 40 min.

Quantum yield determinations. Emission quantum yields were measured on an SLM8000 steady-state fluorimeter and were determined relative to $\Phi_{Ru(bpy)_3^{2+}} = 0.012$ in aerated CH_3CN.[24] For damage quantum yield determination, samples (20 µl) were irradiated at 436 nm, treated with piperidine, and analyzed by gel electrophoresis (*vide supra*). The yield of damage was quantitated by phosporimagery and was not corrected for

the <1.5 % strand scission/G detected in control experiments with piperidine-treated DNA. Using the same geometry as for sample irradiations, ferrioxalate actinometry[23] was conducted to determine light intensity. The quantum yield of damage (Φ_{damage}) was then calculated as moles of strand breaks/moles photons. Care was taken to perform actinometry and cleavage experiments under the same conditions, and several trials were run to ensure precision. A typical determination of Φ follows:

time (s)	A_{510}	I (x 10^9 E/s)
0	0.048	--
5	0.389	12.0
7	0.523	12.0
10	0.735	12.1
12	0.82	11.4
15	0.977	10.9

Light intensity was calculated from

$$I = (A_{510})(V_{irr})(V_{final})/(\varepsilon)(\Phi_{436})(t)(V_{Fe})$$

where I = light intensity in Einsteins/s; A_{510} = absorbance of actinometry solution of volume V_{final} (ml); V_{irr} = volume of irradiated sample (L); ε = extinction coefficient of $Fe(phen)_3^{2+}$ ($M^{-1}cm^{-1}$); Φ_{436} = quantum yield of actinometer; t = time (s); V_{Fe} = volume of ferrioxalate solution (0.15 M) (ml).

5.3 Results and Discussion:

5.3.1 Studies with noncovalently bound Ru(III) oxidants

5.3.1.1 Photoinduced quenching by groove-bound acceptors

Nonintercalating oxidants such as $Ru(NH_3)_6^{3+}$, methyl viologen, and $Co(NH_3)_5Cl^{2+}$ quench the emission of $^*Ru(phen)_2(dppz)^{2+}$ bound to DNA. In contrast to ultrafast quenching with well-intercalated donors and acceptors (Chapter 2),[4] the weakly bound oxidants quench $^*Ru(phen)_2(dppz)^{2+}$ dynamically on the nanosecond timescale.[2a] The linear Stern-Volmer plots for electron transfer quenching shown in Figure 5.1 indicate

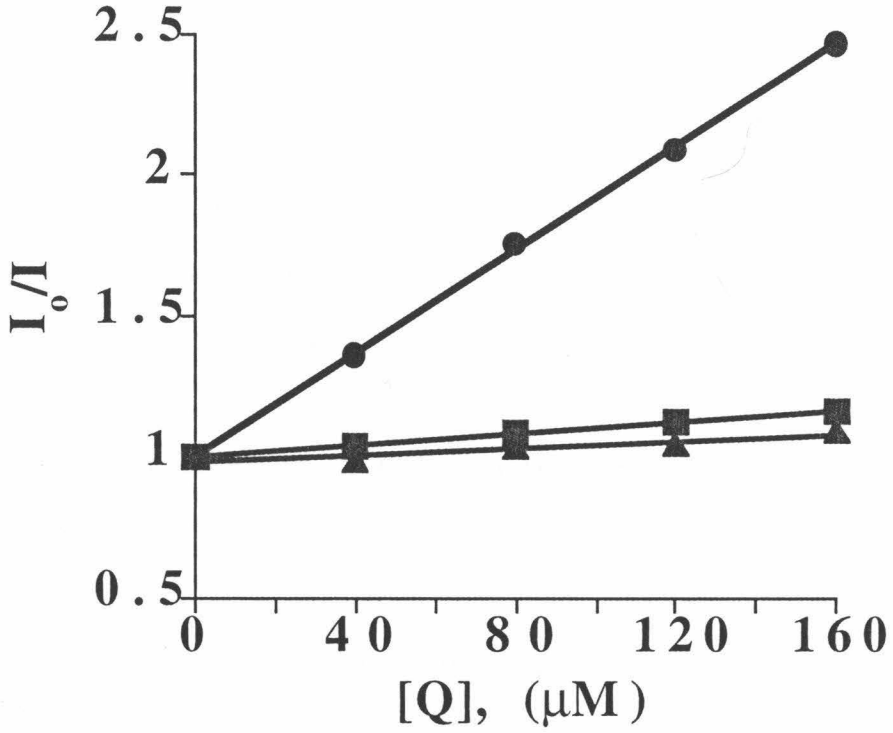

Figure 5.1

Stern-Volmer plots (I_o/I *vs* [Q]) of quenching of *rac*-$Ru(phen)_2(dppz)^{2+}$ intercalated into the oligonucleotide 5'-TGATC**GG**TGCGTCTGAGACT-3' hybridized to complement. I_o = intensity of emission in absence of quencher Q; I = intensity of emission in presence of [Q]. Quenchers are $Ru(NH_3)_6^{3+}$(●), MV^{2+} (■), and $Co(NH_3)_5Cl^{2+}$(▲). Quenching rate constants extracted from Stern-Volmer plots are given in Table 5.1.

that the reaction occurs by a diffusional mechanism. The kinetics of photoinduced electron transfer with these quenchers are similar when $Ru(phen)_2(dppz)^{2+}$ is intercalated into either poly(dG-dC) or poly(dA-dT).[25]

We can monitor the products of the quenching reaction by transient absorption spectroscopy. When *Δ-$Ru(phen)_2dppz^{2+}$ is quenched by $Ru(NH_3)_6^{3+}$ in the presence of poly(dA-dT), we detect a long-lived transient signal corresponding to the decay of Δ-$Ru(phen)_2dppz^{3+}$ on the microsecond timescale. In contrast, when Δ-$Ru(phen)_2(dppz)^{2+}$ is intercalated into poly(dG-dC) and quenched by $Ru(NH_3)_6^{3+}$ (Figure 5.2A), we do not observe a long-lived species with the characteristics of Ru(III). Instead, we detect formation of a new species with differential absorption maxima at ~390 and ~550 nm.

5.3.1.2 Photophysical detection of G•(-H) intermediate

We further characterized the transient formed in poly(dG-dC) as a function of wavelength.[26] Pure enantiomers were used for spectral measurements, since the two intercalated isomers have slightly different absorption spectra; however, both enantiomers gave similar results. The transient spectrum obtained with Δ-$Ru(phen)_2(dppz)^{3+}$, formed after quenching by weakly absorbing $Ru(NH_3)_6^{3+}$,[27] is shown in Figure 5.2B. This UV-visible spectrum corresponds closely to that assigned by Candeias and Steenken[28] as the neutral radical of guanine [G•(-H)] in pulse radiolysis studies with guanosine and guanine monophosphate. Here, the flash-quench method permits the first direct observation of oxidized guanine in duplex DNA by UV-visible absorption spectroscopy.[29] This spectrum indicates that the guanine cation radical, once formed, is rapidly deprotonated in duplex DNA.

Quenching of Δ-$Ru(phen)_2(dppz)^{2+}$ by $Ru(NH_3)_6^{3+}$ occurs concomitantly with the formation of G•(-H). The rise of the radical signal is best monitored at 373 nm, the isobestic point for the *Ru(II) - Ru(II) difference spectrum.[2d,25] Time-resolved measurements indicate that both the *Ru(II) emission decay and the rise of G•(-H)

Figure 5.2

Time-resolved transient absorption spectra of Δ-$Ru(phen)_2(dppz)^{2+}$ (40 μM) bound to poly(dG-dC) (4 mM nucleotides) and quenched by $Ru(NH_3)_6^{3+}$ (0.4 mM). A) Kinetics of emission decay of *Δ-$Ru(phen)_2(dppz)^{2+}$ at 610 nm and the rise of G•(-H) transient at 373 nm, the isobestic point for the *Ru(II) - Ru(II) transient absorption spectrum. The apparent rate constant for the formation of G•(-H) is the same as the rate constant for decay of *Ru(II). B) Absorption difference spectrum after decay of *Ru(II). This spectrum corresponds closely to that assigned[17] as G•(-H). C) The decay of the G•(-H) transient.

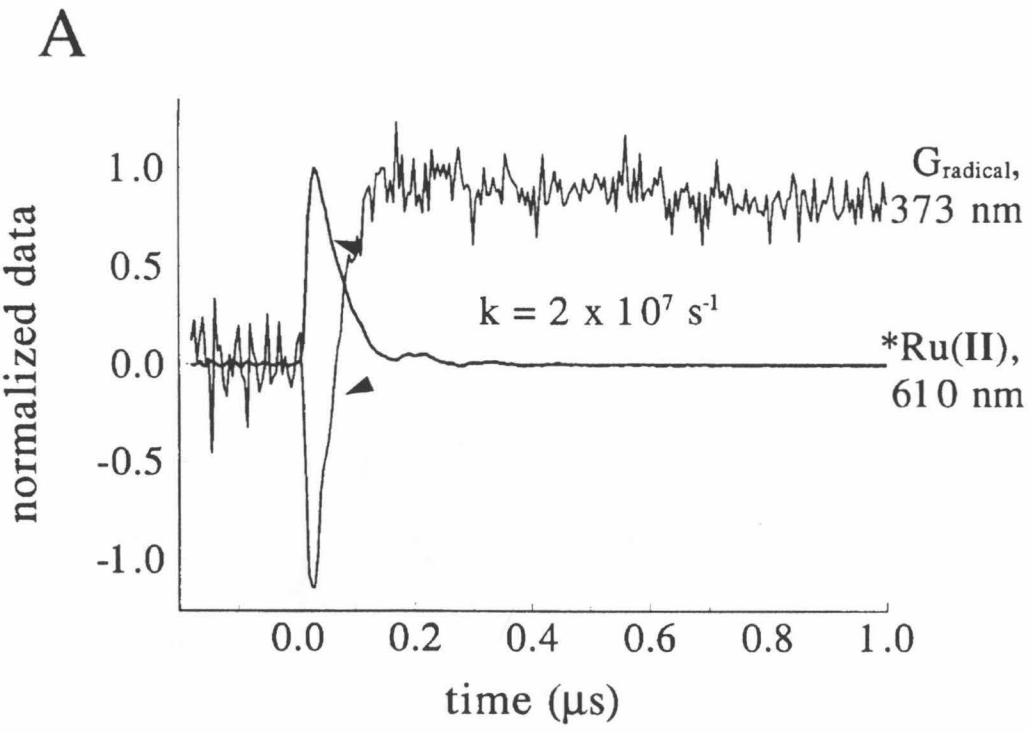

B

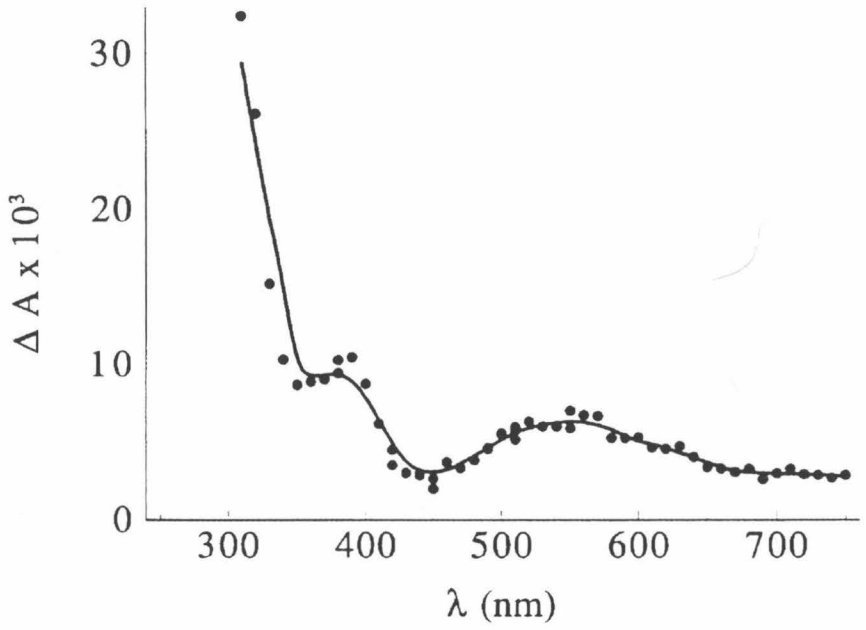
30
20
10
0
Δ A x 10³
300
400
500
600
700
λ (nm)

C

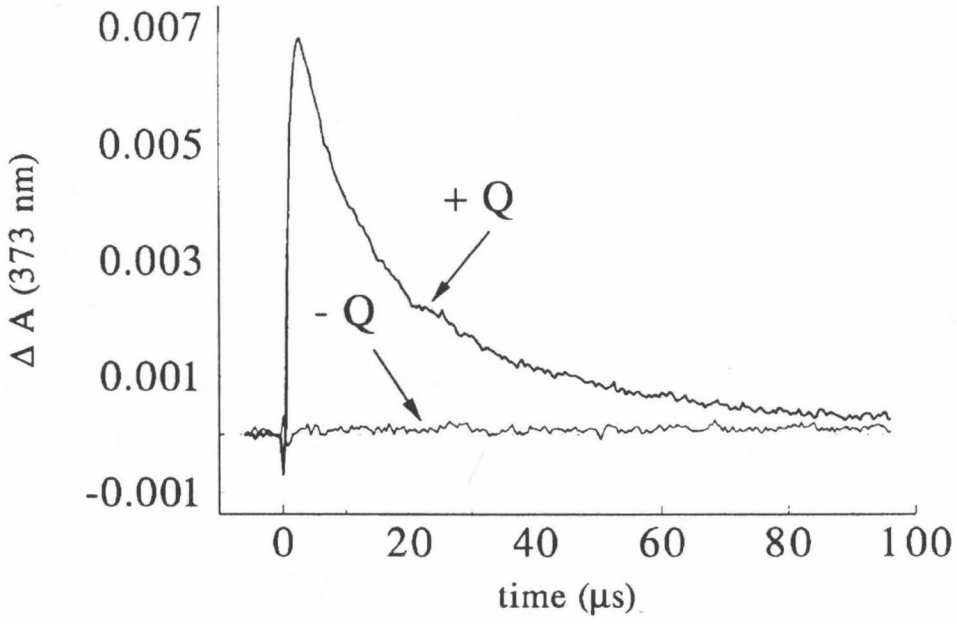
0.007
0.005
0.003
0.001
-0.001
Δ A (373 nm)
+ Q
- Q
0
20
40
60
80
100
time (μs)

absorption occur with $k_{obs} \approx 2 \times 10^7\ s^{-1}$ (Figure 5.2A). Thus, oxidation of guanine by intercalated Δ-$Ru(phen)_2(dppz)^{3+}$ occurs in less than 200 ns and may in fact be much faster.[2,4,30] Nearly all of this guanine radical decays within 100 μs (Figure 5.2C) when $Ru(NH_3)_6^{3+}$ serves as the quencher. With MV^{2+} as quencher, the transient spectrum is complicated by the absorption of reduced MV^{+}. Finally, when $Co(NH_3)_5Cl^{2+}$ serves as a sacrificial quencher, the decay of G•(-H) is much slower (> 1ms).

The formation of G•(-H) by the flash-quench method with different DNAs and intercalators is consistent with the calculated reduction potentials of the reactants.[2,4,11] Rapid formation of G•(-H) is observed for $Ru(phen)_2dppz^{3+}$ bound to either poly(dG)•poly(dC) or poly (dG-dA)•poly(dC-dT). In the presence of poly(dG-dT)•poly(dC-dA), however, a long-lived Ru(III) signal dominates the transient absorption spectrum, indicating that most of the Ru(III) does not react. This trend may reflect the sequence-dependent redox potential of guanine;[11] additionally, the lack of the guanine radical signal could reflect structural variations within the poly(dG-dT)•(dC-dA) polymer.[31] Moreover, Ru(4,7-dimethylphen)$_2$(dppz)$^{3+}$ and Os(phen)$_2$(dppz)$^{3+}$, which both have lower reduction potentials than Ru(phen)$_2$(dppz)$^{3+}$,[2d,32] do not appear to react with guanine.[2c,32] Quenching of these M(II) intercalators by $Ru(NH_3)_6^{3+}$ in poly(dG-dC) produces long-lived signals characteristic of oxidized metal complexes M(III) and no evidence for G•(-H).

We also examined the formation of the G•(-H) intermediate in a mixed sequence of DNA with $Ru(NH_3)_6^{3+}$ as quencher. At short times, the transient spectrum is dominated by the spectral characteristics of $Ru(phen)_2dppz^{3+}$. After the 100 μs decay of the Ru(III) intermediate, however, a small, long-lived transient consistent with decay of a G•(-H) is detected (Figure 5.3). This decay occurs on the millisecond timescale and may reflect the reactions which lead to stable oxidized products (*vide infra*). As Scheme 5.1 indicates, there are several pathways for the decay of G•(-H). Clearly, the relative yields and rate

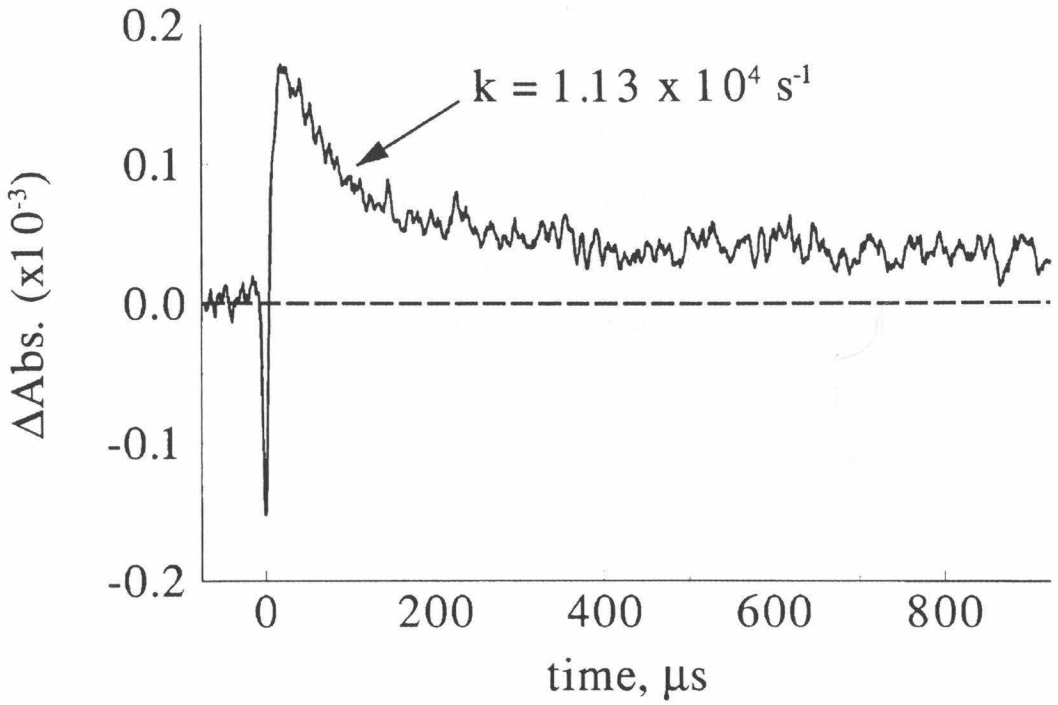

Figure 5.3

Transient absorption spectroscopy monitoring the kinetics of decay of G•(-H) in the oligonucleotide duplex 5'-TGATC**GG**TGCGTC-TGAGACT-3' hybridized to its complement. Samples contained 30 μM duplex, 30 μM $Ru(phen)_2(dppz)^{2+}$, and 0.6 mM $Ru(NH_3)_6^{3+}$ in an aerated buffer of 5 mM phosphate, 50 mM NaCl, pH 7.

constants of G•(-H) formation and decay are a function of the concentrations of Ru(III), Q^{red}, and G•(-H), which differ for the mixed-sequence oligomer versus poly(dG-dC).

5.2.1.3 Analysis of oxidation of 5'-GG-3' by gel electrophoresis

The yield of permanent DNA damage which results from the flash-quench experiment has been analyzed by gel electrophoresis. Oxidized guanine nucleotides have been shown to be labile upon treatment with piperidine; therefore, the yield and position of guanine oxidation can be revealed by strand scission in a gel electrophoresis experiment.[33] When an oligonucleotide duplex containing a 5'-GG-3' doublet is irradiated at 436 nm in the presence of both *rac*-$Ru(phen)_2(dppz)^{2+}$ and quencher, damage, revealed by treatment with piperidine, is observed selectively at the 5'-G of the GG step, with little damage at other sites (Figure 5.4). Thus, the ET reactions in the flash-quench experiment lead to significant permanent damage of DNA.

Other characteristics of these gel electrophoresis experiments are noteworthy. When the Δ isomer was employed for *in situ* oxidation,[26] the sites of oxidative damage were the same as for the racemic intercalator and the quantum yield for damage was slightly higher, consistent with the higher emission quantum yield and more efficient electron transfer observed for the Δ isomer.[4,6] More work with the pure enantiomers is required before quantitative comparisons can be made. Some damage, albeit at a low level, is also evident at all 5'-GX-3' sites (Figure 5.4). This damage is found in all experiments above the control level and likely reflects some oxidation at single G sites. For a given quencher, the yield of damage scales with the fraction of emission quenched and thus increases with quencher concentration (Figure 5.5). Additionally, the yield of oxidative damage is shown to depend on which quencher is used to initiate the flash-quench cycle. This yield of damage is not directly correlated with the efficiency of quenching, however. Thus, the amount of oxidative damage can be varied not only by the intercalator, but by the quencher as well.

Figure 5.4

Autoradiograms after denaturing polyacrylamide gel electrophoresis of ^{32}P-5'-TGATC**GG**TGCGTCTGAGACT-3' after oxidation of the oligonucleotide duplex by *rac*-$Ru(phen)_2(dppz)^{3+}$. A) Samples shown are as follows: lane 1, DNA + $Ru(phen)_2(dppz)^{2+}$ without irradiation; lane 2, DNA + $Ru(phen)_2(dppz)^{2+}$ after 60 min irradiation; lanes 3 and 4, DNA + $Ru(phen)_2(dppz)^{2+}$ + 20 equiv $Ru(NH_3)_6^{3+}$, irradiated for 30 and 60 min, respectively; lanes 5 and 6, DNA + $Ru(phen)_2(dppz)^{2+}$ + 10 equiv MV, irradiated for 2 and 10 min, respectively; lanes 7 and 8, DNA + $Ru(phen)_2(dppz)^{2+}$ + 10 equiv $Co(NH_3)_5Cl^{2+}$, irradiated for 2 and 10 min, respectively; lanes 9 and 10, Maxam-Gilbert sequencing reactions for G and C+T, respectively. Note that with $Ru(NH_3)_6^{3+}$ as quencher, an additional band with higher molecular weight is evident. B) Histograms representing oxidative damage of the oligonucleotide duplex by $Ru(phen)_2(dppz)^{3+}$.

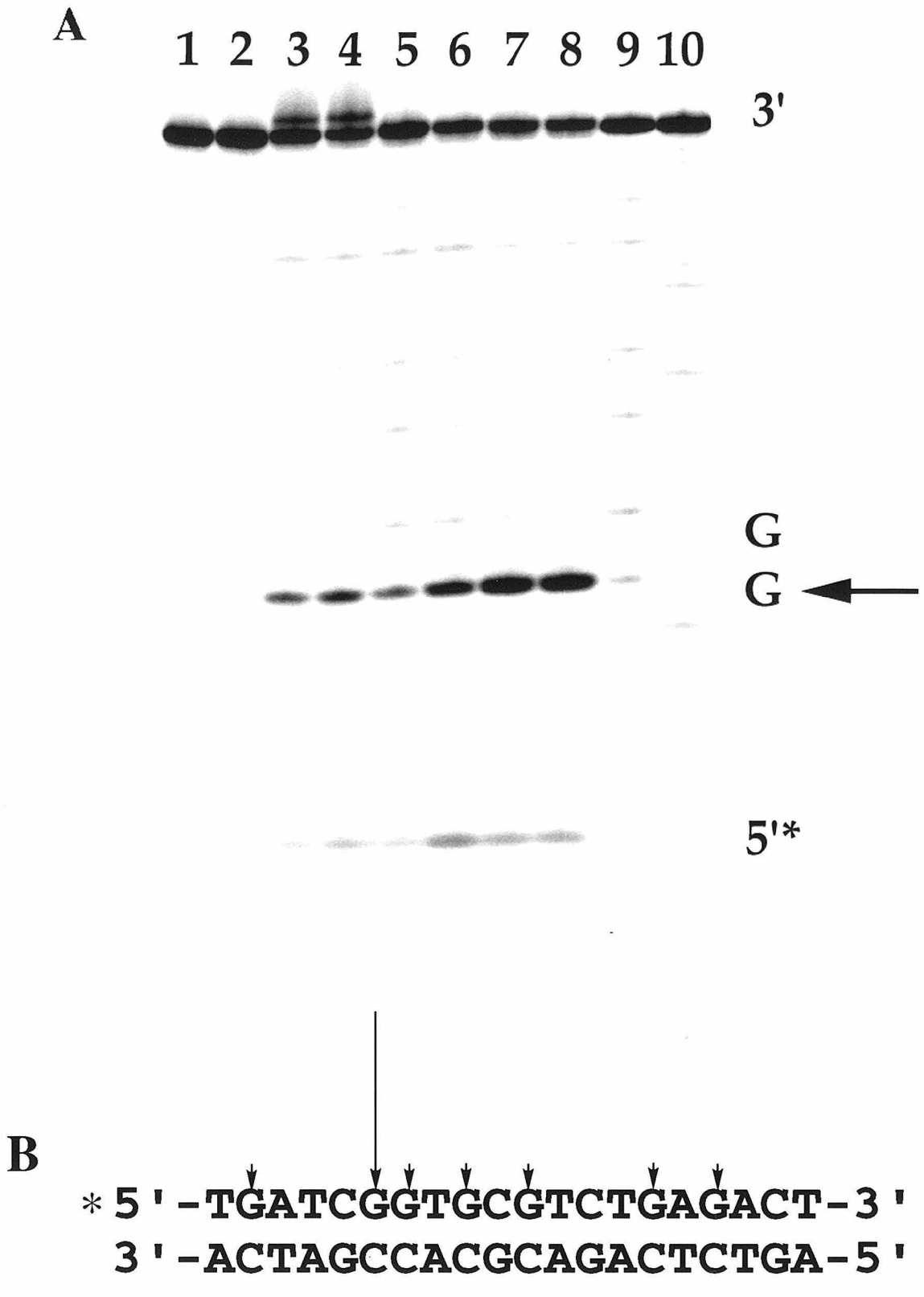
A
1 2 3 4 5 6 7 8 9 10
3'
G
G
5'*
B
*5'-TGATCGGTGCGTCTGAGACT-3'
3'-ACTAGCCACGCAGACTCTGA-5'

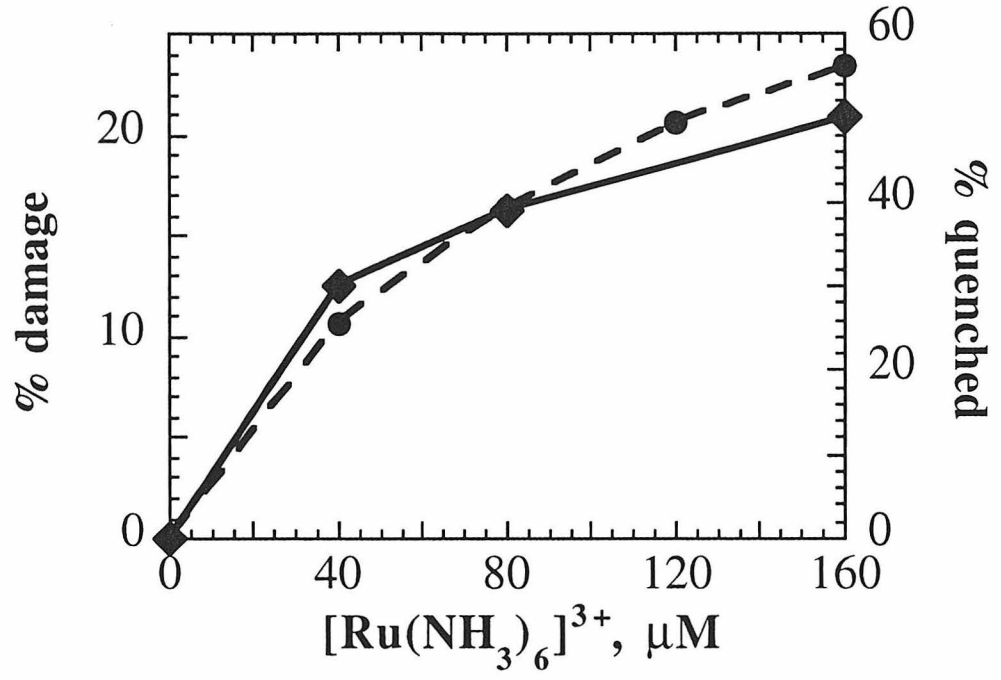

Figure 5.5

Plot showing the yield of piperidine-labile DNA damage (■) and the fraction of emission quenching of *rac*-*Ru(phen)$_2$(dppz)$^{2+}$ (●) as a function of concentration of Ru(NH$_3$)$_6^{3+}$. Samples contained 5'-TGATC**GG**TGCGTCTGAGACT-3' hybridized to complement (8 μM duplex), *rac*-*Ru(phen)$_2$(dppz)$^{2+}$ (8 μM) in a buffer of 5 mM phosphate, 50 mM NaCl, pH 7. The fraction of oxidative damage was determined by phosphorimagery of ^{32}P-labeled DNA; the fraction of emission quenching was measured by integration of time-resolved luminescence decays at 616 nm.

5.2.1.5 Oxidation of a 5'-GGG-3' - containing sequence

The data in Figure 5.6 illustrate the damage of an oligonucleotide containing both a 5'-GGG-3' triplet and 5'-GG-3' doublet. The yield of oxidized guanine is highest for the 5'-G of the 5'-GGG-3' triplet, followed by the central G of 5'-GGG-3' and the 5'-G of 5'-GG-3', in accordance with other experiments[6] and calculated oxidation potentials.[11] For comparison of Figures 4 and 6, it should be noted that the overall yield of damage is greater for the oligonucleotide containing the 5'-GGG-3' sequence. Furthermore, samples containing $Co(NH_3)_5Cl^{2+}$ in Figure 5.6 are irradiated for only 10 and 20 seconds, compared to 10 and 20 minutes for $Ru(NH_3)_6^{3+}$and MV^{2+} samples. For each quencher, damage increases with quencher concentration and irradiation time; indeed complete reaction can be observed for MV^{2+} after only 20 minutes of irradiation. As has been demonstrated with organic intercalators,[8] a high yield of DNA damage by metallointercalators is achieved by this method.

5.2.1.6 Damage of DNA by $^1O_2$-sensitization versus electron transfer

Oxidative damage caused in the flash-quench experiment can be contrasted with DNA damage caused by a $^1O_2$ mechanism. Luminescent diimine complexes of ruthenium(II) are known to sensitize the formation of singlet oxygen,[35] and this reactive radical species has also been shown to cause piperidine-labile oxidation of guanines in duplex DNA.[34] The efficiency of sensitized damage depends directly on the excited-state lifetime[35] and therefore should vary as a function of Ru(II) complex and DNA intercalation site. Lane 2 in Figures 4 and 6 show that $^1O_2$ damage has a relatively low quantum yield in this system and causes DNA damage at all Gs with little sequence-selectivity. This observation is consistent with the low $\Phi_{emission}$[17] of $Ru(phen)_2(dppz)^{2+}$ bound to DNA and the low sequence-selectivity of the metal complex. The slight variations in base damage are likely due to preferences in the sites of Ru(II) intercalation and/or differences in the accessibility of guanine to molecular oxygen.

Figure 5.6

Autoradiograms after denaturing polyacrylamide gel electrophoresis of ^{32}P-5'-ACGGGCATGGCAGTTCGT-3' after oxidation of the oligonucleotide duplex by *rac*-$Ru(phen)_2(dppz)^{3+}$. A) Samples shown are as follows: lane 1, DNA + 10 equiv $Co(NH_3)_5Cl^{2+}$ irradiated 60 sec; lane 2, DNA + $Ru(phen)_2(dppz)^{2+}$ irradiated for 60 min; lanes 3 and 6, DNA + $Ru(phen)_2(dppz)^{2+}$ + 10 equiv methyl viologen, irradiated 10 and 20 min, respectively; lanes 4 and 7, DNA + $Ru(phen)_2(dppz)^{2+}$ + 20 equiv $Ru(NH_3)_6^{3+}$, irradiated 10 and 20 min, respectively; lanes 5 and 8, DNA + $Ru(phen)_2(dppz)^{2+}$ + 10 equiv $Co(NH_3)_5Cl^{2+}$, irradiated 10 and 20 sec, respectively; lanes 9 and 10, Maxam - Gilbert sequencing reactions for G and C+T, respectively. Note that the samples containing $Co(NH_3)_5Cl^{2+}$ were irradiated for *seconds*, while MV^{2+} and $Ru(NH_3)_6^{3+}$ samples were irradiated for several *minutes*. B) Histograms representing oxidative damage of the oligonucleotide duplex by $Ru(phen)_2(dppz)^{3+}$.

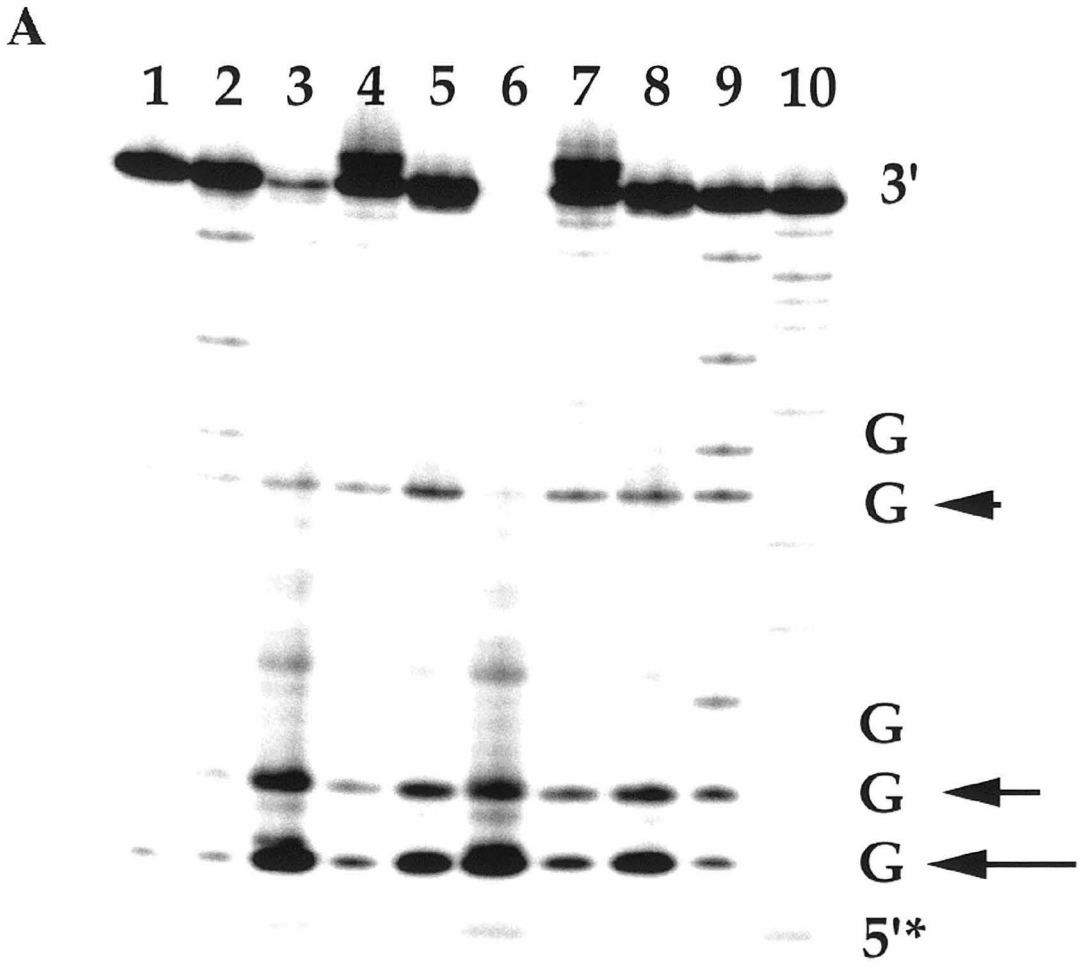
A
1 2 3 4 5 6 7 8 9 10
3'
G
G
G
G
G
5'*

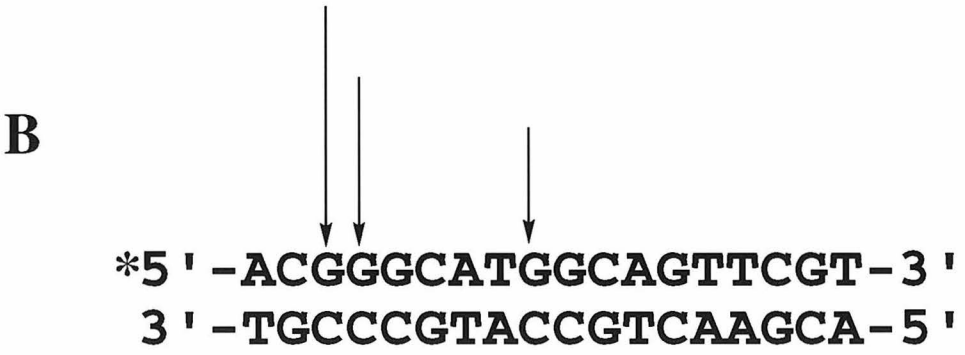
B
*5'-ACGGGCATGGCAGTTCGT-3'
3'-TGCCCGTACCGTCAAGCA-5'

The $^1O_2$-sensitized damage is markedly different, both in position and intensity, from that seen in the flash-quench experiment. By contrast to $^1O_2$-mediated damage, lanes 3-8 in Figures 4 and 6 indicate that the pattern of oxidative damage correlates with the relative reduction potentials of guanine-rich sequences[11] and does not seem to be related to the position of the intercalator on the oligonucleotide duplex. Additionally, no increase in oxidation is observed in D_2O compared to H_2O, despite the longer excited-state lifetimes of both *Ru(II) and $^1O_2$ in D_2O.[2b,35] For a given quencher, the yield of G oxidation increases with the amount of emission quenching; the opposite trend is expected for $^1O_2$-mediated damage. Lastly, the yields of G oxidation far exceed those obtained from $^1O_2$-sensitized cleavage with dppz complexes of Ru(II).

5.2.1.7 Enzymatic digestion of oxidatively damaged DNA

The resultant damage from the flash-quench experiment can also be characterized directly by chemical analysis. Guanine damage has been examined by enzymatic digestion[6,10] without piperidine treatment. Separation of the nucleoside products by HPLC and coelution with authentic samples indicate that the major product was 8-oxo-G[6,8,10,36,37] for samples in which $Ru(NH_3)_6^{3+}$ served as a quencher (Figure 5.7A). The yield of piperidine-sensitive damage identified by gel electrophoresis and the amount of 8-oxo-G identified by HPLC are comparable, indicating that piperidine treatment reveals the primary damage. HPLC analysis also indicates several minor products of the reaction; these are likely due to $Ru(phen)_2(dppz)^{2+}$ and $Ru(NH_3)_6^{3+}$ degradation as well as secondary oxidative products. Interestingly, we do not detect formation of 8-oxo-G in the presence of MV^{2+} or $Co(NH_3)_5Cl^{2+}$ (Figure 5.7B). Given that complete strand cleavage can be obtained with these quenchers, it is not likely that oxidative damage is left undetected in the gel electrophoresis assay. Additionally, it is possible that 8-oxo-G, which is easily oxidized,[38] reacts further in the presence of these quenchers. It is noteworthy that ~20% less dG is observed in the $Co(NH_3)_5Cl^{2+}$-treated sample compared

Figure 5.7

HPLC traces of nucleosides produced by enzymatic digestion of damaged oligonucleotides. The duplex 5'-TGATC**GG**TGCGTCTGAGACT-3' hybridized to complement (20 μM) was irradiated in the presence of *rac*-*$Ru(phen)_2(dppz)^{2+}$ (20 μM) and Q. The oligonucleotide was then subjected to digestion with nuclease P_1 and alkaline phosphatase and analyzed by HPLC chromatography. A) When Q = $Ru(NH_3)_6^{3+}$ (400 μM), 8-oxo-G is formed (retention time = 9.2 min). Wavelengths shown are 260 nm (top trace) and 295 nm (bottom trace). B) When Q = $Co(NH_3)_5Cl^{2+}$ (200 μM), 20% less G is observed compared to unirradiated control reactions, and no 8-oxo-G is obtained. The degradation products with retention times from 30-36 min are not observed in samples quenched by $Ru(NH_3)_6^{3+}$. Wavelengths shown are 260 nm (top trace) and 295 nm (bottom trace).

B

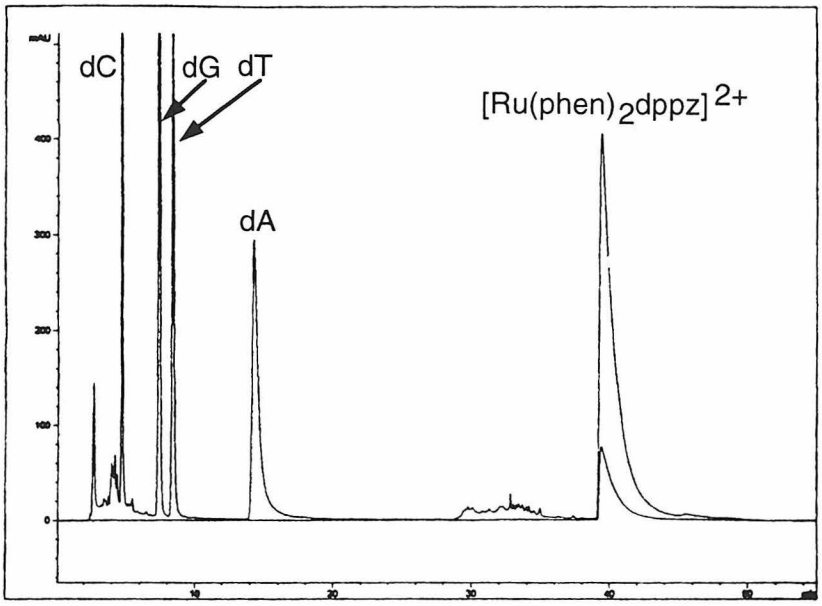

A

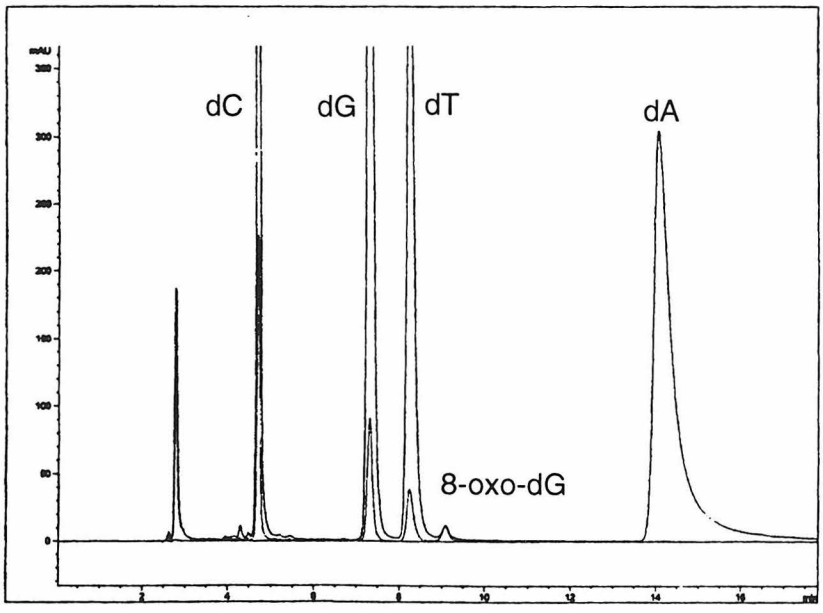

to unirradiated DNA digestions. The loss of dG in the presence of MV^{2+} is difficult to quantitate since the MV^{2+} peak overlaps with the dT and dG nucleoside products.

5.2.1.8 Tuning yield of oxidation with quencher

The amount of damage incurred at G is clearly modulated by the choice of quencher. As suggested by Scheme 5.1, the yield for base oxidation is found to depend on the rates of several competing reactions. Table 5.1 shows the yield of damage as a function of quencher and some of the factors which contribute to these yields. First, some Ru(III) recombines with reduced quencher to give the starting materials Ru(II) and Q. This recombination reaction occurs readily for $Ru(NH_3)_6^{3+}$; thus, even though $Ru(phen)_2(dppz)^{2+}$ is highly quenched by $Ru(NH_3)_6^{3+}$, the quantum yield for damage (Φ_{damage}) is low. Second, the yield of damage depends on how rapidly G•(-H) reacts with Q^{red}, and is thus correlated with the instability of the reduced quencher. For example, since MV^+ reacts with O_2 on the 100 μs timescale,[39] more damage is observed at 5'-GG-3' with MV^{2+} as quencher than $Ru(NH_3)_6^{3+}$. The superoxide formed in reaction of O_2 and MV^+ can also quench the guanine radical,[8a] resulting in an intermediate Φ_{damage}. Finally, the lability of Co(II) complexes is exploited by using $Co(NH_3)_5Cl^{2+}$ as a sacrificial quencher. Since reduced quencher irreversibly degrades on the microsecond timescale,[40a] the highest quantum yield for damage is obtained with $Co(NH_3)_5Cl^{2+}$.

Given that the flash-quench reaction is modulated by the quencher, other observations are understandable in this context. For example, transient absorption spectroscopy indicates that nearly all of the G•(-H) formed in poly(dG-dC) is re-reduced by $Ru(NH_3)_6^{3+}$ within 100 μs; in the presence of $Co(NH_3)_5Cl^{2+}$, by contrast, the G• signal in poly(dG-dC) does not decay measurably within 1 ms. The persistence of the G• with $Co(NH_3)_5Cl^{2+}$and MV^{2+} as quenchers may contribute to the different oxidative products observed by enzymatic digestion. The characteristics of the quencher thus provide a novel means to tune yields of both intermediates and products.

Table 5.1. Parameters for Flash-quench cycle with *rac.*-$Ru(phen)_2(dppz)^{2+}$ + DNA.[a]

Quencher	Φ_{damage}[b]	damage yield[c]	equiv. Q	% quenching[d]	k_q ($*Ru^{2+}$ Q)[e]	k_{obsv} (Ru^{3+} - Ru^{2+})[f]
$[Ru(NH_3)_6]^{3+}$	1×10^{-5}	1.4×1^{-5}	20	60	10×10^{10} $M^{-1}s^{-1}$	6×10^4 s^{-1}
methyl viologen^{2+}	2×10^{-4}	0.002	10	8	1×10^{10} $M^{-1}s^{-1}$	1×10^2 s^{-1}
$[Co(NH_3)_5Cl]^{2+}$	9×10^{-4}	0.02	10	3	6×10^9 $M^{-1}s^{-1}$	N/A[g]

[a] Conditions are: 8 μM $Ru(phen)_2(dppz)^{2+}$, 8 μM DNA duplex (sequence in Figure 5.4B), in an aerated buffer of 5 mM phosphate, 50 mM NaCl, pH 7. [b] Φ_{damage} = quantum yield of piperidine-mediated strand breaks at main damage site. Uncertainty in Φ_{damage} is ~20%. [c] damage yield = Φ_{damage}/Φ_{ET}; the yield of damage per Ru(III). $\Phi_{ET} = k_q[Q]/k_{obs}$ where k_{obs} is the weighted average of a biexponential fit of *Ru(II) emission in the presence of Q. [d] Measured by steady-state emission; uncertainty is ~5%. [e] $Io/I = 1 + [Q](k_q/k_o)$; k_o = weighted average of a biexponential fit of *Ru(II) emission. $k_1 = 4.2 \times 10^6$ s^{-1} (35%), $k_2 = 1.5 \times 10^7$ s^{-1} (65%). Uncertainty is ~10%. [f] k_{obsv} = observed decay of Ru(III)-Ru(II) transient at 440 nm; uncertainty is ~10%. [g] Signal too small to determine kinetics accurately.

5.3.2 Long-range oxidation with Ru(II) tethered oligonucleotides

We have further characterized oxidative damage of DNA by tethering a Ru(II) intercalator to a DNA oligonucleotide duplex (Ru-DNA). Using Ru-DNA, where Ru = $Ru(phen)(bpy')(Me_2\text{-}dppz)^{2+}$, we can also investigate the distance and sequence dependence of G oxidation, differentiate diffusion-controlled from static reactions, and compare the flash-quench system with Ru(II) to the photooxidation of DNA by $Rh(phi)_2(bpy')^{3+}$.[6]

Figure 5.8 illustrates how we determine the sites of Ru(II) intercalation and base oxidation. Oligonucleotides bearing tethered $Ru(phen)(bpy')(Me_2\text{-}dppz)^{2+}$ are prepared as described in Chapter 4 and hybridized to the ^{32}P- or unlabelled complementary strand. Intercalation by the pendant ruthenium(II) complex is measured by singlet oxygen ($^1O_2$) sensitization (left pathway), since irradiation of Ru(II) polypyridyl complexes in the presence of DNA and O_2 leads to $^1O_2$ damage at G residues nearest to the binding site of the complex.[34] By contrast, in the flash-quench experiment (right pathway), photoexcited Ru(II) [*Ru(II)] is quenched by ET to an externally-bound oxidant (Q); the ground state Ru(III) intercalator thus formed leads to oxidation of DNA at the site of lowest reduction potential. As in experiments with noncovalently bound Ru(II), the resultant base damage is revealed by strand scission following treatment with piperidine. Hence, by photolyzing the oligonucleotide assemblies in the absence and presence of ET quenchers, we may assay both the position of intercalation and the yield of base oxidation.

5.3.2.1 Intercalation and long-range DNA damage

Figure 5.9 presents the damage caused by the $^1O_2$ and flash-quench experiments on an oligonucleotide containing tethered Δ-$Ru(phen)(bpy')(Me_2\text{-}dppz)^{2+}$ and a single 5'-GG-3' sequence. For these experiments, the oligonucleotide sequence 5'-TGATCGGTGCG-TCTGAGACT-3' was 5'-labeled with ^{32}P and hybridized to 5'-ruthenated complement.

Figure 5.8

Schematic illustration of oxidation reactions. The position of binding can be monitored by $^1O_2$ sensitization (left pathway). $^1O_2$, sensitized by *Ru(II), reacts with nearby guanine bases; oxidation products are revealed as strand breaks after treatment with piperidine. Long-range ET from guanine is initiated by excitation of Ru(II) in the presence of externally-bound, oxidative quenchers such as $Ru(NH_3)_6^{3+}$ or MV^{2+} (right pathway). Electron transfer from *Ru(II) to the quencher creates a hole on the Ru(III) intercalator; this hole is filled by back-reaction with reduced quencher or by oxidation of guanine. Piperidine treatment reveals the ultimate site of guanine base oxidation.

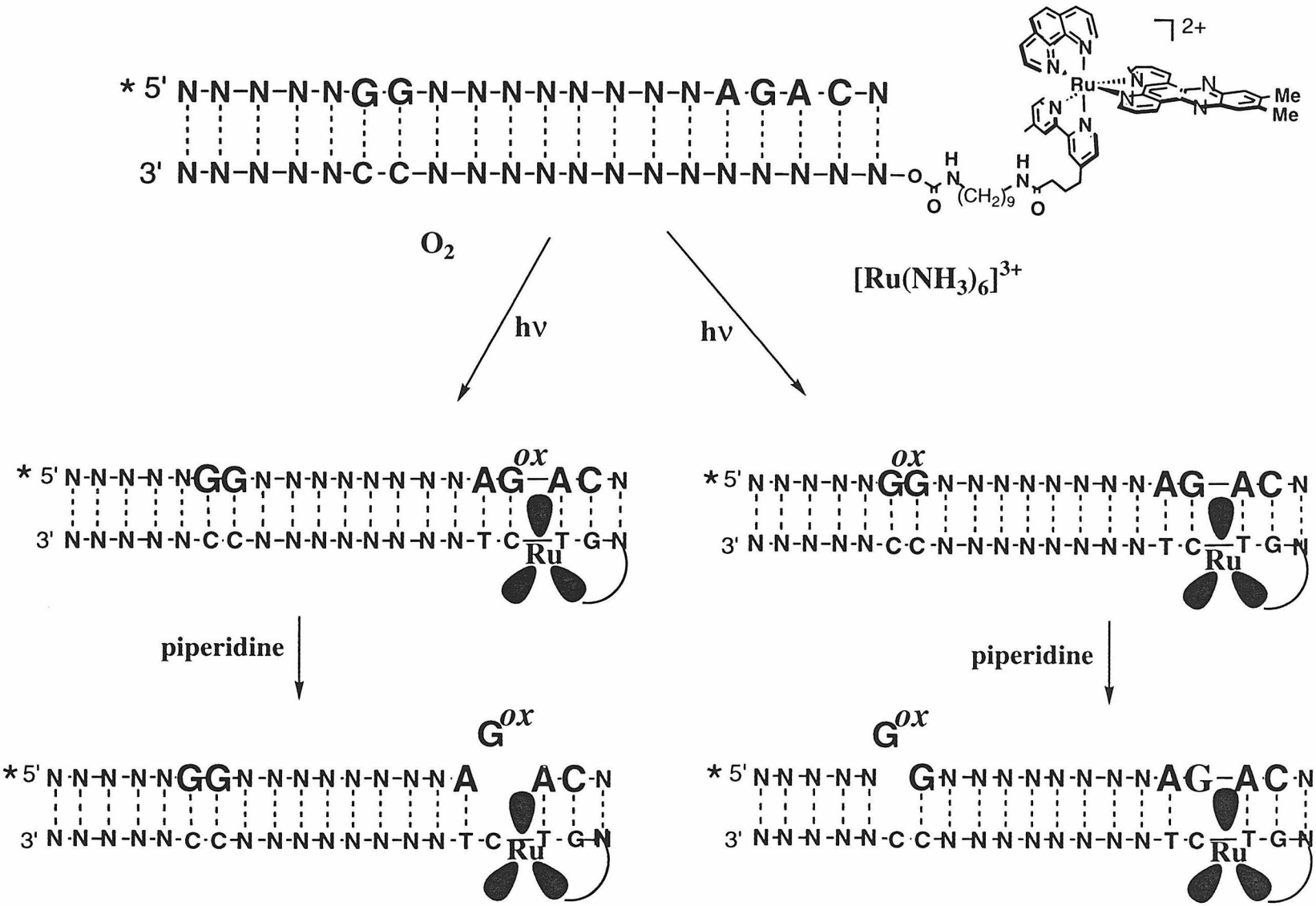
* 5' N-N-N-N-N-G-G-N-N-N-N-N-N-N-N-A-G-A-C-N
3' N-N-N-N-N-C-C-N-N-N-N-N-N-N-N-N-N-N-N-N-O
2+
Ru
Me
Me
O2
hν
hν
[Ru(NH3)6]3+
ox
piperidine
piperidine
Gox

Lane 2 shows $^1O_2$-sensitized damage generated by irradiation (436 nm) of Ru-DNA (8 μM) followed by piperidine treatment.[33] Cleavage occurs primarily at the G closest to the site of Ru(II) attachment and indicates that the complex is intercalated only in that region of the oligonucleotide duplex. In contrast, all guanine residues are damaged when $Ru(phen)_2dppz^{2+}$ is noncovalently bound to the oligonucleotide (lane 14). The lower cleavage intensity in lane 14 versus lane 2 is due to the four-fold lower $\Phi_{emission}$ of $Ru(phen)_2dppz^{2+}$ compared to Δ-$Ru(phen)(bpy')(Me_2\text{-}dppz)^{2+}$ (*vide infra*) and to the increased local concentration of $^1O_2$ caused by specific binding of the tethered complex. As expected, the extent of damage increases two-fold for Ru-DNA in D_2O (20% vs 45% cleavage after one hour irradiation), since D_2O increases the lifetimes of both $^1O_2$ and *Ru(II).[2b,35] These data demonstrate that $^1O_2$ sensitization can be used to mark the site of intercalation.

In the flash-quench experiment, we add an ET quencher, photolyze Ru-DNA, and monitor the yield and position of damage to DNA initiated by electron transfer. As predicted by experiments with noncovalently bound $Ru(phen)_2dppz^{2+}$, oxidative damage to DNA is observed at the 5'-G of the 5'-GG-3' doublet. However, it is important to note that this 5'-GG-3' doublet is placed 11 bp away from the ruthenium binding site, and thus damage is observed ~37Å from the Ru(III) reactant. As shown in Figure 5.9, this reaction requires light (lane 1), quencher (lane 2), $Ru(phen)(bpy')(Me_2\text{-}dppz)^{2+}$ (lanes 3, 9), and piperidine treatment (not shown). In contrast to $^1O_2$-mediated damage, the yield of oxidation of DNA by ET does not increase in D_2O.

5.3.2.2 Choice of Ru complex and acceptors

The two Ru(II) donors utilized in experiments with tethered and untethered complexes have important similarities and interesting differences. $Ru(phen)_2dppz^{2+}$ and $Ru(phen)(bpy')(Me_2\text{-}dppz)^{2+}$ have very similar absorption and emission spectra (Chapters 2, 4), both are "molecular light switches" in aqueous solution,[17] and Ru(II)-Ru(III)

Figure 5.9

Autoradiogram after 20% denaturing polyacrylamide gel electrophoresis showing oxidation reactions of Ru-DNA. The oligonucleotide 5'-TGATC**GG**TGCGTCTGA-GACT-3' was 5'-^{32}P-end-labeled, hybridized to Ru(II)-labeled complement or to unmodified strand, and irradiated as described in section 5.2.3. A) Samples shown are as follows: lanes 1 and 13, Ru-DNA without irradiation; lane 2, Ru-DNA irradiated for 60 min in the absence of quencher; lane 3, unmetallated DNA with MV^{2+} irradiated for 5 min; lanes 4-6, Ru-DNA + MV^{2+} irradiated for 1, 2, 5 min, respectively; lanes 7 and 8, Maxam-Gilbert sequencing reactions G and C+T, respectively; lane 9, unmetallated DNA with $Ru(NH_3)_6^{3+}$ irradiated for 30 min; lanes 10-12, Ru-DNA + $Ru(NH_3)_6^{3+}$ irradiated for 10, 20, 30 min, respectively; lane 14, $Ru(phen)_2(dppz)^{2+}$ + DNA, irradiated for 60 min; lane 15, $Ru(phen)_2(dppz)^{2+}$+ DNA with MV^{2+} irradiated 5 min; lane 16, $Ru(phen)_2(dppz)^{2+}$+ DNA with $Ru(NH_3)_6^{3+}$ irradiated 30 min. B) Histogram representing oxidative damage of the oligonucleotide duplex by Δ-$Ru(phen)(bpy')(Me_2\text{-}dppz)^{3+}$-DNA. The position of intercalation is estimated based on $^1O_2$ sensitization.

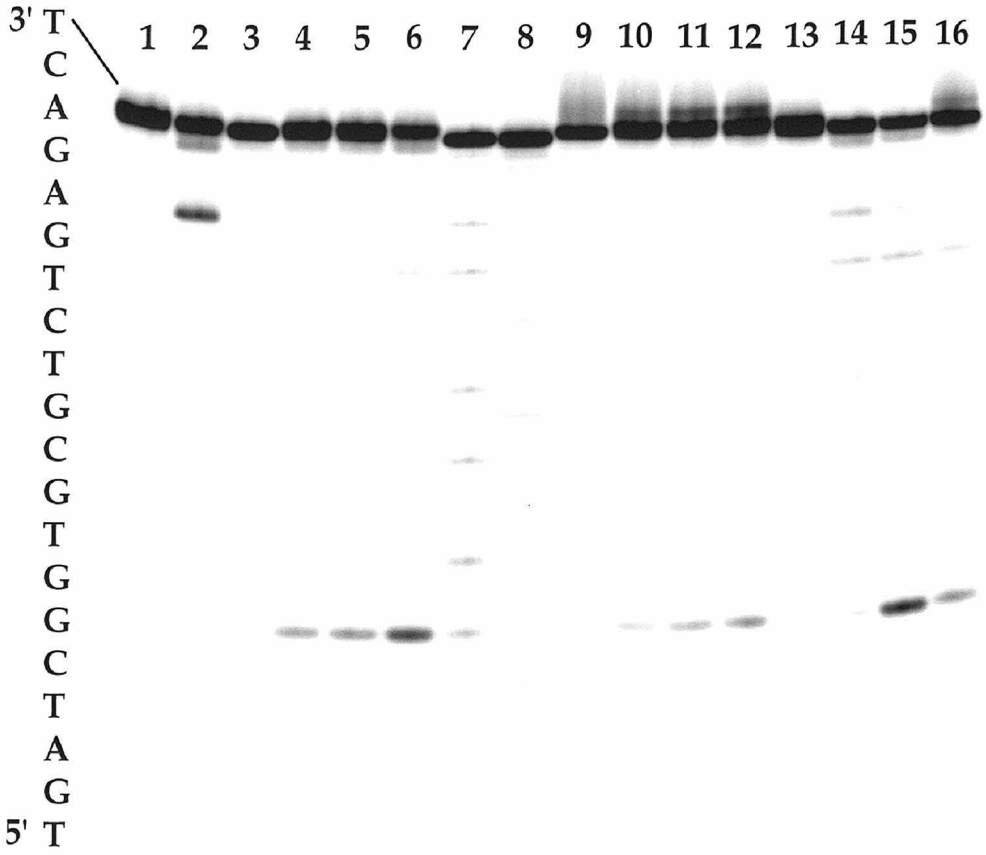
3' T
C
A
G
A
G
T
C
T
G
C
G
T
G
G
C
T
A
G
5' T
1 2 3 4 5 6 7 8 9 10 11 12 13 14 15 16


*5'-TGATCGGTGCGTCTGAGA CT-3
3'-ACTAGCCACGCAGACTCT GA-5
Ru

oxidation potentials are very similar for both complexes.[4] Interestingly, although Ru(II) complexes bearing the ligand Me_2-dppz bind DNA analogously to dppz complexes, their luminescent lifetimes in DNA are substantially longer (Chapter 2), and thus the $\Phi_{emission}$ is ~4-fold higher (0.0074 vs 0.03, respectively). As discussed in Chapter 4, the preferred binding sites for the two intercalators are somewhat distinct, but neither complex seems to show large sequence-selectivity. These two complexes are thus used analogously in the flash-quench measurements described here.

As in experiments with noncovalently bound Ru(II) intercalators, the yield of the G oxidation reaction in Ru-DNA is modulated by the choice of quencher. For both quenchers shown in Figure 5.9, methyl viologen (MV^{2+}) and $Ru(NH_3)_6^{3+}$, damage increases with irradiation time (lanes 4-6, 10-12, respectively) and with the concentration of quencher. Damage also correlates with the instability of the reduced quencher, as expected from Section 5.3.1.8 and Table 5.1; the yield of damage in the presence of MV^{2+} is ~25-fold higher than with $Ru(NH_3)_6^{3+}$. It is noteworthy that the Φ_{damage} is very similar when the donor is *rac*-$Ru(phen)_2dppz^{2+}$ or tethered Δ-Ru(phen)(bpy')$(Me_2\text{-dppz})^{2+}$ despite the differences in $\Phi_{emission}$. Factors contributing to the Φ_{damage} could include either the efficiency of quenching, and thus formation of Ru(III), or the geometry of intercalation, and thus the efficiency of hole transfer from Ru(III) to DNA. For both quenchers, the quenching rate constants (k_q) are ~ 50% smaller for *Δ-Ru(phen)(bpy')$(Me_2\text{-dppz})^{2+}$-DNA than for *rac*-$Ru(phen)_2dppz^{2+}$, indicating that quenching is indeed less efficient for tethered Ru-DNA. There is no evidence to suggest that the yield of damage is altered in Ru-DNA due to the separation between the Ru(III) intercalator and 5'-GG-3'.

Chemical analysis of the products of G oxidation also yields similar data for flash-quench experiments with tethered and untethered Ru(II) intercalators. Ru-DNA was irradiated in the presence of MV^{2+} and $Ru(NH_3)_6^{3+}$ and then subjected to enzymatic digestion (Sections 5.2 and 5.3.1.7). Again, only quenching by $Ru(NH_3)_6^{3+}$ led to significant production of 8-oxo-G products as identified by HPLC. We attempted to

correlate the yield of strand scission with the yield of 8-oxo-G obtained and found that 8-oxo-G was the major product; however, it is difficult to quantitate the total amount of strand scission since there are several G residues on the unlabeled DNA strand. We therefore estimate that the yields of piperidine-labile sites and 8-oxo-G are the same within a factor of 2.

5.3.2.3 Diffusion *versus* long-range oxidation

We can distinguish long-range oxidation in the flash-quench experiment from a reaction mediated by a diffusible species. First, the $^1O_2$ pattern (lane 2 in Figure 5.9) exemplifies damage caused by a reactive, diffusible species generated at the Ru(II) binding site; damage is strongest nearest the Ru(II) and tapers off as the distance from the site increases. Second, we monitored oxidative damage to a radiolabeled DNA duplex in the presence of unlabeled Ru-DNA (Figure 5.10) and found that no damage occurs to the radiolabeled but unmetallated duplex when the quencher is $Ru(NH_3)_6^{3+}$ (lane 5). This control experiment indicates that a) $Ru(NH_3)_6^{2+}$ does not damage DNA , b) Δ-$Ru(phen)(bpy')(Me_2\text{-}dppz)^{3+}$ is only intercalated into the DNA to which it is covalently attached, and c) damage is not caused by a species which can diffuse to another duplex. When the same experiment is done with a sample containing MV^{2+} as quencher, no interstrand damage is observed after one minute of irradiation (lane 6) and minimimal damage (~ 10% of intramolecular damage) at the 5'-GG-3' is observed after five minutes of irradiation. We attribute this cross-reactivity to a small amount of long-lived Ru(III) intercalating into other duplexes, since the rate of decay of Δ-$Ru(phen)(bpy')(Me_2\text{-}dppz)^{3+}$ (~ 10^{-2} s^{-1}; Table 5.1) is similar to the exchange rate of this intercalator (~ 10^{-3} s^{-1}).[20] When $Co(NH_3)_5Cl^{2+}$ serves as quencher, significant intermolecular damage is observed and is similarly attributed to the long lifetime of the Ru(III) intercalator. $Co(NH_3)_5Cl^{2+}$, therefore, has not been used in further studies of long-range G oxidation. For all three quenchers, similar results were obtained when the labeled duplex was identical to the

Figure 5.10

Autoradiogram after 20% denaturing polyacrylamide gel electrophoresis monitoring the extent of interduplex 5'-GG-3' oxidation. 5'-^{32}P-TGATC**GG**TGCGTCTGAG-ACT-3' was hybridized to unmetallated complement and incubated with unlabeled Ru-DNA of the same sequence. Samples shown are as follows: lane 1, ^{32}P-DNA without irradiation; lanes 2 and 3, Maxam-Gilbert sequencing reactions G and C+T, respectively; lane 4, Ru-DNA + ^{32}P-DNA irradiated for 60 min; lane 5, Ru-DNA + ^{32}P-DNA + $Ru(NH_3)_6^{3+}$ irradiated for 30 min; lanes 6 and 7, Ru-DNA + ^{32}P-DNA + MV^{2+} irradiated for 1 and 5 min, respectively.

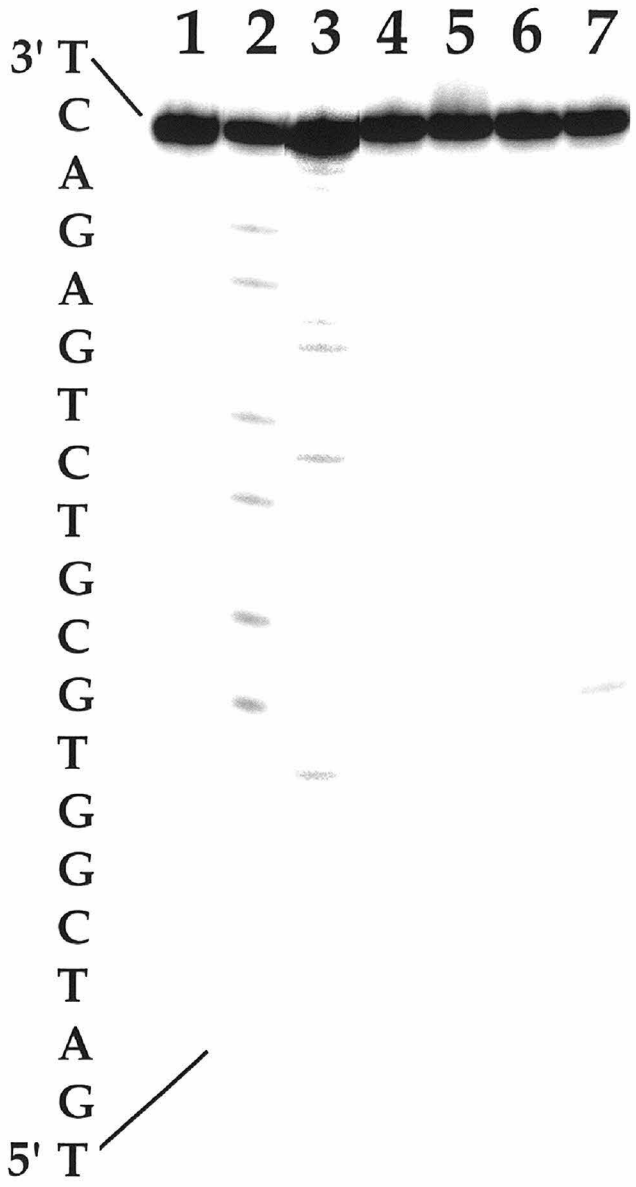
1 2 3 4 5 6 7
3' T
C
A
G
A
G
T
C
T
G
C
G
T
G
G
C
T
A
G
5' T


5'-TGATCGGTGCGTCTGAGA CT-3'
3'-ACTAGCCACGCAGACTCT GA-5'
Ru
+
* 5'-TGATCGGTGCGTCTGAGACT-3'
3'-ACTAGCCACGCAGACTCTGA-5'

metallated DNA (Figure 5.10) or when the ^{32}P-labeled duplex had a different sequence from Ru-DNA; thus, the rates of strand exchange are negligible in the experiments shown in Figure 5.10. Taken together, these data indicate that oxidation of G by Ru(III) is effected by complexes intercalated into DNA, not by a diffusible species, and thus occurs between reactants separated by ~11 bp.

5.3.2.4 Sequence containing 5'-GGG-3' and 5'-GG-3'

Section 5.3.1.5 and Figure 5.6 describe the high yield of G oxidation obtained in the sequence 5'-AC**GGG**CAT**GG**CAGTTCGT-3' hybridized to its complement. When the complementary strand was labeled with Δ-Ru(phen)(bpy')(Me$_2$-dppz)$^{2+}$, however, $^1O_2$ sensitization data indicated that the complex was not intercalated intramolecularly near the site of covalent attachment. Further analysis of the 5'-AGCA-3'/3'-TCGT-5' binding site with this and other sequences[41] indicates that this sequence is not an appropriate intercalation site for Δ-Ru(phen)(bpy')(Me$_2$-dppz)$^{2+}$.

5.3.2.5 Sequence containing 5'-GG-3' separated from Ru(II) by A/Ts

Tethered assemblies such as Ru-DNA provide a good opportunity to describe the effect of sequence on G oxidation. Towards this goal, we prepared the 17 mer sequence ^{32}P-5'-CGCTCA**GG**TATTAATAT-3' and its 5'-ruthenated complement. Given intercalation of Δ-Ru(phen)(bpy')(Me$_2$-dppz)$^{2+}$ two basepairs from the site of attachment, this assembly places the Ru(II) intercalator seven A/T basepairs from 5'-GG-3'. Since the Ru-terminus contains only A and T, however, $^1O_2$ sensitization is not a suitable method to determine the intercalation site,[34] and future experiments are needed to prove that the duplex is well-formed (Chapter 4) and to identify the binding site by footprinting.

We had intended to use this Ru-DNA duplex to study the kinetics of G• formation over ~25Å. However, when this AT-rich Ru-DNA was irradiated in the presence of Ru(NH$_3$)$_6^{3+}$ or Co(NH$_3$)$_5$Cl^{2+}, virtually no damage was observed after treatment with

piperidine (Figure 5.11). Time-resolved emission and transient absorption spectroscopies suggest two reasons for this lack of reactivity. First, emission quenching of this Ru-DNA sequence (24%) is much less efficient than quenching observed under the same conditions for the GC-rich Ru-DNA (83%) described in Section 5.3.2.1 and Figure 5.9. The poor quenching of Δ-*Ru(phen)(bpy')(Me_2-dppz)$^{2+}$ tethered to the AT-rich sequence indicates that little Δ-Ru(phen)(bpy')(Me_2-dppz)$^{3+}$ acceptor is generated and could also suggest that the Ru(II) complex is particularly well intercalated.[25] Figure 5.12 shows the ground state recovery for Δ-Ru(phen)(bpy')(Me_2-dppz)$^{3+}$ bound to the AT- and GC-rich Ru-DNA oligonucleotides in the presence of $Ru(NH_3)_6^{3+}$. In the GC-rich oligonucleotide duplex, Δ-Ru(phen)(bpy')(Me_2-dppz)$^{3+}$ decays with a rate constant of ~6 x 10^4 s^{-1} (Figure 5.12A), similar to the rate obtained for *rac*-Ru(phen)$_2$(dppz)$^{3+}$ bound to the same sequence (Section 5.2.1.2). By contrast, Δ-Ru(phen)(bpy')(Me_2-dppz)$^{3+}$ tethered to the AT-rich sequence decays much more slowly, with a rate constant of ~7 x 10^3 s^{-1} (Figure 5.12B). The slow ground state recovery observed for this oligonucleotide indicates either that back reaction between Δ-Ru(phen)(bpy')(Me_2-dppz)$^{3+}$ and $Ru(NH_3)_6^{2+}$ is particularly slow, perhaps due to protection of the intercalator by the DNA helix, or that ET is highly inefficient between Δ-Ru(phen)(bpy')(Me_2-dppz)$^{3+}$ and the remotely placed 5'-GG-3'.

Two conclusions can thus be drawn from these experiments. First, the AT-rich binding site could perturb the intercalation of the Ru(II) complex such that the flash-quench cycle is inefficient to generate Ru(III) and then G•. Additionally, it is possible that the intervening A/T basestack serves as a poor medium for hole transfer. By preparing a series of oligonucleotides containing 1, 2, or 3 GC basepairs between the intercalator and the 5'-GG-3' doublet, we will be able to analyze the effect of intervening GC basepairs on the yield and rate of long-range G oxidation.

Figure 5.11

Autoradiogram after 20% denaturing polyacrylamide gel electrophoresis showing oxidation reactions of Ru-DNA. The oligonucleotide 5'-CGCTCA**GG**TATTAATAT-3' was 5'-^{32}P-end-labeled, hybridized to Ru(II)-labeled complement, and irradiated as described in section 5.2.3. Samples shown are as follows: lane 1, unirradiated Ru-DNA; lane 2, Ru-DNA irradiated for 40 min; lanes 3-5, Ru-DNA + $Co(NH_3)_5Cl^{2+}$ (1, 5, 10 equiv, respectively) irradiated for 1 min; lanes 6 and 7, Maxam-Gilbert sequencing reactions G and C+T, respectively; lanes 8-10, Ru-DNA + $Ru(NH_3)_6^{3+}$ (2, 10, 20 equiv, respectively) irradiated for 10 min; lanes 11-13, Ru-DNA + $Ru(NH_3)_6^{3+}$ (2, 10, 20 equiv, respectively) irradiated for 30 min.

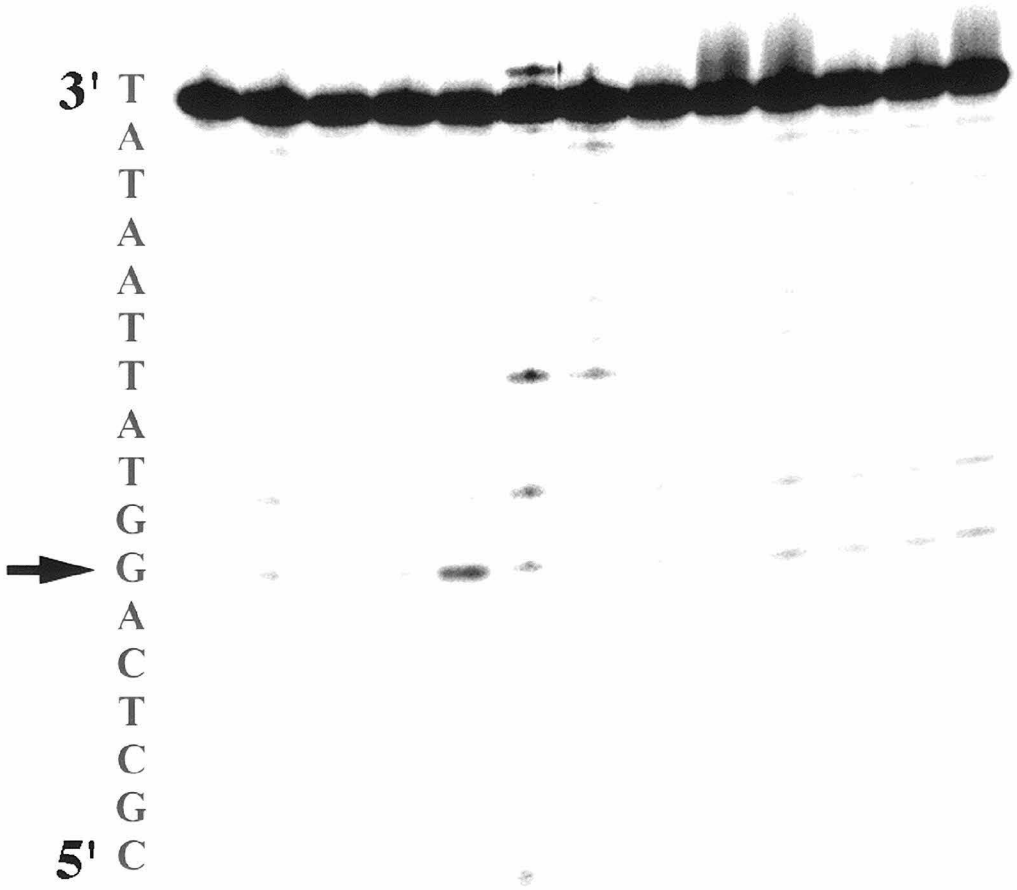
3'
T
A
T
A
A
A
T
T
A
T
G
G
A
C
T
C
G
C
5'
C


*5'-CGCTCAGGTATTAAT AT-3'
3'-GCGAGTCCATAATTA TA-5'
Ru

Figure 5.12

Time-resolved transient absorption spectroscopy of Ru-DNAs quenched by $Ru(NH_3)_6^{3+}$. A) Ground-state recovery of Δ-Ru(phen)(bpy')$(Me_2\text{-dppz})^{2+}$ at 380 nm in the absence (top trace) and presence (bottom trace) of 400 μM $Ru(NH_3)_6^{3+}$. Samples contained the oligonucleotide 5'-TGATC**GG**TGCGTCTGAGACT-3' hybridized to 5'-ruthenated complement (20 μM duplex) in phosphate buffer (Section 5.2). B) Ground-state recovery of Δ-Ru(phen)(bpy')$(Me_2\text{-dppz})^{2+}$ at 380 nm in the absence (top trace) and presence (bottom trace) of 400 μM $Ru(NH_3)_6^{3+}$. Samples contained the oligonucleotide 5'-CGCTCA**GG**TATTAATAT-3' hybridized to 5'-ruthenated complement (20 μM duplex) in phosphate buffer (Section 5.2).

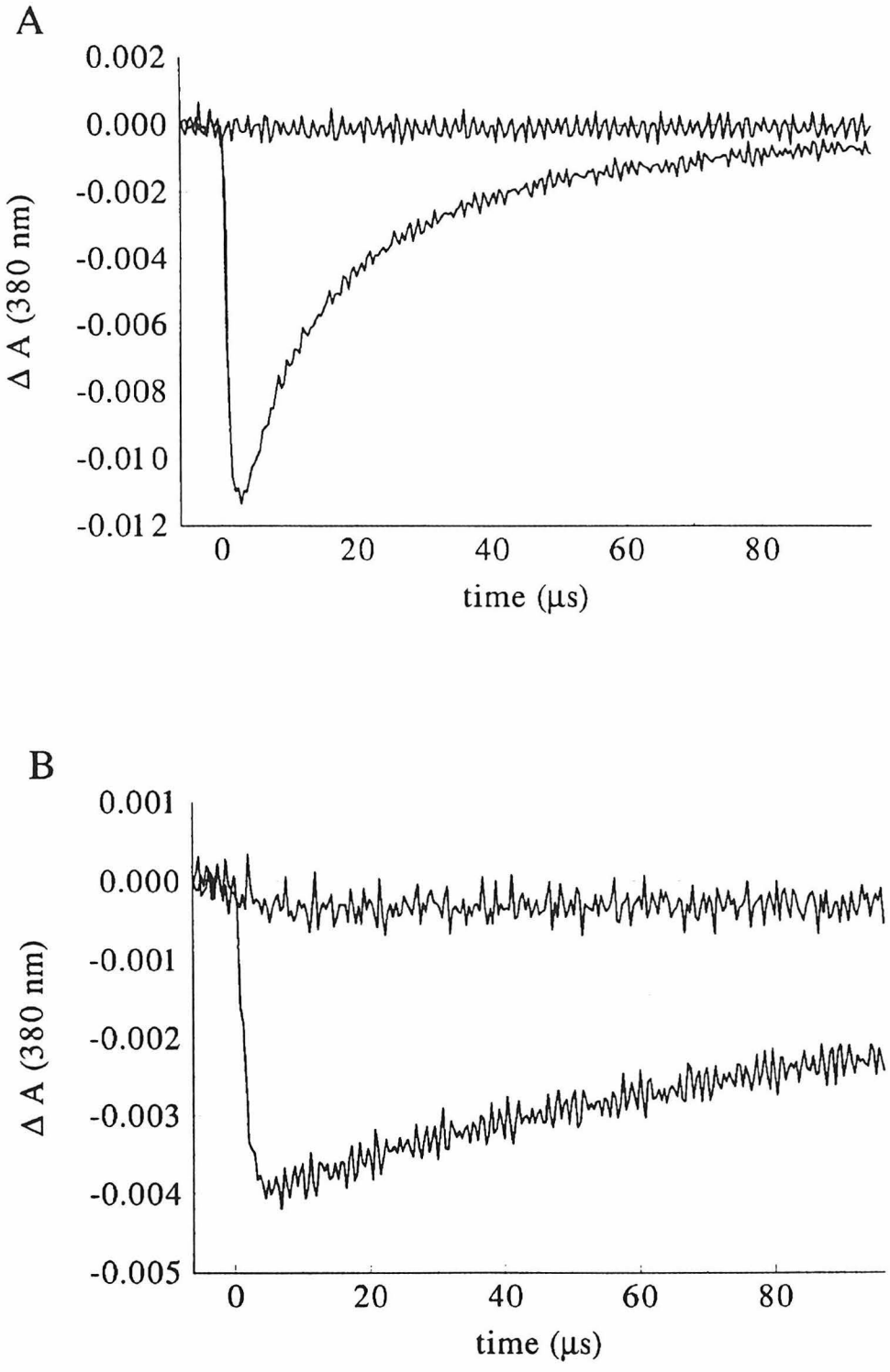
A
0.002
0.000
-0.002
-0.004
-0.006
-0.008
-0.010
-0.012
Δ A (380 nm)
0
20
40
60
80
time (μs)
B
0.001
0.000
-0.001
-0.002
-0.003
-0.004
-0.005
Δ A (380 nm)
0
20
40
60
80
time (μs)

5.3.2.6 Oxidation of DNA containing no 5'-GG-3' sequences

We have also considered long-range oxidation in an oligonucleotide duplex constructed without a 5'-GG-3' doublet (Figure 5.13), using a sequence which differs by only one basepair from the duplex described in Section 5.3.2.1 and Figure 9. These experiments form a bridge between spectroscopic studies which indicate that the poly(dG-dC) is oxidized by Ru(III) and gel electrophoresis experiments which indicate that permanent damage occurs primarily at 5'-GG-3' doublets. Importantly, when no 5'-GG-3' sequences are present, oxidative damage is observed at all Gs on the labeled strand, with no large sequence preference or sensitivity to distance from the oxidant.[8a] The total reaction on the duplex is comparable to that seen with the duplex containing 5'-GG-3' in Figure 5.9. Such comparisons can only be made qualitatively, given the different reaction conditions; however, it is important that the cleavage observed in Figure 5.13 is not simply the background damage observed at other Gs in Figure 5.9. These results suggest that radical damage is able to migrate to the site of lowest redox potential, where a fraction of the radical is subsequently trapped to yield permanent damage. In the absence of a low energy site, the radicals are evenly distributed over the 20-mer DNA duplex. These observations graphically underscore the notion of an equilibration of a radical across the DNA duplex.

5.3.3 Comparison of Rh(III) to Ru(II) systems

Eventual goals of our studies with flash-quench ozxidation of DNA are to determine the mechanism, rate, and energetics of long-range oxidation. We predict that these parameters will be similar for the new flash-quench cycle and the more well-studied photooxidation reaction generated by $*Rh(phi)_2(bpy')^{3+}$,[6] since the reactions seem to differ only in the mechanism of hole generation on the metallointercalator. We have established that there are some similarities between Ru(III)-initiated oxidative damage and the *Rh(III)-initiated reaction, including the sequence-selectivity of damage and the formation of 8-oxo-

Figure 5.13

Autoradiogram after 20% denaturing polyacrylamide gel electrophoresis showing oxidation reactions of Ru-DNA. The oligonucleotide 5'-TGATCGCTGC-GTCTGAGACT-3' was 5'-^{32}P-end-labeled, hybridized to Ru(II)-labeled complement, and irradiated as described in Section 5.2.3. Samples shown are as follows: lanes 1 and 2, Maxam-Gilbert sequencing reactions G and C+T, respectively; lane 3, unirradiated Ru-DNA; lane 4, Ru-DNA irradiated for 60 min; lane 5, Ru-DNA + $Ru(NH_3)_6^{3+}$ irradiated for 30 min; lane 6, Ru-DNA + MV^{2+} irradiated for 5 min. B) Histogram representing oxidative damage of the oligonucleotide duplex by Δ-Ru(phen)(bpy')(Me_2-dppz)$^{3+}$-DNA. The position of intercalation is estimated based on $^1O_2$ sensitization.

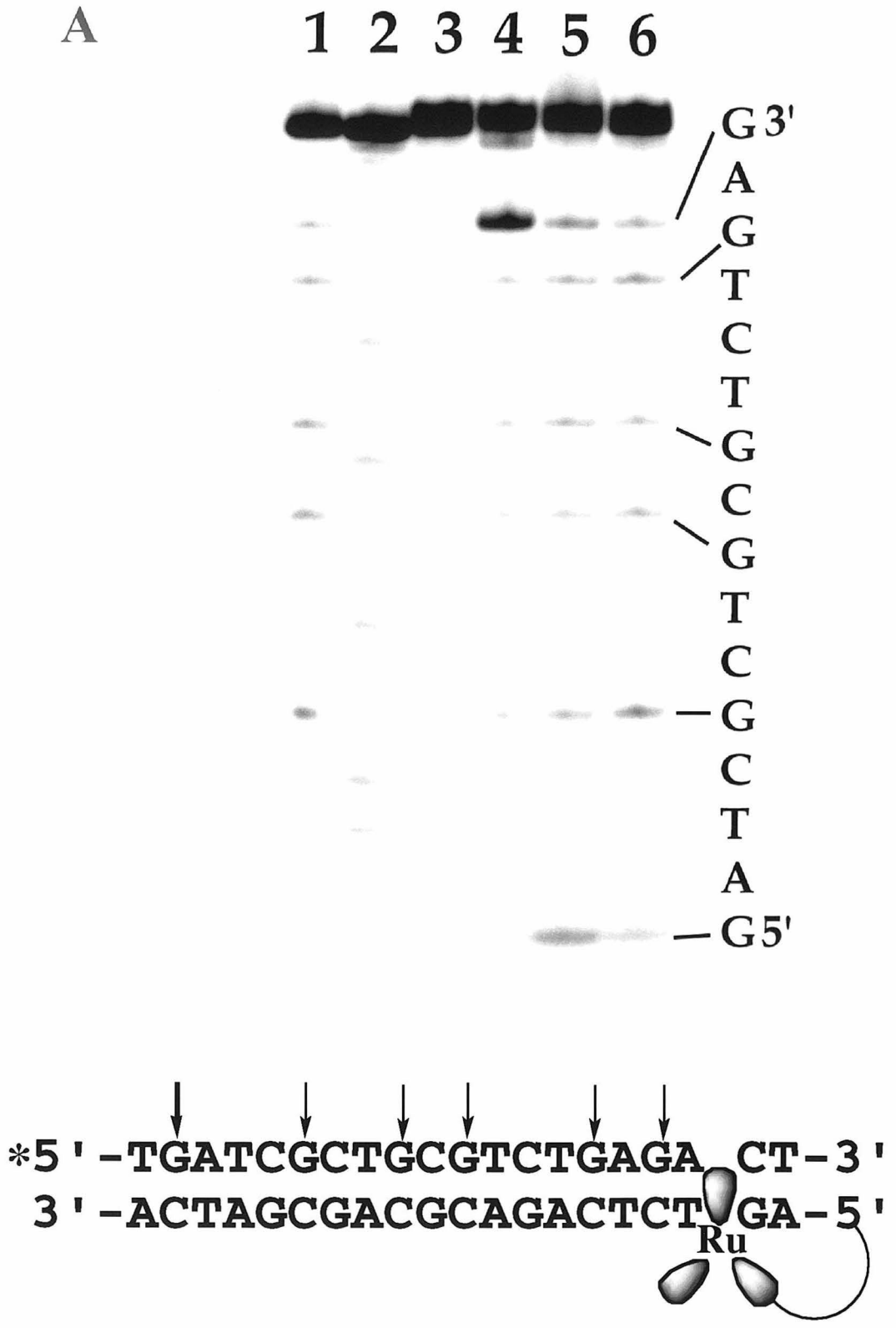
A
1 2 3 4 5 6
G 3'
A
G
T
C
T
G
C
G
T
C
G
C
T
A
G 5'
*5'-TGATCGCTGCGTCTGAGA CT-3'
3'-ACTAGCGACGCAGACTCT GA-5'
Ru

G. However, it has yet to be determined whether the flash-quench cycle will manifest the same sensitivity to bulges, flanking sequence, or molecular oxygen. Initial studies with noncovalently bound and intercalated *Ru(phen)$_2$dppz^{2+} quenched by Ru(NH$_3$)$_6^{3+}$ suggest at most a modest dependence on oxygen (see Section 5.2), in contrast to the strong oxygen dependence observed for *Rh(phi)$_2$(DMB)$^{3+}$. It is noteworthy that O_2-dependent generation of piperidine-labile sites has been observed for G oxidation systems involving anthraquinones,[8a] although this dependence was complex. By contrast, O_2 does not seem to be required for oxidation of DNA by ethidium/methylene blue,[9] and water was found to supply the O atom of 8-oxo-G formed by photoionization of DNA.[37]

There are important technical differences between the Ru(III) and *Rh(III) systems which will direct the choice of oxidant in future studies. Possible advantages of the flash-quench system include high damage yields, low wavelength of irradiation, and tunability of oxidation potential of the Ru(II) donor. First, the quantum yields for oxidative damage are ~10^4-fold higher for the flash-quench system, and suitable quenchers can be chosen for a particular experiment. For example, the good stability and low absorptivity of Ru(NH$_3$)$_6^{3+}$ make it ideal for photophysical measurements, while MV^{2+} gives high yields and thus allows short irradiation times. Second, in contrast to the Rh(phi)$_2$(bpy')$^{3+}$ photooxidant, which shows evidence of direct photocleaves DNA at 365 nm,[6,42] the flash-quench reactions result in a very low background of DNA damage. This relatively clean reaction results from the low wavelength of irradiation and high photochemical stability of Ru(II) polypyridyl complexes. Finally, we expect that the reactivity and sequence-selectivity of oxidation reactions may be tuned by varying the redox potential of the Ru(II) complex. It is important to note that the use of novel photooxidants[43] in place of Rh(phi)$_2$(DMB)$^{3+}$ may incorporate several of the benefits currently found in the flash-quench experiment.

For some experiments, the photooxidation system is more suitable than the flash-quench method. In particular, the flash-quench cycle as described utilizes a diffusible

species which can complicate the interpretation of results, particularly if other noncovalent interactions, such as protein-DNA binding, are involved. For such experiments, a covalently tethered photooxidant may provide a more straightforward system.[6] Secondly, the binding site preferences and intercalation geometries are much better defined for phi complexes of Rh(III) than for dppz complexes of Ru(II). This greater detail is possible due to the direct photocleavage of the DNA backbone by complexes such as $Rh(phi)_2(bpy')^{3+}$.[42] $^1O_2$-sensitization provides the analogous information in Ru(II) polypyridyl chemistry. It is difficult to obtain detailed information from this reaction, however, since this mechanism involves the binding of metal complex, the reactivity of bases near the binding site, the quantum yield of emission, and the diffusion of $^1O_2$.[34] At this time, therefore, we are better able to design and test binding sites for Rh(III) than for Ru(II).

Perhaps the most important point is that both *Rh(III) and ground-state Ru(II) intercalators can effect the same G oxidation chemistry. Contrasting the energetics and timescales for these two systems could therefore provide insight into the reaction mechanism(s). For example, since the two metal complexes are likely to have different absolute energies, the long-range oxidation of DNA seems not to be highly sensitive to the energy of the generated hole. Additionally, the difference in Φ_{damage} observed for these two systems could relate to the timescales for the two reactions; the *Rh(III) lifetime is less than 100 ns, whereas Ru(III) is stable for hundreds of microseconds. Futher comparisons between photooxidation and ground-state hole formation will help define the parameters for long-range oxidative damage of DNA.

5.4 Future Directions

Many interesting experiments are suggested by the work described here. Future work will likely define the mechanism of DNA oxidation in more detail. In order to correlate the flash-quench system with photooxidation, it will be useful to analyze the effect

of bulges on 5'-GG-3' oxidation[6] and the O_2 dependence of piperidine-labile damage. Presently, the flash-quench method is being used to investigate damage to Gs in GA mismatches[41] and the distance-dependence of G oxidation over >50 Å.

Two additional future directions are of particular interest. First, it will be very useful to determine if the reactivity of Ru(III) intercalators can be manipulated by varying the ligands on the complex. For example, both adenines (A) and thymine dimers (T<>T) have a higher redox potential than guanine.[7,44,45] Can the addition of electron-withdrawing groups to the ancillary ligands of $Ru(phen)_2dppz^{2+}$ raise the oxidation potential enough to permit oxidation of A and T<>T? Second, Section 5.3.2.7 presented preliminary results which could indicate that intervening G residues are required to mediate hole transfer from the tethered Ru(III) intercalator to a remotely placed 5'-GG-3'. Further studies could utilize Ru-DNA sequences containing one, two, and three intervening GC basepairs. Data with Ru-DNA containing no 5'-GG-3' sequences (Section 5.3.2.8) suggest that damage can be observed at single G residues if no lower energy sequences are present. Thus, it may be that G-containing sequences can be isolated by intervening A/T stretches,[29b] or perhaps initial formation of the G• is the limiting step in the reaction sequence. Such information will be important in delineating the mechanism of long-range electron transfer in DNA.

5.5 Conclusions

We have demonstrated that a flash-quench methodology can be used to combine spectroscopy and product analysis in the description of long-range ET reactions of DNA. This methodology permits the direct spectroscopic characterization of the neutral guanine radical in duplex DNA and the biochemical description of stable oxidation products at 5'-GG-3' sequences. With tethered Ru-DNA, reactions are shown to occur even when Ru(II) and 5'-GG-3' are separated by 11 bp. The flash-quench reaction with ruthenium intercalators therefore adds to the growing number of ET reactions involving DNA both as

a bridge and as a reactant and permits reaction intermediates and products to be readily identified and compared. In addition, the rich photochemical properties of polypyridyl complexes of Ru(II) provide a means to tune the selectivity and efficiency of these DNA-mediated reactions.

5.6 References

1. a) Stemp, E. D. A.; Barton, J. K. *Metal Ions Biol.* **1996**, *33*, 325. b) Meade, T. J. *Metal Ions Biol.* **1996**, *32*, 453. c) O'Neill, P.; Fielden, E. M. *Adv. Rad. Biol.* **1993**, *17*, 53.
2. a) Murphy, C. J.; Arkin, M. R.; Ghatlia, N. D.; Bossmann, S.; Turro, N. J.; Barton, J. K. *Proc. Nat. Acad. Sci., USA* **1994**, *91*, 5315. b) Arkin, M. R.; Stemp, E. D. A.; Turro, C.; Turro, N. J.; Barton, J. K. *J. Am. Chem. Soc.* **1996**, *118*, 2267. c) Holmlin, R. E.; Stemp, E. D. A.; Barton, J. K. *J. Am. Chem. Soc.* **1996**, *118*, 5236. d) Stemp, E. D. A.; Arkin, M. R.; Barton, J. K. *J. Am. Chem. Soc.*, **1995**, *117*, 2375.
3. a) Baguley, B. C.; Le Bret, M. *Biochemistry* **1984**, *23*, 937. b) Brun, A. M.; Harriman, A. *J. Am. Chem. Soc.* **1992**, *114*, 3656. c) Meade, T. J.; Kayyem, J. F. *Angew. Chem. Int. Ed. Engl.* **1995**, *34*, 352.
4. Arkin, M. R.; Stemp, E. D. A.; Holmlin, R. E.; Barton, J. K.; Hörmann, A.; Olson, E. J. C.; Barbara, P. F. *Science*, **1996**, *273*, 475.
5. a) Murphy, C. J.; Arkin, M. R.; Jenkins, Y. C.; Ghatlia, N. D.; Bossmann, S.; Turro, N. J.; Barton, J. K. *Science*, **1993**, *262*, 1025. b) Kelley, S. O.; Holmlin, R. E.; Stemp, E. D. A.; Barton, J. K. submitted for publication.
6. a) Hall, D. B; Holmlin, R. E.; Barton, J. K. *Nature*, **1996**, *382*, 731. b) Hall, D. B. and Barton, J. K., submitted for publication.
7. Dandliker, P. J.; Holmlin, R. E.; Barton, J. K., *Science*, in press, **1996**.
8. a) Ly, D.; Kan, Y.; Armitage, B.; Schuster, G. B. *J. Am. Chem. Soc.* **1996**, *118*, 8747. b) Breslin, D. and Schuster, G. B. *J. Am. Chem. Soc.* **1996**, *118*, 2311. c) Armitage, B.; Yu, C.; Devadoss, C.; Schuster, G. B. *J. Am. Chem. Soc.*, **1994**, *116*, 9847.
9. Dunn, D. A.; Lin, V. H.; Kochevar, I. E. *Biochemistry*, **1992**, *31*, 11620.
10. Ito, K.; Inoue, S.; Yamamoto, K.; Kawanishi, S. *J. Biol. Chem.* **1993**, *268*, 13221.

11. a) Saito, I.; Takayama, M.; Sugiyama, H.; Nakatani, K.; Tsuchida, A.; Yamamoto, M. *J. Am. Chem. Soc.* **1995**, *117*, 6406. b) Sugiyama, H. and Saito, I. *J. Am. Chem. Soc.* **1996**, *118*, 7063.

12. Chang, I. J.; Gray, H. B.; Winkler, J. R. *J. Am. Chem. Soc.*, **1991**, *113*, 7056.

13. Johnston, D. H.; Glasgow, K. C.; Thorp, H. H. *J. Am. Chem. Soc.*, **1995**, *117*, 8933.

14. Manoharan, M.; Tivel, M. L.; Zhao, M.; Nafisi, K.; Netzel, T. L. *J. Phys. Chem.*, **1995**, *99*, 17461.

15. Colson, A.-O.; Besler, B.; Sevilla, M. D. *J. Phys. Chem.*, **1992**, *96*, 9787.

16. Solvent-accessible guanines, as in bulged sequences, have also been oxidized by activated nickel and cobalt complexes. See a) Burrows, C. J.; Rokita, S. E. *Accts. Chem. Res.* **1994**, *27*, 295. b) Muller, J. G.; Zheng, P.; Rokita, S. E.; Burrows, C. J. *J. Am. Chem. Soc.*, **1996**, *118*, 2320.

17. a) Friedman, A. E.; Chambron, J.-C.; Sauvage, J.-P., Turro, N. J.; Barton, J. K. *J. Am. Chem. Soc.* **1990**, *112*, 4960. b) Jenkins, Y.; Friedman, A. E.; Turro, N. J.; Barton, J. K. *Biochemistry*, **1992**, *31*, 10809.

18. a) Beaucage, S. L.; Caruthers, M. H. *Tet. Lett.* **1981**, *23*, 1859. b) Goodchild, J. *Bioconj. Chem.* **1990**, *1*, 165.

19. Amouyal, E.; Homsi, A.; Chambron, J. C.; Sauvage, J. P. *J. Chem. Soc. Dalton Trans.* **1990**, *6*, 1841.

20. a) Dupureur, C. M.; Barton, J. K. *J. Am. Chem. Soc.* **1994**, *116*, 10286. b) Dupureur, C. M.; Barton, J. K. submitted for publication.

21. Jenkins, Y. C., Ph.D. Thesis, *California Institute of Technology*, **1996**.

22. Sambrook, J.; Fritsch, E. F.; Maniatis, T. *Molecular Cloning: A Laboratory Manual*, 2nd ed., NY: Cold Spring Harbor Laboratory, **1989.**

23. Calvert, J. G.; Pitts, J. N. Jr. *Photochemistry*, New York: John Wiley & Sons, Inc., **1966**, 780-786.

24. Calvert, J. M.; Casper, J. V.; Binstead, R. A.; Westmoreland, T. D.; Meyer, T. J. *J. Am. Chem. Soc.* **1982**, *104*, 6620.

25. Stemp, E. D. A.; Holmlin, R. E.; Arkin, M. R., unpublished results.

26. Stemp, E. D. A. unpublished results.

27. Navon, G.; Sutin, N. *Inorg. Chem.* **1974**, *13*, 2159.

28. Candeias, L. P. and Steenken, S. *J. Am. Chem. Soc.* **1989**, *111*, 1094.

29. G radicals have also been detected after direct ionization of DNA at 193 nm [see a) Melvin, T.; Botchway, S. W.; Parker, A. W.; O'Neill, P. *J. Chem. Soc. Chem. Comm.* **1995**, 653. b) Melvin, T.; Plumb, M. A.; Botchway, S. W.; O'Neill, P.; Parker, A. W. *Photochem. Photobiol.* **1995**, *61*, 584] and following pulse radiolysis in single-stranded DNA [See Jovanovic, S. V. and Simic, M. G. *Biochim. et Biophys. Acta,* **1989**, *1008*, 39].

30. a) Atherton, S. J.; Harriman, A. *J. Am. Chem. Soc.* **1993**, *115*, 1816. b) Brun, A. M.; Harriman, A.; *J. Am. Chem. Soc.*, **1991**, *113*, 8153. c) Lecomte, J.-P.; Kirsch-De Mesmaeker, A.; Feeney, M. M.; Kelly, J. M.; Görner, H. *Photochem. Photobiol*, **1992**, *55*, 681.

31. Mujeeb, A.; Kerwin, S. M.; Kenyon, G. L.; James, T. L. *Biochemistry* **1993**, *32*, 13419.

32. Welch, T. W.; Corbett, A. H.; Thorp, H. H. *J. Phys. Chem.*, **1995**, *99*, 11757.

33. Chung, M.-H.; Kiyosawa, H.; Nishimura, S.; Kasai, H. *Biochem. Biophys. Res. Comm.* **1992**, *188*, 1.

34. a) Mei, H.-Y.; Barton, J. K. *J. Am. Chem. Soc.* **1986**, *108*, 7414. b) Mei, H.-Y.; Barton, J. K. *Proc. Natl. Acad. Sci. USA* **1988**, *85*, 1339.

35. Rodgers, M. A. J.; Snowden, P. T. *J. Am. Chem. Soc.* **1982**, *104*, 5543.

36. 8-oxo-G is a common lesion in oxidatively damaged DNA, see a) Sibutani, S.; Takeshita, M.; Grollman, A. P. *Nature,* **1991**, *349*, 431. b) Barciszewski, J.;

Barciszewska, M. Z.; Rattan, S. I. S.; Clark, B. F. C. *Polish J. Chem.* **1995**, *69*, 841.

37. Cullis, P. M.; Malone, M. E.; Merson-Davies, L. A. *J. Am. Chem. Soc.* **1996**, *118*, 2775.
38. Sheu, C.; Foote, C. S. *J. Am. Chem. Soc.* **1995**, *117*, 6439.
39. Atherton, S. J. and Beaumont, P. C. *J. Phys. Chem.*, **1987**, *91*, 3993.
40. a) Simic, M.; Lilie, J. *J. Am. Chem. Soc.* **1974**, *96*, 291. b)Liang, N.; Mauk, A. G.; Pielak, G. J.; Johnson, J. A.; Smith, M. A.; Hoffman, B. M. *Science*, **1988**, *240*, 311.
41. Coates, S., unpublished results.
42. Sitlani, A.; Long, E. C.; Pyle, A. M.; Barton, J. K. *J. Am. Chem. Soc.***1992**, *114*, 2303.
43. Hall, D. B., unpublished results.
44. Kittler *et al. J. Electroanal. Chem.* **1980**, *116*, 503 (values converted to NHE by adding+0.65 V).
45. Heelis, P. F.; Debble, D. J.; Kim, S.-T.; Sancar-A. *Int. J. Radiat. Biol.* **1992**, *62*, 137.